Exploring Critical Vehicle Parameters for the Design of Multitargeted Nanoparticles for Cancer Specific Gene Delivery

A Thesis
SUBMITTED TO THE FACULTY OF THE
UNIVERSITY OF MINNESOTA
BY

Rachel Mae Levine

IN PARTIAL FULFILLMENT OF THE REQUIREMENTS
FOR THE DEGREE OF
DOCTOR OF PHILOSOPHY

Adviser: Efrosini Kokkoli

October, 2015

Acknowledgements

I'd like to thank my adviser, Efie Kokkoli, for supporting me through the challenges and successes of my PhD work. Communication in science is critical to the advancement of technologies and application of discoveries, and Efie impressed upon me the importance and art of telling a story through my research. I'm so appreciative of the many opportunities she gave me to teach and mentor, and the freedom she gave me to pursue my own ideas. I would also like to thank Professor Victor Barocas, Professor Ben Hackel and Professor Scott McIvor for serving on my committee and for sharing with me their scientific insight and enthusiasm, as well as their mentoring and management philosophies.

Chapters 1 and 2 present previously published work, reproduced by permission of The Royal Society of Chemistry, Levine, R. M., Scott, C. M. & Kokkoli, E. Peptide Functionalized Nanoparticles for Nonviral Gene Delivery. *Soft Matter* **9,** 985–1004 (2013) and reprinted with permission from Levine, R. M., Pearce, T. R., Adil, M. M., & Kokkoli, E. Preparation and Characterization of Liposome-Encapsulated Plasmid DNA for Gene Delivery. *Langmuir* (2013), Copyright 2013 American Chemical Society, respectively. Carolyn Scott collaborated closely with me to help compile a thorough, insightful review of the peptide-targeted gene delivery literature in Chapter 1, Maroof was instrumental in the intellectual development of Chapter 2, and Tim Pearce provided cryo-TEM images for Chapter 2. Christina Dinh, an undergraduate researcher who worked with me for three years, contributed significantly to the experimental execution, analysis and direction of Chapter 3, and was responsible for data collection for several figures in that chapter. I'm very proud of the work we accomplished and of her acceptance to MIT, where she will be starting her own graduate career in chemical engineering in the fall. I could never have been so successful without the past and present members of the Kokkoli Group. Thanks are due to Dr. Brett Waybrant, Dr. Matt Petersen, Dr. Nicole Atchison, Dr. Maroof Adil, Dr. Tim Pearce, Carolyn Scott, Frankie Peleaz and Mike Harris for creating a supportive, collaborative, intellectually challenging and fun work environment. Special thanks go to Dr. Maroof Adil, who has become prominent in my life as a role model, mentor, and friend.

I am grateful to the Hackel group for use of their equipment, but especially to Larry Stern and Sadie Johnson, as well as Carolyn from the Kokkoli lab, for our many thought provoking scientific discussions. Their questions and ideas led to many solutions to experimental and conceptual challenges. I'd like to thank Colleen Witzenburg for reintroducing me to Matlab and helping me

troubleshoot the code presented in Chapter 4. Our deep discussions about science and academia challenged and expanded my point of view, and her dedication to her craft and to constantly learning and improving have been a great inspiration to me.

The support and love of my friends and family has always been critical to my success. I'd like to thank my parents for telling me I could be anything I set my mind to, because I believed them, and that belief has brought me here. Emily, Cassie, Ali and Phillip have always been there for me, and I have so much gratitude for them. I am grateful for my time volunteering with Alpha Epsilon Phi, whose passionate group of women taught me to be a better leader in so many ways, and I am proud of all they have accomplished and all they will become. Melissa and Phil Olsen, Boris and Tammy Chernomordick, Patrick Smadbeck and Caryn Krakauer, Tim Gillard and Colleen Crook, Garrett Swindlehurst and Anna Haugen, and Kevin Pustulka were the source of my sanity and social life throughout my time in Minnesota, and truly became my graduate school family. Thank you to Boris for the philosophical conversations, to Mel for being able to talk with me about absolutely anything for hours, to Anna for the much needed life distractions, and to Tammy for the creative inspirations. Bruce and Colleen Witzenburg are especially important among my support system in Minnesota. I'd like to thank them deeply for their friendship; for Doctor Who marathons, nerdy obsessions, passionate debates and unconditional support. And lastly, I'd like to thank Corrie and Ian Hill for their friendship through the final stretch of my PhD; for the late night psychology discussions, kitty-inspired giggles and empathy through the thesis writing process.

Abstract

The greatest obstacle to clinical application of cancer gene therapy is lack of effective delivery tools. Gene delivery vehicles must protect against degradation, avoid immunogenic effects and prevent off target delivery which can cause harmful side effects. The stealth liposomes has greatly improved tumor localization of small molecule drugs and is a promising tool for nucleic acid delivery as the polyethylene glycol coating its surface protects against immune recognition and blood clearance. In this study, DNA was fully encapsulated within in stealth liposomes by complexing the macromolecule with a cationic polymer before encapsulation. Formation methods and material compositions were then investigated for their effects on encapsulation. This technology was translated for protective delivery of siRNA designed for HPV viral gene silencing and cervical cancer treatment. Stealth liposomes encapsulating siRNA were functionalized with a targeting peptide which binds to the alpha6 integrin, a cervical cancer biomarker. It was found that both targeting and polymer complexation before encapsulation were critical components to effective transfection. Varying the siRNA:polymer ratio revealed an optimal concentration for enhanced transfection, but no improvement to internalization, suggesting polymer complexation enhances transfection through an intracellular mechanism.

Nanoparticles functionalized with cancer-targeting ligands have shown promise but are still limited by off-tumor binding to healthy tissues that nevertheless express low levels of the molecular target. Targeting two unique cancer biomarkers using dual-targeted heteromultivalent nanoparticles presents a solution to this challenge by requiring overexpression of two separate ligands for localization. In order to guide experimental design, a kinetic model was built to explore how the affinity and valency of dual-ligand liposomes affect the binding and selectivity of delivery to cells with various receptor expression. $\alpha_5\beta_1$ and $\alpha_6\beta_4$ integrin expression levels were then quantified on 20 different cell lines to identify appropriate model cells for in vitro investigation. Dual-targeting heteromultivalent liposomes were synthesized using the alpha6 targeting peptide and an alpha5beta1 targeting peptide. Heteromultivalent liposomes with varying peptide ratios were delivered to cells with varying integrin concentrations. Binding and internalization was then evaluated to understand the effect of valency and avidity on binding kinetics and delivery. Dual-ligand liposomes with equal valencies of each targeting peptide achieved enhanced binding efficiency and selectivity for cells expressing equal and high receptor levels. This liposome formulation was used as a gene delivery vehicle to achieve improved transfection to dual-receptor

expressing cells. The insights gained from this study inform rational design of modular heteromultivalent nanoparticles for enhanced specificity to target tissue, for the creation of more effective cancer treatments.

Table of Contents

Table of Tables

Table of Figures

Abbreviations

bPEI – branched polyethyleneimine

Cryo-TEM – Cryo-transmission electron microscopy

DLS – dynamic light scattering

DPPC – 1,2-dipalmitoyl–sn-glycero-3-phosphocholine)

HPV – human papillomavirus

ITC – isothermal calorimetry

N:P – amine to phosphate ratio

pDNA – plasmid DNA

PEG – Polyethylene glycol

PEG2000 – 1,2-dipalmitoyl-sn-glycero-3-phospho ethanolamine-N-[methoxy(polyethylene glycol)-2000] (ammonium salt)

TBP – gene for the TATA box binding protein

TF – thin film

REV – reverse phase xivaporation

RNAi – RNA interference

siRNA – short interfering RNA

YWHAZ – gene for the tyrosine 3-monooxygenase/tryptophan 5-monooxygenase activation protein

Chapter 1 Peptide Functionalized Nanoparticles for Nonviral Gene Delivery

Introduction

Gene therapy has the potential to treat a myriad of diseases currently in need of improved therapies. Though viruses were evolutionarily designed to transfer their genetic information into foreign cells with various tissue tropisms and highly efficient genetic transfer, their use as vehicles for therapeutic gene delivery is limited by their minimal DNA cargo capacity,[1] immunogenic concerns,[2,3] and insertional mutagenic potential[4,5] with possible oncogenic effects. The development of nonviral vectors with virus-like traits of efficient transfection and specific delivery that still minimize viral disadvantages remains a challenge to effective gene delivery. Nonviral vectors are often easier to manufacture, can encapsulate much larger DNA loads and avoid the dangerous immune responses associated with viral vectors[6–10] but lack the high transduction efficiency of viruses. Many different materials and constructs have been investigated as synthetic gene delivery vehicles: Cationic polymers and lipids such as polyethyleneimine (PEI) and 1,2-di-(9Z-octadecenoyl)-3-trimethylammonium-propane (DOTAP), natural molecules like poly-L-Lysine (pLL), albumin and chitosan, and complex structures such as dendrimers have all been used as nucleic acid vectors. The nonviral vectors discussed in this review are included in Figure 1. Functionalization with polyethylene glycol (PEG) for stealth capabilities, cell penetrating peptides for increased uptake, polycationic peptides and lipids for endosomal escape, nuclear localization signals, and antibodies and peptides for targeting have been used to augment the function of these vectors.[7,11–17] The focus of this review is on efforts within the last ten years to target gene delivery vehicles using peptides, both carefully designed biomimetic peptides and peptides identified through library screening. The target, method of discovery, disease application and sequence of each peptide explored is listed in Table 1.

Peptide targeted gene delivery and expression within a cell follows the general pathway outlined in Figure 2. Once the vector comes in contact with its target cell, the peptide can bind to its specific receptor. The receptor bound peptide and its gene vector will then enter the cell through receptor mediated endocytosis, placing the delivery vehicle within an endosome or other intracellular vesicle. The specific intracellular trafficking of the vehicle depends on the mechanism of endocytosis: Clathrin-mediated, caveolae-mediated or clathrin- and caveolae-independent endocytosis.[10,18] The nucleic acid and its vehicle will then escape the vesicle with a mechanism that

depends on the vector composition. If the genetic cargo is siRNA, once it is released into the cytosol it will interact with RNA interference enzymes to downregulate its target gene. If the genetic cargo is DNA, it will need to enter the nucleus where it can be transcribed into mRNA.[18,19] Since receptor binding of the peptide ligand is the first step in the gene delivery vehicle pathway, it is obvious that the target receptor must be chosen carefully, and the proper peptide must be paired with an efficient delivery vector. The receptor should be specific to the cell type being targeted for delivery and should be naturally internalized within the cell. The gene delivery vehicle has to be stable enough to reach the target cells and may possess endosome- or vesicle- escape abilities. An efficient delivery vehicle combined with a highly specific receptor-ligand pair can mediate successful targeting and delivery of a nucleic acid cargo. The ability to target the systemic delivery of nucleic acids, or any drug, can minimize side effects, maximize treatment to the target site and allow for more flexibility in dosing limits.

Peptides are ideal as *in vivo* targeting molecules because they are small with low toxicity and immunogenicity, can be selected for high affinity and specificity for their targets and are easily produced and chemically modified.[20,21] Targeting peptides for a particular receptor can be designed using knowledge of the natural ligand's binding site, sequence, and secondary structure to create a biomimetic peptide, or by screening of a large peptide library using phage display. Combining high affinity, high specificity peptide ligands with effective nonviral vectors that target disease tissue and avoid healthy tissue has the potential to make gene therapy a reality for cancer, cystic fibrosis, neurodegenerative diseases and an unlimited number of other pathologies.

Peptide Targeted Cancer Gene Therapy

The development of malignant cancer requires multiple aberrant genetic events, some of which include the mutation and subsequent inactivation of tumor suppressor genes and proteins whose normal function is to regulate cell growth and correctly initiate apoptosis.[22] One possible treatment, therefore, lies in the restoration of the functional tumor suppressor gene through gene therapy. p53, for example, is a cell cycle regulatory protein that is frequently mutated in human cancers resulting in a loss of its tumor suppression function. The successful transfection of this gene in ovarian cancer patients has caused upregulation of p53 and other enzymes downstream from p53.[23] Another common cancer genetic event comes from a mutation that causes the overexpression or overactivation of an oncogene, which then facilitates uncontrolled proliferation and cell survival. One such oncogene commonly mutated in cancers, K-Ras, has been targeted for inhibition using siRNA. RNA interference effectively inhibits the expression of the mutant protein and limits cell tumorigenicity.[24] RNA interference can be used to inhibit other oncogenes such as

the anti-apoptosis gene livin, and cyclin-E.[25] Prodrug activation is another potential cancer gene therapy application. Prodrug activation involves expressing an exogenous enzyme within the target tissue that can convert a systemically delivered nontoxic prodrug into a potent anti-tumor drug. An example of an enzyme-prodrug combination is the pair herpes simplex virus (HSV) thymidine kinase and phosphorylated gancyclovir. If gancyclovir is administered to a cell which has been transfected to express HSV thymidine kinase, the thymidine kinase will phosphorylate the gancyclovir converting it to a DNA synthesis inhibitor.[26] Some of the other enzyme-prodrug pairs that have been suggested and tested for therapeutic efficacy include another DNA synthesis inhibitor cytosine deaminase and 5-Fluorouracil, and the DNA cross-linking agents nitroreductase and CB1954, and CYP and cyclophosphamide.[26,27] The delivery of anti-angiogenic gene therapy also holds potential for tumor therapy by depriving tumors of necessary blood supply.[28] While several of these gene therapy schemes have shown promise preclinically and in clinical trials, much of their success is limited by low transfection and the insufficient ability to target tumor tissue.[29,30] Peptide targeted gene therapy could potentially resolve some of these clinical limitations.

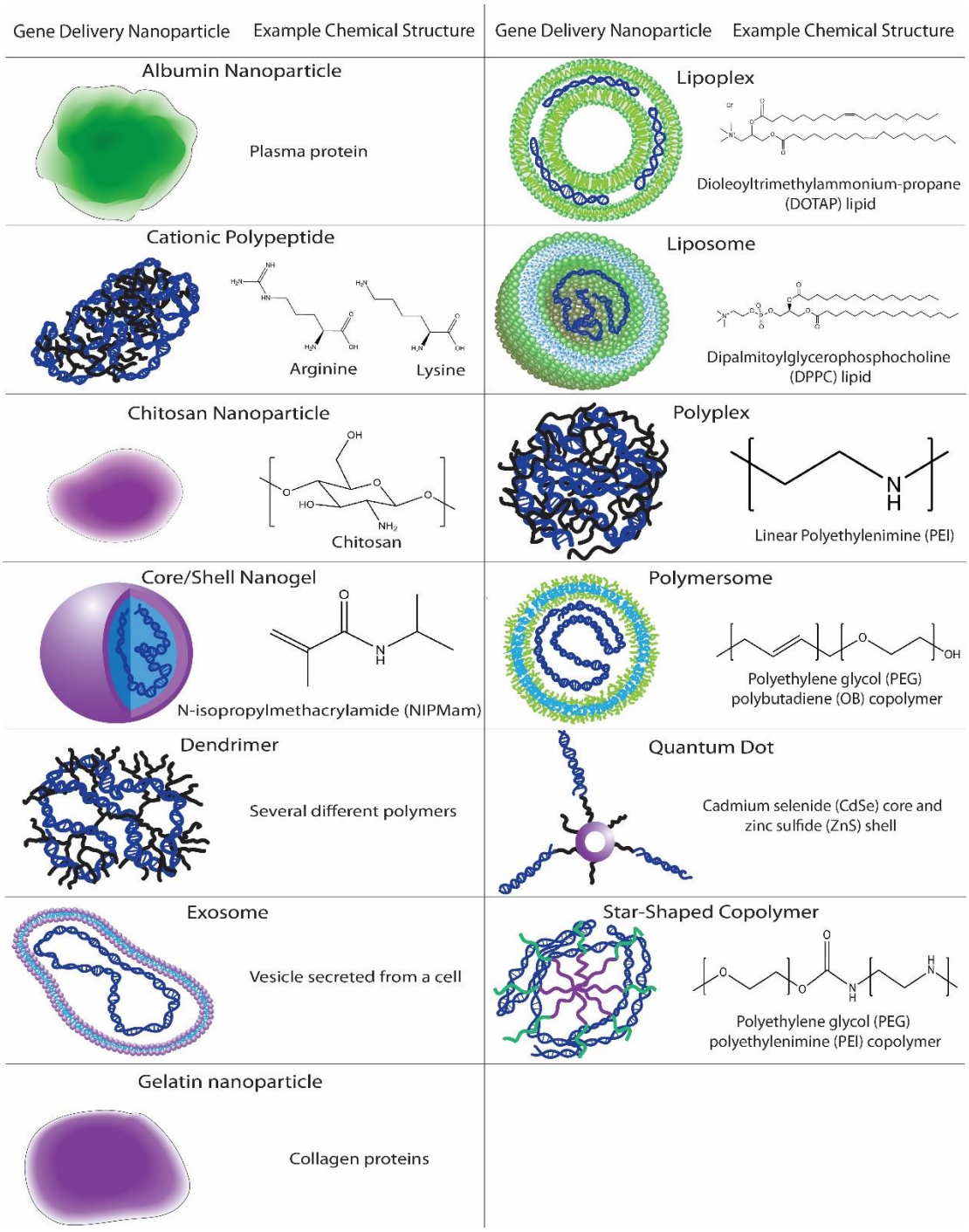

Figure 1. Structures of nanoparticles used for peptide targeted gene delivery.
Adapted with permission from (84, 17, 93). Copyright (2009, 2007) American Chemical Society, Copyright (2004), from Elsevier.

Table 1. Peptide Targeted Gene Delivery Vehicles

Name	Peptide Sequence	Application	Nanoparticle	Molecular Target	Peptide Density	Discovery Method	Reference
MC11	MQLPLAT	cancer	lipoplex, pLL, star-shaped copolymer, PEI	FGFR	2.5 – 10[a] 7-10[b]	phage display	31, 33, 35
GE11	YHWYGYTPQNVI	cancer	PEI, gel-based	EGFR	30 – 50[a]	phage display	38-40
RGD	RGDSPASSKP	cancer	poly(amidoamine) polyplex	$\alpha_v\beta_3$ integrin	19[c]	biomimetic*	47
RGD	cRGDfK	cancer	albumin, pLL, silsesquioxane dendrimer, lipoplex, chitosan	$\alpha_v\beta_3$ integrin	2 – 500[b]	phage display	12, 49, 50, 52, 53
RGD4C	ACDCRGDCFC	cancer	pLL, polycaprolactone polyplex, PEI, lipid protamine lipoplex	$\alpha_v\beta_3$ integrin	5 – 20[a] 1 – 20[b]	biomimetic	11, 56-58, 60-63
	GACRRETAWACG	cancer	pLL	$\alpha_5\beta_1$ integrin	50[a]	phage display	65
PR-b	KSSPHSRN$(SG)_5$RGDSP	cancer	Polymersome, liposome	$\alpha_5\beta_1$ integrin	0.7 – 6.9[a]	biomimetic	77, 78
SIG	SIGYPLPGGGSK$_{16}$	cancer	pHPMA coated pLL	angiogenic vessels	-	phage display	59
	APRPG	cancer	PEI	angiogenic vessels	15.86[c]	phage display	82
YSA	YSAYPDSVPMMS	cancer	core/shell nanogel	EphA2	225[b]	phage display	84, 85
F3	AKVKDEPQRRSARLSAKPAPPKPEPKPKKAPAKK	cancer	quantum dots	nucleolin	20[b]	phage display	93
NGR	GNGRGGVRSSSRTPSDKYC	cancer	lipid protamine lipoplex	aminopeptidase/ CD13	-	phage display	96
B6	CGHKAKGPRK	cancer	PEI	transferrin	50 – 70[a]	phage display	8
PF4zip	CGGRMKQLEDKVKKLLKKNYHLENEVARLKKLVG	cancer	star-shaped PEG polyplex	heparin	-	biomimetic	104

***Biomimetic peptides are those developed through rational design mimicking the function of or selecting specific peptide sequences from the target's natural ligand protein.**

Peptide densities reported as [a] mole percent, [b] peptides per nanoparticle, or [c] peptides per PEI molecule.

Name	Peptide Sequence	Application	Nanoparticle	Molecular Target	Peptide Density	Discovery Method	Reference
HIP	CRPKAKAKAKAKDQTK	cancer	star-shaped PEG polyplex	heparin	-	biomimetic	104
LHRH	(pyroE)-HWSY-(dK)-LRP(amide)	cancer	PEI	LHRH	-	biomimetic	108, 109
NL4	CTTTHTFVKALTMDGKQAAWRFIRIDTAC	neurological disease	pLL, PEI	TrkA	100[a]	biomimetic	117, 118
Leptin30	YQQVLTSLPSQNVLQIANDLENLRDLLHLL	neurological disease	pLL dendrimers	leptin receptor	100[a]	biomimetic	119, 120
RVG	YTIWMPENPRPGTPCDIFTNSRGKRASNG	neurological disease	exosomes, polypeptide	AchR	-	biomimetic	126-129
Tet1	HLNILSTLWKYRC	neurological disease	PEI	trisialoganglioside	0.6[c]	phage display	132, 133
NT	Pyr-LYENKPRRPYIL	neurological disease	PEI	neurotensin receptor	8.2[c]	biomimetic	132
HC	AA 408-859 of tetanus toxin heavy chain	neurological disease	PEI	trisialoganglioside	5 – 25[a]	biomimetic	134
Secretin	HSDGTFTSELSRLRDSARLQRLLQGLVGGC	cystic fibrosis	PEI	secretin receptor	-	biomimetic	140
Tenascin	PLAEIDGIELA	cystic fibrosis	lipoplex	$\alpha_9\beta_1$ integrin	0.05 – 5[a]	biomimetic/ phage display	144
Peptide Y	GACYGLPHKFCG	cystic fibrosis	lipoplex	human airway epithelial cells	4[b]	phage display	145, 146
Peptide E	SERSMNF	cystic fibrosis	lipoplex	human airway epithelial cells, ICAM-1	2,750[b]	phage display	147
Molossin	ICRRARGDNPNNRCT	corneal disorder	pLL	$\alpha_v\beta_3$ and $\alpha_5\beta_1$ integrins	-	biomimetic	154
CAP	DWRVIIPPRPSA	osteoarthritis	PEI	rabbit cartilage	4.86[a]	phage display	157
LAB	NSMIAHNKTRMHGGGSC	bone regeneration	poly(amidoamine) dendrimers	bone tissue	2 – 4[b]	phage display	156
HAB	SGHQLLLNKMPNGGGC	bone regeneration	poly(amidoamine) dendrimers	bone tissue	2 – 8[b]	phage display	156
NGR	GNGRGGVRSSSRTPSDKYC	DNA vaccination	PLGA coated PEI	aminopeptidase/ CD13	10[c]	phage display	160

***Biomimetic peptides are those developed through rational design mimicking the function of or selecting specific peptide sequences from the target's natural ligand protein.**

Peptide densities reported as [a] mole percent, [b] peptides per nanoparticle, or [c] peptides per PEI molecule.

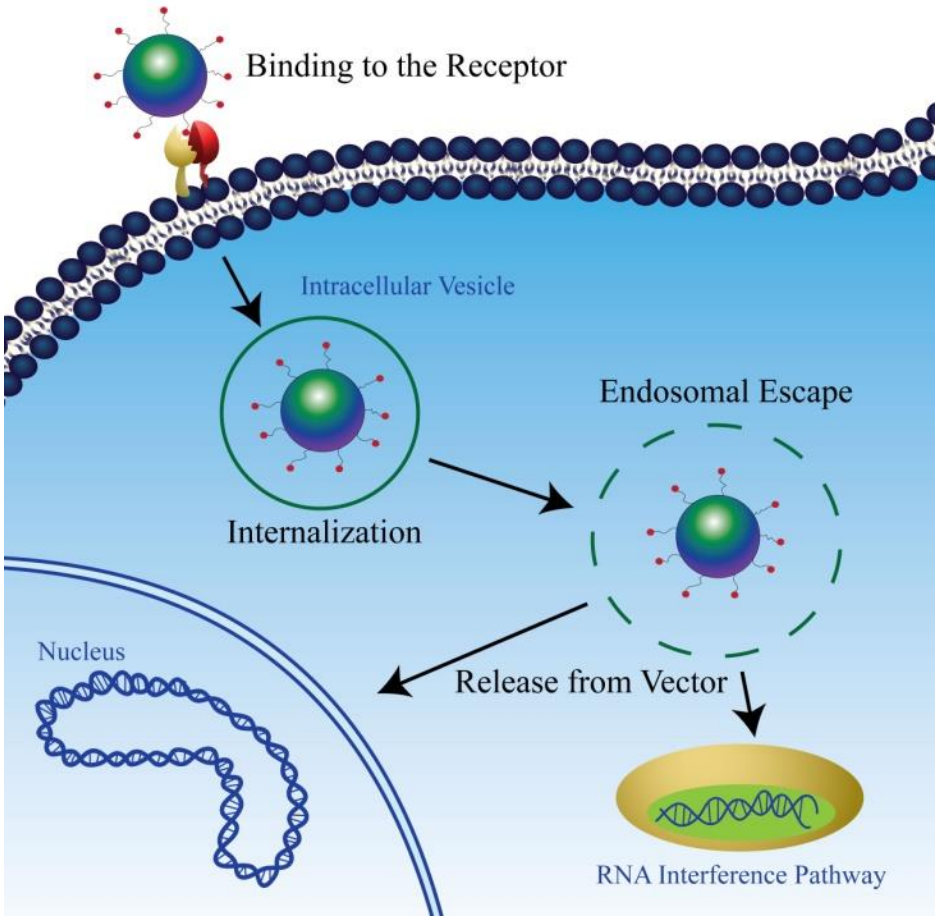

Figure 2. General pathway of cell binding, entry, and gene expression for peptide targeted gene delivery.

Gene Delivery with Peptides Targeting Growth Factors

One approach to targeted gene delivery for the treatment of cancer takes advantage of elevated levels of growth factor receptor expression in tumors and tumor vasculature. For example, fibroblast growth factor receptors (FGFR) have been shown to be overexpressed in various cancer cells, including breast, colon, ovarian, renal, and lung carcinomas,[31] as well as on proliferating endothelial cells during angiogenesis. Fibroblast growth factor (FGF) is a known mitogen which stimulates cell division when bound to FGFR. FGFR is a promising target for delivery of therapeutic agents to cancerous cells and tumors where angiogenic vessels grow rapidly to feed the surrounding tumor tissue; yet the size, stability, and mitogenic effects of FGF are not ideal for nanoparticle functionalization.[32] In the hope of avoiding these mitogenic effects within an FGFR targeting molecule, Seymour et al identified a linear FGFR binding peptide, MQLPLAT, via phage display and biopanning against cells expressing FGFR.[33] Phage display and biopanning are techniques used to study peptide-substrate interactions and select for peptides bound to a specific target using affinity selection. Briefly, random peptide libraries are fused to a phage protein coat,

these peptide displaying phages are incubated with cells expressing FGFR, and unbound phages are removed with a wash. Addition of FGF allows FGFR specific phages to be eluted, cloned, and sequenced. The most successful peptide sequence, MQLPLAT, was also delivered on phages to an *ex vivo* human tumor model to confirm tumor specificity and was found to preferentially accumulate in tumor tissue over healthy tissue.[33]

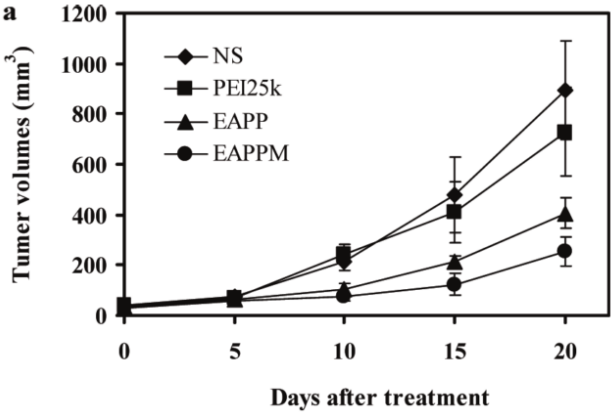

Figure 3. *In vivo* tumor therapy using FGFR targeted star-shaped polymers.
Tumor growth profile after injection of therapeutic plasmid complexed with PEI25k, EAPP (nontargeted star-shaped polymer) and EAPPM (targeted star-shaped polymer) or NS (normal saline) via tail vein. Reprinted with permission from (35). Copyright (2010) American Chemical Society.

The identified peptide was found to be non-mitogenic and has been shown to improve cellular uptake and transfection efficiency when conjugated to PEGylated-PEI polyplexes, or polymer-DNA complexes.[34] PEI is an extremely common, extremely successful polycationic transfection agent. The high transfection efficiency of PEI has been attributed to its ability to escape from vesicles mediated by its 'proton sponge effect'. When PEI is encapsulated within an intracellular vesicle with low pH, the high concentration of amines present within its structure lead to buffering which causes an influx of ions and subsequent osmotic swelling and vesicle rupture.[35]

Niu et al used the FGFR specific, phage display identified peptide to target a glioma mouse model for delivery of plasmid DNA. The plasmid was carefully designed to include a cytotoxic domain to induce cell apoptosis and membrane permeability and secretory domains to encourage the expressed protein to travel intercellularly, also known as the bystander effect. The targeting peptide was attached at the end of the PEG stealth functionalized lipid based delivery agent. The *in vitro* results indicated a 2 fold increase in plasmid expression and a 3 fold improvement in cell death achieved with the cytotoxic designed plasmid compared to delivery with nontargeted lipoplexes. However, the targeted lipoplexes provided no statistical improvement to tumor growth inhibition *in vivo* compared to the nontargeted lipoplexes, and biodistribution was not investigated.[32]

Li et al modified the same peptide sequence, MQLPLAT, to include a spacer sequence, GGGC,

for conjugation to PEI and to improve peptide accessibility on the nanoparticle surface.[36] This peptide was attached to the end of an eight armed block copolymer of PEG for stealth properties and PEI for DNA condensation. The star copolymer was designed to effectively deliver DNA while minimizing the toxicity usually associated with PEI. When these targeted polyplexes were delivered to FGFR positive cells, they achieved a 10 fold increase in expression over nontargeted star polyplexes, and 100 fold increase compared to nonPEGylated PEI polyplexes. *In vivo* biodistribution measured in the tumor, lung and liver of a mouse liver carcinoma model showed much higher transfection in tumor cells with the targeted star copolymers compared to nontargeted delivery agents and compared to the other tissues. When the load included a cytotoxic gene, tumor growth inhibition was observed with the targeted polyplexes. The tumors in the mice receiving targeted polyplex gene therapy were only a quarter of the size of those treated with PEI polyplexes as shown in the tumor growth profile in Figure 3.

Overexpression of epidermal growth factor receptors has also been identified to play a role in several types of cancer. Of the four EGFR family members, HER1 and HER2 have recently been targeted for gene delivery using peptide ligands. Both receptors are frequently overexpressed in several common human cancers, and HER2 is associated with particularly aggressive tumors and poor prognosis. HER1 has several known native ligands, while HER2 has no known native ligands, but participates in EGFR activation.[37,38] A HER1 specific peptide, GE11 (YHWYGYTPQ NVI), was identified via *in vitro* phage display and biopanning against purified HER1.[39] The binding affinity and specificity of the GE11 peptide were quantified *in vitro* and *in vivo* using ^{125}I labeled peptides. Intravenous delivery of GE11 peptide showed that 6% of the peptide accumulated in tumor tissue 30 minutes after injection and that co-injection of unlabeled GE11 peptide resulted in an almost threefold decrease in accumulation in the tumor. Four hours after injection GE11 accumulation was limited to the tumor and the blood, each with about 3% accumulation. The K_d of GE11 for EGFR was found to be 22 nM, 10 times less than that of native EGF; yet GE11 was found to be 5 times less mitogenically stimulative than EGF. This GE11 peptide has been used to improve targeted gene delivery in applications including prostate and pancreatic cancer and has demonstrated superior mitogenicity and binding to cancer cells compared to several other designed and discovered EGFR peptide ligands.[39–41] The GE11 peptide was conjugated to gel-based engineered nanocarrier systems (GENS), which can encapsulate and protect plasmid DNA, while preserving its natural supercoiled structure. When delivered to a pancreatic cancer cell line, these EGFR targeted gene delivery vehicles achieved 48% transfection efficiency, better than both a commercial transfection agent and nontargeted GENS.[41] When conjugated to PEI for condensation with DNA, the GE11 peptide achieved up to a 10 fold increase in transfection efficiency *in vitro*

with EGFR positive cells.[39,40] These targeted PEI polyplexes have up to 1000 fold higher transfection efficiency compared to nontargeted polyplexes when delivered to tumor mouse models either intratumorally or intravenously. Biodistribution of the expression of the delivered plasmid shows that the agents preferentially accumulate in the tumor compared to 7 other organs, including liver.[39,40]

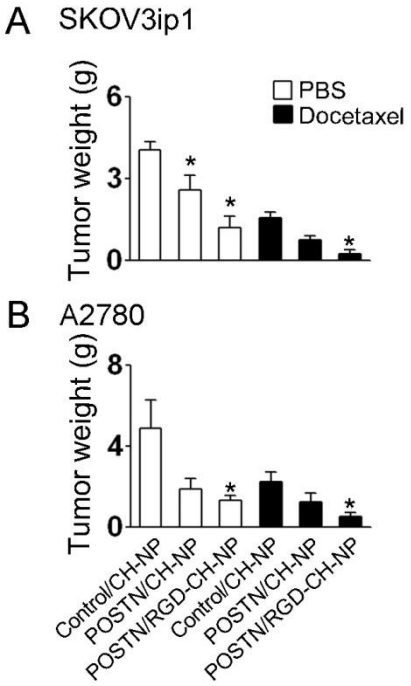

Figure 4. Effect of chitosan nanoparticles on ovarian cancer growth.
Treatment was started 1 week after intraperitoneal (I.P.) injection of tumor cells into mice. A) Integrin positive cell line (SKOV3ip1). B) integrin negative cell line (A2780). Either control or POSTN-targeted siRNA-incorporated into nontargeted (CH-NP) or targeted (RGD-CH-NP) was given twice weekly at a dose of 150 μg/kg body weight through intravenous injection. Docetaxel was diluted in PBS and injected i.p. once per week, at a dose of 100 μg, in 200 μL of PBS. Treatment was continued until mice in any group became moribund (typically 4 to 5 weeks depending on tumor cell) Reprinted with Permission from (54). Copyright (2010) American Association for Cancer Research.

Gene Delivery with Peptides Targeting Integrins

The $\alpha_v\beta_3$, $\alpha_v\beta_5$, and the $\alpha_5\beta_1$ integrins are promising targets for specific delivery of cancer therapeutics. Expression of these integrins is upregulated in many tumor cells and tumor endothelium. The $\alpha_v\beta_3$ and $\alpha_v\beta_5$ integrins bind vitronectin and the $\alpha_5\beta_1$ integrin specifically binds fibronectin. The RGD motif is found in many components of the extracellular matrix, including fibronectin, vitronectin, laminin, and collagen, and has been found to facilitate cell adhesion and nanoparticle delivery. The motif is also found in the penton base, the protein that forms the vertex of the capsid of adenovirus, where it is known to bind to the $\alpha_v\beta_3$ integrin.[11] The RGD peptide has

been used to functionalize PEI, PEI-PEG conjugates, gold nanoparticles, magnetic nanoparticles for combined molecular imaging, poly-L-lysine and many other vector molecules for improved specific *in vitro* uptake and transfection of genetic material.[42–45] The RGD containing peptides RGDSPASSKP and GRGDSP were identified as conserved sequences within the cell binding region of fibronectin, and their integrin binding affinity and specificity were suggested by their ability to reversibly inhibit fibronectin-mediated cell spreading.[46,47] The RGDSPASSKP peptide was used to functionalize PEG polyamidoamine DNA nanoparticles for integrin targeting, but did not show any improvement to plasmid transfection to A549 or 3T3 cells with the conjugation of the RGD peptide to their polyplexes, which was suggested to be caused by poor release of the DNA after internalization.[48]

While some groups have successfully enhanced gene delivery via functionalization with the linear RGD sequence, others have investigated the effect of a constrained secondary structure in cyclic forms of RGD on targeted gene delivery.[12] In particular, the effect of additional amino acids on the conformation, activity, and affinity of cyclic RGD pentapeptides of the form RGDXY was investigated, where X and Y represent both L- and D- natural and non-natural amino acids. This study found that the c(RGDfK) sequence maintained a higher affinity for the $\alpha_v\beta_3$ integrin compared to linear RGD containing sequences.[49]

c(RGDfK) targeted silsesquoxane dendrimers delivering siRNA achieved 50% gene silencing.[50] c(RGDfK) conjugated to a PEG molecule attached to albumin was used to deliver antisense oligonucleotides attached to the surface of the albumin to a cell line derived from lung metastases.[51] The antisense oligonucleotide induced expression of luciferase by correction of incorrect splicing sites.[52] The targeted albumin oligonucleotide vector induces high levels of luciferase expression compared to nontargeted PEGylated albumin, and expression was comparable to that achieved by delivering the oligonucleotides with lipofectamine.[53] Kunath et al found that the transfection efficiency of DNA delivery strongly depended on the ratio of the PEI-RGD vector to DNA concentration. The dependence of transfection efficiency on the amount of PEI-RGD could either be caused by increased integrin targeting with RGD or increased endosomal escape induced by PEI, or a combination of these effects.[54] DNA vectors formed from c(RGDfK) conjugated to cationic convertible detergent lipids with DOPE for endosomal escape still required the addition of chloroquine, a lysosomotropic agent, in the media to achieve 1000 times lower transfection levels than PEI *in vitro.*[12]

c(RGDfK) functionalized chitosan nanoparticles with encapsulated siRNA targeting the oncogene POSTN were delivered to mice with tumors produced from ovarian cancer cells positive for $\alpha_v\beta_3$ integrin expression. Targeting the chitosan nanoparticles resulted in negligible delivery to

the brain, heart, lung, spleen, kidney and liver compared to nontargeted nanoparticles, and a 50% reduction in POSTN expression in the tumor tissue. These targeted vectors resulted in 71% reduction in tumor weight compared to control siRNA and 24% reduction compared to nontargeted siRNA nanoparticles (Figure 4). Tumor weight was furthered reduced when delivered with docetaxol.[55] Similar results were seen with siRNA targeting the oncogene FAK, where tissue specificity and therapeutic efficacy of RGD-functionalized chitosan nanoparticles for siRNA delivery were demonstrated.[55]

Other cyclic RGD-containing peptides targeting the $\alpha_v\beta_3$ integrin have been developed using a combination of rational biomimetic design and phage display techniques. The RGD4C peptide (ACDCRGDCFC) was identified via phage display of a random peptide library in which sequences were flanked with cysteines on either end (CX_5C, CX_6C, CX_7C, and CX_9C).[56] The RGD4C peptide contains two disulfide bonds and was found to inhibit cell attachment to vitronectin surfaces 20 fold, indicating that the peptide binds to the $\alpha_v\beta_3$ and $\alpha_v\beta_5$ integrins in a way that blocks vitronectin binding.[56,57] Despite the effective integrin blocking, the disulfide bonds present in the RGD4C peptide increased the hydrophobicity of the molecule, causing poor solubility in aqueous systems. Additionally, these disulfide bonds have the potential to form improper crosslinks yielding inactive peptides. These features made incorporating functional RGD4C peptides into targeted delivery systems more challenging due to the limited solubility and activity of the peptide.

Linear and cyclic structures of RGD4C inspired peptides with one or two disulfide bonds were investigated to address the necessity of the potentially problematic disulfide linkages. Methionine was substituted for cysteine as shown in Figure 5, and the CDMRGDMFC peptide-functionalized lipoplexes gave promising results compared to the CDCRGDCFC peptide-functionalized lipoplexes. [57,58]

Figure 5. RGD4C and modified RGD4C analogs with disulfide bonds between indicated cysteine residues.

The RGD4C peptide was modified to include a positively charged pLL tail to facilitate the condensation of negatively charged DNA resulting in 100 times greater transfection than nontargeted pLL condensed DNA.[59,60] Other groups have addressed the poor solubility of the RGD4C peptide in aqueous environments by conjugating a PEG spacer to the N-terminus tail of

the peptide to improve the physicochemical properties of the DNA containing polyplex and to reduce the surface charge.[11,61,62] This RGD4C modification to target PEG-polycaprolactone polyplexes, combined with a cell penetrating peptide derived from HIV termed TAT, only achieved a level of transfection that was comparable to a commercially available transfection reagent, however, PEG-RGD4C conjugated to PEI in DNA polyplexes caused significant improvement in gene delivery both *in vitro* and *in vivo*.[11,61–63] Anti-VEGF siRNA delivered *in vivo* with targeted RGD4C-PEG-PEI significantly inhibited tumor growth compared to all controls, as measured by tumor volume of sub-cutaneous tumors established from CT26 cell inoculation.[61] The moderate transfection levels achieved with the targeted PEG-polycaprolactone vectors could be caused by the lack of endosomal escape function, which is probably achieved by the other polyplex systems with the presence of PEI. Kim et al investigated the specificity of PEI-PEG-RGD4C with gene delivery to angiogenic and angiostatic endothelial cells, modelling tumor vasculature compared to healthy vasculature. The RGD4C targeted polyplexes improved transfection in angiogenic cells compared to PEI and inhibited transfection in angiostatic cells, indicating a strong *in vivo* targeting potential to the rapidly proliferating tumor vasculature.[64]

The $\alpha_5\beta_1$ integrin, like the $\alpha_v\beta_3$ integrin, is overexpressed on tumor and tumor endothelial cells. Unlike $\alpha_v\beta_3$, which is expressed on platelets, macrophages and endothelial cells throughout adulthood, the expression of $\alpha_5\beta_1$ decreases during development and is expressed at low levels in healthy adult cells.[65] The decreased expression of the $\alpha_5\beta_1$ integrin in healthy cells and tissues makes it a potentially more selective target for the delivery of cancer therapeutics. Ruoslahti et al performed extensive integrin affinity studies using phage display and biopanning of RGD-containing ligands and identified an $\alpha_5\beta_1$-specific peptide (GACRRETAWACG).[56] Hart et al modified this $\alpha_5\beta_1$-specific peptide with a pLL tail for complexation with plasmid DNA and significantly improved transfection efficiency.[66]

The Kokkoli group has designed a fibronectin mimetic peptide,[67] PR_b (KSSPHSRN$(SG)_5$RGDSP), with high affinity and specificity for the $\alpha_5\beta_1$ integrin, and has conjugated it to a dialkyl ester tail, shown in Figure 6, or to diblock polymers.[67–69] The peptide was designed to include both the primary cell adhesion site (RGDSP) and the synergy site (PHSRN) as well as a linker ($(SG)_5$) that mimics both the length and hydrophobicity/ hydrophilicity of the distance between binding sites in the native fibronectin protein.[67,70,71] PR_b functionalized liposomes and polymersomes have shown enhanced binding, intracellular uptake, and delivery of their encapsulated loads compared to non targeted and GRGDSP-functionalized nanoparticles delivered to colon, prostate, and breast cancer cells, and porcine islets of Langerhans, as well as the capability to deliver a wide variety of therapeutic cargoes including siRNA.[69,72–78] PEGylated PR_b

liposomes and polymersomes internalized via receptor-mediated endocytosis and were initially found in early endosomes, but localized within late endosomes and lysosomes at later times.[77,78] PR_b has been used to functionalize both liposomes and polymersomes for delivery of DNA and siRNA for cancer therapy.[78,79] PR_b functionalized stealth liposomes encapsulating condensed plasmid DNA mediated improved transfection compared to nontargeted stealth liposomes and free condensed DNA, specifically in colon cancer cells overexpressing the $\alpha_5\beta_1$ integrin *in vitro*. Furthermore, when administered *in vivo* to metastatic tumor bearing mice, imaging showed that PR_b functionalized stealth liposomes outperformed nontargeted liposomes and delivered genes specifically to the tumor site, thereby distinguishing between healthy and tumor sites on the liver.[79]

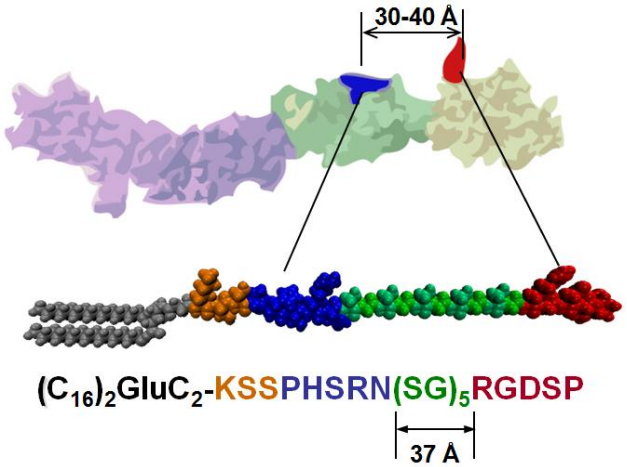

Figure 6. The PR_b peptide is a fibronectin mimetic specific for the $\alpha_5\beta_1$ integrin.
The four repeats of the fibronectin (FN) fragment III7–10 are shown. The synergy site PHSRN is in the III9 repeat and RGDSP is in the III10. The schematic drawing of the PR_b peptide-amphiphile shows the four building blocks of the peptide headgroup (a KSS spacer, the PHSRN synergy site, a $(SG)_5$ linker, and the RGDSP binding site) as well as the dialkyl ester tail ($(C_{16})_2GluC_2$). Reproduced with permission from (19). Copyright (2012) John Wiley and Sons.

Gene Delivery with Peptide Targeting to Other Receptors

Tumor vascular cells grow and divide more rapidly than most healthy vasculature, and changes in the expression of cell surface molecules and receptors have been characterized for many cancer types and tumor vasculature. Targeting the delivery of therapeutic nanoparticles to tumor vasculature attempts to utilize these biological and molecular differences to achieve improved specificity in delivery. Nicklin et al used phage display and biopanning methods to identify a peptide, SIG (SIGYPLP), which specifically binds proliferating endothelial cells. Four rounds of biopanning against human umbilical vein endothelial cells (HUVECs) were followed by counter selection or preclearing steps to remove all phages which bound vascular smooth muscle cells, hepatocytes, or peripheral blood mononuclear cells.[80] The identified sequence was originally used

for applications to treat atherosclerosis, hypertension, and postangioplasty restenosis. Parker et al used the SIG peptide as a more generally applicable target for cancer treatments, targeting angiogenic vessels rather than tumor specific cell markers. By modifying the SIG peptide with a GGGS spacer sequence to mimic the phage stalk and a pLL tail to facilitate DNA condensation ($SIGYPLPGGGSK_{16}$), the peptide was incorporated into poly[N-(2-hydroxypropyl) methacrylamide] (pHPMA) coated pLL polyplexes.[60] The SIG-labeled pHPMA coating of these polyplexes facilitated serum stability without compromise of transfection efficiencies. These HUVEC targeted polyplexes achieved up to a 2 fold increase in uptake in endothelial cells compared to epithelial cells, however, this uptake was lower or comparable to that achieved with RGD functionalized polyplexes. While significant uptake was seen in endothelial cells, little transfection was achieved, which was attributed to the slow cell division rate of these cells. High transfection efficiency was achieved in epithelial cells, but efficiencies higher than RGD mediated gene delivery were only achieved with addition of chloroquine to the media. The investigators then used the SIG peptide to alter adenovirus tropism for DNA delivery.[60]

Recently, a short peptide sequence homing to angiogenic vasculature (APRPG) has been identified using an angiogenic mouse model for *in vivo* phage display.[81] The APRPG peptide selectively binds to angiogenic vessels and not to tumor cells, making it a potential candidate for tumor dormancy therapy, in which the angiogenic vessels feeding the tumor are destroyed via targeted delivery to tumor vasculature.[82] This vessel homing peptide was used to target stealth siRNA PEI polyplexes for downregulation of VEGF and inhibition of vascular growth. The *in vitro* transfection efficiency using both targeted and nontargeted nanoparticles correlated with their internalization efficiency. The gene delivery vector was then used to deliver a fluorescent model molecule to mice with established tumors to investigate biodistribution. While much higher levels of delivery to the tumor were achieved with the APRPG vector than with the free molecule or with nontargeted vectors, higher levels of fluorescent protein were measured in the heart, kidney and liver than in the tumor with the targeted nanoparticles. Intratumoral protein expression and tumor growth was monitored after *in vivo* delivery of VEGF silencing siRNA complexed within APRPG functionalized polyplexes. The tumor growth inhibition and VEGF mRNA knockdown achieved with the targeted siRNA delivery was significant compared to the PBS treated control but showed no improvement over PEI complexed or free siRNA.[83]

The erythropoietin producing hepatocellular A2 (EphA2) receptor is a tyrosine kinase target whose expression is limited to activated adult blood vessels and several tumor cells, including breast, prostate, colon, skin, and esophageal cancers. The YSA peptide (YSAYPDSVPMMS), identified via phage display, is a functional mimetic of ephrin-A as it has been shown to bind to

its receptor, the EphA2 receptor, with a nanomolar K_d and to stimulate EphA2 receptor signaling.[84] Blackburn et al coupled the YSA peptide to the surface of poly(N-isopropylmethacryl amide) core/shell nanogels (nanogels with different polymer compositions within the core and the outer shell) to improve targeted delivery of siRNA to ovarian cancer cells.[85]

The targeted nanogels exhibited high siRNA encapsulation efficiencies and retention (66% after 36 hours in serum) and low cytotoxicity. When EGFR specific siRNA was encapsulated within the YSA functionalized nanogels and delivered to ovarian cancer cells, up to an 80% reduction in EGFR expression was achieved, and significant gene silencing was maintained for up to 120 hours. The specificity of the targeted nanogel was confirmed through delivery to EphA2 positive and negative cell lines, resulting in low delivery and gene silencing in EphA2 negative cells. Since EGFR expression has been found to be closely related to chemosensitivity in cancer cells, the effect of EGFR silencing on docetaxel induced cell death using the targeted nanogel encapsulated siRNA was investigated. An 8 fold increase in sensitivity to docetaxel induced cell death was observed with this targeted gene therapy, and controls performed with YSA peptide and with YSA-nanogels not loaded with siRNA caused a less significant increase in sensitivity. This could be caused by the interactions between the EphA2 receptor and EGFR.[85,86]

An N-terminal fragment of human high mobility group protein 2 (HMGN2) that selectively binds to both bonemarrow endothelial progenitor cells and tumor vasculature was identified via phage display of complimentary DNA libraries generated from mRNA using reverse transcriptase.[87] This peptide, designated the F3 peptide (AKVKDEPQRRSARLAKPAPPKPEPKPKKAPAKK), binds nucleolin expressed on the surface of rapidly growing tumor cells and vasculature. Nucleolin is a phosphoprotein which is localized in the nucleolus of cells and plays a role in control of ribosomal DNA transcription, ribosomal RNA maturation, and transport between the cytoplasm and nucleus. It has been shown that the amount of nucleolin is highly elevated in rapidly proliferating cells, such as cancerous cells and virus harboring cells.[88–91] More recently, it has been shown that nucleolin localizes on the cell surface in several cancer cell lines and that it acts as a receptor for cytokines and the HIV virus.[92] Cell surface nucleolin of cancerous cells readily binds and internalizes the F3 peptide trafficking it to the cell nucleus, making F3 an ideal targeting molecule for gene therapy applications.[93] Derfus et al utilized the F3 peptide to functionalize PEGylated quantum dots to deliver siRNA to HeLa cells, resulting in 30% knockdown in the target protein expression.[94]

Another tumor vasculature homing peptide was identified from *in vivo* phage display and termed the NGR peptide (GNGRGGVRSSSRTPSDKYC). The molecular target of this peptide was not known at the time, though the binding affinity of NGR to integrins was significantly lower than that of RGD-containing peptides.[95] The molecular target for the NGR peptide was later identified

as aminopeptidase N (also called CD13), a membrane protein expressed in endothelial cells and macrophages involved in chemokine processing and invasion. CD13 expression has been shown to be limited to tumor blood vessels and vasculature undergoing angiogenesis.[96] NGR functionalized LPD (lipid-polycation-DNA) nanoparticles have been shown to increase transfection efficiency and to decrease nonspecific accumulation in the liver, kidneys, and other organs indicating that the NGR peptide preferentially binds CD13 and is a promising homing peptide for angiogenic tumor vasculature.[97]

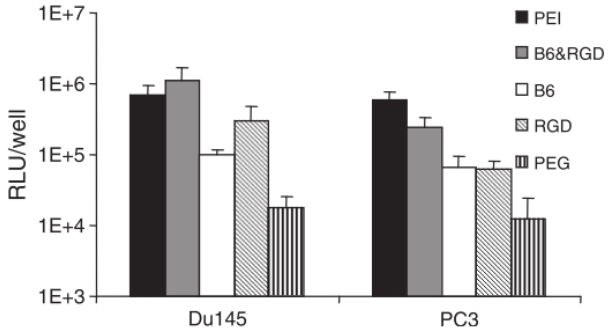

Figure 7. Transfection efficiency of dual ligand PEI polyplexes targeted to transferrin receptor and $\alpha_v\beta_3$. Transfection efficiency was measured by luciferase activity of B6- and RGD- dual targeted polyplexes (B6&RGD) vs. B6- or RGD- single targeted polyplex formulations and nontargeted (PEI) and nontargeted stealth (PEG) polyplex formations in DU145 (transferrin+ and integrin+) and PC3 (transferrin + and integrin -) cells. Reprinted from (8).Copyright (2011), with permission from Elsevier.

The rapid cell division characteristic of cancerous tumors leads to an increased metabolic demand; as a result of increased oxygen consumption, expression of transferrin receptors is often upregulated on tumor cells. The B6 peptide (CGHKAKGPRK) was identified via phage display and was able to bind to transferrin receptors with high affinity.[98] Nie et al created B6-RGD dual targeted PEI polyplexes for the delivery of siRNA to prostate cancer cells *in vivo*. The dual targeting was intended to improve transfection efficiency and specificity of delivery. It was observed that the B6 peptide mediated the majority of polyplex internalization while integrin mediated internalization via the RGD binding sequence played only a minor role in this system.[8] Dual targeting of DNA polyplexes improved their transfection efficiency almost 4 fold compared to the single ligand complexes and 60 fold compared to nontargeted complexes, in a prostate cancer cell line with high expression of both target molecules (Figure 7). The results of the competition and internalization assays performed suggested a synergistic targeting method, where the RGD peptide mediated cell association, and cell uptake occurred primarily through the B6-transferrin receptor interactions.

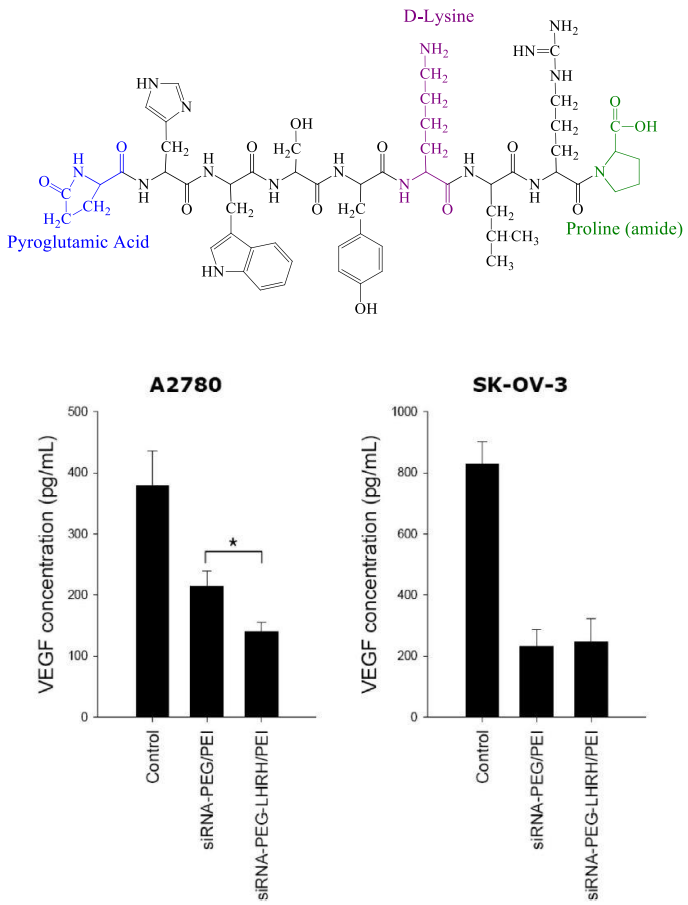

Figure 8. VEGF silencing from siRNA delivery using LHRHR targeted PEGylated polyplexes.
A) Modified LHRH peptide. Modifications are labeled and highlighted B) VEGF silencing in LHRHR positive (A2780) and LHRH negative (SK-OV-3) human ovarian carcinoma cells compared to untreated control. Cells were transfected with anti-VEGF siRNA in targeted (siRNA/PEG-LHRH/PEI) and nontargeted (siRNA-PEG/PEI) complexes. Reprinted with permission from (108). Copyright (2008) American Chemical Society.

Three heparin binding peptides previously identified in the literature to improve internalization and transfection efficiency of star-PEG polyplexes were investigated as potential ligands for gene delivery. By substituting the lysine residues of the heparin binding domain of platelet factor 4 (PF4) into the GCN4 leucine zipper, a peptide called $PF4_{zip}$ (CGGRMKQLEDKVKKLLKKN YHLENEVARLKKLVG) was produced that successfully reproduced the natural heparin binding affinity of PF4.[99–101] A heparin interacting peptide analogue, HIP (CRPKAKAKAKAKDQTK), was identified by analysis of sequence homology of mouse, rat, and human heparin binding proteins to deduce the functional heparin binding sequence.[102] The third peptide used was the K^{121}-A^{134} heparin binding segment of the antithrombin III protein and was designated ATIII (CK(βA)FAKLAARLY RKA).[103,104] Star-shaped PEG polyplexes functionalized with $PF4_{zip}$ and HIP were found to increase the heparin affinity and cellular internalization of the polyplexes compared to PEI, while functionalization with the ATIII peptide was found to be very cytotoxic to

hamster kidney cells (BHK-21).[105] The high internalization rates of the $PF4_{zip}$ and HIP targeted star PEG polyplexes did not mediate efficient transfection compared to PEI alone, suggesting that improving internalization does not necessarily augment transfection efficiency.

For some types of cancer, hormone receptors are promising targets for specific gene delivery. Luteinizing hormone releasing hormone (LHRH) receptors are expressed on breast, ovarian and prostate cancer cells but not expressed in healthy visceral organs. The activity of the native LHRH decapeptide is limited due to rapid degradation by potent enzymes present in the hypothalamus, the site of release, and the pituitary, the site of action.[106] These enzymes have been shown to preferentially cleave LHRH at the Gly^6-Leu^7 bond. To increase the potency of LHRH signalling a LHRH peptide analogue was developed, replacing the Gly^6 residue with a D-Lys residue to slow enzymatic degradation ((pyroE)HWSY(D-K)LRP(amide)) (Figure 8a).[107,108] This LHRH peptide has been used in targeted, PEGylated dendrimers and polyplexes for the delivery of siRNA. The presence of the LHRH peptide significantly increased the gene silencing abilities and the specificity of siRNA stealth nanoparticles to LHRH positive and negative cell lines (Figure 8b).[109,110]

Gene Therapy Targeted to the Central Nervous System for the Treatment of Neurological Diseases

While palliative treatments exist for many neurodegenerative diseases, including Parkinson's, Alzheimer's and Multiple Sclerosis, neural-targeted gene delivery offers the possibility of new curative treatments. Inducing the expression of enzymes found within the dopamine production pathway or delivering genes encoding glial cell line-derived neurotrophic factor has improved behavior in mouse models of Parkinson's[111–113] and the viral transduction of growth factors has been used for neuroprotection in a Huntington's disease model.[114] Neuronal transfection must overcome the additional challenges of crossing the blood brain barrier and internalizing and trafficking within polarized, morphologically elongated cells, challenges that could be solved with receptor-ligand targeting.[10] Several peptides which specifically bind neural cells with high affinity have been identified and used to improve targeted delivery of plasmid DNA and siRNA.

One approach to gene delivery for neurodegenerative diseases targets peptides to receptors specifically expressed in various brain cell types. Neuronal cells in the central nervous system (CNS) express the potential neural target, neurotrophic tyrosine kinase receptor (TrkA). Binding of nerve growth factor (NGF) to TrkA causes dimerization and autophosphorylation of the tyrosine residues in TrkA which results in a transduction of activation signaling.[115] Studies of the structure of NGF, including site-directed mutagenesis and crystal structure analysis, have identified several regions responsible for binding TrkA; the N-terminus, hairpin loop2, and loop4. Small peptide

mimetics of the loop4 region were explored as ligands for TrkA, and several have been shown to bind and activate TrkA and promote neurotrophic effects similar to NGF.[116,117] The cyclic 29 amino acid sequence of loop4 (C80-C108), termed NL4, was modified with a 10 Lysine (10K) tail to facilitate DNA binding and condensation. It was confirmed that the NL4 peptide maintained the biological function of NGF as well as its binding capabilities. The NL4-K10 complexed DNA delivered to TrkA positive cells achieved marked improvement in specific transfection, but only when delivered with an endosomolytic agent.[118] Condensation with PEI eliminated the need for the addition of an endosomolytic agent.[118,119]

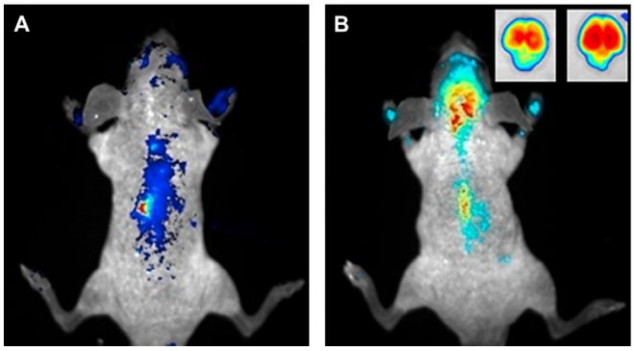

Figure 9. DNA delivery to the brain via leptin receptor targeted, PEGylated pLL polyplexes.
The *in vivo* distribution of labeled DNA intravenously administered and delivered within A) unPEGylated nontargeted nanoparticles and B) PEGylated nanoparticles functionalized with the leptin 30 peptide. Images were taken 80 min after injection. Reprinted from (120). Copyright (2010), with permission from Elsevier.

Another potential target for delivery to the nervous system is leptin, a 16 kDa hormone secreted by adipocytes, which is involved in regulation of appetite and metabolism through leptin receptor binding in the hypothalamus and other regions of the brain. The high molecular weight of leptin prevents its passive diffusion across the blood brain barrier. Thus, to explain leptin accumulation in the brain, leptin receptor mediated transport across the blood brain barrier is thought to be a possible mechanism of transport. Barret et al identified the leptin30 peptide, comprised of amino acids 61-90 in the native leptin protein, which specifically binds leptin receptors in the hypothalamus and brain with a higher affinity than other leptin derived peptides studied.[120] PEGylated pLL nanocarriers functionalized with the leptin30 peptide improved the transfection efficiency and specificity of delivery of plasmid DNA *in vitro* and *in vivo*.[121] Intravenous administration of leptin targeted DNA pLL dendrimers into mice resulted in significant delivery and transfection within the brain compared to nontargeted dendrimers (Figure 9). Protein expression measured in the brain of the mice that received leptin-targeted nanoparticles was twice that measured in the control mice. Biodistribution of the gene delivery vehicle was measured in major organs, showing that the extent of transfection was unaltered by the targeting peptide in liver

and spleen and was decreased in the kidney. High levels of transfection were measured in the heart with the delivery of unPEGylated, nontargeted nanoparticles but these levels were decreased with PEGylation and by the addition of the leptin30 peptide, indicating that the accumulation in the heart was caused by the DNA dendrimers.[121]

The neural acetylcholine receptor (AChR) has been targeted for gene delivery with the RVG peptide (YTIWMPENPRPGTPCDIFTNSRGKRASNG) derived from the native CNS specific rabies virus (RV) glycoprotein. The RV glycoprotein is responsible for cell attachment and internalization of the virus, and studies of infection progression have shown that the rabies virus localizes in regions containing high densities of acetylcholine receptors.[122,123] Neurotoxins from snakes are known to bind with high affinity to the nicotinic AChR, and homology studies have revealed conserved sequences and similarities between snake venoms and the RVG peptide.[124] Lentz et al showed that the RVG peptide sequence competitively and specifically bound to nicotinic acetylcholine receptors.[125,126] Alvarez et al designed AChR targeted exosomes for gene delivery using the RVG peptide.[127] Exosomes are vesicles that can be released by cells for intracellular communication. They have been found to deliver functional mRNA from one cell to another and are therefore hypothesized to be a potential cell derived nonviral gene delivery vehicle.[128] Exosomes were isolated from dendritic cells which had been stably transfected to express Lamp2b-RVG fusion proteins as exosome cell surface markers. The RVG functionalized exosomes significantly improved siRNA delivery and gene silencing in neuronal cells (Neuro2a), comparable to the knockdown achieved with lipofectamine.[127] Immunological tolerance was evaluated both *in vitro*, with a mixed splenocyte reaction measuring lymphocyte growth after RVG exosome addition, and *in vivo*, by monitoring the change in expression of immunostimulatory molecules. RVG exosomes did not trigger T cell proliferation *in vitro* and caused no significant change in the expression of immunostimulatory molecules monitored, suggesting that the targeted exosomes are highly immunologically tolerable.[127] *In vivo* gene delivery and biodistribution of the targeted exosomes was compared to naked siRNA targeting a model gene (GAPDH) which silenced approximately 50% of its target mRNA in liver, spleen, and kidney, and caused no significant silencing in brain, muscle or heart. When the siRNA was delivered within the RVG functionalized exosomes, mRNA silencing was achieved only in the brain and the kidney. The siRNA targeted protein expression, however, was not found to be significantly silenced, even after two doses of the targeted siRNA delivery.[127] Significant protein expression silencing was achieved when the target protein was BACE1, an enzyme responsible for β-amyloid generation and thought to be significant in Alzheimer's pathology.[129] In addition, β-amyloid levels were significantly decreased, suggesting therapeutic potential for this gene delivery system.[127]

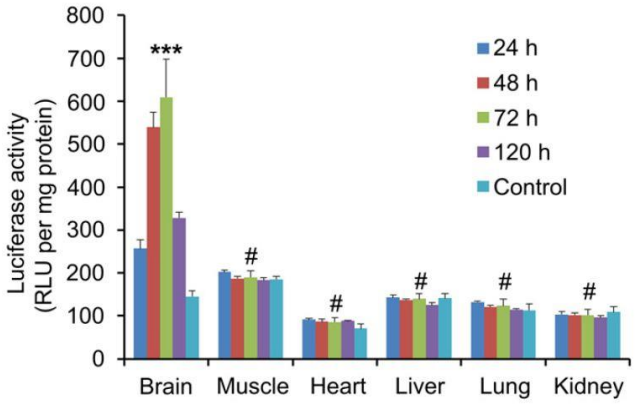

Figure 10. Transfection within the brain using AChR targeted polyplexes.
Luciferase expression measured in different tissues at 24, 48, 72 and 120 hours after intravenous administration of RVG-targeted polyplexes into mice. Reprinted from (129). Copyright (2012) with permission from Elsevier.

The RVG peptide was also used as a ligand to target plasmid DNA delivery to the brain. Gong et al conjugated the RVG peptide to a polyhistidine buffering peptide and a polyarginine DNA binding peptide and complexed this multifunctional peptide to plasmid DNA. This targeted peptide DNA complex achieved higher levels of transfection in Neuro2a cells than DNA delivered with lipofectamine, an improvement over the *in vitro* results seen with RVG-targeted exosomes.[130] This enhanced transfection compared to lipofectamine appears to be from its superior endosomal escape capabilities. Highly specific *in vivo* transfection was also achieved with this targeting peptide. Biodistribution of reporter gene expression was measured in six different organs, and expression within the brain was approximately 5-6 fold that in all other organs (Figure 10).[130]

The Tet1 peptide (HLNILSTLWKYRC) was identified by screening a 12mer phage peptide library on trisialoganglioside (G_{T1b}), and eluting with tetanus toxin fragment C (HC). Fragment C of tetanus toxin is known to specifically interact with motor neurons through interaction with G_{T1b}, a major component of neural cell membranes. The Tet1 peptide binds with high specificity and high affinity to G_{T1b} positive cells, such as primary motor neurons and dorsal root ganglion cells, but unlike the tetanus toxin, Tet1 is non-toxic.[131] Another neuron-targeted ligand is neurotensin (NT), a short neuropeptide which is rapidly internalized upon binding to its high affinity receptor, neurotensin receptor which is specifically expressed on motor neurons.[132] Both Tet1 and NT peptides have been used to functionalize PEI nanoparticles and both peptides have been shown to improve the transfection efficiency of PC-12 cells undergoing neuron-like differentiation induced by NGF, though Tet1 conjugated PEI (Tet-PEI) performs better.[133,134] Tet1-PEI modified with a membrane lytic peptide increased transfection 2 fold over Tet1-PEI and 1000 fold over unmodified PEI.[134] Neither Tet nor NT successfully improved transfection efficiency or specificity in mature

neurons or NGF-differentiated PC-12 cells, indicating that these peptides may not be useful for targeted gene delivery in adult disease states.[133,134] Oliveira et al found that thiolated PEI conjugated to tetanus toxin fragment C via a bifunctional PEG spacer improved transfection efficiency in fully differentiated neurons and dissociated dorsal root ganglion cells.[135] Though Tet1 and HC peptides competitively bind to the same target, HC functionalized polyplexes achieved transfection in primary neuron cells while Tet1 and NT functionalized polyplexes could not. It was suggested that the ability of the HC peptide to traffic to the neuronal cell body via retrograde axonal transport facilitates this improvement in transfection.[135–137]

Peptide Targeted Gene Therapy for the Treatment of Cystic Fibrosis

Cystic fibrosis (CF) is a recessive genetic disorder characterized by the lack of a functional cystic fibrosis transmembrane regulator (CFTR) gene. The lack of CFTR causes abnormal chloride and sodium ion transport in epithelial cells, resulting in thick viscous mucosa secretions which inhibit normal respiratory and digestive functions. The replacement or supplementation of this CFTR gene is a promising therapy for the treatment of cystic fibrosis.[138,139]

McKay et al used a secretin receptor (SR) targeted cationic polyplex system to improve delivery and transfection efficiency of plasmid DNA delivered to modified SR-expressing CHO cells. SR is specifically expressed on biliary and pancreatic duct epithelial cells, the same cells that normally express CFTR in the non-disease state. Another feature of this targeting system attractive for gene delivery is the rapid internalization of the secretin-SR complex into endosomes.[140] The C- and N-termini of the secretin have no secondary structure and the N-terminus is responsible for the high SR affinity, leaving the C-terminus free for manipulation and conjugation.[141] McKay et al used full length secretin with a GGC spacer at the C-terminus where the neutral glycines act as a physical spacer between the bioactive sequence and the charged DNA binding region, and the cysteine was required to form a disulfide linkage with linear PEI (HSDGTFTSELSRLRDSARLQRLLQGLVGGC-PEI).[140] When compared to plasmid DNA transfection with nontargeted linear PEI, the secretin-conjugated PEI improved transfection in cells expressing the secretin receptor, and actually inhibited transfection in cells not expressing the secretin receptor, causing 10 fold transfection efficiency improvement in SR expressing cells over the control cell line.[140] This suggests that specific targeting could be achieved when delivered *in vivo*.

The $\alpha_9\beta_1$ integrin is another attractive target for gene therapy treatment of cystic fibrosis because it is expressed on epithelial cells of the upper airways. Yokosaki et al identified the tenascin peptide which specifically binds the $\alpha_9\beta_1$ integrin via substitution mutagenesis of the third fibronectin type

III repeat in the tenascin-C (TNfn3) protein. Alanine residues were sequentially substituted for acidic residues in or adjacent to the exposed loops of the expected structure as determined by the solved crystal structure of TNfn3. Only substitutions in the B-C loop region resulted in a marked reduction in the attachment of $\alpha_9\beta_1$-expressing cells, indicating that this region is critical to $\alpha_9\beta_1$ integrin binding.[142] Peptides based on the human sequence of the exposed A-B and B-C loops of TNfn3 were evaluated for their ability to block adhesion of α_9-transfected SW480 cells to wild type TNfn3. The AEIDGIEL sequence was identified as the only sequence to effectively block the $\alpha_9\beta_1$ integrin and inhibit binding to wild type TNfn3.[142] The sequence PLAEIDGIELTY was also identified by Schneider et al by screening a phage library of overlapping regions of human TNfn3 and by competitive binding inhibition assays.[143] The tenascin peptide sequence (PLAEIDGIELA) has been used in lipid based nanoparticle carriers to improve specificity of delivery and transfection efficiency of tracheal cells.[144] Incorporating the tenascin peptide into DNA lipoplexes increased transfection in both α_9-integrin expressing and non α_9-integrin expressing cell lines. Some improvement to specificity was achieved by altering the overall particle charge, but nonspecific cell association was still significant.[145]

Several peptide sequences have been identified via phage display of a CX_7C disulfide-constrained peptide library against human airway epithelial cells. The most frequent phage clones were peptide E (GACSERSMNFCG) and peptide Y (GACYGLPHKFCG), both of which were analyzed with Basic Local Alignment Search Tool (BLAST) to identify similarities between the peptide sequences and known protein sequences.[146] Peptide Y resembles a protein of the respiratory pathogen legionella pneumophila whose function and receptors are not yet known; peptide Y was found to improve transfection efficiency in multiple cell types, including human microvascular endothelial cells, human keratinocytes, human fibrosarcoma, and rabbit adventitial fibroblasts.[146] Peptide E shares similarities with the receptor targeting proteins of the respiratory pathogens rhinovirus and listeria monocytogenes known to bind intercellular cell adhesion molecule 1 (ICAM-1).[146] *In vitro* delivery of siRNA lipoplexes targeted with peptide Y resulted in 80% knockdown in the expression of the gene of interest, compared with only 20% with nontargeted siRNA.[147] Manunta et al investigated the aerosolisation of peptide E functionalized plasmid DNA-lipid nanoparticles for nebulized inhaler delivery and subsequent transfection within the upper respiratory tract of mice. These targeted lipoplexes achieved significant transfection within the tracheas of mice treated with nebulized nanoparticle solutions.[148]

Peptide Targeted Gene Therapy for Additional Disease Treatment

Corneal transplantation as well as corneal disorders stand to benefit from targeted gene therapies.

For example, graft rejection could be limited by the expression of soluble tumor necrosis factor alpha (TNF-α) receptors or interleukin-10 (IL-10).[149,150] Expression of the enzyme β-glucuridonase has been used to treat corneal clouding caused by mucosaccharidosis, genetic transfer of the genes for interferon alpha-1 (IFNα-1) and interleukin-2 (IL-2) can prevent herpes-simplex virus reinfection and keratitis, and pathological angiogenesis within the cornea can be prevented with gene therapy using a soluble VEGF receptor.[151–153] The use of viral vectors for these treatments has been known to trigger immune response, indicating that they would greatly benefit from the development of efficient nonviral vectors for corneal gene therapy.[149]

The molossin peptide is a cyclic, RGD-containing peptide derived from pit viper venom (ICRRARGDNPNNRCT) which has been shown to bind the $\alpha_v\beta_3$ and $\alpha_5\beta_1$ integrins.[154] Collins et al used the molossin peptide in a bifunctional peptide with a pLL chain for electrostatic condensation of DNA (K_{16}–ICRRARGDNPNNRCT) to target corneal epithelial cells. The bifunctional peptide was used in combination with a membrane disrupting peptide to deliver plasmid DNA to corneal cells; however, the control systems with K_{16}-RGE peptide performed as well as the molossin peptide, indicating that integrin specific internalization was not the mechanism responsible for improved gene delivery.[155]

Gene therapy also has the potential to treat osteoarthritis caused by cartilage degradation. It has been suggested that gene expression of various growth factors, bone morphogenic proteins or regulatory transcription factors, which cannot easily be delivered in their soluble form to cells, or the inhibition of certain inflammatory cytokines could prevent cartilage degradation and even encourage chondrocyte matrix restoration. Targeted gene therapy to chondrocytes, synovium and bone derived mesenchymal stem cells could be useful for this application.[156,157]

A cartilage affinity peptide CAP (DWRVIIPPRPSA), was identified via phage display biopanning of a peptide library against rabbit cartilage, with negative selection procedures against synovial tissue. The phages identified via tissue biopanning and negative selection were then put through rounds of cell biopanning against isolated chondrocytes. The combination of tissue and cell biopanning yielded the CAP peptide with both tissue specificity and high cell affinity. The peptide was subsequently evaluated for species specificity through primary human cell binding measurements and was found to exhibit high affinity and specificity for human as well as rabbit cartilage.[158]

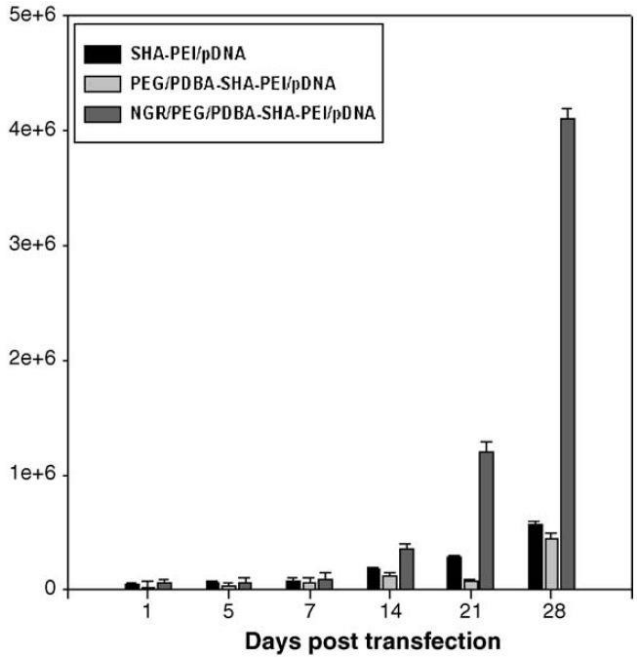

Figure 11. CD13 targeted polyplexes designed for delivery to dendritic cells.
Transfection efficiency was measured by β galactose expression of plasmid DNA delivered within nontargeted, unPEGylated complexes (SHA-PEI/pDNA), nontargeted, PEGylated complexes (PEG/PDBA-SHA-PEI/pDNA) and targeted, PEGylated complexes (NGR/PEG/PDBA-SHA-PDNA). Reprinted from (160). Copyright (2006), with permission from Elsevier.

The CAP peptide was conjugated to PEI for DNA complexation and subsequent *in vivo* delivery to rabbits for cartilage-targeted gene delivery. Transfection efficiencies of CAP-functionalized and scrambled peptide-functionalized vectors were compared between cartilage and synovium 2-7 days after *in vivo* administration. The highest transfection efficiency was achieved after 96 hours. The targeted DNA complex exhibited 9 fold higher transfection than the scrambled peptide DNA complex in harvested cartilage and both complex types achieved significantly lower but indistinguishable transfection in the synovium. The targeted vector fulfilled its design goal of specific *in vivo* gene delivery to cartilage compared to synovium, illustrating its potential for delivery of cartilage disorder gene therapy.[158]

Two bone targeting peptides were identified via *in vivo* phage display in mice; low affinity binding (LAB) peptide: NSMIAHNKTRMHGGGSC and high affinity binding (HAB) peptide: SGHQLLLNKMPNGGGC.[159] Poly(amidoamine) dendrimers were functionalized with LAB and HAB peptides and used to compact plasmid DNA. HAB functionalized dendrimers with 4 and 8 peptides per dendrimer improved transfection compared to both nontargeted dendrimers and a commercial transfection reagent composed of partially degraded dendrimers at 48 hours. Higher levels of transfection were achieved with dendrimers with only 4 peptides attached to their surfaces, possibly because of a local saturation of the target receptors,[157] highlighting the importance of

ligand valency optimization. Using these peptide targeted dendrimer vectors, the specific *in vitro* transfection of multipotent mesenchymal stem cells was significantly improved.[157]

CD13, originally targeted for cancer therapy, is also expressed on dendritic cell precursors and on differentiated dendritic cells.[160] The NGR peptide (GNGRGGVRSSSRTPSDKYC), identified by phage display to specifically target CD13, was therefore used as a targeting ligand for potential DNA vaccine delivery to dendritic cells.[44,95] DNA microparticles were composed of a salicylhydroxamic acid (SHA) derivatized PEI and a NGR peptide conjugated to PEG and phenyl(di)boronic acid, then encapsulated within PLGA-PEG-PLGA. These targeted DNA microparticles improved transfection compared to nontargeted particles, but more markedly, they showed a release profile that extended over weeks, which translates into an extended and increasing transfection efficiency as demonstrated in Figure 11.[161]

Discussion

In order for nonviral gene therapy to become a clinical reality, gene delivery needs to be stable, nontoxic, efficient and specific. To address specificity, several groups have designed nonviral gene delivery vehicles coupled with peptide targeting ligands. These targeting peptides have been designed and selected for tumor associated receptors, epithelial cells, endothelial cells, cartilage tissue, neuron specific receptors and various other targets. They have been used directly or modified with amino acids to act as linkers to vector molecules, to mimic natural ligand spacing, to prevent degradation or to increase solubility. The overwhelming impact of cancer has encouraged countless groups to target malignant tissue for gene therapy. Cancer cells provide many useful receptors for peptide targeting, as the disease state causes abnormal upregulation of many cell surface molecules. The highly proliferative nature of tumor tissue allows for easier access to the nucleus which can facilitate transfection efforts. Peptide targeted gene delivery has therefore seen much success in *in vitro* and *in vivo* models of cancer states. Targeted gene delivery to the CNS provides additional challenges to effective transfection, but a few peptide targeted vectors have addressed these obstacles. Cystic fibrosis is an appealing application for peptide targeted gene delivery because it is caused by a single genetic loss, is localized to a particular tissue type, and has seen success *in vivo* with nebulized, targeted nanoparticles. A few carefully designed phage display investigations have identified useful peptides for bone and cartilage targeting.

Plasmid DNA encapsulated within liposomes bearing the integrin targeting PR_b peptide achieved highly specific *in vivo* tumor targeting. The PR_b peptide has been designed for superior integrin binding and uptake over the many RGD peptides, because it combines the natural RGD binding site with the synergy site found within fibronectin.[67,69–71] Combining this improved integrin

binding peptide with highly stable PEGylated liposomes encapsulating PEI condensed DNA with endosomal escape abilities resulted in an extremely effective *in vivo* gene delivery system.[79] YSA functionalized nanogels, peptide Y functionalized lipoplexes and LHRH peptide functionalized dendrimers achieved 80% or higher specific target gene knockout with delivery of siRNA in vitro.[85,110,147,148] Both YSA and peptide Y were identified by phage display but are functional or sequence mimetics of different ligands. The LHRH peptide is a native ligand with a few careful modifications to increase its stability which provided exceptional gene therapy targeting.[106,107] Peptide E functionalized lipoplexes were also successfully used to transfect the airways of CF model mice.[148] The biomimetic neuron targeting peptide RVG preferentially delivered plasmid DNA to tumor tissue.[127] These targeted vehicles all have great potential for further development and clinical success.

Each *in vivo* study was precluded by extremely successful *in vitro* results indicating specific augmented transfection. However, positive *in vitro* results do not always translate into positive *in vivo* results, as seen with the gene delivery work by Lu et al and Nui et al, emphasizing the importance of *in vivo* biodistribution studies to analyze tissue specificity, as nonspecific delivery can result in poor therapy.[32,83] With respect to increased specificity, the peptide CAP, identified for delivery to cartilage while avoiding synovial tissue, achieved through negative selection screening, highlights the advantages of negative selection to avoid nonspecific delivery.[158] Combining two ligands to target tumor cells improved the targeting capabilities of DNA polyplexes, suggesting the potential improvement of any of these delivery vehicles by combining more than one ligand on one vehicle.[8]

Each disease or tissue however comes with unique challenges. Receptors upregulated and unique to cancer cells often stimulate proliferative effects when activated with their native ligands. Targeted peptides that exhibit antagonistic behaviour will block these stimulatory effects and can be used as inhibitory drugs. Cyclic RGD peptide, for example, has been used as an antagonist for endothelial cell angiogenesis in a tumor vasculature model, because it prevents binding and angiogenic signalling between vitronectin and the $\alpha_v\beta_3$ integrin.[162] As ligands for gene delivery vehicles, a peptide's ability to block binding and signalling from the native ligand is much less important than the affinity and subsequent internalization of the peptide and its load. It is important, however, that the targeting peptide has no agonist action and is nonmitogenic. This is the case for the peptides developed to target the growth factor receptors FGFR and EGFR. FGF stimulates proliferation upon binding with its native receptor FGFR, but the rate of proliferation of cells in the presence of the MC11 FGFR binding peptide was no different than that of untreated cells.[33] EGF also activates mitogenic pathways upon binding with its receptor, EGFR, but the EGFR binding

peptide GE11 was found to have no cell growth stimulating ability.[39] In addition to limiting mitogenicity, both peptides exhibited high affinity for their respective receptors (in the nanomolar or sub-nanomolar range) and were extremely successful gene targeting peptides.[33,34,36,39–41] Biodistribution of phage display identified MC11-functionalized star shaped copolymers and phage display identified GE11 functionalized PEI that showed clear transfection specificity for tumor over healthy tissue, while the MC11 star shaped copolymers provided significant therapeutic benefits to a tumor mouse model.[36,39,40] These growth factor receptors present a valuable gene delivery target because they both hold important nuclear functions such as to interact with transcription factors, and are therefore trafficked to the nucleus after endocytosis.[163,164] Since plasmid DNA must localize to the nucleus for transfection to occur, association with these nuclear-localized receptors enhances transfection efficiency more than simply increased cell association would.

Gene delivery vehicles transfecting neurons must overcome the added intracellular barrier of traversing the axon to reach the nucleus;[165] and neurons and other noncancerous cell types are often post-mitotic which limits access to the nucleus by delivered DNA. Delivery vehicles targeting the CNS *in vivo* have the added obstacle of penetrating the blood brain barrier (BBB).[166] Leptin30, identified from the leptin protein which is known to be taken up into the brain, can cross the BBB and localizes within the parenchyma of the brain. The *in vitro* investigation of the leptin30 functionalized dendrimers was performed with a model primary neuron cell line, and positive results with this model combined with a peptide designed with the *in vivo* challenges in mind, translated to successful *in vivo* transfection.[121] PEI functionalized with Tet1 or NT peptides, though they could transfect PC-12 cells undergoing differentiation, did not successfully transfect fully differentiated PC-12 cells or primary neurons. However, a similar vector with a different neuron targeting peptide, HC peptide, significantly improved transfection in differentiated neurons and primary ganglion cells.[133–135,167] The HC and Tet1 peptides traffic rapidly toward the cell body where the neuronal nucleus is contained, using retrograde axonal transport that avoids late endosomes and lysosomes.[168] This transport ability could indicate the superior performance of these peptides compared to NT. The HC peptide was combined with thiolated PEI complexes, a vector designed to readily release DNA within the reducing intracellular environment.[169] The HC peptide's ability to traffic towards the nucleus combined with the ability of thiolated PEI to release its cargo within the cell accounts for the exceptional neuronal transfection achieved with this vector.

The results of the last ten years in peptide-targeted gene delivery have proven that efficiency and specificity are closely intertwined. Carefully designed peptides do not necessarily achieve positive results with every gene delivery vector. For example, lipoplexes functionalized with an integrin targeting peptide c(RGDfK) achieved 1000 fold lower transfection efficiency than nontargeted PEI,

but c(RGDfK) functionalized chitosan nanoparticles encapsulating siRNA provided therapeutic effect that reduced 71% of tumor weight compared to controls when delivered to tumor mouse models.[12,55] Chitosan is thought to mediate a simultaneous escape from intracellular vesicles and decondensation with nucleic acids, releasing its genetic cargo into the cytosol.[170] When the gene therapy consists of gene silencing siRNA, the nucleic acids need only to be released into the cytosol to be functional, so condensation within chitosan which mediates efficient cytosolic release and targeting with an RGD peptide is therapeutically effective. The transfection efficiency of the RGD functionalized lipoplexes was enhanced with the addition of a lysosomotropic agent, indicating that the targeted lipoplexes alone were limited by their lack of this intrinsic function. The same targeting peptide performed so poorly with one vector and so successfully with another because gene delivery involves several potential rate limiting steps and each one is important to consider when designing an efficient gene delivery vehicle. The addition of a lysosomolytic agent to the media for *in vitro* gene delivery with SIG labeled polyplexes resulted in significant improvements in transfection,[57] and condensation with PEI of NL4 peptide polyplexes eliminated the need for additional endosomolytic agents.[60,105,118,119] Both of these examples suggest that endosomal escape may be an important aspect of many targeted vectors.

In other instances, peptides that achieve highly efficient, specific internalization do not always translate to high levels of transfection. In certain cell types, SIG labeled polyplexes achieved high levels of internalization but low levels of transfection.[57] The addition of endosomolytic agents had no effect on transfection, indicating that an inability to traffic to or penetrate the cell nucleus was the barrier to efficient SIG-mediated gene therapy. Star polyplexes functionalized with several heparin binding peptides exhibited higher levels of internalization than nontargeted PEI, but with several different targeting vector compositions could not achieve even 100 fold less transfection than nontargeted PEI.[60,105] The star polyplexes in this investigation are composed only of PEG, with no intrinsic vesicle escape function or intracellular trafficking mechanism. Though the vectors are efficient for targeted delivery, they have no mechanism for reaching the cell nucleus and did not mediate highly efficient transfection.[105]

Once gene delivery vehicles bind and internalize within a target cell, the nucleic acids must often be released from both the intracellular vesicle and the vehicle. Plasmid DNA must also travel to and enter the nucleus. The mechanisms of transport and escape strongly depend on the ligand-receptor interactions and subsequent internalization pathway. Gene delivery with EGFR or FGFR needs no endosomal escape ability, because the growth factor receptors travel directly to the nucleus. Most of the receptors targeted with the peptides in this review are internalized primarily via clathrin mediated endocytosis[53,171–189] which eventually traffics to endosomes and lysosomes.

The transferrin receptor, for example, is internalized via clathrin mediated endocytosis, requiring peptides targeted to transferrin to be combined with gene vectors with efficient endosomal escape capabilities such as the PEI polyplexes used with the transferrin receptor targeting peptide B6.[8] LHRH has been shown to internalize via caveolae[190] which may not traffic to vesicles with low pH such as late endosomes and lysosomes, so that PEI, which relies upon low pH for its escape mechanism, may be unnecessary. EphA2, AChR, Secretin, and ICAM-1 internalize via caveolae- and clathrin-independent internalization mechanisms.[191–194] Pairing appropriate gene delivery vehicles with peptide ligands targeting these receptors may be more challenging since much less characterization of the mechanisms and subsequent intracellular trafficking of these more recently described internalization schemes has been done.

Efficiency and specificity could be simultaneously improved by carefully pairing vectors and ligands that exploit the cell's natural intracellular trafficking pathways. Unfortunately, our knowledge of intracellular trafficking and vesicle and vector release are still very limited, preventing the implementation of well characterized targeting peptides with consistently successful transfection agents.[19,170,195,196] We continue to improve each piece of the gene delivery vehicle separately, but what is really needed to advance gene delivery into the clinic is intelligent, integrated design methods.

Conclusions

Peptide targeting has been used to improve nonviral gene delivery for several disease states that could potentially be treated with gene therapy. The applications for targeted gene delivery include cancer therapy, genetic treatment for central nervous system diseases, genetic correction of cystic fibrosis and a few other tissue specific disorders, with cancer applications receiving the most attention. The addition of a targeting peptide to the surface of a gene delivery vehicle often results in an increase in transfection and cell specificity, with the best formulations achieving efficiently targeted *in vivo* gene expression localized to the target tissue and even positive therapeutic results. These successful targeting peptides were identified via phage display to particular receptors, cells or tissues or designed via biomimetic function and sequence of natural ligands. The method of discovery, choice of target, affinity and specificity of each of these peptides was discussed with respect to its gene transfection potential and ability. It was found that the most successful gene delivery vehicles utilize a peptide with high affinity and specificity and take advantage of the appropriate intracellular pathways. Strategic pairing of well characterized peptide ligands with effective gene delivery vehicles with respect to the overall route of gene delivery could make targeted clinical gene therapy a reality.

Acknowledgements

This work was supported in part by a National Science Foundation (NSF) Graduate Research Fellowship to RML and by the CAREER award NSF/CBET-0846274.

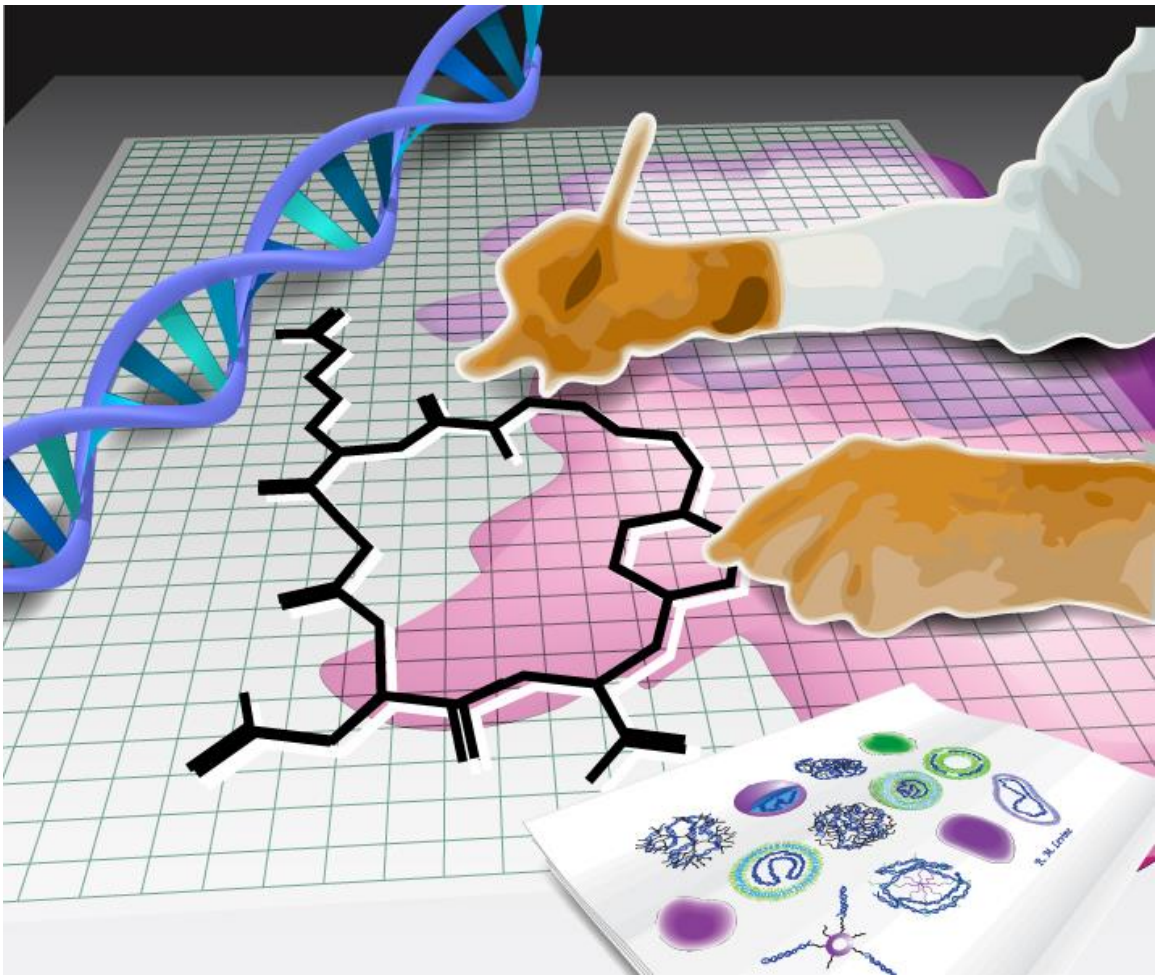

Chapter 2 Preparation and Characterization of Liposome-Encapsulated Plasmid DNA for Gene Delivery

Introduction

Effective non-viral delivery remains a major obstacle to clinical gene therapy. Non-viral vehicles overcome the issues of toxicity, tumorigenicity and low versatility of viral vectors but still struggle to achieve the same high transfection efficiencies.[197,198] The nonviral vectors that have received the most attention and have been most thoroughly investigated are lipoplexes and polyplexes. Lipoplexes and polyplexes consist of cationic lipids, liposomes or polymers that electrostatically condense nucleic acids into nanoparticles. However, these charged complexes maintain several disadvantages during *in vivo* delivery including rapid aggregation, high clearance from the blood stream and inflammatory toxicity. [197,199] Attempts have been made to improve the pharmacokinetics and reduce inflammatory toxicity of these nanoparticles by adding polyethylene glycol (PEG) to the surface of the nanoparticle as a stealth moiety.[200–202] While this addition has been shown to increase circulation time of cationic liposomes, PEGylated neutral liposomes containing doxorubicin maintained higher plasma concentration, achieved higher localization within the target tissue and delivered more effective therapy *in vivo* than the cationic liposomes when directly compared.[202]

PEG modified liposomes (stealth liposomes) exhibit prolonged blood circulation times and avoid aggregation, improving delivery and *in vivo* distribution and are currently approved for clinical use for the treatment of several cancer types including Kaposi's sarcoma and ovarian cancer.[203–205] Stealth liposomes present a potential solution to the disadvantages associated with cationic polyplexes and lipoplexes. They are also easily modified with targeting molecules for improved specific delivery.[18,20,72,73,77,79,198,206] While cationic DNA lipoplexes have been extensively studied,[17,63,197,200,201,207–209] DNA encapsulation within neutral PEGylated liposomes has been investigated less often.[79,210] Previous work has shown that plasmid DNA (pDNA) encapsulated in neutral stealth liposomes that were functionalized with a targeting peptide, exhibited efficient and specific gene delivery to cancer cells *in vitro* and *in vivo*.[79] Therefore, further characterization and investigation of parameters that can influence pDNA encapsulation in neutral stealth liposomes is warranted.

Quantification of condensed pDNA encapsulated in liposomes, or other nanoparticles, is crucial for appropriate evaluation of the performance of the gene therapy nanoparticles. However, no simple and reliable quantification methods have been verified for this gene delivery vehicle that has the condensed pDNA encapsulated in a stealth liposome. On the other hand, most cationic lipoplexes undergo no purification, therefore requiring no final quantification.[17,63,208,209] Synthetic vectors were first quantified for DNA content by measuring radioactivity from radioactively labeled nucleotides, which is a reliable method of quantification, however, the associated risk of radioactive exposure limit its convenience.[210] Ethidium bromide or the PicoGreen DNA quantification reagent are often used to measure the extent of condensation of lipoplexes,[211,212] as they fluoresce when bound to uncomplexed double stranded DNA, but cannot intercalate within complexed DNA. PicoGreen has been used to measure encapsulation efficiency of lipoplexes, calculating the encapsulation efficiency using the difference in fluorescence intensity before and after addition of the detergent Triton X-100, which releases the complexed DNA.[213] However, extreme inconsistencies have been identified between PicoGreen analysis and UV absorbance measurement of DNA extracted and purified from plant tissues.[214] UV spectrophotometric analysis is another common DNA quantification tool, but is inappropriate for gene delivery vehicles because the method is sensitive to contamination from lipids and polymers.[215] Since DNA quantification is vital for gene delivery studies with nanoparticles that encapsulate DNA, it was necessary to develop and verify a simple, accurate DNA quantification tool for condensed DNA encapsulated within stealth liposomes. Covalently labeled DNA presents a possible improvement to the limitations of the current quantification methods. Intracellular imaging of transfected nucleic acids uses covalent labeling to visualize DNA and RNA.[216] Fluorescently labeled DNA has been used as an alternative to PicoGreen and other intercalating dyes for the measurement of complexed DNA released from polymer scaffolds.[217] A DNA quantification method based on fluorescently labeled DNA was developed for liposomal vectors encapsulating condensed DNA and verified for accuracy and consistency with radioactively labeled DNA, as well as compared to the commercially available PigoGreen reagent.

Unilamellar liposomes can be produced via several different means, including detergent dialysis, ethanol injection and thin film (TF) hydration. The detergent dialysis method begins with a solution of mixed micelles that convert to bilayered vesicles as detergent is removed from solution.[218] It is effective at encapsulating lipophilic drugs within its forming bilayer, and is often used to incorporate membrane proteins into bilayers for functional studies.[219,220] Detergent dialysis is also useful for production of lipoplexes.[207] Ethanol injection, which involves injecting ethanol-dissolved lipids into an aqueous phase to form liposomes, is a simple, easily scalable liposome

formulation method, but is more efficient at encapsulating ethanol soluble molecules.[221,222] Ethanol injection can be used to produce cationic liposomes for later complexation with nucleic acids.[223,224] Since plasmid DNA is neither lipophilic nor ethanol-soluble, these methods are not feasible for DNA encapsulated liposome formation. For TF hydration, liposomes are formed by adding an aqueous solution to an adsorbed lipid film, which causes it to swell and detach, forming bilayered vesicles.[225,226] It is a useful method for encapsulating hydrophilic drugs, and is appropriate for DNA encapsulation, however, it relies on the lipid film reforming into vesicles around the DNA, so it has to be determined if it is the most efficient DNA encapsulation method. Two preparation methods, reverse phase evaporation (REV) and asymmetric liposome formation, have been proposed as alternative encapsulation methods, specifically for gene delivery. REV uses biphasic emulsion solvent dispersion, where the encapsulant and the lipid solutions are immiscible, to maximize internal aqueous space. REV has been used for encapsulation of many drugs, including small molecules for cancer chemotherapy, antimicrobial oils, and even oligonucleotides.[227–229] Asymmetric liposome preparation is an inverse emulsion method that has been used to encapsulate oligonucleotides and siRNA for gene delivery.[230,231] These methods were compared to the common TF method to determine the most efficient DNA-encapsulating liposome preparation method.

Here we describe the optimized preparation and characterization of liposome encapsulated plasmid DNA as a nonviral gene delivery vehicle. A simple, accurate DNA quantification method was verified for this gene delivery vehicle and the effect of different parameters, such as preparation method, lipid content and DNA concentration on DNA encapsulation was also evaluated. This analysis provides the basis for production of neutral stealth liposomes for the delivery of plasmid DNA for gene therapy.

Materials and Methods

Plasmid DNA Labeling and Quantification

pT2/Cal (7.5 kbp)[232] encoding firefly luciferase was the pDNA used throughout this study. Fluorescently-labeled pDNA was produced by conjugating Cy5 fluorescent dye to pT2/Cal using LabelIT Cy5 nucleic acid labeling reagents (Mirus, Madison, WI) according to the manufacturer's protocol. The fluorescent label is covalently attached to the DNA through an alkylation reaction between the label and the oxygen and nitrogen species within the DNA bases, predominantly with nitrogen species in guanine.[233,234] Radioactively-labeled pDNA was produced using a nick translation kit (Invitrogen, Grand Island, NY) following the manufacturer's protocol, with a reaction replacing deoxycytodine triphosphate (dCTP) bases with [H3] dCTP (Moravek, Brea, CA). pDNA was labeled with approximately 15 mCi/nmol pDNA. A fluorescent or radioactive

DNA concentration standard curve was generated from the condensed pDNA or the pDNA and the liposomes at the hydration phase of the thin film liposome preparation process. Fluorescence intensity was measured using a fluorescence microplate reader (Biotek, Winooski, VT) and radioactivity was measured using a Beckman LS 6500 liquid scintillation counting (Beckman, Fullerton, CA) without liposome release via detergent addition or uncondensation of pDNA via heparin. For quantification using the PicoGreen reagent (Invitrogen, Grand Island, NY), the liposome encapsulated pDNA was released from the liposomes by incubation with 0.5 % Triton X-100 (Sigma Aldrich, St. Louis, MO) and uncondensed by incubation with 5 mg/mL heparin (Sigma Aldrich, St. Louis, MO). The heparin, Triton X-100, branched polyethyleneimine (bPEI) and lipids were removed from this sample via dialysis through 1000 kDa MWCO membranes (Spectrum Labs, Rancho Dominguez, CA) and the remaining pDNA was quantified with PicoGreen according to the manufacturer's protocol. For all pDNA quantification, only the final purified pDNA concentration in the pDNA-encapsulated liposome formulations was quantified.

DNA Condensation

pDNA was condensed with 10% fluorescently labeled pDNA and/or 1% radioactively labeled pDNA. 20 µg pDNA was dissolved in 10 mM tris-HCl buffer and an equal volume of 25 kDa bPEI (Sigma Aldrich, St. Louis, MO) in water was added to the pDNA solution at an amine to phosphate (N/P) ratio of 8, vortexed for 5 min and incubated at room temperature for 30 min.[79] The size of the condensed pDNA was measured using dynamic light scattering (DLS) with a 660 nm laser at ±1 nm reproducibility (Brookhaven Instruments Corporation, Holtsville, NY). 100 nm or smaller condensed pDNA particles were used for subsequent liposomal formulations.

Liposome Formation

Thin film liposome formation

1,2-dipalmitoyl–sn-glycero-3-phosphocholine (DPPC), 1,2-dipalmitoyl-sn-glycero-3-phospho ethanolamine-N-[methoxy(polyethylene glycol)-2000] (ammonium salt) (PEG2000) and cholesterol were purchased from Avanti Polar Lipids, Inc (Alabaster, AL). 60 mol% DPPC, 35 mol% cholesterol and 5 mol% PEG2000 dissolved in chloroform were combined in a round bottom flask in the appropriate amounts (0.5-20 µmol), and dried under argon at 60 °C to produce a homogenous lipid film. This film was hydrated with condensed pDNA at 45 °C until the entire film peeled off of the bottom of the flask. All liposome formation was performed below 45 °C to ensure nanoparticle stability as temperature studies performed with pDNA and DNA nanoparticles indicated that thermal stability of pDNA is maintained up to 90 °C and size stability of

nanoparticles is maintained above 50 °C.[235,236] These liposomes were then extruded 11 times using a manual extruder (Avestin, Ottowa, ON) through 200 nm membranes and the unencapsulated pDNA was removed with overnight dialysis purification through a 1000 kDa MWCO membrane (Spectrum Labs, Rancho Dominguez, CA). Lipid concentration was measured using a phosphorus assay as described elsewhere.[237] Liposome size and charge were measured using DLS and zeta potential analysis (Brookhaven Instruments Corporation, Holtsville, NY). In previous studies, final PEG2000 mol% in liposomal formulations was measured using H-NMR and found to be in consistent agreement with the mol% initially added to the lipid film.[206] Therefore, the final mol% of PEG2000 in all liposomal formulations prepared was estimated to be 5%.

Reverse phase evaporation liposome formation

Films were prepared as described above and liposomes were prepared from these films as described elsewhere.[238] Lipid films were dissolved in a 1:1 ratio of chloroform and diethyl ether. Condensed pDNA dissolved in water was added to this solution and the suspension was homogenized with sonication for at least 2 min. The organic solution was evaporated off with argon at 45 ºC. These liposomes were then extruded using a manual extruder (Avestin, Ottowa, ON) through 200 nm membranes and the unencapsulated pDNA was removed with overnight dialysis purification through a 1000 kDa MWCO membrane (Spectrum Labs, Rancho Dominguez, CA). Lipid concentration was measured using a phosphorus assay as described elsewhere.[237] Liposome size and charge were measured using DLS and zeta potential analysis (Brookhaven Instruments Corporation, Holtsville, NY). In previous studies, final PEG2000 mol% in liposomal formulations was measured using H-NMR and found to be in consistent agreement with the mol% initially added to the lipid film.[206] Therefore, the final mol% of PEG2000 in all liposomal formulations prepared was estimated to be 5%.

Asymmetric liposomes

Liposomes were prepared using the asymmetric liposome formation method.[230] 62.5 mol% DPPC, 35 mol% cholesterol and 2.5 mol% PEG2000 were dissolved in squalene (Fisher Scientific, Hanover Park, IL) were combined to compose the outer lipid membrane, placed on top of 1.5 mL of water in a round bottom flask and allowed to equilibrate for 1.5 h. 65 mol% DPPC and 35 mol% cholesterol dissolved in squalene were combined to compose the inner lipid membrane. Squalene was compared to other solvents in the investigation of siRNA encapsulation using asymmetric liposomes and was found to yield the highest encapsulation efficiency.[230] PEG was included only in the outer lipid membrane solution in an amount equivalent to that included in the outer bilayer of the REV and TF liposomes. The amount was estimated from a geometrical argument comparing

the outer surface area to the inner surface area of the liposomes. Condensed pDNA was added to the inner lipid membrane solution, sonicated for 1 h and extruded using a manual extruder (Avestin, Ottowa, ON) through 200 nm membranes. This inverse emulsion was gently added to the outer lipid membrane mixture and centrifuged for 1 h at 115 g. The squalene was decanted and the unencapsulated pDNA was removed with overnight dialysis purification through a 1000 kDa MWCO membrane (Spectrum Labs, Rancho Dominguez, CA). Lipid concentration was measured using a phosphorus assay as described elsewhere.[237] Liposome size and charge were measured using DLS and zeta potential analysis (Brookhaven Instruments Corporation, Holtsville, NY). In previous studies, final PEG2000 mol% in liposomal formulations was measured using H-NMR and found to be in consistent agreement with the mol% initially added to the lipid film.[206] Therefore, the final mol% of PEG2000 in all liposomal formulations prepared was estimated to be 5%.

Cryo-Transmission Electron Microscopy (Cryo-TEM)

4.5 μL of condensed pDNA or condensed pDNA liposome sample was deposited onto a lacey formvar/carbon copper grid (Ted Pella, Redding, CA) and vitrified in liquid ethane by Vitrobot (Vitrobot parameters: 4 sec blot time, -1 offset, 5 sec wait time, 5 sec relax time, 95% humidity). Following vitrification, the grid was transferred to a Tecnai G2 Spirit TWIN 20-120 kV / LaB6 TEM. Images were captured using an Eagle 2k CCD camera with an accelerating voltage of 120kV.

Results and Discussion

Liposome Formulation Method Comparison

Liposomes are commonly formed by addition of an aqueous solution to an adsorbed film of lipids that will then swell and detach to form unilamellar and multilamellar vesicles, encapsulating the aqueous volume nearest to the lipids when they form. Encapsulating condensed pDNA presents more challenges than encapsulation of small molecule drugs because of its large size. REV and asymmetric liposome formation have been proposed as methods that could improve the encapsulation of large oligonucleotides. [210,230,238] These methods were compared to the common TF method for their encapsulation yields.

REV liposomes are produced by first introducing an aqueous solution of the cargo to an organic phase containing lipids, and sonicating this mixture to produce small bubbles of aqueous phase within the organic solvent. The amphiphilic lipids will form reverse micelles around the bubbles of aqueous phase and cargo and, as the organic phase is dried off, will form liposomes containing aqueous phase and the encapsulant.[238,239] Asymmetric liposomes are prepared by again creating reverse micelles around small droplets of water and encapsulant within an oil phase. These droplets

are passed through a monolayer of lipids that form the outer liposomal layer, forming bilayered vesicles encapsulating the cargo. Since the inner and outer layers are added separately, their compositions can be separately controlled, for example, to alter the charge of the inner layer while maintaining a neutral outer layer, or including bulky PEG functionalizations only outside the liposomes. Asymmetric liposomes have been used successfully to encapsulate small oligomers.[230]

To ensure consistent encapsulant size for direct comparison between liposomes formation methods, the liposomes within each experiment were prepared from the same batch of condensed pDNA. The prepared liposomes had an average effective diameter of 150 nm with an average polydispersity index of 0.19 (polydispersity is a measure of the relative width of the size distribution), as measured by DLS, with a charge of -20 ± 2.4 mV. This liposome size is in agreement with other reports of liposomes (157 nm) produced via extrusion using the same apparatus and extrusion membrane size.[240] The size of extrusion membrane (200 nm) resulting in 150 nm liposomes was chosen based on the range of liposome size that take advantage of the rapidly formed vasculature within tumor tissue in a disorganized, irregular and 'leaky' blood vessel structure, allowing nanoparticles to more easily extravasate into the surrounding tissue. In a study identifying optimal liposome size for tumor drug delivery, PEGylated liposomes of different sizes were delivered intravenously to a tumor mouse model and the liposome distribution was measured. Liposomes of 100-200 nm accumulated most efficiently into the tumor compared to the blood and other organs, while liposomes above 300 nm did not.[241] Since the pDNA to be encapsulated is 100 nm or smaller, liposomes were prepared at the upper limit of the range of sizes of liposomes that achieve efficient tumor accumulation.

pDNA-encapsulated liposomes were prepared using the three liposome formation methods, and pDNA yield was determined by measuring radioactivity from radioactively labeled pDNA. As seen in Figure 12 the REV formation method provided no advantage over the TF method in terms of overall pDNA yield. REV and TF liposomes retained 9.0 ± 1.4 and 10.6 ± 1.2 μg/mL pDNA respectively from the initial pDNA concentration of 13.3 μg/mL. The asymmetric method gave very low yields in comparison to both REV and TF, with final pDNA concentrations of 2.2 ± 0.6 μg/mL, and preparing asymmetric liposomes with negatively charged lipids (1,2-dipalmitoyl-sn-glycero-3-phospho-(1'-rac-glycerol)) in the inner layer provided no improvement to pDNA yield. REV uses organic solvents during liposome formation which could have adverse effects on the stability of biological encapsulants, and any residual solvent could introduce toxicity concerns.[239] Since the TF method avoids the use of organic solvents during liposome formation and produced statistically the same yield of pDNA concentration as the REV method, the TF method was chosen as the best plasmid encapsulation method for further experiments. A comparison of cationic

lipoplexes prepared using REV, TF and ethanol injection methods also identified the TF method as the best lipoplex formation method because it resulted in highly stable particles with a lower tendency to aggregate even after 60 days.[224]

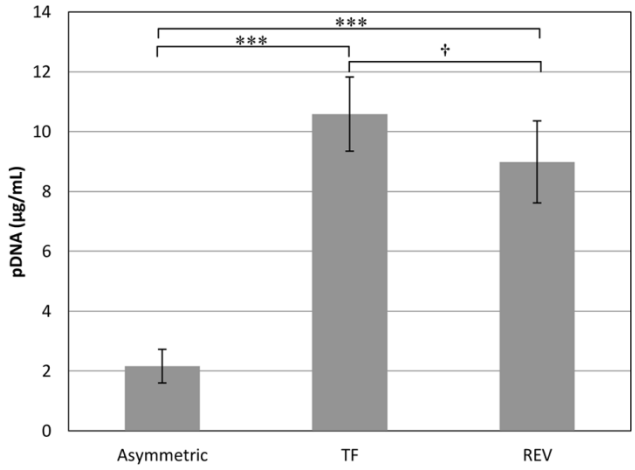

Figure 12. Comparison of liposome-encapsulated pDNA formulation methods.
pDNA, condensed with bPEI, was encapsulated in stealth liposomes prepared using asymmetric, TF or REV formation methods and final pDNA concentration was measured using radioactively labeled pDNA. Data are shown as the mean ± standard error of three separate experiments (n=3), each performed in triplicate. Student's t test statistical analysis was performed and statistical significance noted for the bracketed data (*** $p < 0.005$). Comparison of a pair resulting in a $p > 0.5$ is noted with a †.

Electron Microscopy and Characterization of TF Prepared Liposomes

The condensed pDNA and pDNA encapsulated stealth liposomes produced by the TF method were visualized using cryo-TEM (Figure 13). Unencapsulated bPEI condensed pDNA formed 100 nm or smaller spherical particles and the particle sizes shown in Figure 13A are consistent with the DLS analysis of condensed pDNA with an average effective diameter of 88 nm and an average polydispersity index of 0.26. Representative DLS data is shown in Figure 14 to illustrate the liposome size distribution. pDNA encapsulated liposomes formed by the TF method existed as unilamellar vesicles with some liposomes appearing to contain spheres enclosed within them that resemble the unencapsulated pDNA particles. This unilamellar structure is in contrast to the bilayered structures observed with cationic DNA lipoplexes, which can form multilamellar vesicles, bilamellar invaginated vesicles and liposomes with DNA condensed on their outer surfaces.[17,242–245] These images suggest successful encapsulation of condensed pDNA particles inside unilamellar liposomes.

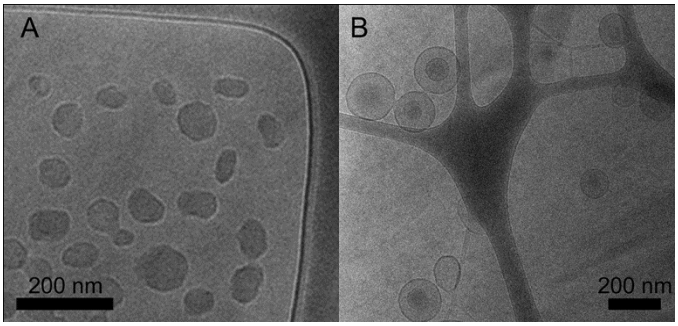

Figure 13. Cryo-TEM images of bPEI condensed pDNA and condensed pDNA encapsulated in stealth liposomes.
A) bPEI condensed pDNA prepared with an N to P ratio of 8. B) bPEI condensed pDNA (N/P=8) encapsulated in stealth liposomes prepared using the TF method from a 20 µmol lipid film.

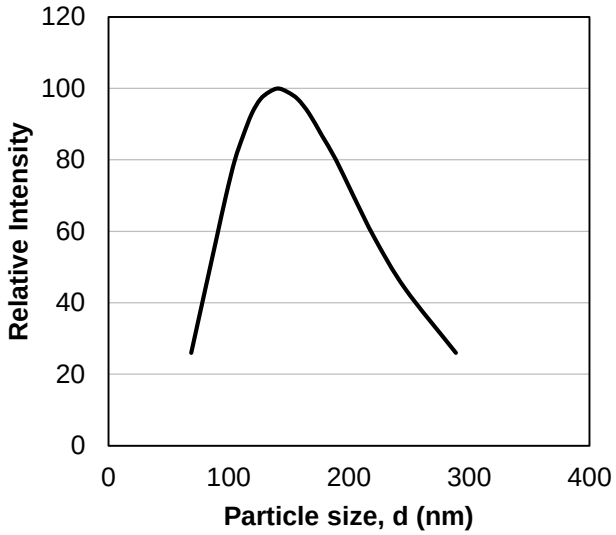

Figure 14. Representative DLS particle sizing data from pDNA-encapsulated liposomes. Distribution is typical of pDNA encapsulated liposomes with polydispersity index of 0.26.

DNA Quantification

A DNA quantification method based on fluorescently labeled pDNA was developed for liposome encapsulated pDNA. Fluorescent labeling was chosen as an appropriate assay because of its relative ease of conjugation, the linear dependence of fluorescence intensity with the pDNA concentration and the ability to measure fluorescent intensity of pDNA without sample destruction (i.e. without addition of detergents to release pDNA). With the goal of encapsulating pDNA in our 150 nm liposomes (in order to best take advantage of the leaky vasculature of tumor tissue[241]), the pDNA was electrostatically condensed using the cationic polymer bPEI. Condensation of DNA brings the strands and fluorophores conjugated to backbone atoms in close proximity causing some

degree of quenching of the fluorescent signal.[246] The extent of quenching then depends on the extent of condensation. A fluorescent signal standard was therefore produced after the pDNA condensation reached a stabilized state, immediately after lipid hydration occurs (Figure 15A). Figure 15B confirms that the presence of lipids and PEG have little effect on the fluorescent signal measured in the concentration standards. To ensure the pDNA condensation is stable and that the Cy5 fluorescently labeled pDNA provides an accurate quantification tool for this application, this method was compared, along with the method using the common pDNA quantification reagent PicoGreen, to quantification using radioactively labeled pDNA. Radioactive decay is unaffected by environment, so it provides a reliable standard by which to compare the other quantification methods.

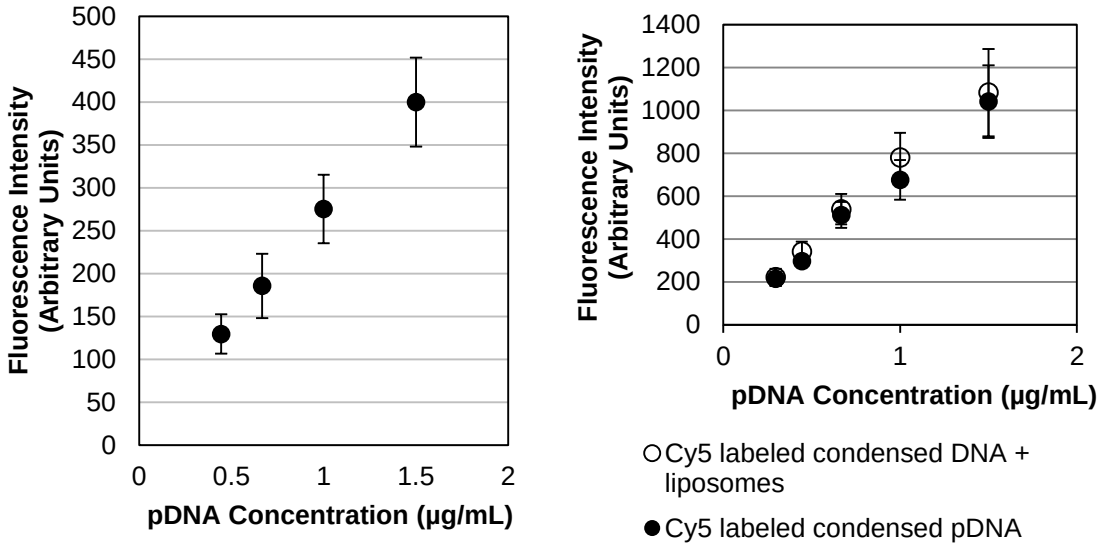

Figure 15. Cy5 labeled condensed pDNA concentration standards
A) Concentration standard for 10% Cy5 labeled condensed pDNA after hydration step of liposome formation, showing the linear dependence of fluorescence intensity on pDNA concentration. Concentration standard for 10% Cy5 labeled condensed pDNA and 10% Cy5 labeled pDNA in the presence of empty liposomes, showing the linear dependence of fluorescence intensity on pDNA concentration and the invariance of fluorescence intensity in the presence of lipids and PEG. Data are shown as the mean ± standard error of three separate experiments (n=3), each performed in triplicate.

Liposomes were prepared with condensed pDNA containing both fluorescently labeled and radioactively labeled pDNA, and after purification, final pDNA concentration was quantified via fluorescence (either by using the Cy5-labeled DNA or the PicoGreen assay) or radioactivity as shown in Figure 16. The pDNA concentration determined by Cy5 fluorescence and radioactivity are not statistically different while the concentrations measured using PicoGreen are significantly different. It was also found that the PicoGreen assay was extremely inconsistent when measuring the same sample more than once (data not shown). PicoGreen is a DNA intercalating dye that relies

on access to the space between DNA bases in uncondensed DNA to bind and fluoresce.[217] PicoGreen, therefore, cannot access the condensed pDNA or pDNA encapsulated within liposomes, necessitating the use of additional reagentss to break the liposomes, uncondensed the pDNA and purify the reagents before PicoGreen can be effective, introducing many opportunities for error, loss and contamination that inhbits PicoGreen fluorescence. The fluorescence and radioactivity from fluorescently and radioactively labeled DNA are measurable in their condensed, encapsulated state, simplifying the assay and ensuring greater accuracy. Cy5 fluorescently labeled pDNA therefore has been validated with radioactively labeled pDNA as an appropriate and useful tool for pDNA quantification of liposome encapsulated pDNA.

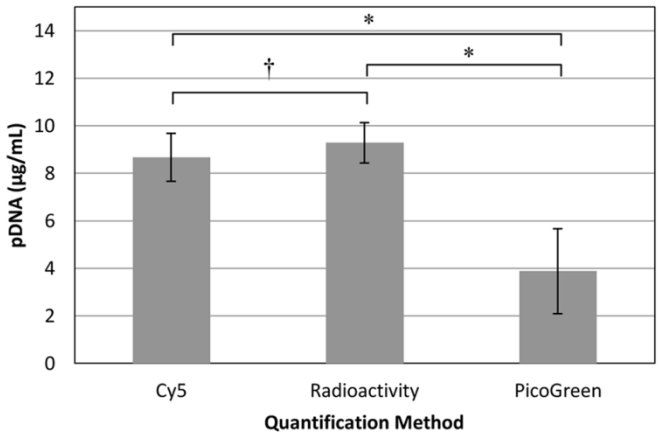

Figure 16. Comparison of liposome-encapsulated pDNA quantification methods.
pDNA (condensed with bPEI) concentration of prepared stealth liposomes measured using Cy5 labeled pDNA, radioactively labeled pDNA and the PicoGreen reagent. Data are shown as the mean ± standard error of five separate experiments (n=5), each done in triplicate. Student's t test statistical analysis was performed and statistical significance noted for the bracketed data (* $p < 0.05$). † indicates statistical similarity ($p > 0.7$).

Effect of Lipid Concentration on pDNA Encapsulated Stealth Liposomes

Using the Cy5 fluorescently labeled pDNA as the quantification method, neutral stealth liposomes encapsulating condensed pDNA via bPEI were further characterized for the effect of lipid content on yield and fraction of pDNA filled liposomes.

Liposomes were produced from lipid films containing several different amounts of lipids (0.5 – 20 µmol, lipid content). The pDNA and liposome concentrations of the purified liposomes were then measured to evaluate plasmid encapsulation. The pDNA yield was calculated as the pDNA content within the liposome formulation after purification divided by the pDNA content initially added to the lipid film. In general, lipid films with fewer lipids resulted in lower pDNA yields, with 20 µmol lipids giving 27.4 ± 6.2 % pDNA yield and 0.5 µmol of lipids resulting in only 10.6 ± 1.6% pDNA yield, as shown in Figure 17A.

In order to estimate the fraction of prepared liposomes containing condensed pDNA (Figure 17B), the final number of liposomes and condensed pDNA particles were estimated. The final liposome concentration of each formulation was calculated using the following equation

$$L = \frac{l\, N_A\, SA_{lipid}}{2 * 4\pi\, r^2} \qquad (1)$$

where L is liposome concentration [liposomes/mL], l is lipid concentration [mol/mL], SA_{lipid} is the surface area of DPPC (0.65 nm^2),[247] N_A is Avagadro's number and r is the radius of spherical liposomes (75 nm).

A maximum number of pDNA molecules per condensed pDNA particle can be calculated from the volume occupied by a pDNA molecule assuming a cylindrical shape[248,249]

$$V = l * bp * \pi * r^2 \qquad (2)$$

where r is 1.35 ± 0.2 nm,[250] the radius of a DNA helix,[248] l is 0.34 nm, the length of one base pair,[248] and bp is the number of base pairs in the plasmid, which for pT2/Cal is 7537. Using Equation 2, the minimum volume of a monomolecular pDNA particle is $14.7*10^3$ nm^3. A spherical pDNA particle with a diameter of 88 nm occupies a volume of $356*10^3$ nm^3, corresponding to a maximum number of pDNA molecules condensed in an 88 nm particle of 24. The calculated maximum number significantly overestimates the number of molecules actually found within a condensed pDNA particle. The length of a base pair is a well characterized parameter, but the radius of a DNA helix is less studied. Since the volume calculation depends on the square of the radius, the estimation of this parameter has a larger effect on the volume estimations for condensed DNA than the value of the length of a base pair, however, underestimating the radius by the experimental error of 0.2 nm changes the calculated number of DNA molecules per particle by only 24%, and overestimating by 0.2 nm changes the result by 38%. The overestimation is therefore most likely caused by the fact that the solvent and the bPEI polymer also occupy particle volume and this volume is not taken into account in the calculations.[248,251] Previous work has shown that a 6 kbp pDNA molecule occupies only 10% of the volume of a bPEI-condensed pDNA particle.[249] Therefore, 2.4 pDNA molecules would occupy 10% of the volume of our 88 nm particle. Other experimental investigations of the number of pDNA molecules per bPEI-condensed particle have reported 90 molecules per particle for 5 kbp pDNA complexed with bPEI at a N/P ratio of 15,[248] and 3.5 molecules per particle for 6 kbp pDNA complexed at a N/P ratio of 6 and 10.[249] The condensation conditions used for this study correspond more closely to those used in the latter study. Using the theoretical calculations with a 10% volume occupancy per particle and the literature values, 3 molecules per particle was determined as an appropriate estimate for calculating the fraction of pDNA filled liposomes. It was also assumed that all the condensed pDNA particles

were encapsulated within the liposomes in order to calculate the maximum fraction of stealth liposomes with encapsulated condensed pDNA.

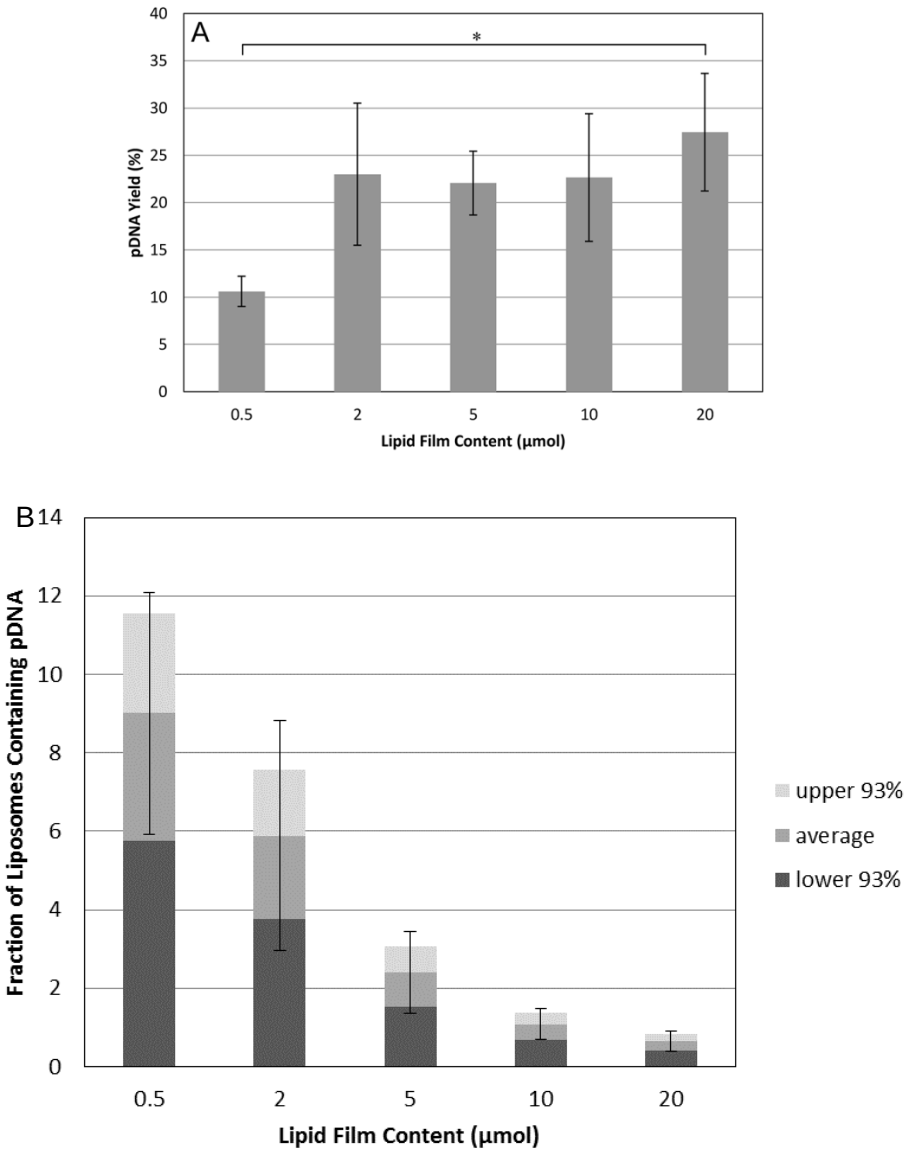

Figure 17. Yield and load fraction of liposome-encapsulated pDNA prepared with varying lipid film content. A) Comparison of the yield of pDNA measured using 20 µg Cy5 labeled pDNA that was condensed with bPEI and encapsulated in stealth liposomes prepared via the TF method. B) Theoretical calculation of the fraction of liposomes with encapsulated condensed pDNA from the liposomes shown in (A). Fraction is calculated using the average liposome size and the liposome size at 93% relative intensity above (170 nm) and below (120 nm) average as measured by DLS. Data are the mean ± standard error of three separate experiments (n=3), each performed in triplicate. Student's t test statistical analysis was performed and statistical significance noted for the bracketed data (* $p < 0.05$, ** $p < 0.02$, *** $p < 0.005$, † $p > 0.05$).

Though liposomes produced with lower initial lipid content had lower overall yields, they were estimated to have a larger fraction of pDNA filled liposomes, with 9.0 ± 1.6% full liposomes (Figure 17B). This means that approximately 90% of the stealth liposomes contain no pDNA.

For stealth liposomes, the fraction of pDNA filled liposomes can be controlled by increasing or decreasing the lipid film content. Previous characterization of liposomes encapsulating small molecules have shown that increasing lipid concentration decreases encapsulation efficiency, because increasing the lipid concentration encourages the formation of multilamellar vesicles.[252] However, the liposomes formed in this study even at the highest lipid content of 20 µmol formed unilamellar vesicles, as seen in Figure 13B, therefore an increase in concentration correlates with an increase in the total number of available liposomes, which improves the potential for pDNA encapsulation, but also increases the number of empty liposomes. Figure 18 quantitatively relates the lipid film content and theoretical calculation of the fraction of liposomes with encapsulated condensed pDNA.

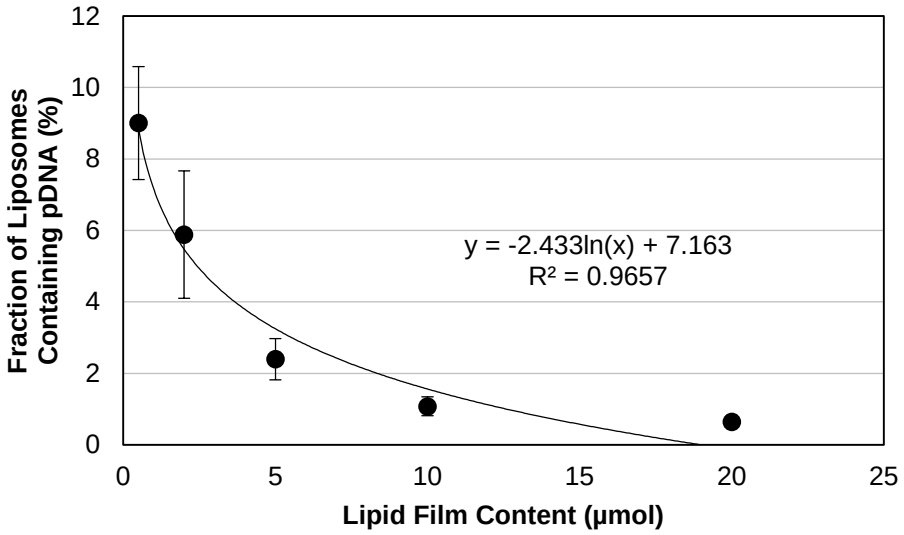

Figure 18. Quantitative relationship between the lipid film content and theoretical calculation of the fraction of liposomes with encapsulated condensed pDNA.
Stealth liposomes were prepared via the TF method with varying lipid film content using 20 µg Cy5 labeled pDNA that was condensed with bPEI. pDNA concentration was measured using fluorescence. Data are the mean ± standard error of three separate experiments (n=3), each performed in triplicate.

Liposomes were also prepared with two different amounts of pDNA to understand the effect of initial pDNA content on the fraction of liposomes containing pDNA. Liposomes prepared from a 20 µmol lipid film with 13.3 µg/mL pDNA had a 2 fold higher fraction of filled liposomes compared to liposome prepared with 6.6 µg/mL pDNA (Figure 19). This suggests that higher initial pDNA concentrations will result in more liposomes loaded with pDNA and fewer empty liposomes.

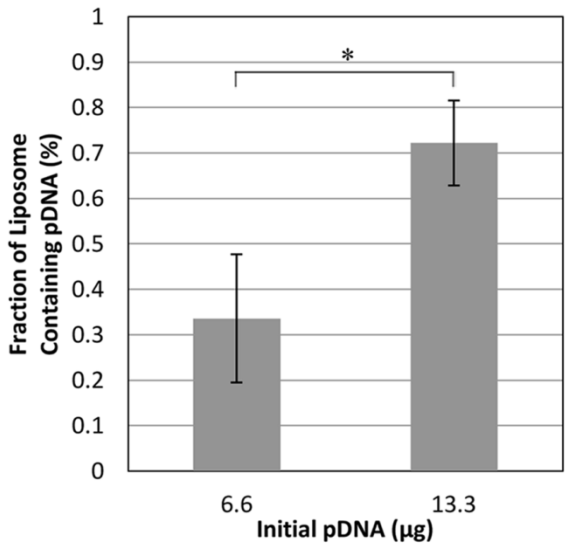

Figure 19. Load fraction of liposome-encapsulated pDNA prepared with varying initial pDNA content. Theoretical calculation of the fraction of liposomes with encapsulated condensed pDNA measured using Cy5 labeled pDNA that was condensed with bPEI and encapsulated in stealth liposomes prepared via the TF method from a 20 µmol lipid film. Data are the mean ± standard error of three separate experiments (n=3), each performed in triplicate. Student's t test statistical analysis was performed and statistical significance noted for the bracketed data (* $p < 0.05$).

These results provide a guide for pDNA encapsulated liposome production, depending upon the optimization goals of the process. In order to maximize overall pDNA encapsulation, the lipid concentration should be increased, but in order to minimize the number of empty carriers within the formulation higher pDNA concentrations should be used along with lower lipid concentrations.

Conclusions

Different processes of forming stealth liposomes that can encapsulate pDNA and pDNA quantification methods were examined. Comparing three different liposome formation methods thought to be beneficial for pDNA capture, it was determined that the TF method was best for pDNA encapsulation because of its higher yield and use of aqueous solvents for film hydration. The gene delivery field has, until recently, been lacking a simple, reliable quantification method that is compatible with the presence of lipids and PEI polymer and can be performed without sacrificing any amount of sample. Many pDNA quantification tools exist, but few are accurate for unpurified gene delivery vehicles. A fluorescence quantification method using Cy5 labeled pDNA was therefore developed for this delivery system and was verified for accuracy by comparing it to a radiolabeled pDNA assay. This comparison also confirmed that the commonly used commercial PicoGreen pDNA quantification assay is unreliable for this type of delivery vehicle. The effect of initial lipid concentration on pDNA encapsulation and fraction of pDNA loaded liposomes was

also explored. Higher lipid concentrations encapsulated a higher amount of pDNA but produced a high number of empty liposomes as well. Conversely, a lower lipid concentration encapsulated fewer pDNA particles, but the resulting formulation contained a higher fraction of pDNA loaded liposomes. Increasing pDNA concentrations also increased the number of filled liposomes. Therefore, the careful control of pDNA yield and fraction of pDNA encapsulated liposomes may be beneficial during production. For example, maximizing DNA yield may be an important aspect of production because of the cost of plasmid production. Inversely, for DNA liposomes that are targeted to bind to cell surface receptors, high encapsulation fraction may be more desirable to minimize the binding of unloaded liposomes to cells. Gene therapy has the potential to treat and cure many common ailments, but its success is limited by the lack of efficient delivery vehicles. The tools described here could contribute to the advancement of the stealth liposome as a delivery vehicle of encapsulated pDNA for gene therapy.

Acknowledgements

This work was supported in part by a National Science Foundation (NSF) Graduate Research Fellowship to R.M.L., by the CAREER award NSF/CBET-0846274, and by the Shell Chair.

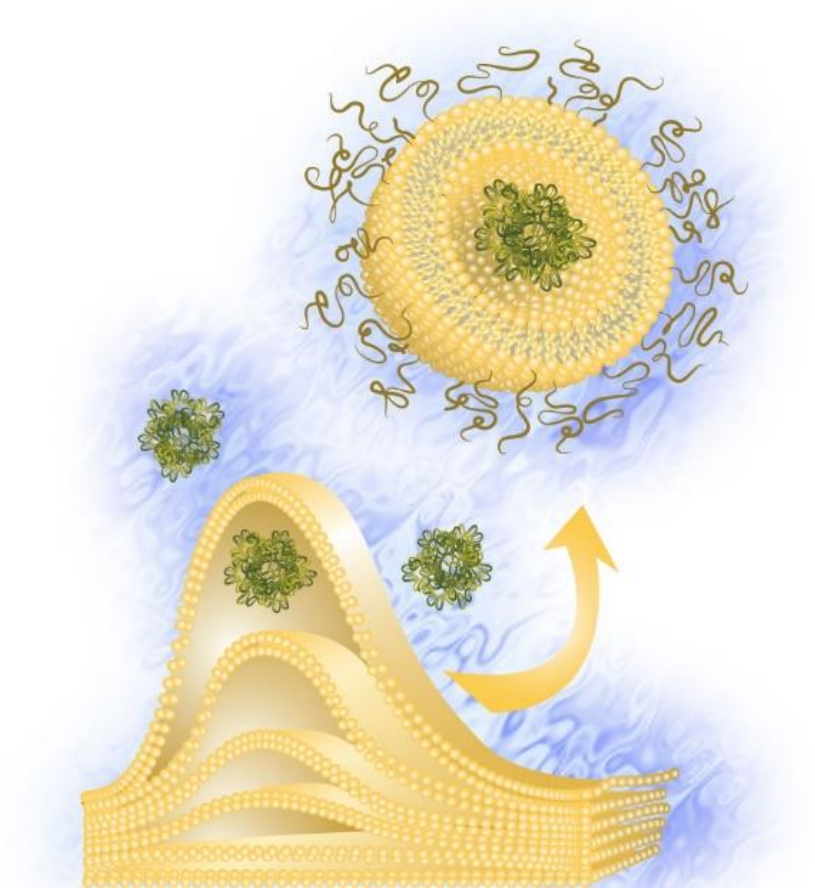

Chapter 3 Targeting HPV-Infected Cervical Cancer Cells with Stealth Liposomes Encapsulating siRNA and the Role of siRNA Complexation with Polyethylenimine

Introduction

Rapid advancements in genetic technologies have given researchers the ability to target and modify individual genetic events involved in disease progression, providing potential treatment avenues for previously untreatable diseases.[253–255] A particularly valuable tool for characterization and modification of disease-associated genes is RNA interference (RNAi), a cellular pathway which can selectively silence the expression of a target gene. When short (~22 base pair) RNA sequences are introduced into the cytoplasm of a cell, they can be incorporated into an RNA-induced silencing complex (RISC), molecular machinery which identifies the complementary mRNA sequence of the incorporated RNA for degradation, thus preventing translation and expression of the target gene. Selective gene silencing can be especially useful for treating diseases such as cancer or viral infection, where disease progression is driven by undesirable or aberrant gene expression.[254,256,257] One such example of the potential of RNAi therapy is demonstrated by the treatment of cervical cancer by silencing key genes within the cellularly integrated genome of the oncovirus human papillomavirus (HPV). The oncogenic nature of HPV has been attributed to the aberrant expression of the E6 and E7 viral proteins, and their interference with native cell cycle regulatory pathways. E6 and E7 bind to tumor suppressor proteins p53 and pRb, marking them for degradation or blocking their binding sites, thereby preventing apoptosis and driving cellular proliferation.[258,259] With the knowledge of the genetic mechanism of this oncovirus, several siRNA sequences targeting the gene sequences that encode the E6 and E7 proteins have been developed, demonstrating rescue of the p53 and pRb tumor suppression pathways, resulting in cell cycle arrest and apoptosis in HPV-infected cancer cells both *in vitro* and *in vivo*. [260–264]

In order for the potential of clinical gene therapy to be realized, several key obstacles to efficient *in vivo* delivery need to be overcome. For successful transfection and therapy to occur, siRNA must be internalized into the cells and released into the cytosol to mediate gene silencing. While traversing the blood stream to reach the target tissue, siRNA must avoid degradation by nucleases, recognition by the immune system, and renal clearance. Several technologies have been developed to address each of these barriers to siRNA delivery, including chemical modification, nanoparticle complexation, and addition of targeting moieties.[253–257,265] In this study, we developed

cancer gene therapy delivery vehicles composed of targeted stealth liposomes encapsulating siRNA. Stealth liposomes are hollow, spherical phospholipid nanoparticles functionalized with a layer of polyethylene glycol (PEG) which have seen clinical success for the delivery of chemotherapeutic agents.[203–205] The addition of the PEG layer prolongs blood circulation times and minimizes immunogenicity of the liposomes, promoting tumor accumlation.[203–205] Stealth liposomes are also less immunogenic than cationic lipoplexes and polyplexes, the most common siRNA transfection agents.[197,199] Stealth liposomes functionalized with ligands designed to bind to upregulated surface receptors can enhance cellular association and internalization into cancer cells. The $\alpha_6\beta_4$ integrins are upregulated surface receptors associated with metastatic behavior in several cancer types, including cervical cancer.[266–268] The AG86 peptide was identified as an α_6 integrin binding ligand,[269] and was investigated here for specificity for the $\alpha_6\beta_4$ integrin and for targeting to HeLa cervical cancer cells. Polyethyleneimine (PEI) complexation with nucleic acids alone has been shown to aid in endosomal escape through the proton sponge effect, whereby the high buffering capacity of PEI can cause osmotic swelling and rupture of intracellular organelles.[35,270,271] Previously, we have demonstrated successful encapsulation of plasmid DNA (pDNA) complexed with PEI within the aqueous core of stealth liposomes.[272] With the addition of a targeting ligand, liposome encapsulated PEI-complexed pDNA achieved efficient transfection in colorectal cancer cells.[273,274] We therefore hypothesized that siRNA/PEI complexation could enhance transfection efficiency within stealth liposomes as well. We engineered AG86-functionalized stealth liposomes encapsulating PEI complexed siRNA as a delivery scheme to address each of the barriers to effective gene delivery. Optimal targeting and complexation properties of this vehicle were identified for successful gene silencing of the HPV-E7 gene in cervical cancer cells.

Experimental Section

siRNA Labeling and Quantification

si18E7-674 (CTAGCACGAGCAATTAAGCGA), shown to silence the HPV-E7 gene,[264] (GE Dharmacon, Lafayette, CO) and used throughout this study, was fluorescently labeled using Cy5 Label IT Tracker Intracellular Nucleic Acid Localization Kit (Mirus, Madison, WI). The conjugation was carried out according to the manufacturer's protocol using the maximum recommended reagent volume and a reaction time of 3 h. For liposome encapsulated siRNA used for silencing, 5% of the total siRNA encapsulated was labeled with Cy5. For liposome encapsulated siRNA used for siRNA binding and internalization studies, 25% of the total siRNA encapsulated was labeled with Cy5. An siRNA concentration standard curve was produced from the complexed siRNA following the hydration step of liposome formation.[272] Fluorescence intensity of the

standard and of the liposome sample were measured using a Synergy H1 fluorescence microplate reader (Biotek, Winooski, VT). Yield was calculated as final siRNA content after purification compared to initial siRNA content used for encapsulation (100 pmol).

siRNA/PEI Complexation

100 pmol of total siRNA (5% fluorescently labeled siRNA, si18E7-674[264]) was complexed using 25 kDa branched PEI (Sigma-Aldrich, St. Louis, MO). 100 pmol of siRNA was dissolved in 6 mM HEPES buffer, mixed with an equal volume of PEI in 6 mM HEPES at the desired amine to phosphate (N:P) ratio at a final siRNA concentration of 67 nM, was vortexed for 5 sec and incubated at room temperature for 20 min. The size of complexed siRNA nanoparticles was measured using a NanoSight LM10 (Malvern Instruments, Malvern, UK) with a 405 nm laser, and zeta potential analysis (Brookhaven Instruments Corporation, Holtsville, NY) was used to measure the surface charge of the particles.

Isothermal Calorimetry (ITC)

siRNA and PEI were prepared in the same buffer to minimize mixing effects. PEI was then injected at 2 μL increments into the siRNA solution using a MicroCal Auto-iTC 200 System to measure the power required to maintain a constant chamber temperature. Using the MicroCal Auto-iTC200 software, the resulting power versus time data were integrated to determine heat exchange associated with each injection. The heat of dilution was accounted for by subtracting the heat data obtained from injections of PEI into buffer from the heat data obtained from injecting PEI into an siRNA solution. The resulting heat curve was fitted to a "one set of sites" binding model, which uses n, the number of binding sites, K, the binding association constant, and ΔH, the enthalpy of binding, as fitting parameters where all n binding sites have the same K and ΔH.[275,276] The data were fitted to the following equations:

$$K = \frac{\theta}{(1-\theta)[X]} \tag{3}$$

$$X_t = [X] + n\theta M_t \tag{4}$$

$$Q = n\theta M_t \Delta H V_o \tag{5}$$

$$\Delta Q(i) = Q(i) + \frac{dV_i}{V_o}\left[\frac{Q(i) + Q(i-1)}{2}\right] - Q(i-1) \tag{6}$$

where θ is the fraction of sites occupied by the siRNA, $[X]$ is the free siRNA concentration, X_t is the bulk siRNA concentration, M_t is the bulk PEI concentration, Q is the total heat content of the solution, $\Delta Q(i)$ is the heat released from the ith injection, V_o is the volume of the chamber, and dV_i is the injection volume at the ith injection.

Liposome Formation

1,2 Dipalmitoyl-sn-glycero-3-phosphocholine (DPPC), 1,2-dipalmitoyl-sn-glycero-3-phospho ethanolamine-N-[methoxy(poly(ethylene glycol))-2000] (ammonium salt) (PEG2000), and cholesterol were purchased from Avanti Polar Lipids, Inc. (Alabaster, AL). AG86 peptide (KSSLGGLPSHYRARNI)[269] was purchased from United Biosystems (Herndon, VA) and the peptide-amphiphile was synthesized as described previously.[67] x mol% AG86 peptide-amphiphile (x = 0-10), (60-x) mol% DPPC, 35 mol% cholesterol and 5 mol% PEG2000 dissolved in chloroform were combined in a round bottom flask at a total lipid content of 5 μmol and dried under a stream of argon. The solution was dried under argon at 60 °C to produce a homogeneous lipid film, followed by overnight incubation in a vacuum oven. This film was hydrated with 0.75 mL of 2 mM calcein or 1.5 mL of complexed siRNA/PEI at 45 °C for 1.5 h. These liposomes were extruded 11 times using a manual extruder (Avestin, Ottowa, ON) through 200 nm membranes. For siRNA liposomes, the unencapsulated siRNA was removed with overnight dialysis purification through a 1000 kDa MWCO cellulose ester membrane (Spectrum Laboratories, Rancho Dominguez, CA) and stored at 4–8 °C for up to 4 weeks.[79,272] Calcein liposomes were purified using a Sepharose CL-4B gel filtration column to remove unencapsulated material and stored at 4–8 °C for up to 4 weeks. Lipid concentration was measured using a phosphorous assay as described elsewhere[237] and peptide concentration was measured using a BCA Protein Assay Kit (Pierce Biotechnology, Rockford, IL). Liposome size and charge were measured using dynamic light scattering (DLS) and zeta potential analysis (Brookhaven Instruments Corporation, Holtsville, NY). A fluorescence standard relating calcein fluorescence to total lipid concentration was used to quantify the amount of bound and internalized lipid for calcein liposome experiments. siRNA quantification is described above.

Binding and Internalization of Fluorescent Liposomes

HeLa cervical cancer cells (American Type Culture Collection, Manassas, VA) were subcultured in black 96-well plates at 5,000 cells/well containing 200 μL Minimum Essential Media (MEM) supplemented with 10% fetal bovine serum, 100 units/mL penicillin and 0.1 mg/mL streptomycin. Targeted stealth liposomes encapsulating calcein with varying AG86 content (0-10

mol%) were incubated with HeLa cells for 3, 6, and 24 h at 37 °C and 5% CO_2 at a lipid concentration of 100 μM. After incubation, the cells were washed 3 times with phosphate buffered saline (PBS) and maintained at -80 °C for 24 h. The frozen cells were then thawed, lysed with lysis buffer (Promega, Madison, WI) and the calcein fluorescence was quantified at excitation/emission wavelengths of 485/515 nm. The total amount of bound and internalized lipids was calculated based on a standard curve relating fluorescence and lipid concentration.

Peptide and Antibody Blocking of Fluorescent Liposome Binding

HeLa cervical cancer cells were fixed by incubation in 4% paraformaldehyde (Sigma, St. Louis, MO) for 10 min at 25 °C, and aliquoted in 4 °C 1% w/v bovine serum albumin (ThermoFisher, Grand Island, NY), 0.9 mM $CaCl_2$, 0.5 mM $MgCl_2$ PBS at $5x10^6$ cells/mL. Cells were incubated with 10 μg/mL AG86 peptide, 1:100 dilution of rat anti-human CD49f/α_6 (eBioscience, Inc., San Diego, CA), or 1:100 dilution of MAB1964 mouse anti-human β_4 (EMD Millipore, Darmstadt, Germany) at 4 °C for 30 min. 50 μM AG86-functionalized stealth liposomes were added and incubated at 4 °C for 1 hr, then washed twice with 4 °C PBS and analyzed immediately on a BD Accuri C6 flow cytometer (Masonic Cancer Center, University of Minnesota).

Silencing of HPV-E7 Gene mRNA

HeLa cells were subcultured in clear 12-well plates at 50,000 cells/well in 2 mL of MEM and incubated for 24 h. 2.5 nM si18E7-674[264] was delivered to each well with the different transfection agents for 24 h at 37 °C and 5% CO_2. RNA extraction was conducted using the E.Z.N.A Total RNA Isolation Kit I (Omega Biotek, Norcross, GA) according to the manufacturer's protocol. The concentration of extracted RNA was quantified using an absorbance microspot reader (Biotek, Winooski, VT) and 1 μmol of RNA was converted to cDNA using RNA to cDNA EcoDry™ Premix (Double Primed) according to the manufacturer's protocol (Clontech, Mountain View, CA). HPV-E7 expression was quantified through a reverse-transcription polymerase chain reaction (RT-PCR) using PerfeCTa qPCR mix (Quanta Biosciences, Gaithersburg, MD) in a MX3000P qPCR machine (Agilent, Santa Clara, CA). The geometric mean of the reference gene threshold cycles ($C_{t,ref1}$, $C_{t,ref2}$) were used to normalize the HPV-E7 threshold cycle for each sample. TATA-binding protein (TBP) and tyrosine 3-monooxygenase activation protein-zeta (YWHAZ) were chosen as reference genes to minimize the effect of apoptosis on reference gene expression and subsequent mRNA expression measurements.[277] A buffer and RNA control were included for each experiment. The reference gene threshold was calculated as

$$C_{t,ref} = \sqrt{C_{t,ref1} x C_{t,ref2}} \quad (7)$$

where $C_{t,ref1}$ and $C_{t,ref2}$ are the threshold cycles of the individual reference genes.

HPV-E7 gene silencing was calculated using the following equations. First, the normalized sample threshold cycle, ΔC_t, was determined by subtracting the reference gene threshold cycle ($C_{t,ref}$) from the target gene threshold cycle ($C_{t,x}$) for each sample.

$$\Delta C_t = C_{t,x} - C_{t,ref} \quad (8)$$

The difference between treated and untreated threshold cycles, $\Delta\Delta C_t$, was then calculated by subtracting the $\Delta C_{t,untreated}$ of the untreated sample from the $\Delta C_{t,treated}$ of the treated sample.

$$-\Delta\Delta C_t = -(\Delta C_{t,treated} - \Delta C_{t,untreated}) \quad (9)$$

The fold silencing that was achieved in the treated sample relative to the untreated sample was calculated as follows.

$$Fold\ Decrease = 2^{-\Delta\Delta C_t} \quad (10)$$

Binding and Internalization of siRNA Liposomes

HeLa cells were subcultured in clear 12-well plates at 50,000 cells/well in 2 mL of MEM and incubated for 24 h. 2.5 nM encapsulated si18E7-674 was delivered and allowed to incubate for 24 h at 37 °C and 5% CO_2. Cells were then harvested with TrypleE Express cell dissociation agent (ThermoFisher Scientific, Grand Island, NY), pelleted by centrifugation at 500 g for 2.5 min, washed twice with 4 °C PBS and analyzed immediately on a BD Accuri C6 flow cytometer (Masonic Cancer Center, University of Minnesota). Fluorescence intensities were normalized to siRNA concentration with the concentration standard used to determine yield.

Cell Viability

HeLa cells were subcultured in clear 96-well plates at 5,000 cells/well in 200 µL of MEM and incubated for 24 h. 2.5 nM liposome encapsulated si18E7-674, nonsilencing siControl siRNA (siGENOME Nontargeting siRNA #2, GE Dharmacon, Lafayette, CO) or 750 nM (lipids) empty liposomes were delivered and allowed to incubate for 24 h at 37 °C and 5% CO_2. Cell viability was then measured using a WST-1 Cell Proliferation Reagent (Roche, Indianapolis, IN) following the manufacturer's protocol. Absorbance was measured using a Synergy H1 microplate reader (Biotek, Winooski, VT). Cell viability was normalized to untreated cells.

Statistics

ANOVA analysis and Tukey Kramer honest significant difference (HSD) test were performed to calculate p-values and determine statistical significance between means. When only two means were compared within an experiment, student's t test was used to calculate p-values.

Results

Binding and Internalization of Fluorescent Liposomes Delivered to HeLa Cells

To investigate the ability of AG86-functionalized stealth liposomes to target cervical cancer cells, calcein loaded liposomes were prepared with 0-10 mol% AG86 targeting peptide and delivered to HeLa cells for 3, 6 and 24 h at 37 °C. As delivery time increased, binding and internalization increased for all targeting peptide concentrations. Increasing the concentration of the targeting peptide results in a nonlinear increase in binding and internalization (Figure 20), which is likely mediated by increased peptide valency resulting in binding avidity.[278,279] Liposomes prepared with 5 mol% AG86 achieved significantly more efficient delivery compared to 0, 2 and 3 mol% peptide at all time points (Table 2), and was chosen as a sufficient targeting peptide formulation for subsequent gene delivery studies. To further verify that the AG86 peptide was responsible for liposome binding to HeLa cells, the binding of AG86-functionalized stealth liposomes was measured after incubation with free AG86 peptide and compared to binding without peptide blocking (Figure 21A). The presence of the free peptide decreased liposome binding by 98%, confirming AG86-mediated binding. The initial discovery of the AG86 peptide demonstrated specific interaction with the α_6 integrin.[269] The presence of anti-α_6 antibodies disrupted 40% of cellular adhesion to AG86 peptide coated surfaces.[269] The α_6 integrin is known to dimerize with either the β_1 or the β_4 integrin,[280] and while blocking with a β_1 specific antibody demonstrated that AG86 binding is not specific for the $\alpha_6\beta_1$ heterodimer, binding to the β_4 integrin was not explored.[269] We therefore investigated the binding interactions of the AG86 peptide using antibody blocking of AG86-functionalized stealth liposome binding to cells (Figure 21B). In the presence of anti-α_6 and anti-β_4 integrin antibodies, liposome binding is decreased by 66% and 86% respectively, verifying the $\alpha_6\beta_4$ integrin as the binding target of the AG86 peptide.

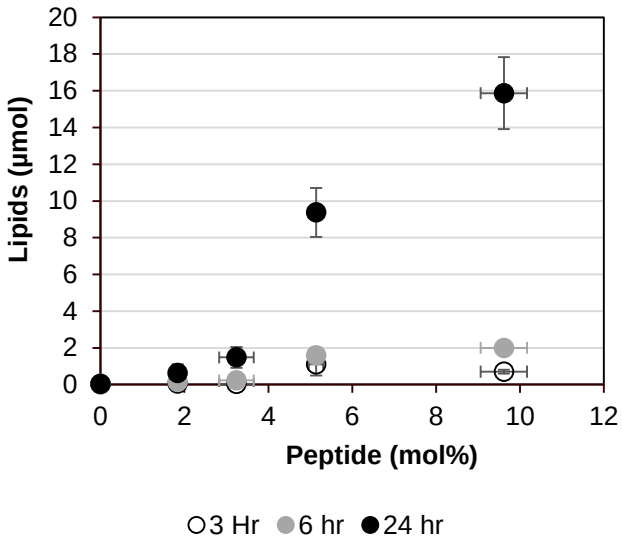

Figure 20. Binding and internalization of fluorescent targeted stealth liposomes.
0-10 mol% AG86-functionalized, calcein loaded, stealth liposomes were delivered at 100 µM lipids to HeLa cells for 3, 6, and 24 h at 37 °C and binding and internalization was examined by lysing cells and measuring fluorescence. Data are presented as the mean ± SE (n = 3-4, performed in triplicate). All p-values from statistical analysis are listed in Table 2.

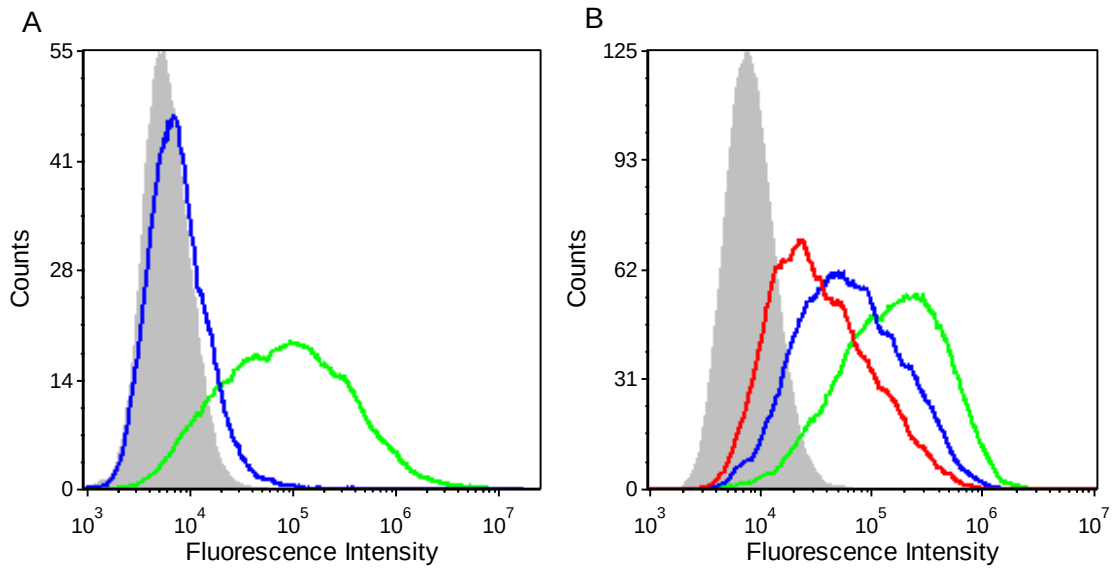

Figure 21. Peptide and antibody blocking of AG86-functionalized stealth liposomes
5-6 mol% AG86-functionalized, calcein loaded, stealth liposomes (green) were delivered at 50 µM lipids to HeLa cells at 4 °C for 1 h after a 30 min incubation of (A) 10 µg/mL free AG86 peptide (blue) or (B) 100x dilution of anti-α_6 (blue) and anti-β_4 (red) integrin antibodies. Binding was measured using flow cytometry. Untreated cells (grey) were measured for background fluorescence.

Table 2. p-values from ANOVA statistical analysis for Figure 20 showing binding and internalization of fluorescent liposomes with varying peptide concentration and incubation times.

3 h

0	1.8	3.2	5.1	9.6	Peptide (mol%)
	>0.05	>0.05	**<0.05**	>0.05	0
		>0.05	**<0.05**	>0.05	1.8
			<0.05	>0.05	3.2
				>0.05	5.1
					9.6

6 h

0	1.8	3.2	5.1	9.6	Peptide (mol%)
	>0.05	>0.05	**<0.01**	**<0.01**	0
		>0.05	**<0.01**	**<0.01**	1.8
			<0.05	**<0.01**	3.2
				>0.05	5.1
					9.6

24 h

0	1.8	3.2	5.1	9.6	Peptide (mol%)
	>0.05	>0.05	**<0.01**	**<0.01**	0
		>0.05	**<0.01**	**<0.01**	1.8
			<0.01	**<0.01**	3.2
				<0.01	5.1
					9.6

Characterization of siRNA/PEI Complexes

Before encapsulation in targeted liposomes, anionic siRNA was complexed with the cationic polymer PEI. siRNA was complexed at several different nitrogen:phosphate ratios (N:P) to investigate the effect of N:P ratio on yield and transfection efficiency. None of the particle sizes are significantly different between different N:P ratios (Figure 22).[281] As N:P ratio was increased from 2 to 8 and more positively charged polymer was added during complexation, the zeta potential increased from -11 to 13 mV (Figure 22). The larger standard error of the average particle size for siRNA/PEI complexes at N:P = 4 is indicative of the high size polydispersity observed from these complexes, as is commonly seen at N:P ratios that produce particles approaching a neutral charge or at the transition from negative to positive zeta potential associated with increasing N:P.[282–284]

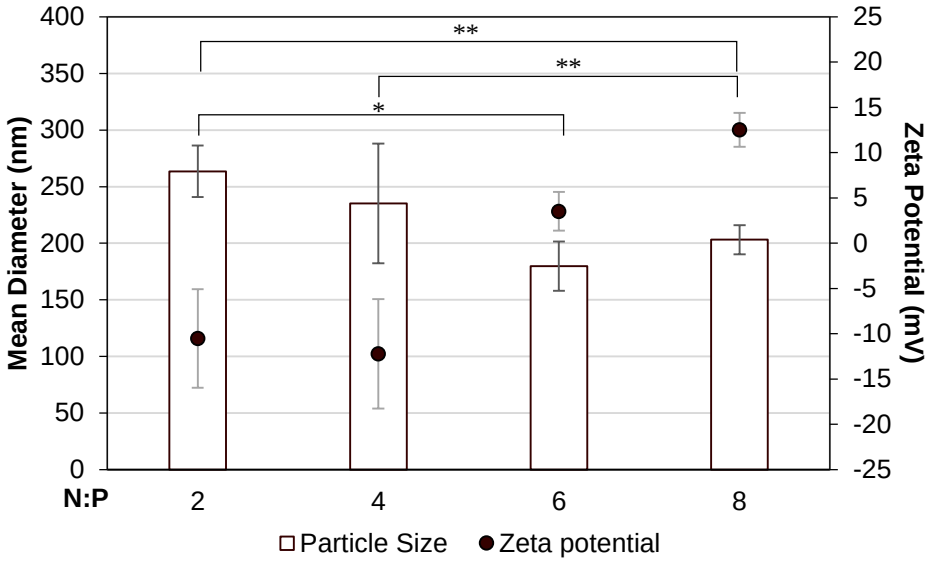

Figure 22. Size and zeta potential measurements of siRNA/PEI complexes.
siRNA/PEI particles were complexed at various N:P ratios, and size and charge were determined. Data are presented as the mean ± SE (n = 4-11). * p-value <0.05, ** p-value <0.005 comparing zeta potential measurements. There was no significant statistical difference for pairs without brackets.

Isothermal Calorimetry (ITC) Exploring siRNA/PEI Complexation

Microcalorimetric titrations of PEI into siRNA solutions were performed to monitor the thermodynamic properties associated with the formation of siRNA/PEI complexes. Titrations were performed over the entire range of N:P ratios investigated for transfection (Figure 23A, C). The calorimetry results over this N:P range showed complete saturation of siRNA with PEI between N:P 1 and 2. Others have observed DNA/PEI saturation between N:P of 2-3 using branched PEI of similar size,[276,282,285] and between 1-2.5 for siRNA/PEI.[286] In order to better observe the transition from free to fully complexed siRNA, titrations were also performed spanning N:P ratios of 0-2.5 (Figure 23B, D). A "one set of sites" model was used to calculate binding affinity, enthalpy and entropy of binding, and stoichiometry (Figure 23 and inset). The calculated binding affinity $K = 3.1 \times 10^6 \pm 1.2 \times 10^6\ M^{-1}$ and stoichiometry $n = 0.57 \pm 0.02$ are similar to those measured from ITC experiments of DNA/PEI complexes.[276,282] An n of 0.57 corresponds to an siRNA:PEI ratio of 25 and a negative to positive charge ratio of 1.7:1. This deviation from a charge ratio of 1:1 could be explained by a difference in linear intercharge spacing between siRNA (0.17 nm)[275] and PEI (0.25-0.35 nm).[287] Normalizing to the charge ratio, it's reasonable to expect the interaction of siRNA and PEI to resemble the interaction of DNA with PEI. The binding of siRNA and bPEI in distilled water was characterized using similar thermodynamic parameters, however an n of 2.26 was identified, requiring more PEI molecules for condensation of 1 siRNA molecule.[286] This discrepancy could

be caused by differing buffer conditions.[275] In Figures 23 A and B, large endothermic (positive) peaks are observed at the transition between free and complexed siRNA, and this has been attributed to an endothermic reorganization of saturated siRNA:PEI complexes into less siRNA-dense particles.[286]

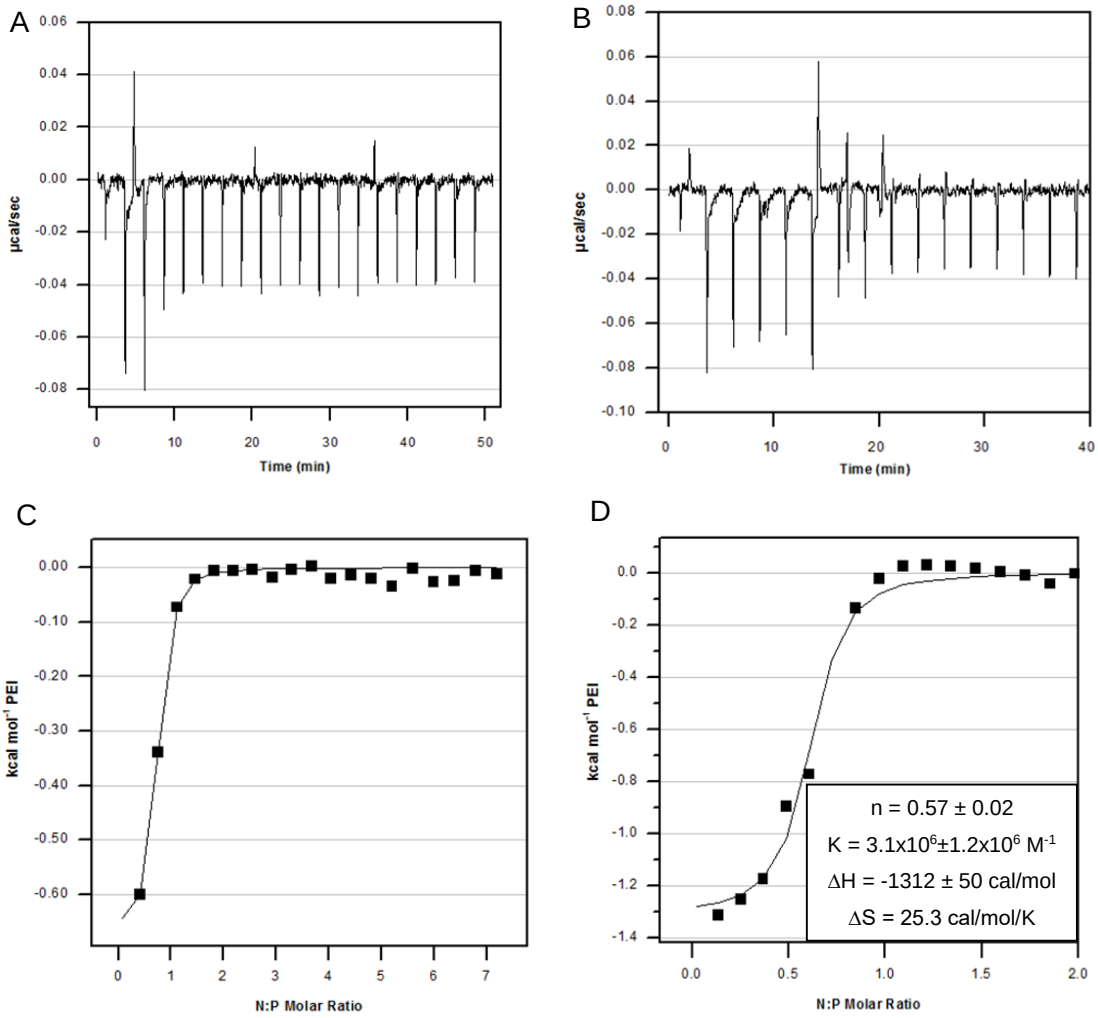

Figure 23. Representative ITC experiments showing raw (A-B) and integrated (C-D) data for the titration of PEI into siRNA in 6 mM HEPES buffer.
PEI was titrated into siRNA over N:P ranges of 0-8 (A, C) and 0-2.5 (B, D).

Characterization of Targeted Stealth Liposomes Encapsulating siRNA

siRNA/PEI complexes (N:P = 2-8) or uncomplexed siRNA (N:P = 0; no PEI) were encapsulated within 5 mol% AG86-functionalized stealth liposomes. The N:P ratio had no significant effect on liposome size or zeta potential and results were no different than size or zeta potential measured for empty stealth liposomes (Figure 24). The yield of siRNA encapsulation was measured using a standard created from the fluorescently labeled siRNA included in the complexes

(Figure 25).[272] Encapsulation of siRNA in neutral lipid delivery systems is historically limited by low entrapment efficiency.[288] However, targeted stealth liposomes encapsulating siRNA complexed to PEI achieved yields of up to 60% as shown in Figure 25.

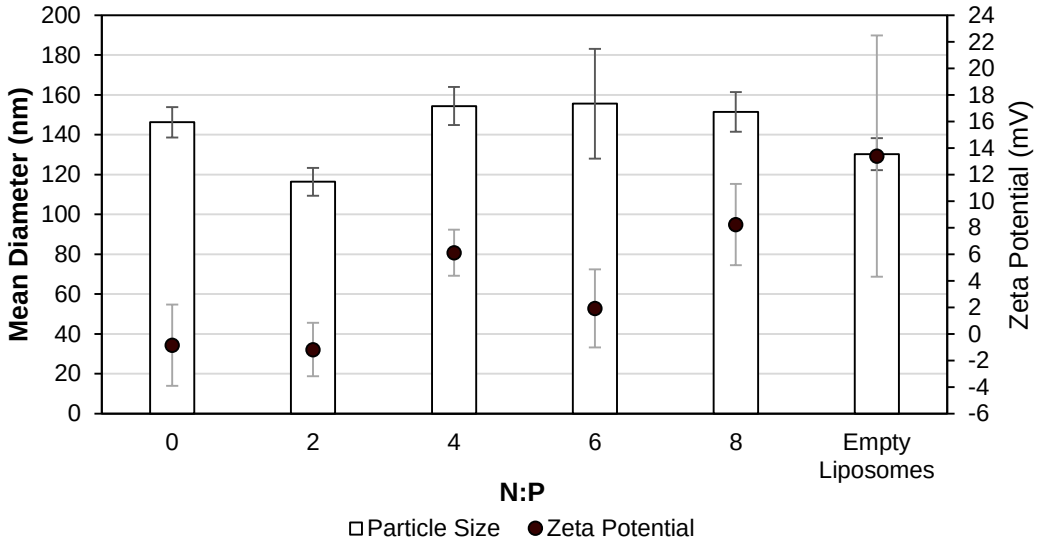

Figure 24. Size and zeta potential measurements of targeted stealth liposomes encapsulating siRNA. siRNA/PEI complexes were prepared at various N:P ratios, then encapsulated in stealth liposomes (5-6 mol% AG86) for characterization. N:P = 0 indicates encapsulation of uncomplexed siRNA (no PEI). There was no significant statistical difference for pairs without brackets. Empty stealth liposomes (5.3 mol% AG86) were prepared by hydrating lipid films with buffer. Data are presented as the mean ± SE (n = 3-6).

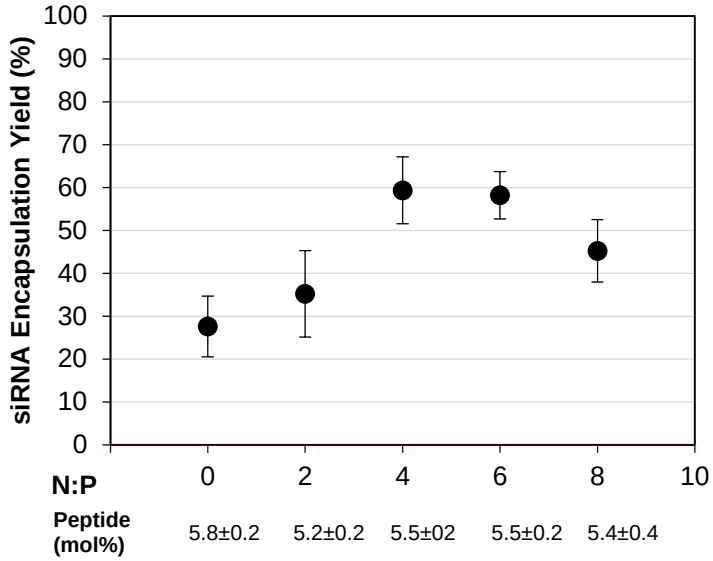

Figure 25. siRNA encapsulation yield in targeted stealth liposomes.
siRNA/PEI complexes were first prepared at various N:P ratios, then encapsulated in the targeted stealth liposomes for characterization. N:P = 0 indicates encapsulation of uncomplexed siRNA (no PEI). Yield is calculated as siRNA present in final liposomes solution compared to initial siRNA. Data are presented as the mean ± SE (n = 3-6, performed in triplicate). There was no significant statistical difference for all pairs.

mRNA Silencing from Targeted Stealth Liposomes Encapsulating siRNA

siRNA/PEI complexes encapsulated in targeted stealth liposomes and free siRNA/PEI were delivered to HeLa cells, and the resulting mRNA silencing from the delivery of HPV-E7 specific siRNA was measured 24 h after delivery using RT-PCR (Figure 26). The level of mRNA silencing increased with increasing N:P ratio up to N:P = 6 for both the free and encapsulated siRNA/PEI complexes. The encapsulated siRNA/PEI formed at N:P = 6 achieved significantly higher levels of silencing compared to the unencapsulated complexes at N:P = 6 and to targeted stealth liposome encapsulated siRNA/PEI formed at N:P = 0-4. HPV-E7 mRNA expression was reduced to 32 ± 7% of control levels with the N:P = 6 encapsulated siRNA/PEI complexes, a 10 fold improvement in silencing over free siRNA delivery (unencapsulated and uncomplexed siRNA, N:P = 0). Notably, the encapsulated siRNA/PEI complexes at N:P = 6 achieved a 2.6 fold decrease in expression compared to targeted stealth liposomes encapsulating uncomplexed siRNA (N:P = 0). Since the same siRNA concentration was used for all formulations, this suggests a benefit to transfection from the presence of PEI. The silencing achieved by the highest performing targeted stealth liposome formulation (complexed siRNA/PEI at N:P = 6 encapsulated in targeted stealth liposomes) was also compared to the silencing efficiency from nontargeted liposomes encapsulating siRNA/PEI complexes at the same N:P ratio and from Lipofectamine RNAimax, a commercial RNAi transfection reagent (Figure 27). The siRNA/PEI encapsulated in the targeted stealth liposomes achieved 1.9 fold decreased expression compared to the nontargeted formulations, and 2.2 fold decrease in expression compared to Lipofectamine, displaying superior *in vitro* delivery and transfection ability.

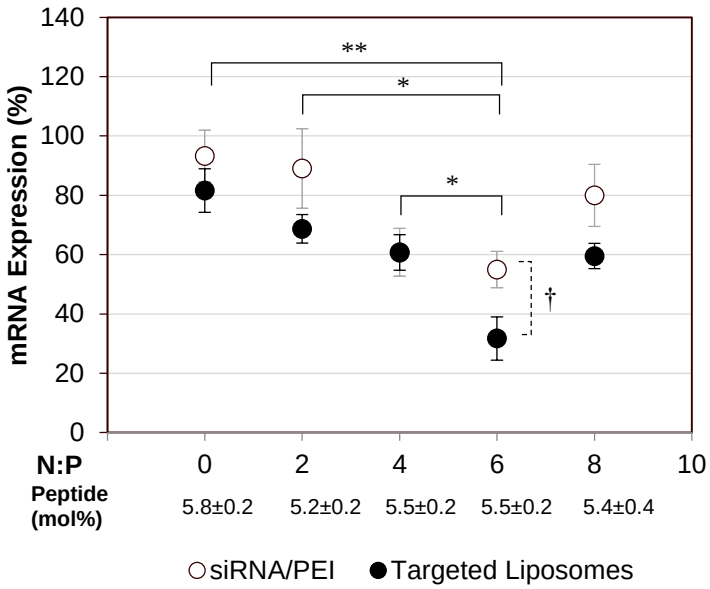

Figure 26. mRNA silencing from siRNA/PEI complexes in solution or encapsulated in targeted stealth liposomes.
HeLa cells were transfected with 2.5 nM siRNA for 24 h. mRNA expression was measured as % expression of HPV-E7 mRNA in HeLa cells compared to untreated cells. N:P = 0 indicates delivery of uncomplexed siRNA (no PEI). Data are presented as the mean ± SE (n = 3-7, performed in triplicate). * p-value <0.05, ** p-value <0.005 comparing targeted stealth liposome-encapsulated siRNA/PEI, and † p-value <0.05 comparing targeted stealth liposome-encapsulated siRNA/PEI to siRNA/PEI complexes in solution at the same N:P. There was no significant statistical difference for pairs without brackets.

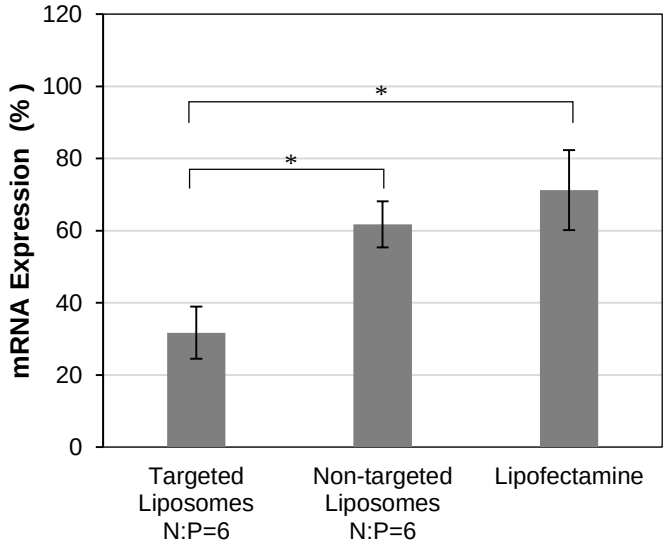

Figure 27. mRNA expression after siRNA transfection with various reagents.
siRNA was complexed with PEI at N:P = 6 and encapsulated in targeted (5.5 ± 0.2 mol% AG86) or nontargeted stealth liposomes, or mixed with Lipofectamine. mRNA silencing of HPV-E7 in HeLa cells was compared to untreated cells, 24 h after delivery of 2.5 nM of siRNA. Data are presented as the mean ± SE (n = 3-7, performed in triplicate). * p-value <0.05. There was no significant statistical difference for pairs without brackets.

Internalization of siRNA Encapsulated in Targeted Stealth Liposomes

In order to investigate further the benefit observed from complexation of siRNA with PEI before encapsulation, targeted stealth liposomes encapsulating uncomplexed siRNA (N:P = 0) or siRNA/PEI complexes (N:P = 6) were delivered to HeLa cells and the fluorescence intensity from the Cy5-labeled siRNA was used to compare the amount of the fluorescently labeled siRNA in the cells through binding and internalization of the two formulations. The fluorescence intensity from delivery of the targeted liposomes encapsulating complexed or uncomplexed siRNA was similar (Figure 28). The effect of siRNA loading in the targeted stealth liposomes was also considered. The theoretical fraction of loaded liposomes was calculated as reported previously,[272] using an average of 26.8 siRNA molecules per siRNA/PEI complex based on the number of siRNA-PEI binding sites (n = 0.57 ± 0.02) calculated using the ITC data shown in Figure 23. The theoretical loading of the uncomplexed siRNA in the targeted stealth liposomes is 100% compared to 34.0 ± 3.9% for the complexed siRNA. A difference in the fraction of loaded liposomes would therefore not explain the difference in transfection efficiency and since the presence of PEI has no apparent effect on the binding and internalization efficiency of the targeted liposomes encapsulating the siRNA, this suggests that the improved transfection efficiency observed in the presence of PEI is realized after internalization.

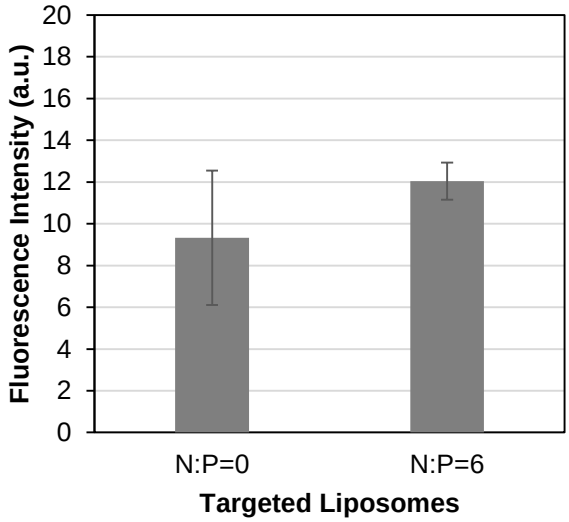

Figure 28. Binding and internalization of targeted stealth liposomes encapsulating siRNA.
Binding and internalization of targeted stealth liposomes encapsulating complexed siRNA/PEI (N:P = 6, 5.5 ± 0.2 mol% AG86) or uncomplexed siRNA (N:P = 0, 5.8 ± 0.2 mol% AG86) quantified using flow cytometry. 2.5 nM of Cy5-labeled siRNA were delivered to HeLa cells for 24 h. Background fluorescence of untreated cells was subtracted from data. Data are normalized to fluorescence vs. concentration standards for each liposome batch. Data are presented as the mean ± SE (n = 6). There was no significant statistical difference between the pair of means.

Cytotoxicity of siRNA Encapsulated in Targeted Stealth Liposomes

The optimized targeted stealth liposomes encapsulating siRNA/PEI at N:P = 6 were evaluated further for their cytotoxicity against $\alpha_6\beta_4$-expressing, HPV-containing cancer cells *in vitro*. The targeted stealth liposomes encapsulating either complexed (N:P = 6) or uncomplexed siRNA (N:P = 0) were delivered to HeLa cells and cell viability was assayed 24 h later. As Figure 29 shows, the nanoparticles with the complexed siRNA decreased cell proliferation by 30%, while those encapsulating the uncomplexed siRNA had no effect on cell proliferation. Increasing the concentration of liposome encapsulated, complexed siRNA delivered did not significantly increase the effect on cell proliferation (data not shown). 2.5 nM siRNA delivered using targeted stealth liposomes achieved 68% mRNA silencing, as shown in Figure 26, however protein expression and subsequent phenotypic effects are not quantitatively predicted by mRNA expression and may account for the observed 30% cell toxicity.[289,290] Our results are in agreement with previous findings where it was shown that silencing of the HPV-E7 gene using RNAi promoted 80-90% mRNA silencing and resulted in 40-60% inhibition of cell proliferation at early time points.[264,291] Therefore, continued doses of siRNA may be necessary to achieve more potent cytotoxicity effects.

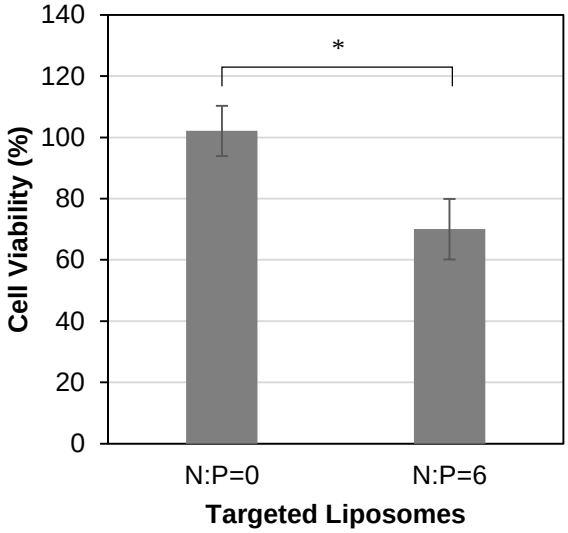

Figure 29. Cytotoxicity of targeted stealth liposomes encapsulating siRNA.
Cytotoxicity of targeted stealth liposomes encapsulating siRNA either complexed with PEI (siRNA/PEI at N:P = 6, 5.5 ± 0.2 mol% AG86) or uncomplexed siRNA (N:P = 0, 5.8 ± 0.2 mol% AG86). 2.5 nM of siRNA were delivered to HeLa cells for 24 h and toxicity from HPV-E7 silencing was measured by comparing cell viability of treated and untreated cells. Data are presented as the mean ± SE (n = 4, performed in triplicate). * p-value <0.05.

The cytotoxicity from the individual components of the targeted stealth liposomes encapsulating siRNA/PEI was also investigated. Empty targeted stealth liposomes and siRNA/PEI

complexes of a nonspecific sequence were delivered to the HeLa cells either free in solution or encapsulated in the targeted liposomes. As Figure 30 shows, none of the isolated components exhibited significant cytotoxicity compared to the untreated control, thus concluding that the toxicity observed in Figure 29 was the result of transfection of the si18E7-674 siRNA sequence.

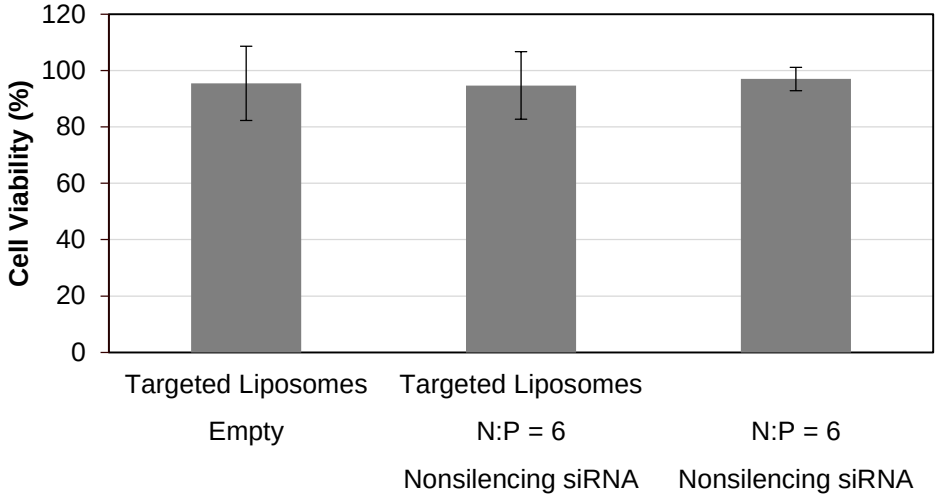

Figure 30. Toxicity from the components of targeted stealth liposomes used for siRNA delivery. The targeted stealth liposomes (750 nM lipids or 2.5 nM siRNA) were delivered to the cells. Empty targeted liposomes (5.3 ± 0.1 mol% AG86), siRNA/PEI particles (N:P = 6) of nonsilencing siRNA, and siRNA/PEI particles (N:P = 6) of nonsilencing siRNA encapsulated in the targeted liposomes (4.9 ± 0.2 mol% AG86) were delivered to HeLa cells for 24 h and toxicity was measured by comparing cell viability of treated and untreated cells. Data are presented as the mean ± SE (n = 3, performed in triplicate). There was no significant statistical difference between any pairs.

Discussion

Numerous gene silencing targets with therapeutic potential to treat cancer, viral infections and respiratory diseases have been identified, but effective systemic gene delivery strategies are critical for successful pursuit of these genetic targets.[255,256,265] While cationic polyplexes or lipoplexes mediate extremely effective RNAi transfection *in vitro*, their instability and immunogenicity *in vivo* preclude their clinical success, which has inspired numerous synthetic alternatives.[197,199,254,257,288,292] Most notably, stable nucleic acid lipid particles (SNALPs), liposome-polycation-DNA, cyclodextrin nanoparticles, and lipidoids are cationic lipid and polymer based nanoparticles that have become extremely popular for preclinical exploration of siRNA delivery for cancer therapy.[253,254,293] Liposome-polycation-DNA particles composed of both DNA and siRNA complexed with protamine, coated with cationic liposomes, shielded with PEG and targeted to a lung cancer biomarker were used to deliver growth receptor silencing siRNA to lung tumors in mice and achieved extremely high tumor localization. Interestingly, the presence of the targeting

ligand didn't improve tumor localization, but did mediate enhanced cellular uptake and therefore silencing and tumor cell apoptosis. However, the targeted nanoparticles also elicited high levels of cytokine production.[294] siRNA complexed with a cationic peptide, encapsulated in cationic liposomes and coated in cleavable PEG were designed for the PEG to be cleaved upon exposure to tumor associated matrix metalloproteinases. The addition of PEG or cleavable PEG improved tumor accumulation 10-20 fold over naked nanoparticles, but silencing was significantly improved only in nanoparticles modified with cleavable PEG, allowing for internalization and transfection.[295] A large lipidoid library was synthesized to develop structure function relationships for amine functionalized lipid molecules used for the production of biodegradable siRNA lipidoid nanoparticles.[296] Structure function relationships developed from transfection efficiency analysis of this lipidoid library were used to predict and design highly efficient siRNA delivery vehicles. The optimal PEGylated siRNA lipidoid nanoparticles achieved more than 95% protein silencing *in vivo* in hepatocytes.[296] Interestingly, surface pKa of a particular lipidoid was a critical parameter for predicting transfection efficiency for a particular lipidoid nanoparticle.[296] The SNALPs are a well-studied nontargeted lipid based delivery vehicle which has seen great success in preclinical studies. In one study, SNALPs were used to silence polo-like kinase 1 in tumors while abrogating activation of innate immune response and reducing tumor size by 75%.[297] Transferrin targeted cyclodextrin particles have also successfully delivered siRNA to tumors *in vivo*, and an accumulation/function study again revealed similar tissue accumulation for targeted and nontargeted nanoparticles, but enhanced transfection associated with targeting.[298] Preclinical results from SNALP and cyclodextrin nanoparticle development motivated clinical trials for oncogene silencing and cancer treatment.[293] With these advances, many biodistribution challenges have been addressed, and often the key barrier lies in specific cellular uptake and appropriate intracellular release.[198,265]

Previous work within our group has shown that pDNA condensed with PEI can be fully encapsulated within neutral stealth liposomes composed of the same materials as FDA approved doxil and other clinical liposomal cancer treatments.[79,272] Stealth liposomes encapsulating pDNA/PEI complexes were functionalized with a targeting peptide for specific delivery to $\alpha_5\beta_1$-expressing cancer cells and demonstrated excellent *in vivo* delivery and transfection in a metastatic colorectal mouse model.[79] Furthermore, a modular multifunctional gene delivery system was prepared in our group by combining the extracellular targeting ability of peptide-functionalized stealth liposomes with a new form of transcriptional targeting, by designing a therapeutic pDNA under the control of an NF-κB responsive element. The targeted nanoparticles (encapsulating pDNA/PEI complexes) specifically killed close to 70% of cancer cells while minimally affecting

healthy cells *in vitro*.[299] Mechanistic investigations revealed that stealth liposomes targeting the $\alpha_5\beta_1$ integrin and encapsulating pDNA/PEI complexes internalized into DLD-1 colorectal cancer cells through macropinocytosis and caveolar mediated endocytosis. The targeted stealth liposomes achieved higher transfection efficiency and more efficient endosomal release than pDNA/PEI complexes alone, suggesting a cooperative effect on internalization and intracellular delivery mediated by the targeted stealth liposomes encapsulating pDNA/PEI complexes.[274]

Our *in vitro* and *in vivo* delivery success with plasmid transfection prompted translation of targeted stealth liposomes encapsulating pDNA condensed with PEI to the equally challenging technology of specifically delivering siRNA. Our discoveries, along with evidence in the literature from various nonviral gene delivery vehicles that the key delivery barriers may lie in intracellular activity,[265,272] inspired the hypothesis that PEI complexation of siRNA, though not necessary for encapsulant size considerations as in the case of pDNA, may provide additional benefits to siRNA delivery using targeted stealth liposomes. In this work, we designed AG86-functionalized stealth liposomes that targeted $\alpha_6\beta_4$-expressing HeLa cervical cancer cells with the goal of delivering the si18E7-674 siRNA sequence, developed to silence the HPV-E7 gene. The delivery vehicle design considerations addressed here included identifying 5 mol% as a sufficient AG86 peptide concentration for binding and internalization, exploring the necessity of PEI complexation before encapsulation, and then identifying the optimal N:P ratio for effective transfection efficiency.

ITC analysis demonstrated that siRNA complexes are saturated with PEI at N:P = 2, however increasing the N:P ratio increased the zeta potential of the complexes. This seemingly conflicting result seems to support the binding model proposed in the literature, where siRNA escapes from initial nanocomplexes near N:P = 1 and reorganizes into nanoparticles with fewer siRNA molecules per particle in the presence of additional polymer,[286,300,301] which would result in more positive charge dense complexes without significantly changing complex size. siRNA complexed with PEI was efficiently encapsulated in targeted stealth liposomes, achieving on average 60% encapsulation yield, where other neutral lipid based vehicles encapsulated 10% or less.[288] It was found that there was no significant statistical difference in encapsulation yield between targeted stealth liposomes encapsulating siRNA/PEI complexed at different N:P ratios, while silencing increased with increasing N:P up to N:P = 6. Others have also observed an increase in siRNA transfection using PEI with increasing N:P up to a certain ratio, followed by a decrease in transfection efficiency. The increase in transfection with increasing N:P ratio was attributed to higher uptake, and the decrease attributed to increasing cytotoxicity at higher N:P ratios.[270,281,284,286] Since binding and internalization of the targeted stealth liposomes is largely driven by the targeting peptide as shown before and in Figure 20,[274] and not by the presence of PEI in the liposomes, this explanation is

insufficient. Therefore, we speculate that the increase in siRNA silencing with an optimal N:P ratio of the encapsulated siRNA/PEI is more likely caused by an optimization of the local buffering capacity within the liposome.[302–304] Since targeted stealth liposomes encapsulating siRNA/PEI complexes at N:P = 6 showed no difference in binding and internalization compared to liposomes encapsulating uncomplexed siRNA (N:P = 0), as shown in Figure 28, but achieved 3.7 fold higher silencing efficiency (Figure 26), this indicates that the PEI complexation of siRNA in these gene delivery vehicles may have improved efficiency either through carrier release, endosomal escape, or a combination of both. PEI mediated endosomal release could minimize immunogenicity, as it has been found that the endosomal acidification process is crucial to siRNA induction of the interferon and cytokine response.[305]

Active targeting has been shown to significantly improve transfection for several other gene delivery vehicles.[294,298,306] Targeting can be desirable as it can both increase the concentration of internalized siRNA and influence trafficking pathways into the cell. Therefore, in addition to any benefit PEI may provide, the actual internalization pathway of the targeted delivery vehicle after binding to the receptor of choice may play a synergistic role, as shown in the case of stealth liposomes targeting the $\alpha_5\beta_1$ integrin and encapsulating pDNA/PEI complexes.[274] The internalization pathways of the $\alpha_6\beta_4$ integrin have yet to be elucidated,[280,307–310] but it is possible that they may play a synergistic role in transfection efficiency.

Targeted stealth liposomes encapsulating siRNA/PEI at N:P = 6 decreased the proliferation of HeLa cells by 30% on average with 2.5 nM si18E7-674, demonstrating a potential therapeutic effect for this system while suggesting that repeated doses of this siRNA sequence may be necessary to achieve more potent cytotoxicity effects.

A significant challenge for cancer therapy lies in the effective discrimination between healthy and tumor tissue. Targeting delivery vehicles to cancer biomarkers in order to improve delivery specificity has been explored in depth, however, off target delivery is a common limitation of this scheme.[311,312] Additional genetically mediated targeting could potentially overcome this obstacle by removing off target effects from the therapy itself.[299,313,314] Each aspect of the targeted stealth liposome encapsulating siRNA/PEI complexes, provided a significant delivery mediator: the vehicle targeting mediating cell internalization and improving bioavailability of the therapy at the tumor site, and the viral-specific gene silencing minimizing off target effects since healthy cells lack the targeted viral genome. Combined with the improvement to intracellular availability and transfection through PEI complexation, targeted stealth liposomes encapsulating siRNA/PEI complexes provide an example of a modular gene delivery vehicle designed to address each barrier to gene therapy.

Acknowledgements

The flow cytometry analysis was performed in the University of Minnesota Flow Cytometry Resource. The ITC experiments were performed in the lab of Prof. Courtney Aldrich and we thank Dr. Feng Liu for his technical support. The PCR experiments were performed in Prof. Wei-Shou Hu's lab. This work was funded by NSF/CBET-1403564.

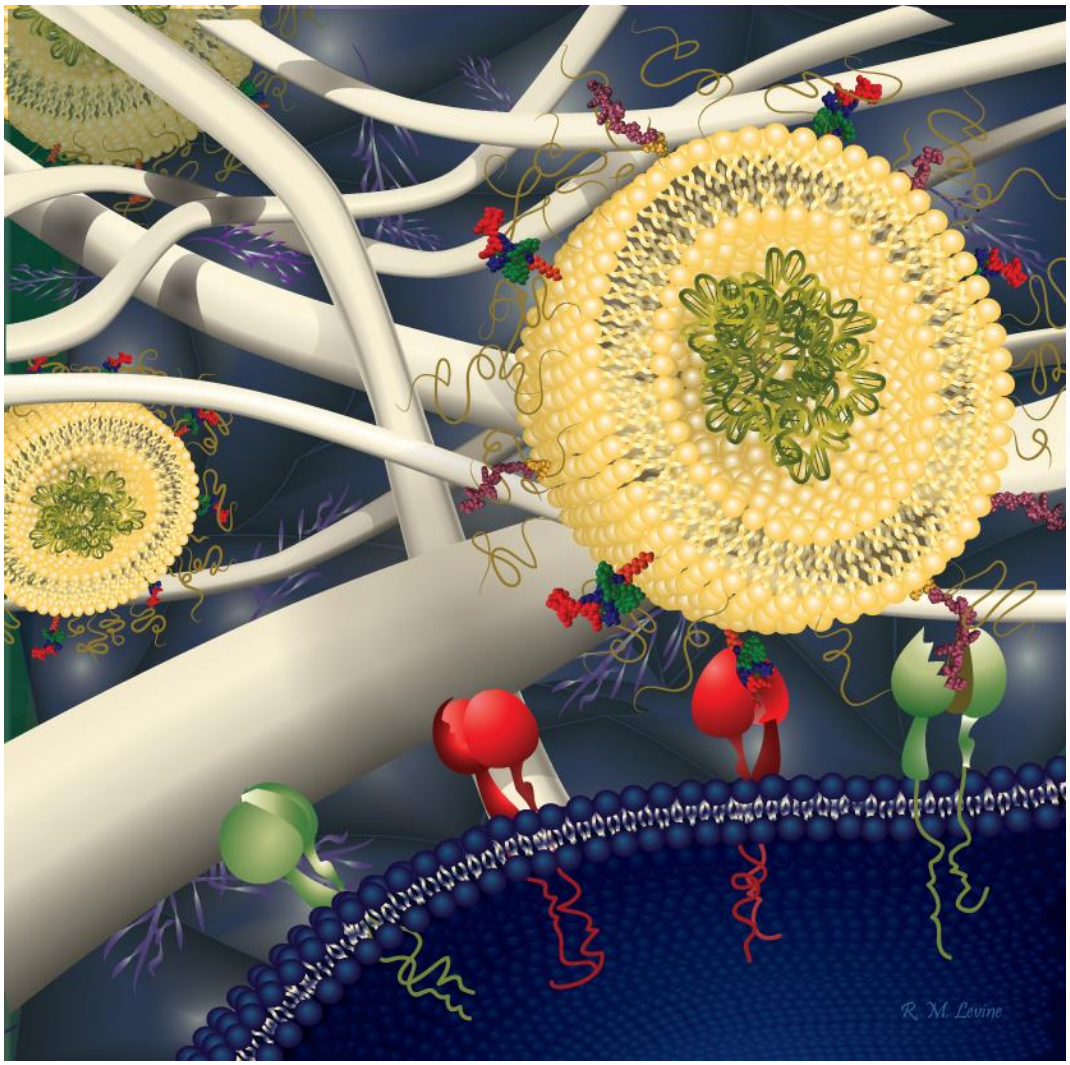
R. M. Levine

Chapter 4 Theoretical and *In Vitro* Understanding of the Effect of Ligand-Receptor Valency on Dual-Ligand Nanoparticle Delivery

Introduction

Effective chemotherapy is limited by the nonspecific delivery of toxic cancer drugs, causing harmful side effects and limiting clinical dosages. Targeted drug delivery strategies have increased the bioavailability of therapeutics to cancer tissue, decreased side effects from off target delivery to healthy tissue, and greatly improved clinical outcomes. Targeting to tumor tissue is mediated by ligands identified or designed to specifically bind to aberrantly expressed cancer biomarkers.[315–318] Specific targeting using antibodies to CD20 and human epidermal growth factors 1 and 2 (EGFR and HER2) has revolutionized clinical treatment of multiple myeloma, colorectal carcinoma, lymphoma, and breast cancer,[316,319] and nanoparticle therapies targeting the transferrin receptor and EGFR have entered clinical trials.[315,318,320] Unfortunately, targeted cancer biomarkers are not entirely unique to cancer, and low or even comparable levels of expression of the same cancer-associated receptors can be found on certain healthy tissues.[321–323] While targeting can decrease nonspecific delivery to most healthy tissue, off-tumor, target-related toxicity can occur through delivery to healthy tissue with measurable expression of the targeted receptor, resulting in the clinical challenge of mechanism-based toxicity.[311,324] As a potential solution to this challenge, dual-ligand nanoparticle drug delivery is explored here with two goals in mind: first, to effectively increase the targeted receptor density on cancer cells by targeting more than one receptor, therefore enhancing delivery, and second, to improve selectivity for cells with overexpression of both targeted receptors.

In this investigation, we have created dual-ligand stealth liposomes functionalized with peptides targeting the $\alpha_5\beta_1$ and $\alpha_6\beta_4$ integrins. Stealth liposomes represent an effective delivery vehicle taking advantage of passive targeting through the enhanced permeability and retention effect.[325] The polyethylene glycol (PEG) layer that decorates the surface of the stealth liposomes provides them with superior serum stability, extended blood circulation kinetics, and immunogenic protection, resulting in clinically relevant tumor accumulation and drug delivery.[203,326,327] In order to exploit these benefits for gene delivery, we have previously developed stealth liposomes encapsulating siRNA or plasmid DNA (pDNA), which have demonstrated effective delivery to

several cancer cell types (See Chapters 2 and 3).[79,272,274,299] The $\alpha_5\beta_1$ and $\alpha_6\beta_4$ integrins were chosen as appropriate receptors for dual-ligand targeting because they are upregulated in many of the same cancer types including breast,[268,323,328–330] colon,[331–333] and prostate[334–337] and are often associated with metastatic development.[337–339] Both integrins are internalized and recycled,[280,308] a desirable characteristic for a drug delivery target.[315] The apparently contrasting expression of each of these integrins in healthy tissues makes them relevant receptors to appropriately distinguish between single-receptor expressing cells and dual-receptor expressing cancer tissue *in vivo*.[323,340]

Peptides are ideal as targeting ligands for delivery applications because they can be designed or selected for high target specificity, and elicit low toxicity and immunogenicity.[20,198] The use of peptide ligands also provides flexibility and control of ligand incorporation into liposomes. Peptide-amphiphiles can be synthesized to directly participate in liposome self-assembly so that peptide valency can be controlled through variation of peptide-amphiphile concentration during assembly. A peptide ligand, PR_b, was developed within the Kokkoli group for enhanced specificity for the $\alpha_5\beta_1$ integrin.[67,70,71] It has been successfully utilized for targeted drug and gene delivery *in vitro* and *in vivo* for applications to prostate, breast, and colon cancer.[69,72,73,75,78,79,206,273] The AG86 peptide was identified through bead display of laminin derived peptides to bind specifically to the α_6 integrin, but not the β_1 integrin.[269] As the α_6 integrin is known to heterodimerize with either the β_1 or β_4 integrin,[341] it was hypothesized that the AG86 peptide was specific for the α_6 integrin or the $\alpha_6\beta_4$ integrin pair. The AG86 peptide was used here for the first time as a targeting ligand, and shown to be an effective ligand for drug delivery.

The potential of dual-ligand functionalized nanoparticles has been explored recently with varied levels of success,[8,312,342–354] however very few investigations attempted to quantify the parameters affecting nanoparticle binding and internalization, which is critical for a systematic understanding of future vehicle design. For example, stealth immunoliposomes targeting CD19 and CD20 showed additive binding effects when comparing the same total antibody concentration between dual- and single-ligand liposomes. However, increasing valency for the dual-ligand liposomes decreased uptake, which was suggested to be caused by steric effects.[342] A fluorescent assay was developed within that study to quantify individual antibody densities but ligand affinities and receptor expressions were not addressed.[342] Stealth immunoliposomes functionalized with folic acid and anti-EGFR antibodies demonstrated an impressive selectivity achieved by combining suboptimal single-ligand densities for dual-ligand delivery, however, lack of characterization of ligand affinities, receptor expression or internalization rates precludes the development of generalizable design parameters from these results.[312]

Dual-ligand nanoparticles have also been explored for gene delivery as a virus-mimetic delivery scheme. Polyethylenimine (PEI) polyplexes functionalized with native ligands targeting the transferrin receptor and EGFR improved transfection compared to single-targeted polyplexes.[344] Discussion of ligand affinities or quantitative receptor expressions were absent. Functionalizing PEI with targeting ligands presents a challenge to ligand valency estimation because polyplex formation results in a large proportion of free PEI,[249] and no further ligand quantification was provided outside of initial ligand concentration.[344] Polyplexes targeted to choroidal neovascularization via transferrin and RGD (to target the transferrin receptor and the $\alpha_v\beta_3$ integrin) and delivered *in vivo* achieved less efficient delivery than single-targeted RGD polyplexes. Expression levels for the two receptors were not confirmed in the target tissue, and delivery localization suggested that the two ligands had targeted two distinct tissues, rather than simultaneously targeting the same cells.[345] PEI polyplexes functionalized with two peptides targeting the transferrin receptor and the $\alpha_v\beta_3$ integrin showed improved *in vitro* transfection in prostate cancer cells when compared to single-ligand polyplexes with half the overall peptide density.[8] Internalization and blocking observations of the dual- and single-ligand polyplexes led to the hypothesis that each ligand provided a unique delivery mechanism, binding via $\alpha_v\beta_3$ and internalization via the transferrin receptor.[8]

Stealth liposomes targeted to $\alpha_v\beta_3$ and galectin-1 for magnetic resonance imaging of tumor angiogenesis showed enhanced uptake *in vitro* when compared to single-ligand liposomes with the same individual peptide density but lower overall peptide density. Dual-ligand liposomes also demonstrated enhanced uptake compared to combinations of single-ligand liposomes delivered simultaneously.[346] *In vivo* delivery of these liposomes resulted in similar tumor accumulation between dual- and single-ligand liposomes, but dual-ligand liposomes mediated endothelium localization while RGD liposomes remained in the lumen.[347] The effect of ligand and receptor density and ratio, as well as mobility on binding of dual-targeted immunoliposomes was also explored. NonPEGylated immunoliposomes targeted to ICAM and E-selectin were produced with constant overall antibody densities but varying antibody ratios. When delivered to cells with similar upregulated expression of both receptors, dual-ligand immunoliposomes with equal antibody valency achieved superior delivery.[348–350] The effect of membrane fluidity and lipid raft formation was also explored using liposomes with immobile surfaces and cells with disrupted lipid rafts. Effective delivery was only achieved in the presence of lipid rafts and fluid liposome surfaces suggesting that clustering effects from both the ligand and the receptor are critical for dual-ligand binding of immunoliposomes.[348] These studies highlight the complex design criteria significant for dual-ligand binding. More recently, gold nanoparticles targeted to the transferrin receptor and

EGFR using peptides with similar affinity and functionalized with a constant number of peptides per nanoparticle exhibited higher accumulation in dual- compared to single-expressing cells, and compared to single-ligand nanoparticles.[354] Similar internalization rates were observed for the two receptors, reiterating the importance of characterizing vehicle parameters in heteromultivalent systems. These results emphasize the need for understanding and characterization of the key parameters that can influence dual-ligand multivalent binding as they can be critical to intelligent vehicle design.

When assessing a multivalent system, there are many parameters which influence the binding kinetics and thus the delivery vehicle's efficiency and selectivity in binding. The affinity of a nanoparticle for a cell is determined by the available valency of interaction, which is affected by the size of the nanoparticle, the affinity of individual binding events between a ligand-receptor pair, the local receptor density, the length of the bound ligand-receptor pair and the local peptide density.[278,279,355–358] When multiple ligands are attached to the same molecule or vehicle and interact with receptors attached to a surface, each additional ligand-receptor pair that participates in a binding event contributes to the apparent affinity of the construct. Importantly, it has been observed that an increase in ligand-receptor valency contributes more than an additive increase to affinity, and this phenomena is referred to as avidity.[279,356,357,359–361] The surface density of a receptor therefore has a significant effect on the delivery efficiency of targeted nanoparticles, and with the introduction of a second ligand to the liposomes, the density of both targeted receptors and the ratios of each receptor on a cell will strongly influence nanoparticle binding. The density and ratio of both ligands, as well as the comparative affinities of the two interactions become additional controllable parameters. This study explores how variations in these parameters affect the efficiency and selectivity of a dual-targeting nanoparticle system both *in vitro* and using a kinetic binding model. In order to identify cell lines with a wide range of receptor expression levels and ratios, the expression of α_6, β_4 and $\alpha_5\beta_1$ integrins were quantified on multiple cell lines. A theoretical model was developed to explore the effects of cellular receptor expression and liposome ligand density on the binding of AG86/PR_b dual-ligand nanoparticles to cancer cells. Guided by the model results, *in vitro* studies were used to explore the actual enhancement to delivery and selectivity achieved with dual-ligand nanoparticles to cells with various receptor expression levels. A fluorescent assay for quantification of the peptide ratios incorporated in the dual-ligand liposomes is described for careful characterization of the peptide ratios. Integrin internalization rates were measured for several cell lines. Dual- and single-ligand liposomes were delivered to cells at 4 °C and 37 °C to evaluate heteromultivalent nanoparticle binding and internalization, and transfection studies demonstrated the potential of dual-ligand liposomal gene delivery.

Materials and Methods

Cell Culture

A-431, LS 174T, MDA-MB-231, MDA-MB-435, MDA-MB-468, and SK-OV-3 were grown in Dulbecco's Modified Eagle Medium (DMEM) (ThermoFisher Scientific, Grand Island, NY). HT-1080, LNCaP, OVCAR-3, PC3-LN4, and SW 1990 were grown in Roswell Park Memorial Institute 1640 medium (RPMI) (ThermoFisher Scientific, Grand Island, NY). HCT116 and HT29 were grown in McCoy's 5A medium (ThermoFisher Scientific, Grand Island, NY). DU145, HEPG2, and RKO were grown in Minimal Essential Medium (MEM) (ThermoFisher Scientific, Grand Island, NY), and BJ-fibroblasts, DLD-1, and MCF7 were grown in DMEM without sodium pyruvate (ThermoFisher Scientific, Grand Island, NY). All media were supplemented with 10% (v/v) fetal bovine serum (FBS), 100 units/ml penicillin, and 0.1 mg/ml streptomycin (ThermoFisher Scientific, Grand Island, NY). Cells were obtained from the American Type Culture Collection and A-431, LS 174T, MDA-MB-435, MDA-MB-468, SK-OV-3, HT-1080, PC3-LN4, SW 1990, HCT116, and HT29 were a gift from Professor Hackel, University of Minnesota. Cells were cultured in T75 flasks in DMEM at 37 °C and 5% CO_2 and passaged when they reached 60-80% confluence by treatment with TrypLE Express cell dissociation agent (ThermoFisher Scientific, Grand Island, NY).

Receptor Expression Quantification

Cells were harvested and resuspended in 4 °C PBSA (1 w/v% bovine serum albumin (BSA) in phosphate buffered saline (PBS)), and incubated with a 1:100 dilution of MAB1969 mouse anti-human $\alpha_5\beta_1$ antibody (EMD Millipore, Darmstadt, Germany), MAB1964 mouse anti-human β_4 (EMD Millipore, Darmstadt, Germany), rat anti-human CD49f/α_6 (eBioscience, Inc., San Diego, CA), IgG from murine serum (Sigma Aldrich, St. Louis, MO), or purified rat myeloma IgG2a (Life Technologies, Grand Island, NY) for 20 min at 4 °C on a rotary shaker. Separate α_6 and β_4 antibodies were used because no $\alpha_6\beta_4$ heterodimer antibody was available at the time of this study. Cells were pelleted by centrifugation at 500 *g* for 2.5 min, washed twice with 4 °C PBSA and incubated with 1:100 dilution of Alexa Fluor 488 goat anti-mouse IgG or Alexa Fluor 488 donkey anti-rat IgG (Life Technologies, Grand Island, NY) for 15 min at 4 °C on a rotary shaker. Following incubation, cells were pelleted by centrifugation, washed twice with 4 °C PBSA and analyzed immediately on a BD Accuri C6 flow cytometer (Masonic Cancer Center, University of Minnesota). Fluorescence intensity from isotype labeled controls were subtracted as background.

To determine the number of cell surface receptors from fluorescence intensity data, antibody binding capacities were compared with a standardized microbead calibration plot using Quantum Simply Cellular Bead standards (Bangs Laboratories, Inc., Fishers, IN) that were stained and measured in the same manner as the cells.

Heteromultivalent Kinetic Model Development

The kinetics of monovalent binding where one ligand binds to one receptor to form a complex, with forward and reverse reaction rates k_f and k_r, is well established, and has frequently been extended to multivalent binding.[355,356,358–360,362] Complexes in multivalent interactions can be formed between *n* ligands and receptors to form a multivalent complex (C_n), with a forward reaction rate k_x governing an additional ligand binding to produce C_{n+1}, and a reverse reaction rate k_{-x} governing the dissocation of one ligand to produce C_{n-1} (Equation 11).

$$R_i + L \underset{k_r}{\overset{k_f}{\rightleftharpoons}} C_1 + R_{i-1} \underset{k_{-x}}{\overset{k_x}{\rightleftharpoons}} C_2 + R_{i-2} \underset{k_{-x}}{\overset{k_x}{\rightleftharpoons}} \dots \underset{k_{-x}}{\overset{k_x}{\rightleftharpoons}} C_n + R_{i-n} \qquad (11)$$

In the case of multivalent binding of two distinct ligand receptor pairs (ligand *a*-receptor *a* and ligand *b*-receptor *b*), we must track which pair participates in each binding event. For example, consider nanoparticle *L* with ligands *a* and *b* which can bind to receptors *a* and *b*. From the state represented by C_{1a1b} in Scheme 1 (where one *a* and one *b* ligands are bound), four different events can proceed: a second ligand *a* can bind at a forward rate of k_{xa} to produce C_{2a1b}, a second ligand *b* can bind at a forward rate of k_{xb} to produce C_{1a2b}, ligand *a* can dissociate at a reverse rate of k_{ra} to produce C_{1b}, or ligand *b* can dissociate at a reverse rate of k_{ra} to produce C_{1a}. Each of these events contribute to the accumulation of bound nanoparticles at that particular binding state, defining the rate equation for C_{1a1b}. Using this general scheme, Caplan and Rosca[362] developed a heterovalent binding model for multiligand molecules containing two of each or three of each ligand. We expanded this model here to incorporate the additional valencies (up to a total valency of 8 for the ligand-receptor pairs) and combinations of valencies encountered between a dual-ligand multivalent nanoparticle and a cell. Scheme 1 represents a nanoparticle with a total valency of 4 and individual ligand valency of 2 for each ligand-receptor pair.

Nanoparticle binding was modeled simultaneously for three representative cell lines; one with receptor expression similar to the high dual-receptor expressing SK-OV-3 cells (R_a=200,000, R_b=200,000), one with higher expression of receptor *a* (R_a=200,000, R_b=25,000) and one with higher expression of receptor *b* (R_a=25,000, R_b=200,000). The kinetic parameters used in the

model, including k_r, k_f, k_x, k_{-x}, and K_d for ligands *a* and *b*, were verified previously,[362] with the assumptions that the reverse reaction rate for binding events occuring after the initial binding of the free nanoparticle is equal to the monovalent reverse reaction rate ($k_{-x}=k_r$), and that the forward reaction rate for events after the initial binding rate is proportional to the monovalent forward reaction rate adjusted by multiplying by the comparative height between the media in a well h_{well} and the ligand-receptor interaction length h_{bound} ($k_{xa}=k_{fa}*h_{well}/h_{bound}$), which was shown to be an appropriate estimation to model monovalent, divalent and trivalent binding to cells.[362] h_{well} was calculated as the height of 200 µL of binding volume in a 6.4 mm diameter well. The fully extended length of an integrin as determined by electron microscopy is 20 nm,[363,364] and the extended peptide length was measured at 2-3 nm,[70] resulting in an h_{bound} of approximately 23 nm. The affinities of the two ligands were assumed to be equal. Equations and corresponding Matlab code can be found in Appendix A.

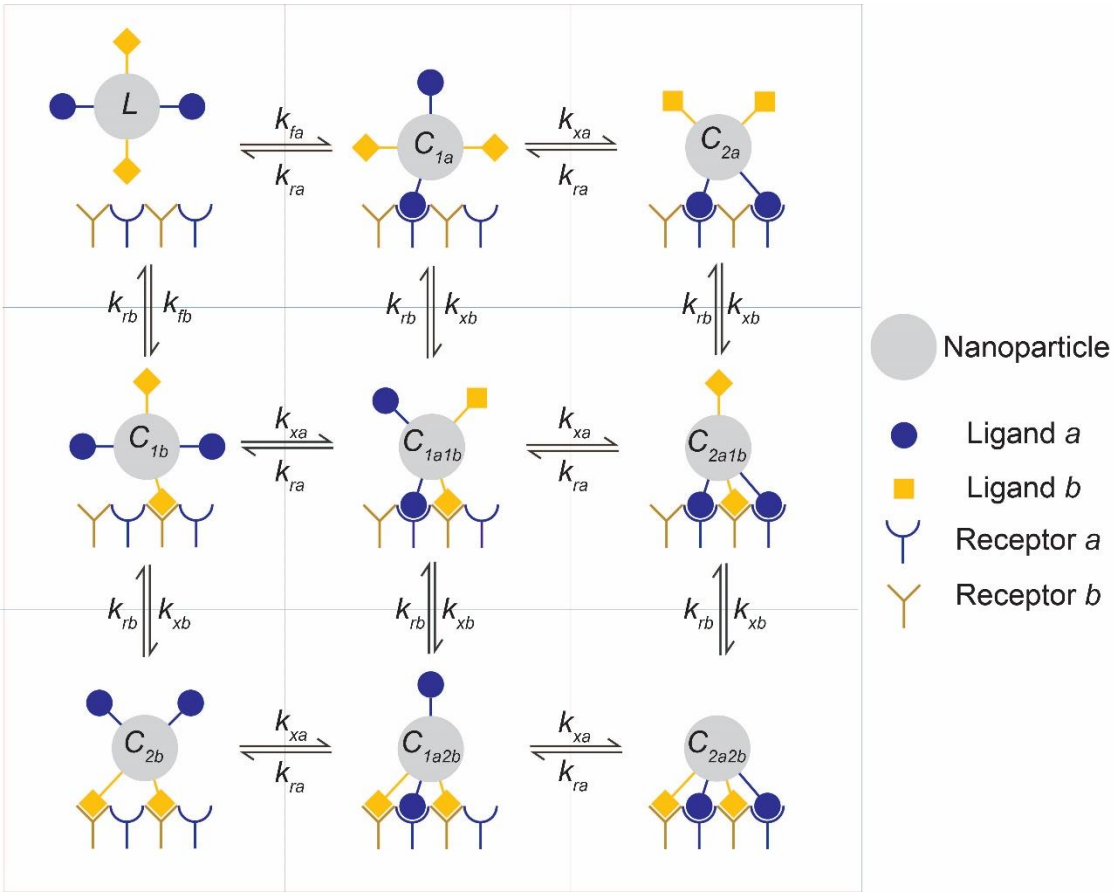

Scheme 1. Representative schematic of the binding model of heteromultivalent nanoparticle binding.
A nanoparticle *L* functionalized with two distinct ligands, each with an available valency of two, can interact with a multivalent surface in 8 unique ways. A free nanoparticle can bind via ligand *a* with a forward reaction rate of k_{fa} and via ligand *b* with a forward reaction rate k_{fb}. From each bound state, any unbound ligand has the potential to associate with a forward reaction rate of k_{xa} or k_{xb}, and each bound ligand has the potential to dissociate with a reverse reaction of k_{ra} or k_{rb}. Adapted from Caplan and Rosca.[362]

Peptide-Receptor Binding Affinity Analysis

Cells were harvested and fixed in 4% paraformaldehyde in PBS for 10 min at room temperature, washed twice in PBS via centrifugation at 500 g for 2.5 min and resuspended into $PBSA^{++}$ (1 w/v% BSA, 0.9 mM $CaCl_2$, 0.5 mM $MgCl_26H_20$ in PBS buffer). A constant concentration of the labeled free PR_b or AG86 peptide was mixed with varying concentrations of unlabeled form of the peptide and incubated with cells for 3 h on an orbital shaker at 4 °C. PR_b (KSSPHSRNSGSGSGSGSGRGDSP) and AG86 (KSSLGGLPSHYRARNI) peptides (unlabeled and with N-terminus conjugated FITC) were purchased from United Biosystems (Herndon, VA). Cells were pelleted by centrifugation at 500 g for 2.5 min, washed twice with 4 °C $PBSA^{++}$ and analyzed immediately on a BD Accuri C6 flow cytometer (Masonic Cancer Center, University of Minnesota). Nonlinear regression was used to fit binding curves to the fluorescence intensities to determine IC_{50} and K_d using Equations 12 and 13,[365]

$$1 - fraction\ bound = \frac{L_0}{L_0 + IC_{50}} \tag{12}$$

$$K_d = IC_{50} - L_0 \tag{13}$$

where $fraction\ bound$ of the labeled ligand is measured as the fluorescence intensity of the sample divided by the maximum fluorescence intensity, and L_0 is the initial concentration of unlabeled ligand.

Fluorescent Liposome Preparation and Characterization

Fluorescent liposomes were prepared as previously described.[76] 1,2- Dipalmitoyl-sn-glycero-3-phosphocholine (DPPC), 1,2-dipalmitoyl-sn- glycero-3-phosphoethanolamine-N-[methoxy(poly(ethylene glycol))-2000] (ammonium salt) (PEG2000), and cholesterol were purchased from Avanti Polar Lipids, Inc. (Alabaster, AL). Peptide-amphiphiles with C_{16} dialkyl tails were made as described previously.[67] 5 μmol of 60-x mol % DPPC, 35 mol % cholesterol, 5 mol % DPPE-PEG2000 and x mol % peptide-amphiphile dissolved in chloroform were combined in a round-bottom flask and dried under argon at 60 °C. The lipid film was hydrated with 2 mM calcein (Sigma-Aldrich, St. Louis, MO) in TNE buffer (10mM Tris, 150 mM NaCl, 1 mM EDTA) at 55 °C for 90 min. Liposomes were extruded 11 times using a manual extruder (Avestin, Ottowa, ON) through 200 nm membranes, and purified over a Sepharose CL-4B gel filtration column. Lipid concentration was measured using a phosphorus assay as described elsewhere.[237,366] Peptide concentration in the liposomes was determined by the BCA protein assay (Thermo Scientific, Waltham, MA) following the manufacturer's protocol. Peptide concentration is expressed as a mole

percentage of total lipid. Liposome size and charge were measured using dynamic light scattering and zeta potential analysis (Brookhaven Instruments Corporation, Holtsville, NY).

Peptide Ratio Quantification

PR_b and AG86 peptides were purchased from United Biosystems (Herndon, VA) with a C-terminal cysteine (PR_b-C and AG86-C) and used to synthesize peptide-amphiphiles as described previously.[67] Maleimide functionalized tetramethylrhodamine-5-maleimide (TAMRA) (Sigma-Aldrich, St. Louis, MO) and N-(7-dimethylamino-4-methylcoumarin-3-yl)) maleimide (DACM) (Life Technologies, Grand Island, NY) were covalently attached to the PR_b-C and AG86-C peptide-amphiphiles respectively using maleimide thiol chemistry[367] and purified using high performance liquid chromatography. The fluorophores were chosen for their non-overlapping excitation emission spectra, small size and neutral charge in order to easily discriminate between the fluorescent signals and minimize the effect of the fluorophore on self-assembly. Fluorophore-functionalized peptide-amphiphiles were used to produce single-ligand liposomes at various peptide densities. Fluorescence intensities of DACM and TAMRA, normalized to lipid content, were measured at 405/450 and 561/582 nm respectively using a Synergy H1 multi-mode reader (Biotek, Winooski, VT), and used to create a peptide density standard. Fluorophore-functionalized peptide-amphiphiles were used to produce 75:25, 50:50 and 25:75 PR_b:AG86 functionalized stealth liposomes and fluorescence intensity was used to measure the density of each peptide to verify the final peptide ratio of the dual-ligand formulations. Nontargeted, single-ligand, and dual-ligand liposomes were analyzed on a BD LSR II/Fortessa flow cytometer (Masonic Cancer Center, University of Minnesota) to verify incorporation of both ligands on individual liposomes.

Antibody Blocking of Fluorescent Liposome Binding

SK-OV-3 cells were fixed by incubation in 4% paraformaldehyde (Sigma, St. Louis, MO) for 10 min at 25 °C, and aliquoted in 4 °C $PBSA^{++}$. Cells were incubated with 1:100 dilution of MAB1969 mouse anti-human $\alpha_5\beta_1$ antibody (EMD Millipore, Darmstadt, Germany), 1:100 dilution of rat anti-human CD49f/α_6 (eBioscience, Inc., San Diego, CA), or 1:100 dilution of MAB1964 mouse anti-human β_4 (EMD Millipore, Darmstadt, Germany) at 4 °C for 30 min. 10 μM PR_b- or AG86-functionalized stealth liposomes were added to the cells blocked with $\alpha_5\beta_1$ or α_6/β_4 antibodies respectively and incubated at 4 °C for 1 hr, then washed twice with 4 °C PBS and analyzed immediately on a BD Accuri C6 flow cytometer (Masonic Cancer Center, University of Minnesota).

Preparation and Characterization of Liposomes Encapsulating pDNA

Condensed plasmid DNA (pDNA) particles were prepared for encapsulation from 95% unlabeled pmaxGFP pDNA (gift from Prof. Hu, University of Minnesota) and 5% Cy5-labeled pmaxGFP for pDNA quantification as described previously.[272] Labeled pDNA was prepared using Cy5 Label-IT tracker (Mirus, Madison, WI) according to the manufacturer's protocol. 20 μg of pDNA were dissolved in water and an equal volume of 25 kDa branched polyethyleneimine (bPEI) (Sigma-Aldrich, St. Louis, MO) in water was added to the pDNA solution at an amine to phosphate (N:P) ratio of 8, vortexed for 5 min, and incubated at room temperature for 30 min. The N:P ratio was chosen for optimal size for subsequent encapsulation, and has demonstrated effective transfection within targeted stealth liposomes.[79] Lipid films were prepared as above, and hydrated with the condensed pDNA particles at 45 °C for 90 min. The liposomes were then extruded 11 times using a manual extruder (Avestin, Ottowa, ON) through 400 nm membranes, and the unencapsulated pDNA was removed with overnight dialysis purification through a 1000 kDa MWCO membrane (Spectrum Laboratories, Rancho Dominguez, CA).[79,272] Final pDNA concentration in the liposomes was determined as described elsewhere using a concentration standard curve.[272] Lipid and peptide concentration, and liposome size and charge were measured as described for fluorescent liposome preparation.

Receptor Internalization

Receptor internalization analysis was performed as reported previously.[368] Cells were plated at 100,000 cells/well in 12 well plates and allowed to adhere overnight. Cells were incubated for 3 h on an orbital shaker at 4 °C in $PBSA^{++}$ with 100 μM fluorescein isothiocyanate (FITC)-labeled free AG86 or PR_b peptides to allow for binding to surface receptors. Cells were washed twice in $PBSA^{++}$ and incubated for various times in prewarmed media and 0.6 μM primaquine (to prevent receptor recycling)[369] at 37 °C. Cells were washed twice in $PBSA^{++}$ and incubated in acid stripping buffer (MEM adjusted to pH 3.5) three times for 5 min each time to remove surface proteins and surface bound fluorescent peptides. Cells were then washed twice in $PBSA^{++}$ and harvested with TrypleE Express cell dissociation agent (ThermoFisher Scientific, Grand Island, NY). Cells were pelleted by centrifugation at 500 *g* for 2.5 min, washed twice with cold $PBSA^{++}$ and analyzed immediately on a BD Accuri C6 flow cytometer (Masonic Cancer Center, University of Minnesota).

Liposome Binding

Cells were harvested and resuspended in $PBSA^{++}$ at 0.5 x 10^6 cells/mL. Calcein-loaded liposomes were added at a final concentration of 10 μM lipids. Liposomes were incubated with

cells for 24 h on an orbital shaker at 4 °C to minimize internalization.[370] Cells were then pelleted by centrifugation at 500 *g* for 2.5 min, washed twice with 4 °C $PBSA^{++}$ and analyzed immediately by flow cytometry on a BD Accuri C6 flow cytometer (Masonic Cancer Center, University of Minnesota). To determine fraction bound for time course experiments, fluorescence intensity was normalized to the maximum intensity measured for each liposome formulation.

Liposome Binding and Internalization

Cells were plated at 25,000 cells/well in 24 well plates and allowed to adhere overnight. Calcein-loaded liposomes were added at a final concentration of 10 μM lipids. Liposomes were incubated with cells for 24 h at 37 °C. Cells were then harvested with TrypleE Express cell dissociation agent (ThermoFisher Scientific, Grand Island, NY), pelleted by centrifugation at 500 *g* for 2.5 min, washed twice with 4 °C PBS and analyzed immediately on a BD Accuri C6 flow cytometer (Masonic Cancer Center, University of Minnesota).

Transfection Using Liposomes Encapsulating pDNA

Cells were plated at 25,000 cells/well in 24 well plates and allowed to adhere overnight. They were transfected with liposomes encapsulating condensed pDNA at various DNA concentrations for 48 h at 37 °C. Cells were then harvested with TrypleE Express cell dissociation agent (ThermoFisher Scientific, Grand Island, NY), pelleted by centrifugation at 500 *g* for 2.5 min, washed twice with PBS and analyzed immediately on a BD Accuri C6 flow cytometer (Masonic Cancer Center, University of Minnesota).

Statistics

ANOVA analysis and Tukey Kramer honest significant difference (HSD) test were performed to calculate p-values and determine statistical significance between means unless otherwise indicated.

Results

Receptor Expression Analysis of Common Cancer Cell Lines

The expression of α_6, β_4 and $\alpha_5\beta_1$ integrins were quantified on 20 commonly investigated cell lines (Table 3 and Figure 31). The quantitative report of receptor expression on several cell lines of various origin allows for direct comparison of expression in different tissues.[268,328,331,333–335] From the characterization of integrin receptor expression levels and relative $\alpha_5\beta_1$:α_6 and $\alpha_5\beta_1$:β_4 expression, six cell lines were chosen for further investigation (Figure 31). The ratio of $\alpha_5\beta_1$ to $\alpha_6\beta_4$

expression was close to unity for MCF7 and SK-OV-3 cells, and the expression levels on SK-OV-3 cells were 100 fold higher than on MCF7 cells, suggesting SK-OV-3 cells would function as an appropriate model for a high dual-receptor expressing cell line. MCF7 cells express 10^3-10^4 receptors/cell, consistent with cancer biomarker expression levels measured on healthy model cells or tissues,[371–373] suggesting MCF7 cells are appropriate as a low receptor expressing or "healthy" cell line.

Four other cell lines were chosen with differential levels of integrin expression. RKO and HT-1080 cells have higher $\alpha_5\beta_1$ than $\alpha_6\beta_4$ expression levels, with RKO exhibiting a higher ratio of $\alpha_5\beta_1$:$\alpha_6\beta_4$ expression, but lower overall expression than HT-1080 cells. LS 174T and SW 1990 cells have higher $\alpha_6\beta_4$ than $\alpha_5\beta_1$ expression, with LS 174T cells exhibiting a higher ratio of $\alpha_6\beta_4$:$\alpha_5\beta_1$ expression and higher expression levels than SW 1990, and both cell lines express higher $\alpha_6\beta_4$ levels than the dual-receptor expressing SK-OV-3 cells. Note that all cells have measurable expression of both receptors.

Table 3. Expression levels of $\alpha_5\beta_1$, α_6 and β_4 integrins on several cell lines.
Many commercially available cancer cell lines, and one embryonic fibroblast line, were analyzed for α_6, β_4, and $\alpha_5\beta_1$ expression levels using flow cytometry. Quantitative receptor expression levels were calculated by subtracting isotype controls as background and comparing fluorescent intensities to a bead calibration curve. Data are presented as the mean ± SE (n = 3-4 of longitudinal samples).

Cell Line	Cell Type	$\alpha_5\beta_1$ (10^3 Receptors/Cell)	α_6 (10^3 Receptors/Cell)	β_4 (10^3 Receptors/Cell)
A-431	Skin Epidermoid Carcinoma	164 ± 25	300 ± 56	356 ± 40
BJ	Embryonic Foreskin Fibroblast	280 ± 65	92 ± 46	4.9 ± 0.5
DLD-1	Colorectal Adenocarcinoma	40 ± 8	226 ± 20	165 ± 5.5
DU 145	Prostate Carcinoma	174 ± 36	213 ± 13	58 ± 7.4
HCT 116	Colorectal Carcinoma	99 ± 18	202 ± 10	165 ± 3.0
HeLa	Cervical Adenocarcinoma	313 ± 28	279 ± 39	80 ± 16
Hep G2	Hepatocellular Carcinoma	0.1 ± 0.8	102 ±16	5.4 ± 2.2
HT-1080	Connective Tissue Fibrosarcoma	240±12	127 ± 21	1.6 ± 1.2
HT-29	Colorectal Adenocarcinoma	36 ± 21	486 ± 23	375 ± 81
LNCaP	Prostate Carcinoma	83 ± 21	77 ± 1.5	1.4 ± 2.3
LS 174T	Colorectal Adenocarcinoma	11 ± 7	3050 ± 1710	1240 ± 647
MCF7	Breast Adenocarcinoma	9.7 ± 3.5	10 ± 2.5	5.8 ± 2.3
MDA-MB-231	Breast Adenocarcinoma	116 ± 49	245 ± 38	189 ± 69
MDA-MB-435	Melanoma	55 ± 6	65 ± 29	0.3 ± 0.5
MDA-MB-468	Breast Adenocarcinoma	4.1 ± 1.9	79 ± 18	36 ± 3.9
OVCAR-3	Ovarian Adenocarcinoma	9.7 ± 1.2	20 ± 1.5	15 ± 2.8
PC3-LN4	Prostate Carcinoma (artificial lymph node metastasis)	48 ± 0.1	208 ± 24	121 ± 3.6
RKO	Colon Carcinoma	33 ± 9.7	2.9 ± 1.1	0.03 ± 0.4
SK-OV-3	Ovarian Adenocarcinoma	193 ± 12	359 ± 20	202 ± 21
SW 1990	Pancreatic Adenocarcinoma	73 ± 38	505 ± 127	648 ± 163

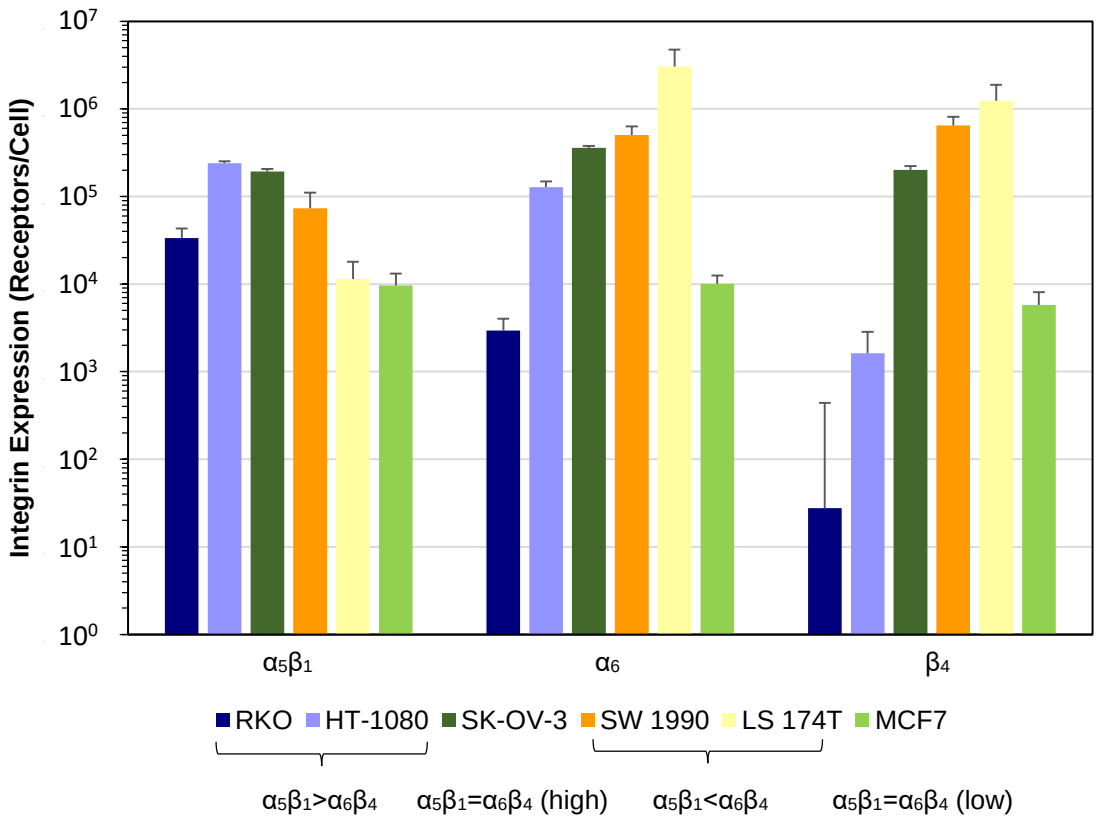

Figure 31. Integrin expression levels of cancer cell lines.
RKO, HT-1080, SK-OV-3, SW 1990, LS 174T and MCF7 were chosen as representative cell lines for *in vitro* investigation of dual-ligand nanoparticles based on their α_6, β_4 and $\alpha_5\beta_1$ expression characterized with flow cytometry. Quantitative receptor expression levels were calculated by subtracting isotype controls as background and comparing fluorescent intensities to a bead calibration curve. Data are presented as the mean ± SE (n = 3-4). Numerical values are also listed in Table 3.

Heteromultivalent Kinetic Model

With an initial nanoparticle concentration of 2.5×10^{-14} M, calculated as described previously,[272] which corresponds to a lipid concentration of 10 μM, the number of liposomes bound to each cell was calculated using the heteromultivalent model for nanoparticles with varying valencies from 0-8 for each ligand and varying ratios of valencies. Selectivity was also calculated for each valency state as the ratio of the total number of nanoparticles bound to the cells with equal receptor concentrations (Figure 32A) to the total number of nanoparticles on whichever of the two other cell types showed greater binding (Figures 32B and 32C). Nanoparticles with higher valencies of ligand *a* were calculated to bind at higher levels to cells with higher expression of receptor *a* (Figure 32B), and nanoparticles with higher valencies of ligand *b* bound at higher levels to cells with higher expression of receptor *b* (Figure 32C).

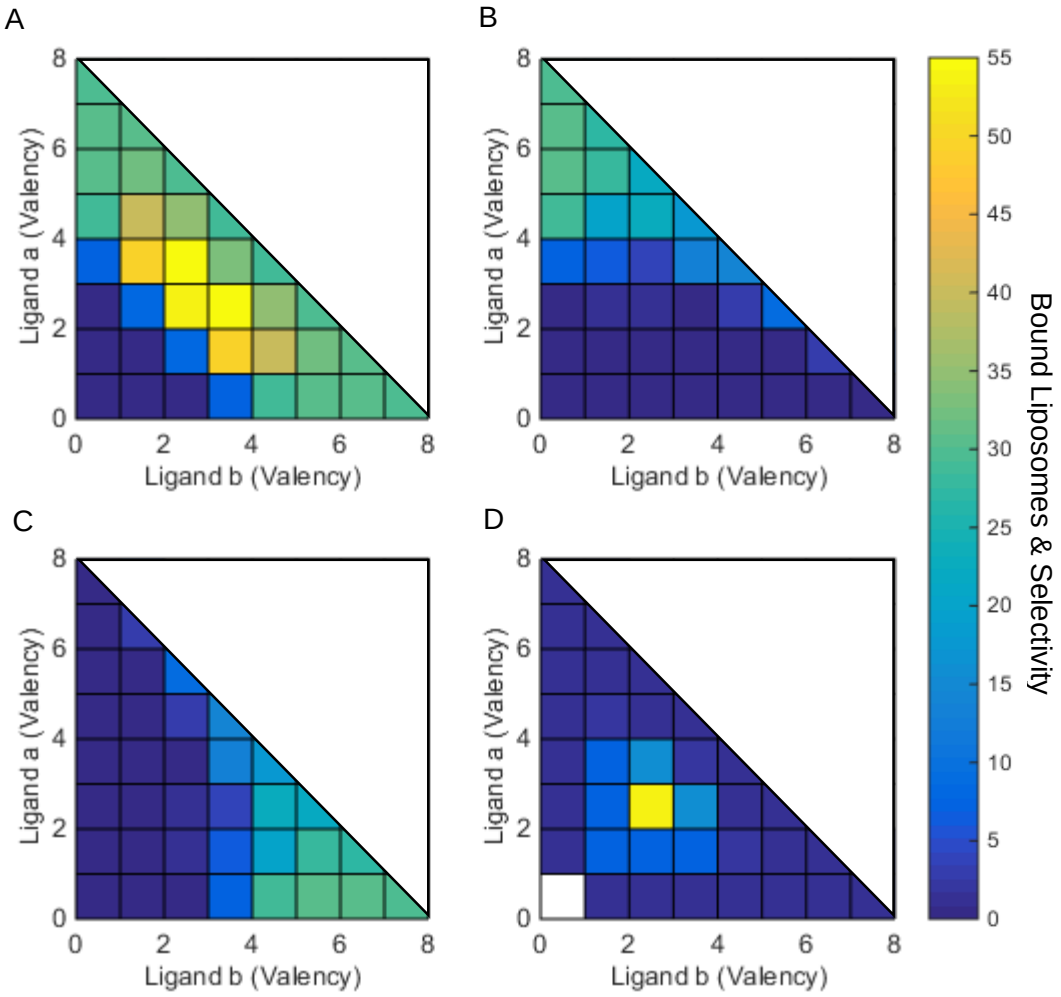

Figure 32. Theoretical binding of heteromultivalent nanoparticles to three cell types.
The heteromultivalent kinetic binding model was used to calculate nanoparticles bound to cells with high expression of both receptors (R_a=200,000, R_b=200,000) (A), higher expression of receptor *a* (R_a=200,000, R_b=25,000) (B), or higher expression of receptor *b* (R_a=25,000, R_b=200,000) (C). Valency of ligand *a* and *b* was varied from 0 to 8 and binding to each cell was measured, as well as selectivity (D) of (A) compared to (B) and (C). $L = 2.5\text{x}10^{-14}$ nanoparticles, $K_{da} = K_{db} = 3.3\text{x}10^{-6}$ M, $k_{fa} = k_{fb} = 300$ $M^{-1}s^{-1}$, $k_{ra} = k_{rb} = K_{da}$ x k_{fa}, $k_{-xa} = k_{-xb} = k_{ra}$, $k_{xa} = k_{xb} = 9.3\text{x}10^{8}$ $M^{-1}s^{-1}$.

Nanoparticles with equal valencies between ligand *a* and *b* bound at higher levels to the cells with equal receptor expression compared to other nanoparticle valencies (Figure 32A). This resulted in the highest selectivity of nanoparticles with equal *a* and *b* ligand valency for the dual-receptor expressing cells compared to the other cell types (Figure 32D). There also appears to be an optimum overall valency of 3 for each ligand-receptor pair, above which binding to the dual-receptor expressing cells decreases, decreasing the selectivity. Notably, the best valency for

targeting cells that expressed higher levels of one receptor is not the best valency to target the dual-receptor expressing cell.

Dual- and Single-Ligand Nanoparticle Delivery

The results of the kinetic binding model suggest that for ligands of similar affinity for their targets, a 50:50 ratio of ligands on a nanoparticle surface will bind most effectively and most selectively to cells with a high and equal level of targeted receptor expression. With a basic theoretical understanding of the effect of valency on dual-targeted nanoparticle binding, this concept was explored *in vitro*. Single-ligand liposomes containing either PR_b or AG86, and dual-ligand liposomes containing 75:25, 50:50 and 25:75 ratios of PR_b:AG86 were produced with similar overall peptide content in order to isolate synergy effects of dual-ligand binding from single-ligand avidity effects. Liposome size and zeta potential for each formulation are reported in Table 4. The ability to achieve the desired peptide ratios in the final dual-targeted liposomes compared to the initial peptide ratio during liposome formation was verified using fluorescently labeled peptide-amphiphiles. PR_b was labeled with TAMRA, and AG86 was labeled with DACM. As shown in Figure 33A, standards were created using single-ligand liposomes, and fluorescence intensity was used to measure peptide ratios in dual-ligand liposomes. A linear fluorescence-concentration response excludes the possibility of fluorescence self-quenching within the investigated concentrations. Final peptide ratios for liposomes initially prepared with 75:25, 50:50 and 25:75 ratios are shown in Figure 33B, and final peptide ratios for 50:50 and 25:75 formulations were not statistically different from initial ratios. Liposomes were also analyzed using flow cytometry to establish the presence of both peptides on individual liposomes. Nontargeted liposomes (Figure 33C) exhibit background fluorescence at both 561/582 (TAMRA) and 405/450 (DACM) excitation/emission wavelengths. Functionalization with PR_b-TAMRA (Figure 33E) increases the TAMRA-positive population measured at 561/582 nm and functionalization with AG86-DACM (Figure 33F) increases the fluorescence intensity measured at 405/450 nm. Liposomes functionalized with both fluorescently labeled peptide-amphiphiles (Figure 33D) exhibit a simultaneous increase in fluorescence intensity measured at both sets of wavelengths, confirming the presence of both peptides on individual liposomes.

Table 4. Size and zeta potential of targeted stealth liposome formulations for delivery.
Data are presented as mean ± SE (n = 5).

Liposome Formulation	Size (nm)	Zeta Potential (mV)
100% PR_b	181±14	-3.5±5.6
75:25 PR_b:AG86	169±15	2.5±4.0
50:50 PR_b:AG86	170±13	-1.8±2.6
25:75 PR_b:AG86	168±15	-5.4±4.0
100% AG86	178±5	8.0±2.6

Binding affinity of PR_b and AG86 for their respective receptors was measured using a competition cellular assay (Figure 34). The affinities of both ligand-receptor pairs were similar, resulting in a K_d of 5.0 ± 3.8 μM and 2.6 ± 0.9 μM for PR_b and AG86 respectively. Similar ligand-receptor affinities allow subsequent binding analysis to focus solely on valency effects. The K_d of PR_b for the $\alpha_5\beta_1$ integrin was previously identified using an ELISA as 76.3 nM.[68] Differences in measured K_d using different assays has been observed for other peptide binders,[374] emphasizing the value of cellular K_d measurements for targeting ligand characterization.

The specificity of the PR_b peptide for the $\alpha_5\beta_1$ integrin has been characterized on endothelial and colon cancer cell lines,[67,375] however the target specificity of the AG86 peptide is less well characterized. The AG86 peptide was initially identified to bind to the α_6 integrin, with little interaction with the β_1 integrin, suggesting an α_6 or $\alpha_6\beta_4$ specific binding interaction, as α_6 can associate only with β_1 or β_4.[269,341] In order to verify the specificity of the PR_b and AG86 liposomes for the $\alpha_5\beta_1$ and $\alpha_6\beta_4$ integrins respectively, single targeted liposomes were delivered to SK-OV-3 cells in the presence and absence of antibodies to block access to the cell surface integrins. The presence of the anti-$\alpha_5\beta_1$ antibodies decreased the PR_b liposome binding by 65%, verifying the specificity of PR_b for the $\alpha_5\beta_1$ on SK-OV-3 cells (Figure 35A). The presence of the anti-α_6 and anti-β_4 antibodies decreased the AG86 liposome binding to SK-OV-3 cells by 79.7% and 70.6% respectively, demonstrating specificity of AG86 peptide binding to the $\alpha_6\beta_4$ heterodimer (Figure 35B).

Single-ligand liposomes were first delivered to cells at 4 °C for 2-24 h to identify a sufficient incubation time for subsequent experiments in this study. 24 h was chosen as a sufficient time point as liposome binding appears to reach saturation before this point (Figure 36).

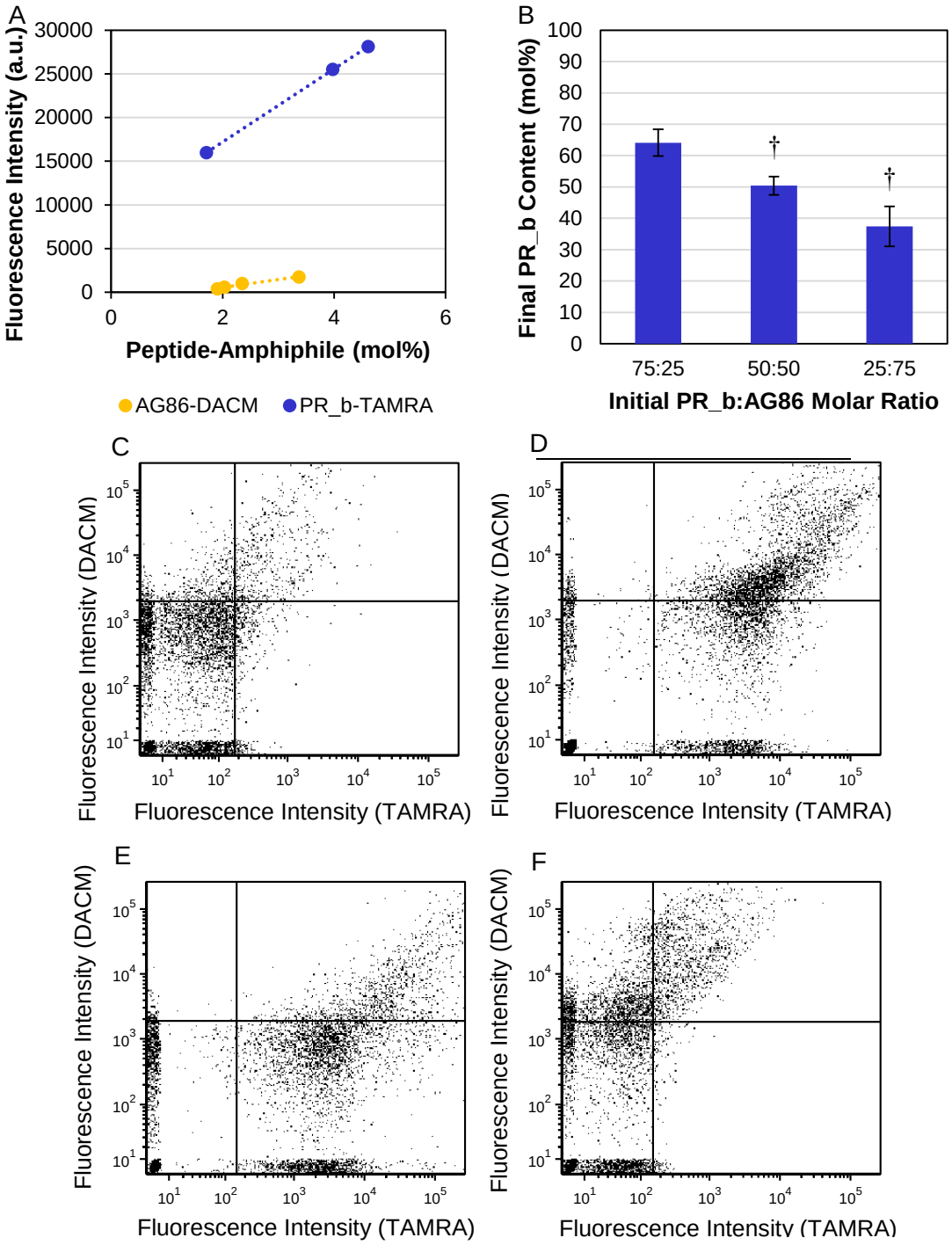

Figure 33. Characterization of peptide ratios in dual-ligand stealth liposomes.
Single-ligand stealth liposomes were prepared with fluorescently labeled peptide-amphiphiles and used to produce a fluorescent concentration standard (A). Dual-ligand stealth liposomes were prepared with 4.5-5.5 mol% of 75:25, 50:50 and 25:75 initial molar ratios of PR_b-TAMRA:AG86-DACM and final peptide percentages were calculated using the single-ligand standards (B). Peptide percentage data are presented as the mean ± SE (n = 3). Z test statistical analysis was performed comparing final to initial peptide contents. † $p > 0.05$. Nontargeted (C), 50:50 dual-ligand (D), 100% PR_b (E), and 100% AG86 (F) stealth liposomes were analyzed using flow cytometry to verify the presence of both fluorescently labeled peptide-amphiphiles in individual cytometry events.

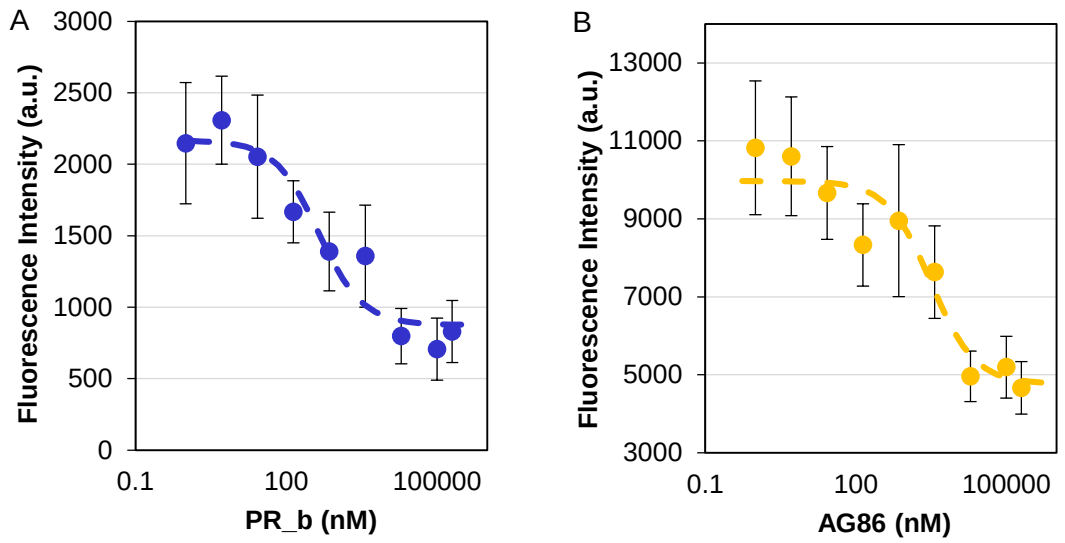

Figure 34. Competition binding curves for PR_b-$\alpha_5\beta_1$ and AG86-$\alpha_6\beta_4$.
Affinity of PR_b for the $\alpha_5\beta_1$ integrin (A) and AG86 for the $\alpha_6\beta_4$ integrin (B) were calculated from competition binding curves generated from delivery of 100 nM of FITC-labeled peptide and varying concentrations of unlabeled peptide to SK-OV-3 cells at 4 °C for 3 h.

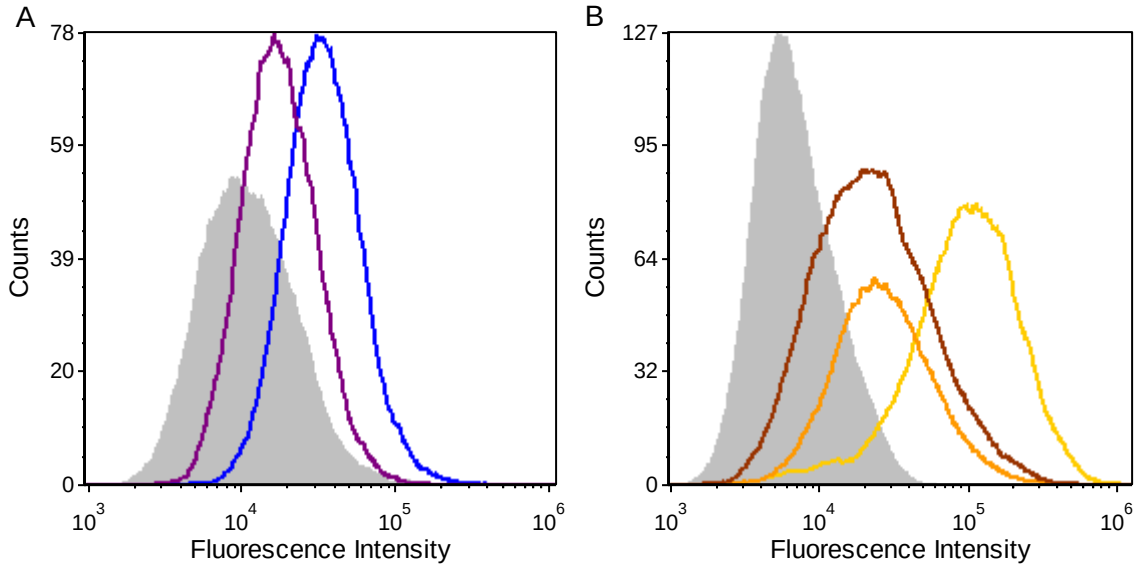

Figure 35. Antibody blocking of liposome binding.
10 µM single-ligand calcein-loaded stealth liposomes were incubated with SK-OV-3 cells at 4 °C for 1 hr in the presence and absence of blocking antibodies, and binding was measured with flow cytometry. (A) PR_b stealth liposomes (5.0 mol% PR_b), blue, blocked with 1:50 anti-$\alpha_5\beta_1$ antibody, purple, and (B) AG86 stealth liposomes (5.9 mol% AG86), yellow, blocked with 1:100 anti-α_6, orange, or anti-β_4, brown, antibody. Untreated cells were measured for background fluorescence (grey).

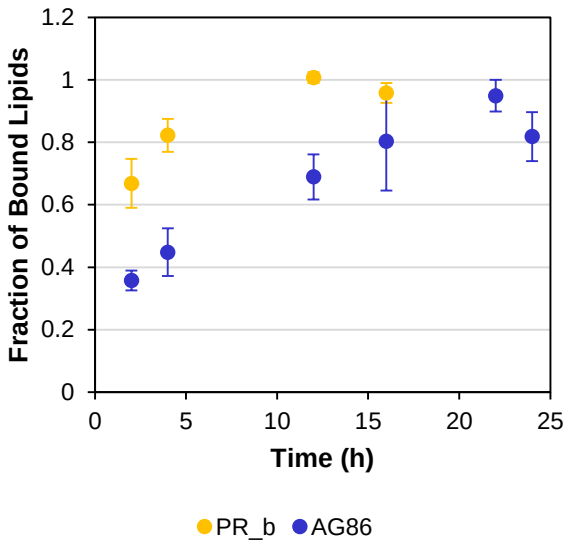

Figure 36. Effect of delivery time on liposome binding.
10 µM of lipids of single-ligand stealth liposomes loaded with calcein and functionalized with 6.5 ± 2.5 mol% PR_b or 6.3 ± 0.9 mol% AG86 peptide-amphiphiles were incubated with SW 1990 cells for various times and liposome binding was determined via flow cytometry. Fraction bound was calculated as fluorescence intensity/maximum intensity. Data are presented as the mean ± SE (n = 4).

Single- and dual-targeted stealth liposomes with 5 mol% total peptide were incubated with several cells, with various receptor concentrations and ratios, for 24 h at 4 °C, to prevent internalization (Figure 37A). Two important observations emerge from the results shown in Figure 37A: First, the 50:50 liposome formulation binds much more efficiently to SK-OV-3 cells, the high dual-receptor expressing cell line, than any of the other liposome formulations, achieving at least 5 fold better binding than either of the single-ligand formulations. Second, the 50:50 formulation binds significantly more efficiently to SK-OV-3 cells than to any other cell, achieving 27 fold selectivity for SK-OV-3 cells compared to MCF7, a low dual-expressing cell line (a cell line with balanced but lower receptor expression), and 8-10 fold selectivity for SK-OV-3 cells compared to cells with unbalanced receptor ratios. Additionally, single- and dual-targeted stealth liposomes were delivered to the same cell lines at 37 °C to allow for binding and internalization (Figure 37B). Similar trends were observed for SK-OV-3 cells with liposome delivery at physiological conditions. 50:50 liposomes bound and internalized 2-3 fold more in SK-OV-3 cells than any other liposome formulation. They also bound and internalized to a higher extent in SK-OV-3 cells compared to RKO, SW 1990, LS 174T and MCF7 cells, however these differences were not statistically significant. Interestingly, in HT-1080 cells, 50:50 liposomes bound and internalized more efficiently compared to all other cells (there was no statistically significant difference between 50:50 liposome binding to SK-OV-3 and HT-1080 cells), which was not the case when considering

binding alone. Differences in $\alpha_5\beta_1$ and $\alpha_6\beta_4$ internalization rates between cells were hypothesized to play some role in differences observed between binding (Figure 37A) and binding with internalization (Figure 37B) and were measured for each cell line (Figure 38). Figure 38 shows that the internalization of $\alpha_5\beta_1$ and $\alpha_6\beta_4$ integrins was similar for each cell. In general, internalization of both integrins was very rapid in HT-1080, SK-OV-3 and SW 1990 cells, with almost all integrins initially present at the surface internalized after 45 min. Integrin internalization was relatively slower in RKO, LS 174T and MCF7 cells, with only 30-60% of integrins internalized after 45 min of incubation at 37 °C.

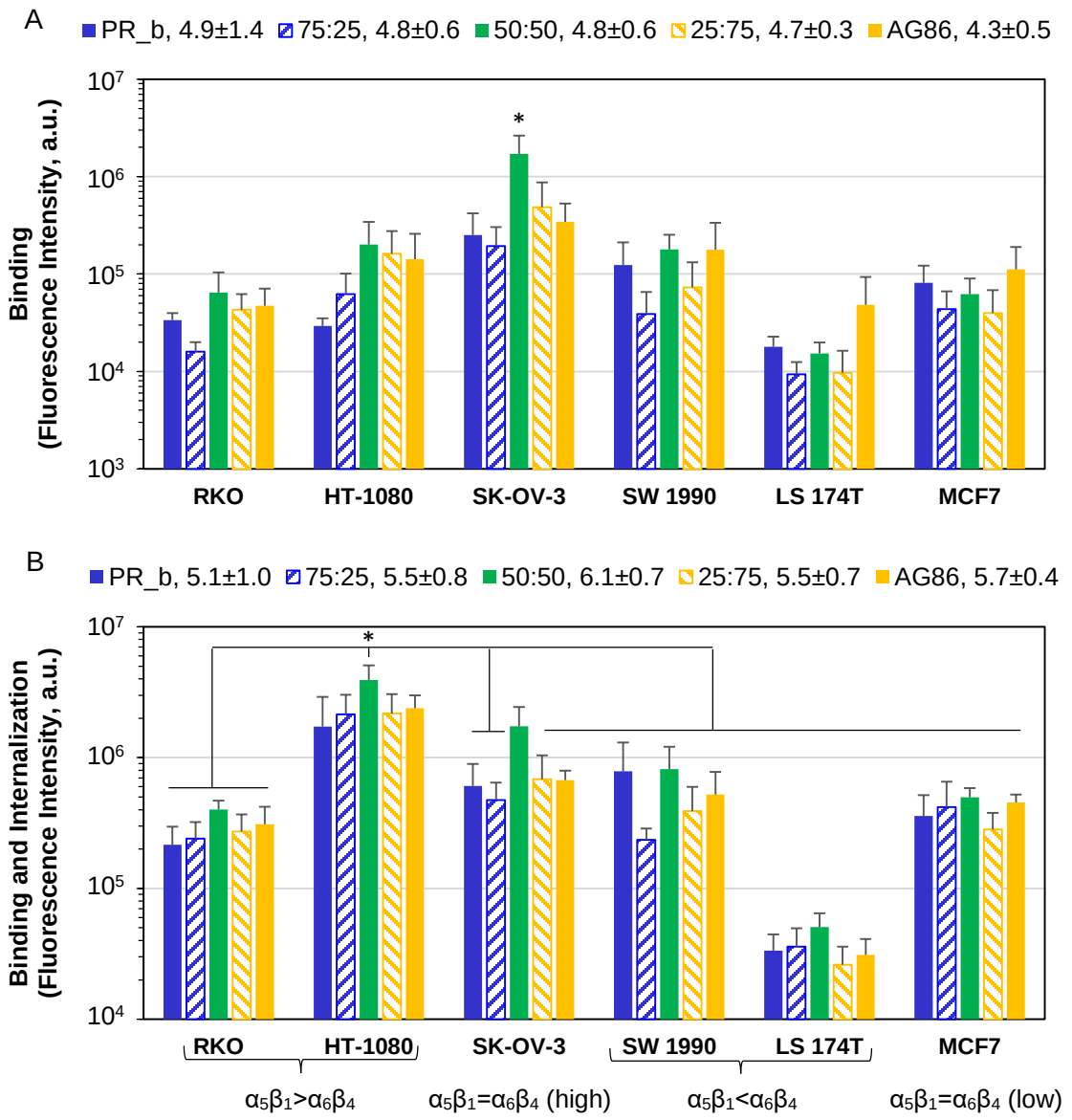

Receptors/cell (10^3)

	RKO	HT-1080	SK-OV-3	SW 1990	LS 174T	MCF7
$\alpha_5\beta_1$	33±10	240±12	190±12	73±38	11±6.6	10±4
α_6	2.9±1.1	127±21	360±20	510±1130	3100±1700	10±3
β_4	0.03±0.4	1.6±1.2	200±21	650±160	1200±650	6±2

Figure 37. Dual- and single-targeted stealth liposome delivery to cells with varying receptor density. Stealth liposomes loaded with calcein and functionalized with 100% PR_b, 75% PR_b:25% AG86, 50% PR_b:50% AG86, 25% PR_b:75% AG86, or 100% AG86, were delivered to RKO, HT-1080, SK-OV-3, SW 1990, LS 174T, and MCF7 cells for 24 h at 4 °C (A) to measure liposome binding, or 37 °C (B) to allow for binding and internalization. Total peptide concentration, shown in the legend for each formulation, was kept constant to keep total valency constant across samples. Data are presented as mean ± SE (n = 5). Fluorescence intensity of bound and internalized liposomes was measured using flow cytometry. * in (A) $p < 0.05$ compared to all other samples. * in (B) shows significant statistical difference ($p < 0.05$) between the 50:50 formulation with the HT-1080 cells and the formulations covered under the horizontal lines. The table shows the integrin expression levels measured for the cell lines. There was no significant statistical difference for pairs without brackets.

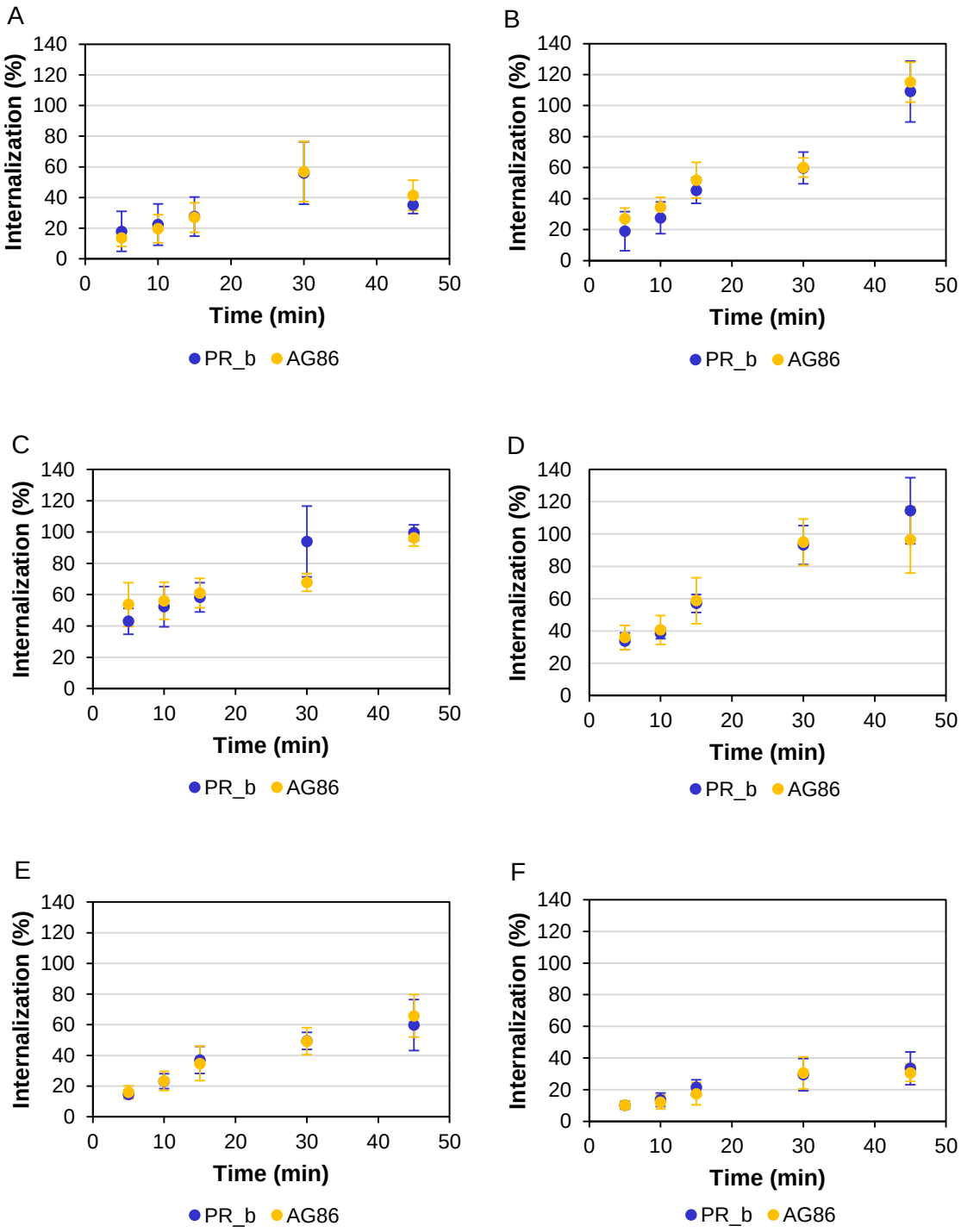

Figure 38. Internalization of $\alpha_5\beta_1$ and $\alpha_6\beta_4$ integrins.
FITC-labeled PR_b and AG86 were allowed to bind for 3 h at 4 °C to $\alpha_5\beta_1$ integrin and $\alpha_6\beta_4$ integrin, respectively, on RKO (A), HT-1080 (B), SK-OV-3 (C), SW 1990 (D), LS 174T (E), and MCF7 (F) cells. Integrin bound peptides were allowed to internalize for 5-45 min at 37 °C in the presence of primaquine before surface bound peptide was removed via acid stripping. Internalized peptide was quantified via flow cytometry. Receptor internalization (%) was calculated as fluorescence intensity/fluorescence intensity in the absence of acid stripping. Data are presented as mean ± SE (n = 3).

Transfection with Single- and Dual-Ligand Liposomes

For a cell line with comparable high levels of expression of two targeted receptors, the best binding and selectivity was achieved using dual-ligand liposomes with equal composition of the two ligands (Figure 32A, D and 37A). This concept was further explored with the delivery of a GFP reporter plasmid to the high dual-receptor expressing SK-OV-3 cells. RKO and LS 174T cells were also used as cells with much higher levels of expression of one receptor, and MCF7 cells were included as low dual-receptor expressing cells. Condensed pDNA was fully encapsulated[79,272] (see Chapter 2) within PR_b or AG86 single-ligand stealth liposomes, or 50:50 dual-ligand stealth liposomes, and delivered to cells for 48 h, before GFP fluorescence and Cy5-labeled pDNA fluorescence were measured to determine transfection efficiency and internalization, respectively. Even with the additional barriers that exist between internalization and transfection, the dual-ligand stealth liposomes were more effective at transfecting the SK-OV-3 high dual-receptor expressing cells than single-ligand stealth liposomes (Figure 39A). Dual-ligand liposomes also mediated selective delivery to SK-OV-3 compared to RKO, LS 174T and MCF7 cells which was observed both in pDNA internalization and transfection (Figure 39A and 39B). Increasing the amount of pDNA delivered to SK-OV-3 cells with the dual-ligand stealth liposomes increased both pDNA internalization and transfection nonlinearly (Figure 40).

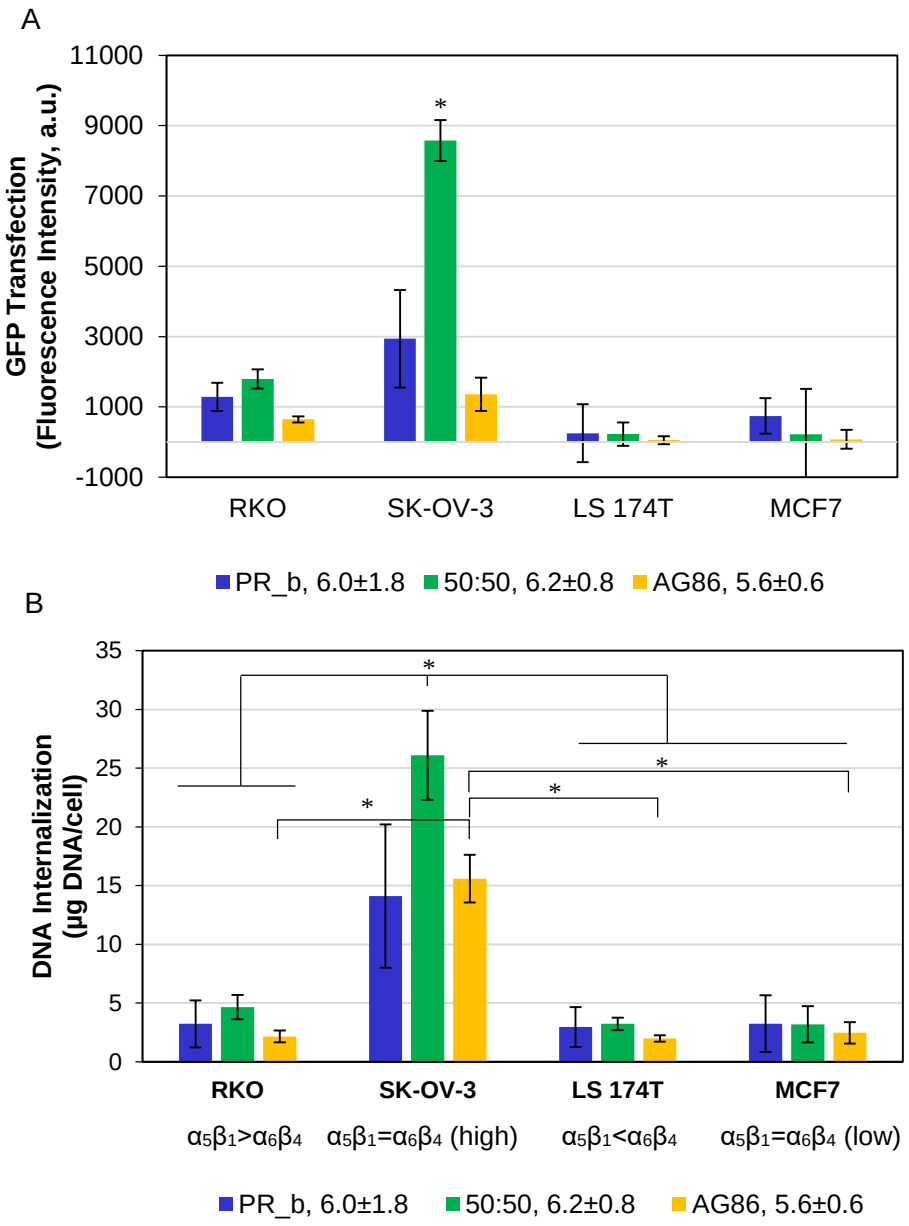

Figure 39. Gene delivery and transfection with dual- and single-targeted stealth liposomes.
Stealth liposomes encapsulating condensed pDNA/PEI, where the pDNA was fluorescently labeled with Cy5, were functionalized with 100% PR_b, 50% PR_b:50% AG86, or 100% AG86 and used to deliver 500 ng of GFP plasmid to RKO, SK-OV-3, LS 174T or MCF7 cells. Total peptide concentration, shown in the legend for each formulation, was kept constant. The liposomes were incubated with the cells for 48 h at 37 °C. (A) Transfection was measured via GFP fluorescence and (B) pDNA internalization was measured via Cy5 fluorescence using flow cytometry. Data are presented as mean ± SE (n = 3). * in (A) $p < 0.05$ compared to all other samples. * in (B) $p < 0.05$. There was no significant statistical difference for pairs without brackets in (B).

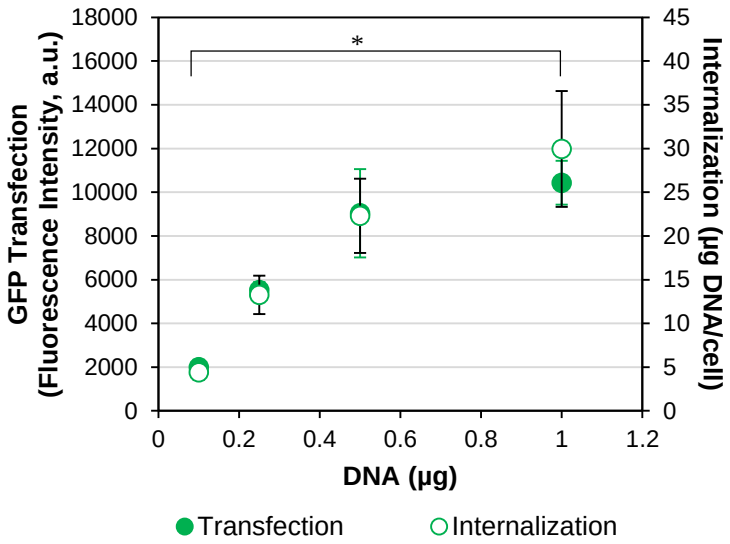

Figure 40. Gene delivery and transfection with dual-targeted stealth liposomes at various concentrations. Stealth liposomes functionalized with 50% PR_b:50% AG86 (total peptide 6.2 ± 0.8 mol%) encapsulating Cy5-labeled condensed pDNA were used to deliver 0.1-1.0 μg GFP pDNA to SK-OV-3 cells for 48 h at 37 °C. Transfection was measured via GFP fluorescence and internalization was measured via Cy5 fluorescence. Data are presented as mean ± SE (n = 3). * $p < 0.05$. There was no significant statistical difference for pairs without brackets.

Discussion

The concept of functionalizing nanoparticles with dual multivalent ligands for improved delivery of chemotherapy has only recently been pursued,[8,312,342,344,345,349,350,354] and with each success, the accompanying challenges emphasize the need for systematic understanding of relevant vehicle parameters and their effect on delivery to guide the design of efficient delivery vehicles. As delivery schemes become more sophisticated, the experiments necessary to fully characterize their cellular interactions become combinatorially complex, and the experimental load becomes unmanageable. Therefore, developing even basic models to establish critical parameters and general trends can guide more strategic experiment design.

Anticipated to significantly contribute to dual-ligand nanoparticle delivery efficiency, receptor expression was quantified for several cancer cell lines. Some general integrin expression trends can be elucidated where multiple cell lines from the same cancer type were characterized. The $\alpha_5\beta_1$ integrin is normally associated with ovarian cancer development and metastasis,[376] however there is conflicting evidence of the involvement of $\alpha_6\beta_4$ in ovarian cancer progression.[377,378] The ovarian cancer cells characterized here (SK-OV-3 and OVCAR-3) both have moderate to high levels of expression of the two integrins, with $\alpha_5\beta_1$:$\alpha_6\beta_4$ expression ratios close to unity, corroborating the evidence that both integrins are associated with ovarian cancer development. Upregulated $\alpha_5\beta_1$

expression has also been observed in breast cancer,[323,330] and poor prognosis[329,379] and metastases[328] in breast cancer patients is commonly associated with high levels of $\alpha_6\beta_4$ expression, particularly in triple negative breast cancer (an especially aggressive and hard to treat type of breast cancer). MDA-MB-231 and MDA-MB-468 cell lines, which have been identified as triple negative breast cancer cell lines,[380] express moderate to high levels of $\alpha_6\beta_4$ integrin (10^4-10^5 receptors/cell) and MDA-MB-231 also expresses high levels of $\alpha_5\beta_1$ (>10^5 receptors/cell). However, MCF7 cells, a breast cancer cell line that is not triple negative, expressed low levels of both integrins. High levels of $\alpha_6\beta_4$ and $\alpha_5\beta_1$ expression also facilitates invasive malignancy in colorectal cancer.[322,331] With the exception of RKO cells which have previously demonstrated negligible $\alpha_6\beta_4$ expression,[331] the characterized colorectal carcinoma cell lines expressed low to moderate levels of $\alpha_5\beta_1$ integrin (<10^5 receptors/cell) and high levels of $\alpha_6\beta_4$ expression (>10^5 receptors/cell). DU145 and PC3-LN4 cells, which are prostate carcinoma cell lines, exhibited $\alpha_5\beta_1$:$\alpha_6\beta_4$ expression ratios that were closer to unity than the colorectal cancer or breast cancer cell lines, with similar overall expression levels. LNCaP cells, another prostate carcinoma cell line, however, had almost 100 fold lower β_4 expression than $\alpha_5\beta_1$ and α_6 expression. While *in vitro* cellular expression analysis cannot always be extrapolated to *in vivo* environments, the characterization of cellular expression reported here of integrins which have been identified as cancer biomarkers highlights the subtleties usually neglected when receptor expression is reported qualitatively. In particular, quantification of receptor expression is critical in nanoparticle drug delivery when designing a vehicle with more than one type of ligand. Biomarker quantification of model tissues in preclinical studies provides correlation between treatment effectiveness and biomarker levels which can lead to accurate prediction of treatment outcomes for personalized medicine strategies.

In pursuit of a paradigm for dual-ligand vehicle design, a kinetic model was created to explore the effect of ligand valency and ratio, and receptor density and ratio on nanoparticle delivery. Implicit within the model are two assumptions. First is the assumption that ligands and receptors are homogenously distributed within the binding area. Peptide-amphiphiles have been observed to mix with PEGylated lipids at peptide-amphiphile concentrations below 10 mol% and above 35 mol%, while they phase separated at 10-35 mol%,[381] but it is unclear how the two ligands would distribute in relation to each other. The assumption of homogenous ligand distribution may therefore underestimate local ligand density, and evaluation of ligand distribution could improve the estimates of available ligand density. The assumption of homogenous distribution of receptors is a clear simplification of cellular biology, as receptor clustering into and out of focal adhesions and hemidesmosomes is well known integrin behavior,[280,382–384] which could be accounted for in the future with a previously developed model of receptor clustering.[356,385,386] Second is the

assumption that k_r is equivalent for every dissociation event and every k_x is proportional to the free nanoparticle k_f. It is difficult to directly measure differences in forward and reverse reaction rates for multivalent binding events, however when multivalent kinetic equations were fit to bivalent and trivalent experimental binding data, the reverse reaction rates for multivalent binding were calculated to be up to 100 fold slower than the k_r for the first ligand to bind, while the forward reaction rates were rarely more than 10 fold slower or faster,[358,387] suggesting that this assumption may be unrealistic. Despite the biological simplifications introduced by these assumptions, the model was able to predict the delivery enhancements achieved with optimal valency ratios for dual ligand nanoparticles targeting dual-receptor expressing cells.

Sensitivity analysis was performed for the input parameters chosen to generate Figure 32. The results varied little with changes in ligand-receptor k_f, however decreases in K_d (increases in affinity) decrease the optimal valency calculated for a dual-ligand nanoparticle binding to a dual-receptor expressing cell, while the potential selectivity reaches a maximum at a K_d of 2×10^{-5} M (Appendix B1), above which increasing affinity decreases binding. Similar results were observed when varying the receptor expression of the dual-receptor expressing cell; higher levels of receptor expression decreased the optimum valency of a dual-ligand nanoparticle, while the selectivity reaches a maximum around 3×10^4 receptors per cell (Appendix B2). The appearance of a maximum selectivity with variations in ligand density, K_d, and receptor expression suggests that increasing valency and affinity of ligand-receptor pairs will increase selectivity to an extent, but this selectivity can be inhibited by high valency or affinity interactions. The dependence of the selectivity on the comparative ligand-receptor affinities was also explored (Appendix B3). Notably, for up to a 9 fold difference in K_d between the two ligand-receptor pairs, the overall selectivity decreased, but maximum selectivity was still achieved with dual-ligand nanoparticles of equal valency. While this result hasn't been verified *in vitro*, it suggests that balancing ligand valency may be more significant to successful delivery than choosing ligands with equal affinities for their targets, and a dual targeted vehicle with a 50:50 ratio of ligands should bind with higher efficiency and selectivity to dual-receptor expressing cells as long as the affinities of the two ligands are within an order of magnitude of each other. The heteromultivalent kinetic model addresses the need for better understanding of the effect of binding parameters on delivery by identifying the ratio of valencies as an extremely critical design constraint. In addition, it revealed the existence of an optimum ligand density and receptor density, indicating that single-ligand delivery optimization is not applicable to dual-ligand construction.

Two important trends emerged from the model and the binding data. For dual-ligand nanoparticles with equal ligand valencies (50:50) delivered to dual-receptor expressing cells with

equal and high receptor expression levels: delivery is enhanced compared to single-ligand liposomes and selectivity for dual-receptor expressing cells is achieved compared to single-receptor expressing cells. The elucidation of these trends effectively guided the design of an efficient and specific gene delivery vehicle targeted to SK-OV-3 cells. Previous studies have identified 5 mol% PR_b as a sufficient concentration for single targeting applications.[74,79] In the 5 mol% 50:50 stealth liposome formulation used here, PR_b and AG86 are present at approximately 2.5 mol% each. The use of a substandard individual ligand concentration for effective dual-ligand targeting is consistent with the conclusion from the model that the optimal dual-ligand density is less than the optimal single-ligand density. Interestingly, when stealth liposomes were allowed to bind and internalize within cells with various receptor densities, the 50:50 dual-ligand stealth liposomes interacted more selectively with HT-1080 cells compared to all other cells, and there was no statistical difference between the liposomes that bound and internalized in HT-1080 and SK-OV-3 cells. HT-1080 cells express higher levels of $\alpha_5\beta_1$ than $\alpha_6\beta_4$, however, the ratio of $\alpha_5\beta_1$:$\alpha_6\beta_4$ expression is much smaller (1.9 fold) than the other cells with higher expression of one receptor out of the two targeted. The unexpected efficiency of dual-ligand liposome delivery to HT-1080 cells emphasizes the need for a more quantitative understanding of the parameter space governing multivalent delivery, perhaps suggesting a threshold of expression level and receptor ratio necessary for effective dual-ligand binding and internalization.

Liposome delivery for all formulations in Figure 37B is more efficient in HT-1080 cells compared to SK-OV-3 cells, which can't simply be explained by expression levels. In addition, binding and internalization within the LS174T cells was surprisingly low considering the expression levels measured for these cells. The high integrin internalization rates for the HT-1080 cells may partially account for the increased binding and internalization of the 50:50 formulation compared to binding for these cells. However, clustering, recycling and trafficking of integrins were not examined and may likely play a significant role as well. Integrin clustering is a significant regulator of extracellular matrix adhesion and cell signalling processes.[280,308,383,384,388] Approximately 20% of surface integrins have been observed in clusters,[382] and of these, integrins can exist in nascent or mature clusters with integrin densities of 365 and 875 integrins/μm^2 respectively, while the density of homogenously distributed receptors would be approximately 200 integrins/μm^2 which is a clear underestimation of available receptor valency.[389] These measurements, however, have only been performed in one cell type, and could vary significantly from cell to cell. The integrin mobility, and therefore ability to cluster, significantly increases with increasing temperature,[390] which could also contribute to unexpected increases in binding for certain cell types when nanoparticles were delivered at 37 °C compared to 4 °C. Intracellular

trafficking of integrins can also vary with cell type. For example, $\alpha_5\beta_1$ internalization is clathrin dependant in fibrosarcoma cells,[388] and caveolin mediated in ovarian and colorectal cancer cells.[274,391] Internalization of active and inactive forms of $\alpha_5\beta_1$ integrin can be regulated via different pathways,[280,388] and internalization of other integrins can even influence internalization rates and pathways of certain integrins.[388] Once internalized, $\alpha_5\beta_1$ and $\alpha_6\beta_4$ are either degraded, or recycled through long-loop recycling, which involves trafficking through early endosomes to the perinuclear recycling complex, and a Rab11 GTPase dependent return to the cell surface.[280,308] The decision between integrin degradation or recycling may depend on integrin activation state mediated by native, and potentially synthetic, ligand binding.[280,308] Further elucidation of integrin biology is therefore required for accurate predictions of nanoparticle-cell interactions for different cell types. The current kinetic model used in this study only addresses binding, however the *in vitro* results at 37 °C suggest that internalization and integrin biology are not negligible in delivery considerations, and a more extensive guide for vehicle design should include these effects.

Though the cells investigated here are cancer cell lines, the comparative receptor expression levels may also be used as a model for tissue types encountered *in vivo*: the high dual-receptor expressing SK-OV-3 cells represent cancer tissue with high levels of expression of both receptors. MCF7 cells have expression levels comparable to levels observed for common cancer biomarkers such as EGFR and VEGFR in healthy cells,[371,372] and therefore represent healthy tissue with much lower expression of both receptors. The cell lines with differential expression levels of the two integrins (RKO, HT-1080, LS 174T and SW 1990) model any healthy tissue with high levels of expression of only one of the cancer biomarkers, which would be the site of toxicity when mechanism based toxicity is encountered in healthy sites. With this potential model of tissue in mind, the work here demonstrates the ability to design an efficient delivery vehicle that may selectively target dual-receptor expressing cancer tissue, while minimizing binding to healthy tissue unintentionally reached by conventional targeted therapies.

Acknowledgements

The flow cytometry analysis was performed in the University Flow Cytometry Resource. This work was funded by NSF/CBET-1403564.

Chapter 5 Concluding Remarks and Future Directions

This thesis addresses the delivery challenges currently limiting the field of cancer gene therapy. Many advances have been made throughout the years, as discussed at great length in Chapter 1, however gene therapy solutions for cancer are still largely absent from clinical treatments. Gene therapy faces several significant hurdles between systemic administration and intracellular expression, and in an attempt to overcome these hurdles, an established small molecule delivery technology, the stealth liposome, was translated for encapsulation and delivery of nucleic acids. Stealth liposome technology is an ideal choice to protect nucleic acids from degradation, clearance and immunogenicity, and the addition of targeting ligands integrates the passive and active targeting effects that can facilitate tumor accumulation, while a combination of the targeting and the nucleic acid-polymer complex contributes to cellular internalization and cytosolic or nuclear delivery of nucleic acids. A major objective throughout the development of this vehicle was the establishment of general design criteria for further vehicle development, and to that end, each layer of vehicle construction was systematically investigated for its significance to vehicle properties and delivery capacity.

As outlined in Chapter 2, stealth liposomes were first developed for plasmid DNA encapsulation. In order to encapsulate plasmid DNA, which is much larger than the small molecules typically encapsulated in stealth liposomes, DNA was first condensed into nanoparticles using PEI. The complex vehicle design required the development and verification of a new quantification tool. General guidelines were then outlined for the encapsulation process, and through exploration of material composition, the ability to tune DNA yield and liposome loading fraction was demonstrated through variations in lipid:DNA ratios. Higher lipid:DNA ratios favor higher yields, while lower ratios favor liposome loading.

With the tools developed for DNA encapsulation, stealth liposome technology was readily translated for siRNA applications in Chapter 3. A lower lipid:nucleic acid ratio was employed to enhance loaded liposome fraction, since targeting was introduced for this vehicle. Another aspect of vehicle design was explored with the goal of addressing the critical gene delivery barrier of appropriate intracellular localization upon delivery. Complexation with PEI, a cationic polymer with high buffering capacity, was necessary for siRNA-mediated gene silencing via targeted stealth liposomes, and the identification of the optimal siRNA:polymer ratio was clearly important to successful transfection.

The next aspect of the gene delivery scheme that was explored was the ability to effectively and selectively target disease tissue through dual-ligand targeting. The addition of a second targeting ligand significantly increased the design complexity which warranted the development of a kinetic model to inform experimental choices and verify experimental trends. With the intention of elucidating design criteria, several aspects of the targeting parameter space were characterized. Optimal delivery and selectivity was described for dual-ligand stealth liposomes targeting dual-receptor expressing cells. By characterizing and varying receptor expression and ratio, and ligand density and ratio, the importance of these parameters in targeting design was demonstrated. Combining the optimal dual targeting formulation with the previously developed nucleic acid encapsulation tools produced a highly efficient and cell line selective gene delivery vehicle for cancer gene therapy applications.

Future Directions

PEI exhibited an important role in targeted stealth liposomes transfection of siRNA, perhaps synergistically with $\alpha_6\beta_4$ targeting, however, the mechanism of transfection enhancement remains elusive. The internalization pathway mediated by the targeting ligand could be identified through pathway disruption, and intracellular localization and cytosolic release could be investigated through confocal imaging and pH sensitive fluorescent probes. Elucidation of the intracellular pathways utilized by the optimized siRNA delivery vehicle could direct targeting ligand choice towards those that rely on similar internalization pathways. PEI can elicit toxicity at high concentrations,[392,393] and although no toxicity was observed with the vehicle concentrations explored in Chapter 2, it may be beneficial to replace PEI with a more biocompatible polymer. PEI could be substituted within the liposomes with other polymers with a broad range of buffering capacity, with the goal of identifying an optimal buffering capacity to inform property characterization for novel polymer design.

Chapter 4 focuses on the influence of variations in receptor and ligand ratios on nanoparticle binding, however, several other vehicle parameters with potential delivery impact are easily modifiable for further characterization of the dual-ligand delivery parameter space. Ligand and receptor mobility proved significant for immunoliposome targeting of ICAM and ELAM,[349] and the impact of mobility on the delivery scheme designed here could be explored using cellular fixation or lipids with various bilayer packing properties. The model revealed the theoretical existence of an optimal overall ligand density above which no further benefit to binding is gained, and also suggested that nanoparticle binding was relatively tolerant to differences in ligand-receptor pair affinities. These concepts could be verified *in vitro*, by comparing dual-ligand liposome

formulations with various overall ligand densities, and by tuning the affinity of one of the ligands. Additional receptors could also be targeted to explore the effect of receptor biology, such as clustering, mobility, internalization pathway and rates, on nanoparticle delivery.

The final goal of the development of targeted gene delivery for cancer therapy is to surmount the *in vivo* barriers to effective gene therapy in order to take advantage of the cellular level benefits demonstrated by this vehicle. Each delivery barrier presents distinct challenges and warrants unique improvements to further vehicle design. It will therefore be important to identify any additional obstacle to delivery effectiveness by assessing biodistribution with *in vivo* and *ex vivo* imaging techniques, intratumoral and intracellular localization with immunohistochemistry, and function using an easily measurable transfection outcome such as fluorescence or luminescence.

Final Words

As our understanding of the mechanisms driving and characterizing cancer becomes more sophisticated, so will our delivery vehicles. The objective in developing targeted stealth liposomes encapsulating gene therapy is therefore not only to achieve superior delivery and transfection, but to contribute to the establishment of a paradigm to guide more intelligent vehicle design. Using modular vehicles, consisting of nucleic acid complexation, stealth liposome encapsulation and one or more targeting moieties, provides extra flexibility in tuning vehicle characteristics to address specific challenges. The concepts presented in this work can be used as a platform upon which to build delivery schemes for innumerable applications.

Bibiography

1. Luo, D. & Saltzman, W. M. Synthetic DNA delivery systems. *Nat. Biotechnol.* **18,** 33–37 (2000).
2. Cichon, G. *et al.* Intravenous administration of recombinant adenoviruses causes thrombocytopenia, anemia and erythroblastosis in rabbits. *J. Gene Med.* **1,** 360–71 (1999).
3. Muruve, D. A., Barnes, M. J., Stillman, I. E. & Libermann, T. A. Adenoviral gene therapy leads to rapid induction of multiple chemokines and acute neutrophil-dependent hepatic injury in vivo. *Hum. Gene Ther.* **10,** 965–976 (1999).
4. Buckley, R. H. Gene therapy for SCID - a complication after remarkable progress. *Lancet* **360,** 1185–1186 (2002).
5. Marshall, E. Clinical research - Gene therapy a suspect in leukemia-like disease. *Science* **298,** 34–35 (2002).
6. Pack, D. W., Hoffman, A. S., Pun, S. & Stayton, P. S. Design and development of polymers for gene delivery. *Nat. Rev. Drug Discov.* **4,** 581–593 (2005).
7. Suk, J. S. *et al.* Gene delivery to differentiated neurotypic cells with RGD and HIV Tat peptide functionalized polymeric nanoparticles. *Biomaterials* **27,** 5143–50 (2006).
8. Nie, Y. *et al.* Dual-targeted polyplexes: one step towards a synthetic virus for cancer gene therapy. *J. Control. Release* **152,** 127–134 (2011).
9. Medina-Kauwe, L. K., Maguire, M., Kasahara, N. & Kedes, L. Nonviral gene delivery to human breast cancer cells by targeted Ad5 penton proteins. *Gene Ther.* **8,** 1753–61 (2001).
10. Perez-Martinez, F. C. *et al.* Barriers to Non-Viral Vector-Mediated Gene Delivery in the Nervous System. *Pharm. Res.* **28,** 1843–58 (2011).
11. Xiong, X.-B. B., Uludag, H., Lavasanifar, A., Uludağ, H. & Lavasanifar, A. Virus-mimetic polymeric micelles for targeted siRNA delivery. *Biomaterials* **31,** 5886–93 (2010).
12. Zuber, G., Dontenwill, M. & Behr, J. P. Synthetic viruslike particles for targeted gene delivery to alphavbeta3 integrin-presenting endothelial cells. *Mol. Pharm.* **6,** 1544–1552 (2009).
13. Andreu, A., Fairweather, N. & Miller, A. D. Clostridium neurotoxin fragments as potential targeting moieties for liposomal gene delivery to the CNS. *Chembiochem* **9,** 219–231 (2008).
14. Talsma, S. S., Babensee, J. E., Murthy, N. & Williams, I. R. Development and in vitro validation of a targeted delivery vehicle for DNA vaccines. *J. Control. Release* **112,** 271–9 (2006).
15. Ferrer-Miralles, N., Vázquez, E., Villaverde, A., Vazquez, E. & Villaverde, A. Membrane-active peptides for non-viral gene therapy: making the safest easier. *Trends Biotechnol.* **26,** 267–75 (2008).
16. Duan, Y. J. *et al.* Poly(ethylene glycol)-Grafted Polyethylenimine Modified with G250 Monoclonal Antibody for Tumor Gene Therapy. *Hum. Gene Ther.* **21,** 191–198 (2010).
17. Martin-Herranz, A. *et al.* Surface functionalized cationic lipid-DNA complexes for gene delivery: PEGylated lamellar complexes exhibit distinct DNA-DNA interaction regimes. *Biophys. J.* **86,** 1160–1168 (2004).
18. Pearce, T. R., Shroff, K. & Kokkoli, E. Peptide Targeted Lipid Nanoparticles for Anti-Cancer Drug Delivery. *Adv. Mater.* **24,** 3803–3822 (2012).
19. Khalil, I. A., Kogure, K., Akita, H. & Harashima, H. Uptake Pathways and Subsequent Intracellular Trafficking in Nonviral Gene Delivery. *Pharmacol. Rev.* **58,** 32–45 (2006).
20. Pangburn, T. O., Petersen, M. A., Waybrant, B., Adil, M. M. & Kokkoli, E. Peptide- and

aptamer-functionalized nanovectors for targeted delivery of therapeutics. *J. Biomech. Eng.* **131,** 074005 (2009).
21. Chen, K. & Conti, P. S. Target-specific delivery of peptide-based probes for PET imaging. *Adv. Drug Deliv. Rev.* **62,** 1005–22 (2010).
22. Khan, J. *et al.* Classification and diagnostic prediction of cancers using gene expression profiling and artificial neural networks. *Nat. Med.* **7,** 673–9 (2001).
23. Wen, S. F. *et al.* Assessment of p53 gene transfer and biological activities in a clinical study of adenovirus-p53 gene therapy for recurrent ovarian cancer. *Cancer Gene Ther.* **10,** 224–238 (2003).
24. Brummelkamp, T. R., Bernards, R. & Agami, R. Stable suppression of tumorigenicity by virus-mediated RNA interference. *Cancer Cell* **2,** 243–7 (2002).
25. Crnkovic-Mertens, I., Hoppe-Seyler, F. & Butz, K. Induction of apoptosis in tumor cells by siRNA-mediated silencing of the livin/ML-IAP/KIAP gene. *Oncogene* **22,** 8330–8336 (2003).
26. Xu, G. & McLeod, H. L. Strategies for enzyme/prodrug cancer therapy. *Clin. Cancer Res.* **7,** 3314–3324 (2001).
27. Westphal, E. M., Ge, J., Catchpole, J. R., Ford, M. & Kenney, S. C. The nitroreductase/CB1954 combination in Epstein-Barr virus-positive B-cell lines: induction of bystander killing in vitro and in vivo. *Cancer Gene Ther.* **7,** 97 (2000).
28. Schmitz, V. *et al.* Treatment of colorectal and hepatocellular carcinomas by adenoviral mediated gene transfer of endostatin and angiostatin-like molecule in mice. *Gut* **53,** 561–567 (2004).
29. Palmer, D. H., Young, L. S. & Mautner, V. Cancer gene-therapy: clinical trials. *Trends Biotechnol.* **24,** 76–82 (2006).
30. McNeish, I. a, Bell, S. J. & Lemoine, N. R. Gene therapy progress and prospects: cancer gene therapy using tumour suppressor genes. *Gene Ther.* **11,** 497–503 (2004).
31. Chandler, L. A. *et al.* Prevalent expression of fibroblast growth factor (FGF) receptors and FGF2 in human tumor cell lines. *Int. J. Cancer* **81,** 451–458 (1999).
32. Niu, G. Q., Driessen, W. H. P., Sullivan, S. M. & Hughes, J. A. In Vivo Anti-Tumor Effect of Expressing p14ARF-TAT Using a FGF2-Targeted Cationic Lipid Vector. *Pharm. Res.* **28,** 720–30 (2011).
33. Maruta, F. *et al.* Identification of FGF receptor-binding peptides for cancer gene therapy. *Cancer Gene Ther.* **9,** 543–52 (2002).
34. Rao, G. a, Tsai, R., Roura, D. & Hughes, J. A. Evaluation of the transfection property of a peptide ligand for the fibroblast growth factor receptor as part of PEGylated polyethylenimine polyplex. *J. Drug Deliv.* **16,** 79–89 (2008).
35. Akinc, A., Thomas, M., Klibanov, A. M. & Langer, R. Exploring polyethylenimine-mediated DNA transfection and the proton sponge hypothesis. *J. Gene Med.* **7,** 657–663 (2005).
36. Li, D. *et al.* Construction of a Star-Shaped Copolymer as a Vector for FGF Receptor-Mediated Gene Delivery In Vitro and In Vivo. *Biomacromolecules* **11,** 2221–2229 (2010).
37. Klapper, L. N. *et al.* The ErbB-2/HER2 oncoprotein of human carcinomas may function solely as a shared coreceptor for multiple stroma-derived growth factors. *Proc. Natl. Acad. Sci.* **96,** 4995–5000 (1999).
38. Singh, A. B. & Harris, R. C. Autocrine, paracrine and juxtacrine signaling by EGFR ligands. *Cell. Signal.* **17,** 1183–1193 (2005).
39. Li, Z. H. *et al.* Identification and characterization of a novel peptide ligand of epidermal growth factor receptor for targeted delivery of therapeutics. *FASEB J.* **19,** 1978–85 (2005).
40. Schäfer, a *et al.* Disconnecting the Yin and Yang Relation of Epidermal Growth Factor Receptor (EGFR)-Mediated Delivery: A Fully Synthetic, EGFR-Targeted Gene Transfer System Avoiding Receptor Activation. *Hum. Gene Ther.* **22,** 1463–73 (2011).

41. Magadala, P. & Amiji, M. Epidermal growth factor receptor-targeted gelatin-based engineered nanocarriers for DNA delivery and transfection in human pancreatic cancer cells. *AAPS J.* **10,** 565–76 (2008).
42. Sun, Y.-X. X. *et al.* The influence of RGD addition on the gene transfer characteristics of disulfide-containing polyethyleneimine/DNA complexes. *Biomaterials* **29,** 4356–65 (2008).
43. Ng, Q. K. T. *et al.* Engineering Clustered Ligand Binding Into Nonviral Vectors: alpha(v)beta(3) Targeting as an Example. *Mol. Ther.* **17,** 828–36 (2009).
44. Zhou, Q.-H. H. *et al.* Cyclic RGD-targeting of reversibly stabilized DNA nanoparticles enhances cell uptake and transfection in vitro. *J. Drug Target.* **17,** 364–373 (2009).
45. Lee, J. H. *et al.* All- in- One Target- Cell- Specific Magnetic Nanoparticles for Simultaneous Molecular Imaging and siRNA Delivery. *Angew. Chemie* **48,** 4174–4179 (2009).
46. Katow, H., Yazawa, S. & Sofuku, S. A fibronectin-related synthetic peptide, pro-ala-ser-ser, inhibits fibronectin binding to the cell-surface, fibronectin-promoted cell-migration in vitro, and cell-migration in vivo. *Exp. Cell Res.* **190,** 17–24 (1990).
47. Yamada, K. M. & Kennedy, D. W. Dualistic nature of adhesive protein function: fibronectin and its biologically active peptide fragments can autoinhibit fibronectin function. *J. Cell Biol.* **99,** 29–36 (1984).
48. Parkhouse, S. M., Garnett, M. C. & Chan, W. C. Targeting of polyamidoamine-DNA nanoparticles using the Staudinger ligation: attachment of an RGD motif either before or after complexation. *Bioorg. Med. Chem.* **16,** 6641–50 (2008).
49. Haubner, R. *et al.* Structural and functional aspects of RGD-containing cyclic pentapeptides as highly potent and selective integrin alpha(v)beta(3) antagonists. *J. Am. Chem. Soc.* **118,** 7461–7472 (1996).
50. Kaneshiro, T. L. & Lu, Z.-R. R. Targeted intracellular codelivery of chemotherapeutics and nucleic acid with a well-defined dendrimer-based nanoglobular carrier. *Biomaterials* **30,** 5660–6 (2009).
51. Studeny, M. *et al.* Bone marrow-derived mesenchymal stem cells as vehicles for interferon-beta delivery into tumors. *Cancer Res.* **62,** 3603–3608 (2002).
52. Sazani, P. & Kole, R. Therapeutic potential of antisense oligonucleotides as modulators of alternative splicing. *J. Clin. Invest.* **112,** 481–486 (2003).
53. Kang, H., Alam, M. R., Dixit, V., Fisher, M. & Juliano, R. L. Cellular delivery and biological activity of antisense oligonucleotides conjugated to a targeted protein carrier. *Bioconjug. Chem.* **19,** 2182–8 (2008).
54. Kunath, K. *et al.* Integrin targeting using RGD-PEI conjugates for in vitro gene transfer. *J. Gene Med.* **5,** 588–99 (2003).
55. Han, H. D. *et al.* Targeted Gene Silencing Using RGD-Labeled Chitosan Nanoparticles. *Clin. Cancer Res.* **16,** 3910–3922 (2010).
56. Koivunen, E., Wang, B. C. & Ruoslahti, E. Phage libraries displaying cyclic peptides with different ring sizes: ligand specificities of the RGD-directed integrins. *Nat. Biotechnol.* **13,** 265–270 (1995).
57. Pasqualini, R., Koivunen, E. & Ruoslahti, E. alpha v Integrins as receptors for tumor targeting by circulating ligands. *Nat. Biotechnol.* **15,** 542–546 (1997).
58. Anwer, K., Kao, G., Rolland, A., Driessen, W. H. P. & Sullivan, S. M. Peptide-mediated gene transfer of cationic lipid/plasmid DNA complexes to endothelial cells. *J. Drug Target.* **12,** 215–21 (2004).
59. Carlisle, R. C., Read, M. L., Wolfert, M. A. & Seymour, L. W. Self-assessing poly(L-lysine)/DNA complexes capable of integrin-mediated cellular uptake and gene expression. *Colloids and Surfaces B-Biointerfaces* **16,** 261–272 (1999).
60. Parker, A. L. *et al.* Enhanced gene transfer activity of peptide-targeted gene-delivery

vectors. *J. Drug Target.* **13,** 39–51 (2005).
61. Kim, J., Kim, S. W. & Kim, W. J. PEI-g-PEG-RGD/Small Interference RNA Polyplex-Mediated Silencing of Vascular Endothelial Growth Factor Receptor and Its Potential as an Anti-Angiogenic Tumor Therapeutic Strategy. *Oligonucleotides* **21,** 101–7 (2011).
62. Suh, W., Han, S. O., Yu, L. & Kim, S. W. An angiogenic, endothelial-cell-targeted polymeric gene carrier. *Mol. Ther.* **6,** 664–672 (2002).
63. Harvie, P. *et al.* Targeting of lipid-protamine-DNA (LPD) lipopolyplexes using RGD motifs. *J. Liposome Res.* **13,** 231–247 (2003).
64. Kim, W. J. *et al.* Soluble Flt-1 gene delivery using PEI-g-PEG-RGD conjugate for anti-angiogenesis. *J. Control. Release* **106,** 224–34 (2005).
65. Muschler, J. L. & Horwitz, A. F. Down-regulation of the chicken alpha5beta1 integrin fibronectin receptor during development. *Development* **113,** 327–337 (1991).
66. Hart, S. L. *et al.* Lipid-mediated enhancement of transfection by a nonviral integrin-targeting vector. *Hum. Gene Ther.* **9,** 575–585 (1998).
67. Mardilovich, A., Craig, J., McCammon, M. Q., Garg, A. & Kokkoli, E. Design of a Novel Fibronectin-Mimetic Peptide-Amphiphile for Functionalized Biomaterials. *Langmuir* **22,** 3259–3264 (2006).
68. Shroff, K., Pearce, T. R. & Kokkoli, E. Enhanced integrin mediated signaling and cell cycle progression on fibronectin mimetic peptide amphiphile monolayers. *Langmuir* **28,** 1858–65 (2012).
69. Pangburn, T. O., Bates, F. S. & Kokkoli, E. Polymersomes functionalized via 'click' chemistry with the fibronectin mimetic peptides PR_b and GRGDSP for targeted delivery to cells with different levels of α5β1 expression. *Soft Matter* **8,** 4449 (2012).
70. Craig, J. A., Rexeisen, E. L., Mardilovich, A., Shroff, K. & Kokkoli, E. Effect of linker and spacer on the design of a fibronectin-mimetic peptide evaluated via cell studies and AFM adhesion forces. *Langmuir* **24,** 10282–10292 (2008).
71. Mardilovich, A. & Kokkoli, E. Biomimetic peptide-amphiphiles for functional biomaterials: The role of GRGDSP and PHSRN. *Biomacromolecules* **5,** 950–957 (2004).
72. Garg, A. & Kokkoli, E. pH-Sensitive PEGylated liposomes functionalized with a fibronectin-mimetic peptide show enhanced intracellular delivery to colon cancer cells. *Curr. Pharm. Biotechnol.* **12,** 1135–1143 (2011).
73. Garg, A., Tisdale, A. W., Haidari, E. & Kokkoli, E. Targeting colon cancer cells using PEGylated liposomes modified with a fibronectin-mimetic peptide. *Int. J. Pharm.* **366,** 201–210 (2009).
74. Demirgöz, D. *et al.* PR_b-Targeted PEGylated Liposomes for Prostate Cancer Therapy. *Langmuir* **24,** 13518–13524 (2008).
75. Demirgöz, D. *et al.* PR_b-targeted delivery of tumor necrosis factor-α by polymersomes for the treatment of prostate cancer. *Soft Matter* **5,** 2011 (2009).
76. Atchison, N. A. *et al.* Binding of the fibronectin-mimetic peptide, PR_b, to alpha5beta1 on pig islet cells increases fibronectin production and facilitates internalization of PR_b functionalized liposomes. *Langmuir* **26,** 14081–8 (2010).
77. Shroff, K. & Kokkoli, E. PEGylated liposomal doxorubicin targeted to α5β1-expressing MDA-MB-231 breast cancer cells. *Langmuir* **28,** 4729–4736 (2012).
78. Pangburn, T. O., Georgiou, K., Bates, F. S. F. & Kokkoli, E. Targeted Polymersome Delivery of siRNA Induces Cell Death of Breast Cancer Cells Dependent upon Orai3 Protein Expression. *Langmuir* **28,** 12816–12830 (2012).
79. Adil, M. *et al.* PR_b Functionalized Stealth Liposomes for Targeted Delivery to Metastatic Colon Cancer. *Biomater. Sci.* **1,** 393–401 (2013).
80. Nicklin, S. A., White, S. J., Watkins, S. J., Hawkins, R. E. & Baker, A. H. Selective targeting of gene transfer to vascular endothelial cells by use of peptides isolated by phage display. *Circulation* **102,** 231–237 (2000).

81. Oku, N. *et al.* Anti-neovascular therapy using novel peptides homing to angiogenic vessels. *Oncogene* **21,** 2662–2669 (2002).
82. Oreilly, M. S., Holmgren, L., Chen, C. & Folkman, J. Angiostatin induces and sustains dormancy of human primary tumors in mice. *Nat. Med.* **2,** 689–692 (1996).
83. Lu, Z. X., Liu, L. T. & Qi, X. R. Development of small interfering RNA delivery system using PEI-PEG-APRPG polymer for antiangiogenic vascular endothelial growth factor tumor-targeted therapy. *Int. J. Nanomedicine* **6,** 1661–1673 (2011).
84. Koolpe, M., Dail, M. & Pasquale, E. B. An ephrin mimetic peptide that selectively targets the EphA2 receptor. *J. Biol. Chem.* **277,** 46974–46979 (2002).
85. Blackburn, W. H., Dickerson, E. B., Smith, M. H., McDonald, J. F. & Lyon, L. A. Peptide-Functionalized Nanogels for Targeted siRNA Delivery. *Bioconjug. Chem.* **20,** 960–8 (2009).
86. Dickerson, E. B. *et al.* Chemosensitization of cancer cells by siRNA using targeted nanogel delivery. *BMC Cancer* **10,** 10 (2010).
87. Porkka, K., Laakkonen, P., Hoffman, J. A., Bernasconi, M. & Ruoslahti, E. A fragment of the HMGN2 protein homes to the nuclei of tumor cells and tumor endothelial cells in vivo. *Proc. Natl. Acad. Sci.* **99,** 7444–7449 (2002).
88. Ginisty, H., Sicard, H., Roger, B. & Bouvet, P. Structure and functions of nucleolin. *J. Cell Sci.* **112,** 761–772 (1999).
89. Hovanessian, A. G. Midkine, a cytokine that inhibits HIV infection by binding to the cell surface expressed nucleolin. *Cell Res.* **16,** 174–181 (2006).
90. Hovanessian, A. G. *et al.* The cell-surface-expressed nucleolin is associated with the actin cytoskeleton. *Exp. Cell Res.* **261,** 312–328 (2000).
91. Nisole, S., Krust, B. & Hovanessian, A. G. Anchorage of HIV on permissive cells leads to coaggregation of viral particles with surface nucleolin at membrane raft microdomains. *Exp. Cell Res.* **276,** 155–173 (2002).
92. Watanabe, T. *et al.* Nucleolin on the Cell Surface as a New Molecular Target for Gastric Cancer Treatment. *Biol. Pharm. Bull.* **33,** 796–803 (2010).
93. Christian, S. *et al.* Nucleolin expressed at the cell surface is a marker of endothelial cells in angiogenic blood vessels. *J. Cell Biol.* **163,** 871–878 (2003).
94. Derfus, A. M., Chen, A. A., Min, D.-H. H., Ruoslahti, E. & Bhatia, S. N. Targeted quantum dot conjugates for siRNA delivery. *Bioconjug. Chem.* **18,** 1391–6 (2007).
95. Arap, W., Pasqualini, R. & Ruoslahti, E. Cancer treatment by targeted drug delivery to tumor vasculature in a mouse model. *Science* **279,** 377–380 (1998).
96. Pasqualini, R. *et al.* Aminopeptidase N is a receptor for tumor-homing peptides and a target for inhibiting angiogenesis. *Cancer Res.* **60,** 722–727 (2000).
97. Chen, Y., Wu, J. J. & Huang, L. Nanoparticles targeted with NGR motif deliver c-myc siRNA and doxorubicin for anticancer therapy. *Mol. Ther.* **18,** 828–34 (2010).
98. Xia, H. B., Anderson, B., Mao, Q. W. & Davidson, B. L. Recombinant human adenovirus: Targeting to the human transferrin receptor improves gene transfer to brain microcapillary endothelium. *J. Virol.* **74,** 11359–11366 (2000).
99. Deuel, T. F., Keim, P. S., Farmer, M. & Heinrikson, R. L. Amino-Acid Sequence of Human Platelet Factor 4. *Proc. Natl. Acad. Sci.* **74,** 2256–2258 (1977).
100. Butcher, D. J. *et al.* A natural motif approach to protein design: A synthetic leucine zipper peptide mimics the biological function of the platelet factor 4 protein. *FEBS Lett.* **409,** 183–187 (1997).
101. Handin, R. I. & Cohen, H. J. Purification and Binding Properties of Human Platelet Factor 4. *J. Biol. Chem.* **251,** 4273–4282 (1976).
102. Liu, S. C. *et al.* cDNA cloning and expression of HIP, a novel cell surface heparan sulfate/heparin-binding protein of human uterine epithelial cells and cell lines. *J. Biol. Chem.* **271,** 11817–11823 (1996).

103. Tylercross, R., Sobel, M., Marques, D. & Harris, R. B. Heparin-Binding Domain Peptides of Antithrombin-III - Analysis by Isothermal Titration Calorimetry and Circular-Dichroism Spectroscopy. *Protein Sci.* **3,** 620–627 (1994).
104. TylerCross, R., Sobel, M., McAdory, L. E. & Harris, R. B. Structure-function relations of antithrombin III-heparin interactions as assessed by biophysical and biological assays and molecular modeling of peptide-pentasaccharide-docked complexes. *Arch. Biochem. Biophys.* **334,** 206–213 (1996).
105. Fichter, K. M., Zhang, L., Kiick, K. L. & Reineke, T. M. Peptide-Functionalized Poly (ethylene glycol) Star Polymers : DNA Delivery Vehicles with Multivalent Molecular Architecture. *Bioconjug. Chem.* **19,** 76–88 (2008).
106. Koch Baram, T., Chobsieng, P. &Fridkin, M., Y. Enzymatic Degradation of Lutenizing Hormone-Releasing Hormone (LH-RH) by Hypothalamic Tissue. *Biochem. Biophys, Res. Commun.* **61,** (1974).
107. Coy, D. H., Vilchezmartinez, J. A., Coy, E. J. & Schally, A. V. Analogs of Luteinizing-Hormone-Releasing Hormone with Increased Biological-Activity Produced by D-Amino-Acid Substitutions in Position 6. *J. Med. Chem.* **19,** 423–425 (1976).
108. Koch Baram, T., Hazum, E. &Fridkin, M., Y. Resistance to Enzymatic Degradation of LH-RH Analogues Possessing Increased Biological Activity. *Biochem. Biophys, Res. Commun.* **74,** 488–491 (1977).
109. Kim, S. H. W. H. W., Jeong, J. H., Lee, S. H., Kim, S. H. W. H. W. & Park, T. G. LHRH receptor-mediated delivery of siRNA using polyelectrolyte complex micelles self-assembled from siRNA-PEG-LHRH conjugate and PEI. *Bioconjug. Chem.* **19,** 2156–62 (2008).
110. Taratula, O. *et al.* Surface-engineered targeted PPI dendrimer for efficient intracellular and intratumoral siRNA delivery. *J. Control. Release* **140,** 284–93 (2009).
111. Mandel, R. J. *et al.* Characterization of intrastriatal recombinant adeno-associated virus-mediated gene transfer of human tyrosine hydroxylase and human GTP-cyclohydrolase I in a rat model of Parkinson's disease. *J. Neurosci.* **18,** 4271–4284 (1998).
112. Bilang-Bleuel, A. *et al.* Intrastriatal injection of an adenoviral vector expressing glial-cell-line-derived neurotrophic factor prevents dopaminergic neuron degeneration and behavioral impairment in a rat model of Parkinson disease. *Proc. Natl. Acad. Sci.* **94,** 8818 (1997).
113. Choi-Lundberg, D. L. *et al.* Dopaminergic neurons protected from degeneration by GDNF gene therapy. *Science* **275,** 838–841 (1997).
114. Kells, A. P. *et al.* AAV-mediated gene delivery of BDNF or GDNF is neuroprotective in a model of Huntington disease. *Mol. Ther.* **9,** 682–688 (2004).
115. Holtzman, D. M. *et al.* TrkA Expression in the CNS - Evidence for the Existence of Several Novel NGF-Responsive CNS Neurons. *J. Neurosci.* **15,** 1567–1576 (1995).
116. Ibáñez, C. F. Neurotrophic factors: from structure-function studies to designing effective therapeutics. *Trends Biotechnol.* **13,** 217–27 (1995).
117. Wiesmann, C., Ultsch, M. H., Bass, S. H. & de Vos, A. M. Crystal structure of nerve growth factor in complex with the ligand-binding domain of the TrkA receptor. *Nature* **401,** 184–8 (1999).
118. Zeng, J., Too, H.-P., Ma, Y., Luo, E. S. E. & Wang, S. A synthetic peptide containing loop 4 of nerve growth factor for targeted gene delivery. *J. Gene Med.* **6,** 1247–56 (2004).
119. Zeng, J. & Wang, S. Enhanced gene delivery to PC12 cells by a cationic polypeptide. *Biomaterials* **26,** 679–86 (2005)
120. Barrett, G. L., Trieu, J. & Naim, T. The identification of leptin-derived peptides that are taken up by the brain. *Regul. Pept.* **155,** 55–61 (2009).
121. Liu, Y. *et al.* A leptin derived 30-amino-acid peptide modified pegylated poly-L-lysine dendrigraft for brain targeted gene delivery. *Biomaterials* **31,** 5246–57 (2010).
122. Lentz, T. L., Burrage, T. G., Smith, A. L., Crick, J. & Tignor, G. H. Is the Acetylcholine-

Receptor a Rabies Virus Receptor. *Science* **215,** 182–184 (1982).
123. Lentz, T. L., Wilson, P. T., Hawrot, E. & Speicher, D. W. Amino-Acid-Sequence Similarity Between Rabies Virus Glycoprotein and Snake-Venom Curaremimetic Neurotoxins. *Science* **226,** 847–848 (1984).
124. Karlsson, E. Chemistry of protein toxins in snake venoms. *Handb. Exp. Pharmacol.* **52,** 159–212 (1979).
125. Kumar, P. *et al.* Transvascular delivery of small interfering RNA to the central nervous system. *Nature* **448,** 39–43 (2007).
126. Lentz, T. L., Hawrot, E. & Wilson, P. T. Synthetic Peptides Corresponding to Sequences of Snake-Venom Neurotoxins and Rabies Virus Glycoprotein Bind to the Nicotinic Acetylcholine-Receptor. *Proteins-Structure Funct. Genet.* **2,** 298–307 (1987).
127. Alvarez-Erviti, L. *et al.* Delivery of siRNA to the mouse brain by systemic injection of targeted exosomes. *Nat. Biotechnol.* **29,** 341–U179 (2011).
128. Valadi, H. *et al.* Exosome-mediated transfer of mRNAs and microRNAs is a novel mechanism of genetic exchange between cells. *Nat. Cell Biol.* **9,** 654–9 (2007).
129. Vassar, R. *et al.* β-secretase cleavage of Alzheimer's amyloid precursor protein by the transmembrane aspartic protease BACE. *Science* **286,** 735–741 (1999).
130. Gong, C., Li, X., Xu, L. & Zhang, Y.-H. H. Target delivery of a gene into the brain using the RVG29-oligoarginine peptide. *Biomaterials* **33,** 3456–63 (2012).
131. Liu, J. K. *et al.* A novel peptide defined through phage display for therapeutic protein and vector neuronal targeting. *Neurobiol. Dis.* **19,** 407–418 (2005).
132. Martinez-Fong, D. *et al.* Neurotensin-SPDP-poly-L-lysine conjugate: a nonviral vector for targeted gene delivery to neural cells. *Mol. Brain Res.* **69,** 249–262 (1999).
133. Park, I.-K. K., Lasiene, J., Chou, Sh.-H. H., Horner, P. J. & Pun, S. H. Neuron-specific delivery of nucleic acids mediated by Tet1- modified poly(ethylenimine). *J. Gene Med.* **9,** 691–702 (2007).
134. Kwon, E. J., Bergen, J. M., Park, I. K. & Pun, S. H. Peptide-modified vectors for nucleic acid delivery to neurons. *J. Control. Release* **132,** 230–5 (2008).
135. Oliveira, H. *et al.* Targeted gene delivery into peripheral sensorial neurons mediated by self-assembled vectors composed of poly(ethylene imine) and tetanus toxin fragment c. *J. Control. Release* **143,** 350–8 (2010).
136. Lalli, G. *et al.* Functional characterisation of tetanus and botulinum neurotoxins binding domains. *J. Cell Sci.* **112,** 2715–2724 (1999).
137. Fishman, P. S. & Carrigan, D. R. Retrograde transneuronal transfer of the C-fragment of tetanus toxin. *Brain Res.* **406,** 275–9 (1987).
138. Guggino, W. B. & Stanton, B. A. New insights into cystic fibrosis: molecular switches that regulate CFTR. *Nat. Rev. Mol. Cell Biol.* **7,** 426–436 (2006).
139. Babinski, D. & Trawinska-Bartnicka, M. Rhinosinusitis in cystic fibrosis: Not a simple story. *Int. J. Pediatr. Otorhinolaryngol.* **72,** 619–624 (2008).
140. McKay, T. & Huang, L. Secretin-Mediated Gene Delivery, a Specific Targeting Mechanism with Potential for Treatment of Biliary and Pancreatic Disease in Cystic Fibrosis. *Mol. Ther.* **5,** 323–8 (2002).
141. Hefford, M. A. & Kaplan, H. Chemical-Properties of the Histidine Residue of Secretin-Evidence for a Specific Intramolecular Interaction. *Biochim. Biophys. Acta* **998,** 267–270 (1989).
142. Yokosaki, Y. *et al.* Identification of the ligand binding site for the integrin alpha9 beta1 in the third fibronectin type III repeat of tenascin-C. *J. Biol. Chem.* **273,** 11423–8 (1998).
143. Schneider, H. *et al.* A novel peptide, PLAEIDGIELTY, for the targeting of alpha(9)beta(1)-integrins. *FEBS Lett.* **429,** 269–273 (1998).

144. Waterhouse, J. E., Jorgensen, M. R., Harbottle, R. P., Kostarelos, K. & Miller, A. D. Synthesis and biological evaluation of alpha 9 beta 1 integrin targeted non-viral gene delivery system. *Mol. Ther.* **7,** S218–S218 (2003).
145. Waterhouse, J. E. *et al.* Synthesis and application of integrin targeting lipopeptides in targeted gene delivery. *Chembiochem* **6,** 1212–23 (2005).
146. Writer, M. J. *et al.* Targeted gene delivery to human airway epithelial cells with synthetic vectors incorporating novel targeting peptides selected by phage display. *J. Drug Target.* **12,** 185–93 (2004).
147. Tagalakis, A. D., He, L., Saraiva, L., Gustafsson, K. T. & Hart, S. L. Receptor-targeted liposome-peptide nanocomplexes for siRNA delivery. *Biomaterials* **32,** 6302–6315 (2011).
148. Manunta, M. D. I. *et al.* Nebulisation of Receptor-Targeted Nanocomplexes for Gene Delivery to the Airway Epithelium. *PLoS One* **6,** (2011).
149. Rayner, S. A., Larkin, D. F. P. & George, A. J. T. TNF receptor secretion after ex vivo adenoviral gene transfer to cornea and effect on in vivo graft survival. *Invest. Ophthalmol. Vis. Sci.* **42,** 1568–1573 (2001).
150. Klebe, S., Sykes, P. J., Coster, D. J., Krishnan, R. & Williams, K. A. Prolongation of sheep corneal allograft survival by ex vivo transfer of the gene encoding interleukin-10. *Transplantation* **71,** 1214–1220 (2001).
151. Jun, A. S. & Larkin, D. F. P. Prospects for gene therapy in corneal disease. *Eye* **17,** 906–11 (2003).
152. Lai, C. M. *et al.* Inhibition of angiogenesis by adenovirus-mediated sFlt-1 expression in a rat model of corneal neovascularization. *Hum. Gene Ther.* **12,** 1299–1310 (2001).
153. Kamata, Y. *et al.* Adenovirus-mediated gene therapy for corneal clouding in mice with mucopolysaccharidosis type VII. *Mol. Ther.* **4,** 307–312 (2001).
154. Shewring, L. *et al.* A nonviral vector system for efficient gene transfer to corneal endothelial cells via membrane integrin. *Transplantation* **64,** 763–769 (1997).
155. Collins, L. & Fabre, J. W. A synthetic peptide vector system for optimal gene delivery to corneal endothelium. *J. Gene Med.* **6,** 185–94 (2004).
156. Trippel, S. B., Ghivizzani, S. C. & Nixon, A. J. Gene-based approaches for the repair of articular cartilage. *Gene Ther.* **11,** 351–9 (2004).
157. Santos, J. L. *et al.* Receptor-Mediated Gene Delivery Using PAMAM Dendrimers Conjugated with Peptides Recognized by Mesenchymal Stem Cells. *Mol. Pharm.* **7,** 763–74 (2010).
158. Pi, Y. B. *et al.* Targeted delivery of non-viral vectors to cartilage in vivo using a chondrocyte-homing peptide identified by phage display. *Biomaterials* **32,** 6324–32 (2011).
159. Balian, G. Bone Targeting Peptides. (2004).
160. Rosenzwajg, M., Canque, B. & Gluckman, J. C. Human dendritic cell differentiation pathway from CD34(+) hematopoietic precursor cells. *Blood* **87,** 535–544 (1996).
161. Moffatt, S. & Cristiano, R. J. Uptake characteristics of NGR-coupled stealth PEI/pDNA nanoparticles loaded with PLGA-PEG-PLGA tri-block copolymer for targeted delivery to human monocyte-derived dendritic cells. *Int. J. Pharm.* **321,** 143–54 (2006).
162. Hammes, H. P., Brownlee, M., Jonczyk, A., Sutter, A. & Preissner, K. T. Subcutaneous injection of a cyclic peptide antagonist of vitronectin receptor-type integrins inhibits retinal neovascularization. *Nat. Med.* **2,** 529–33 (1996).
163. Bryant, D. M., Wylie, F. G. & Stow, J. L. Regulation of Endocytosis , Nuclear Translocation , and Signaling of Fibroblast Growth Factor Receptor 1 by E-Cadherin. **16,** 14–23 (2005).
164. Wang, Y.-N., Yamaguchi, H., Hsu, J.-M. & Hung, M.-C. Nuclear trafficking of the epidermal growth factor receptor family membrane proteins. *Oncogene* **29,** 3997–4006 (2010).
165. Bergen, J. M., Park, I.-K. K., Horner, P. J. & Pun, S. H. Nonviral approaches for neuronal delivery of nucleic acids. *Pharm. Res.* **25,** 983–98 (2008).

166. Pardridge, W. M. Drug and gene targeting to the brain with molecular Trojan horses. *Nat. Rev. Drug Discov.* **1,** 131–9 (2002).
167. Fairweather, N. F., Lyness, V. A., Pickard, D. J., Allen, G. & Thomson, R. O. Cloning, nucleotide sequencing, and expression of tetanus toxin fragment C in Escherichia coli. *J. Bacteriol.* **165,** 21–7 (1986).
168. Lalli, G. & Schiavo, G. Analysis of retrograde transport in motor neurons reveals common endocytic carriers for tetanus toxin and neurotrophin receptor p75NTR. *J. Cell Biol.* **156,** 233–9 (2002).
169. Carlisle, R. C. *et al.* Polymer-coated polyethylenimine/DNA complexes designed for triggered activation by intracellular reduction. *J. Gene Med.* **6,** 337–44 (2004).
170. Thibault, M., Nimesh, S., Lavertu, M. & Buschmann, M. D. Intracellular trafficking and decondensation kinetics of chitosan-pDNA polyplexes. *Mol. Ther.* **18,** 1787–95 (2010).
171. Vandenbulcke, F., Nouel, D., Vincent, J. P., Mazella, J. & Beaudet, A. Ligand-induced internalization of neurotensin in transfected COS-7 cells: differential intracellular trafficking of ligand and receptor. *J. Cell Sci.* **113 (Pt 1,** 2963–75 (2000).
172. Belouzard, S. & Rouillé, Y. Ubiquitylation of leptin receptor OB-Ra regulates its clathrin-mediated endocytosis. *EMBO J.* **25,** 932–42 (2006).
173. Howe, C. L. A Cbl:clathrin complex involved in NGF signaling for neurite outgrowth. *Neurosci. Res. Commun.* **33,** 86–98 (2003).
174. Miki, T. *et al.* The reversion-inducing cysteine-rich protein with Kazal motifs (RECK) interacts with membrane type 1 matrix metalloproteinase and CD13/aminopeptidase N and modulates their endocytic pathways. *J. Biol. Chem.* **282,** 12341–52 (2007).
175. Nesterov, A., Carter, R. E., Sorkina, T., Gill, G. N. & Sorkin, A. Inhibition of the receptor-binding function of clathrin adaptor protein AP-2 by dominant-negative mutant mu2 subunit and its effects on endocytosis. *EMBO J.* **18,** 2489–99 (1999).
176. Kagaya, H. *et al.* Impact of polyplex micelles installed with cyclic RGD peptide as ligand on gene delivery to vascular lesions. *Gene Ther.* **19,** 61–9 (2012).
177. Goh, L. K., Huang, F., Kim, W., Gygi, S. & Sorkin, A. Multiple mechanisms collectively regulate clathrin-mediated endocytosis of the epidermal growth factor receptor. *J. Cell Biol.* **189,** 871–83 (2010).
178. Haugsten, E. M., Malecki, J., Bjørklund, S. M. S., Olsnes, S. & Wesche, J. Ubiquitination of fibroblast growth factor receptor 1 is required for its intracellular sorting but not for its endocytosis. *Mol. Biol. Cell* **19,** 3390–403 (2008).
179. Le Roy, C. & Wrana, J. L. Clathrin- and non-clathrin-mediated endocytic regulation of cell signalling. *Nat. Rev. Mol. Cell Biol.* **6,** 112–26 (2005).
180. Legrand, D. *et al.* Surface nucleolin participates in both the binding and endocytosis of lactoferrin in target cells. *Eur. J. Biochem.* **271,** 303–317 (2004).
181. Huang, F., Khvorova, A., Marshall, W. & Sorkin, A. Analysis of clathrin-mediated endocytosis of epidermal growth factor receptor by RNA interference. *J. Biol. Chem.* **279,** 16657–61 (2004).
182. Vrecl, M. *et al.* Agonist-induced endocytosis and recycling of the gonadotropin-releasing hormone receptor: effect of beta-arrestin on internalization kinetics. *Mol. Endocrinol.* **12,** 1818–29 (1998).
183. Grimes, M. L., Beattie, E. & Mobley, W. C. A signaling organelle containing the nerve growth factor-activated receptor tyrosine kinase, TrkA. *Proc. Natl. Acad. Sci.* **94,** 9909–14 (1997).
184. Cammisotto, P. G. *et al.* Receptor-Mediated Transcytosis of Leptin through Human Intestinal Cells In Vitro. *Int. J. Cell Biol.* **2010,** 928169 (2010).
185. Savdie, C., Ferguson, S. S. G., Vincent, J.-P., Beaudet, A. & Stroh, T. Cell-type-specific pathways of neurotensin endocytosis. *Cell Tissue Res.* **324,** 69–85 (2006).
186. Deinhardt, K., Berninghausen, O., Willison, H. J., Hopkins, C. R. & Schiavo, G. Tetanus

toxin is internalized by a sequential clathrin-dependent mechanism initiated within lipid microdomains and independent of epsin1. *J. Cell Biol.* **174,** 459–71 (2006).
187. Melkebeek, V. *et al.* Targeting aminopeptidase N, a newly identified receptor for F4ac fimbriae, enhances the intestinal mucosal immune response. *Mucosal Immunol.* **5,** 635–45 (2012).
188. Song, N. *et al.* The nuclear translocation of endostatin is mediated by its receptor nucleolin in endothelial cells. *Angiogenesis* **15,** 697–711 (2012).
189. Marchese, C. *et al.* Receptor-mediated endocytosis of keratinocyte growth factor. *J. Cell Sci.* **111,** 3517–27 (1998).
190. Pawson, a. J. Multiple Determinants for Rapid Agonist-Induced Internalization of a Nonmammalian Gonadotropin-Releasing Hormone Receptor: A Putative Palmitoylation Site and Threonine Doublet within the Carboxyl-Terminal Tail Are Critical. *Endocrinology* **144,** 3860–3871 (2003).
191. Zhuang, G., Hunter, S., Hwang, Y. & Chen, J. Regulation of EphA2 receptor endocytosis by SHIP2 lipid phosphatase via phosphatidylinositol 3-Kinase-dependent Rac1 activation. *J. Biol. Chem.* **282,** 2683–94 (2007).
192. Roseberry, A. G. & Hosey, M. M. Internalization of the M2 muscarinic acetylcholine receptor proceeds through an atypical pathway in HEK293 cells that is independent of clathrin and caveolae. *J. Cell Sci.* **114,** 739–46 (2001).
193. Walker, J. K., Premont, R. T., Barak, L. S., Caron, M. G. & Shetzline, M. A. Properties of secretin receptor internalization differ from those of the beta(2)-adrenergic receptor. *J. Biol. Chem.* **274,** 31515–23 (1999).
194. Muro, S. *et al.* A novel endocytic pathway induced by clustering endothelial ICAM-1 or PECAM-1. *J. Cell Sci.* **116,** 1599–609 (2003).
195. Rejman, J., Bragonzi, A. & Conese, M. Role of clathrin- and caveolae-mediated endocytosis in gene transfer mediated by lipo- and polyplexes. *Mol. Ther.* **12,** 468–74 (2005).
196. Ziello, J. E., Huang, Y. & Jovin, I. S. Cellular endocytosis and gene delivery. *Mol. Med.* **16,** 222–229
197. Seow, Y. & Wood, M. J. Biological Gene Delivery Vehicles: Beyond Viral Vectors. *Mol. Ther.* **17,** 767–777 (2009).
198. Levine, R. M., Scott, C. M. & Kokkoli, E. Peptide Functionalized Nanoparticles for Nonviral Gene Delivery. *Soft Matter* **9,** 985–1004 (2013).
199. Zhang, J.-S., Liu, F. & Huang, L. Implications of Pharmacokinetic Behavior of Lipoplex for its Inflammatory Toxicity. *Adv. Drug Deliv. Rev.* **57,** 689–698 (2005).
200. Balazs, D. & Godbey, W. Liposomes for use in gene delivery. *J. Drug Deliv.* **2011,** (2011).
201. Simões, S., Filipe, A. & Faneca, H. Cationic liposomes for gene delivery. *Expert Opin. Drug Deliv.* **2,** 237–254 (2005).
202. Zhao, W., Zhuang, S. & Qi, X.-R. Comparative study of the in vitro and in vivo characteristics of cationic and neutral liposomes. *Int. J. Nanomedicine* **6,** 3087–3098 (2011).
203. Immordino, M. L., Dosio, F. & Cattel, L. Stealth Liposomes: Review of the Basic Science, Rationale, and Clinical Applications, Existing and Potential. *Int. J. Nanomedicine* **1,** 297–315 (2006).
204. Fields, A. L. & Runowicz, C. D. Current Therapies in Ovarian Cancer. *Cancer Invest.* **21,** 148–156 (2003).
205. Brown, S. & Khan, D. R. The Treatment of Breast Cancer Using Liposome Technology. *J. Drug Deliv.* **2012,** (2012).
206. Demirgöz, D., Garg, A. & Kokkoli, E. PR_b-targeted PEGylated liposomes for prostate cancer therapy. *Langmuir* **24,** 13518–13524 (2008).
207. Tros de Ilarduya, C., Sun, Y. & Düzgüneş, N. Gene delivery by lipoplexes and polyplexes. *Eur. J. Pharm. Sci.* **40,** 159–170 (2010).
208. Preuss, M., Tecle, M., Shah, I., Matthews, D. a & Miller, A. D. Comparison between the

interactions of adenovirus-derived peptides with plasmid DNA and their role in gene delivery mediated by liposome-peptide-DNA virus-like nanoparticles. *Org. Biomol. Chem.* **1,** 2430–2438 (2003).
209. Herringson, T. P. P., Patlolla, R. R. R. & Altin, J. G. G. Targeting of plasmid DNA-lipoplexes to cells with molecules anchored via a metal chelator lipid. *J. Gene Med.* **11,** 1048–1063 (2009).
210. Legendre, J.-Y. & Szoka Jr., F. C. Delivery of Plasmid DNA into mammalian cells using pH-sensitive liposomes. *Pharm. Res.* **9,** 1235–1242 (1992).
211. Vonarbourg, A. *et al.* The encapsulation of DNA molecules within biomimetic lipid nanocapsules. *Biomaterials* **30,** 3197–3204 (2009).
212. Lee, L. K. *et al.* Biophysical characterization of an integrin-targeted non-viral vector. *Med. Sci. Monit.* **9,** BR54–61 (2003).
213. Jeffs, L. B. *et al.* A Scalable, Extrusion-Free Method for Efficient Liposomal Encapsulation of Plasmid DNA. *Pharm. Res.* **22,** 362–372 (2005).
214. Holden, M. J. *et al.* Factors affecting quantification of total DNA by UV spectroscopy and PicoGreen fluorescence. *J. Agric. Food Chem.* **57,** 7221–7226 (2009).
215. Bhat, S. *et al.* Comparison of methods for accurate quantification of DNA mass concentration with traceability to the international system of units. *Anal. Chem.* **82,** 7185–7192 (2010).
216. Tagawa, T. *et al.* Characterisation of LMD virus-like nanoparticles self-assembled from cationic liposomes, adenovirus core peptide mu and plasmid DNA. *Gene Ther.* **9,** 564–576 (2002).
217. Holladay, C. *et al.* A reliable method for detecting complexed DNA in vitro. *Nanoscale* **2,** 2718–2723 (2010).
218. Wacker, M. & Schubert, R. From mixed micelles to liposomes: Critical steps during detergent removal by membrane dialysis. *Int. J. Pharm.* **162,** 171–175 (1998).
219. Madani, F., Perálvarez-Marín, A. & Gräslund, A. Liposome Model Systems to Study the Endosomal Escape of Cell-Penetrating Peptides: Transport across Phospholipid Membranes Induced by a Proton Gradient. *J. Drug Deliv.* **2011,** (2011).
220. Lichtenberg, D. & Barenholz, Y. Liposomes: preparation, characterization, and preservation. *Methods Biochem. Anal.* **33,** 337–462 (1988).
221. Pons, M., Merc, F. & Estelrich, J. Liposomes obtained by the ethanol injection method. *Int. J. Pharm.* **95,** 51–56 (1993).
222. Batzri, S. & Korn, E. Single bilayer liposomes prepared without sonication. *Biochim. Biophys. Acta* **298,** 1015–1019 (1973).
223. Maitani, Y., Igarashi, S., Sato, M. & Hattori, Y. Cationic liposome (DC-Chol/DOPE=1:2) and a modified ethanol injection method to prepare liposomes, increased gene expression. *Int. J. Pharm.* **342,** 33–39 (2007).
224. Yang, S., Chen, J., Zhao, D., Han, D. & Chen, X. Comparative study on preparative methods of DC-Chol/DOPE liposomes and formulation optimization by determining encapsulation efficiency. *Int. J. Pharm.* **434,** 155–160 (2012).
225. Lasic, D. D. The mechanism of vesicle formation. *Biochem. J.* **256,** 1–11 (1988).
226. Lasic, D. D. *Liposomes in Gene Delivery*. (CRC Press, 1997).
227. Ko, Y. T. & Bickel, U. Liposome-encapsulated polyethylenimine/oligonucleotide polyplexes prepared by reverse-phase evaporation technique. *AAPS PharmSciTech* **13,** 373–378 (2012).
228. Tong, Q., Li, H., Li, W. & Chen, H. In Vitro and In Vivo Anti-Tumor Effects of Gemcitabine Loaded with a New Drug Delivery System. *J. Nanosci. Nanotechnol.* **11,** 3651–3658 (2011).
229. Crosasso, P. *et al.* Antitumoral activity of liposomes and immunoliposomes containing 5-fluorouridine prodrugs. *J. Pharm. Sci.* **86,** 832–839 (1997).

230. Whittenton, J. *et al.* Evaluation of asymmetric liposomal nanoparticles for encapsulation of polynucleotides. *Langmuir* **24,** 8533–8540 (2008).
231. Mokhtarieh, A. A., Cheong, S., Kim, S., Chung, B. H. & Lee, M. K. Asymmetric liposome particles with highly efficient encapsulation of siRNA and without nonspecific cell penetration suitable for target-specific delivery. *Biochim. Biophys. Acta* **1818,** 1633–1641 (2012).
232. Belur, L., McIvor, R. & Wilber, A. Liver-directed gene therapy using the sleeping beauty transposon system. *Methods Mol. Biol.* **434,** 267–276 (2008).
233. Fu, D., Calvo, J. a & Samson, L. D. Balancing repair and tolerance of DNA damage caused by alkylating agents. *Nat. Rev. Cancer* **12,** 104–20 (2012).
234. Osborne, M. R., Wilman, D. E. V & Lawleyt, P. D. Alkylation of DNA by the nitrogen mustard Bis (2-chloroethyl)methylamine. *Chem. Res. Toxicol.* **8,** 316–320 (1995).
235. Vijayanathan, V., Lyall, J., Thomas, T., Shirahata, A. & Thomas, T. J. Ionic, structural, and temperature effects on DNA nanoparticles formed by natural and synthetic polyamines. *Biomacromolecules* **6,** 1097–103 (2005).
236. Lobo, B. a *et al.* Differential scanning calorimetric studies of the thermal stability of plasmid DNA complexed with cationic lipids and polymers. *J. Pharm. Sci.* **91,** 454–66 (2002).
237. Chen, P. S., Toribara, T. Y. & Warner, H. Microdetermination of Phosphorus. *Anal. Chem.* **28,** 1756–1758 (1956).
238. Szoka, F. & Papahadjopoulos, D. Procedure for Preparation of Liposomes with Large Internal Aqueous Space and High Capture by Reverse-Phase Evaporation. *Proc. Natl. Acad. Sci. U. S. A.* **75,** 4194–4198 (1978).
239. Cortesi, R. *et al.* Preparation of liposomes by reverse -phase evaporation using alternative organic solvents. *J. Microencapsul.* **16,** 251–256 (1999).
240. Ramana, L. N., Sethuraman, S., Ranga, U. & Krishnan, U. M. Development of a liposomal nanodelivery system for nevirapine. *J. Biomed. Sci.* **17,** 57 (2010).
241. Unezaki, S., Maruyama, K. & Hosoda, J. Direct measurement of the extravasation of polyethyleneglycol-coated liposomes into solid tumor tissue by in vivo fluorescence microscopy. *Int. J. Pharm.* **144,** 11–17 (1996).
242. Semple, S. C. *et al.* Efficient encapsulation of antisense oligonucleotides in lipid vesicles using ionizable aminolipids : formation of novel small multilamellar vesicle structures. *Biochim. Biophys. Acta* **1510,** 152–166 (2001).
243. Xu, Y., Hui, S. W., Frederik, P. & Szoka, F. C. Physicochemical characterization and purification of cationic lipoplexes. *Biophys. J.* **77,** 341–353 (1999).
244. Sternberg, B., Sorgi, F. & Huang, L. New structures in complex formation between DNA and cationic liposomes visualized by freeze—fracture electron microscopy. *FEBS Lett.* **356,** 361–366 (1994).
245. Templeton, N. S. Nonviral delivery for genomic therapy of cancer. *World J. Surg.* **33,** 685–697 (2009).
246. Agbavwe, C. & Somoza, M. M. Sequence-dependent fluorescence of cyanine dyes on microarrays. *PLoS One* **6,** (2011).
247. Lupyan, D., Mezei, M., Logothetis, D. E. & Osman, R. A molecular dynamics investigation of lipid bilayer perturbation by PIP2. *Biophys. J.* **98,** 240–247 (2010).
248. Bhise, N. S., Shmueli, R. B., Gonzalez, J. & Green, J. J. A novel assay for quantifying the number of plasmids encapsulated by polymer nanoparticles. *Small* **8,** 367–373 (2011).
249. Clamme, J., Azoulay, J. & Mely, Y. Monitoring of the formation and dissociation of polyethylenimine/DNA complexes by two photon fluorescence correlation spectroscopy. *Biophys. J.* **84,** 1960–1968 (2003).
250. Lerman, L. S., Wilkerson, L. S., Venable, J. J. H. & Robinson, B. H. DNA packing in single crystals inferred from freeze-fracture-etch replicas. *J. Mol. Biol.* **108,** 271–293 (1976).
251. Hou, S. *et al.* Formation and structure of PEI/DNA complexes: quantitative analysis. *Soft*

Matter **7,** 6967–6972 (2011).
252. Benita, S., Poly, P. a, Puisieux, F. & Delattre, J. Radiopaque liposomes: effect of formulation conditions on encapsulation efficiency. *J. Pharm. Sci.* **73,** 1751–1755 (1984).
253. Kanasty, R., Dorkin, J. R., Vegas, A. & Anderson, D. Delivery Materials for siRNA Therapeutics. *Nat. Mater.* **12,** 967–977 (2013).
254. Whitehead, K. A., Langer, R. & Anderson, D. G. Knocking Down Barriers: Advances in siRNA Delivery. *Nat. Rev. Drug Discov.* **8,** 129–138 (2009).
255. Seyhan, A. A. RNAi: A Potential New Class of Therapeutic for Human Genetic Disease. *Hum. Genet.* **130,** 583–605 (2011).
256. Haasnoot, J. & Berkhout, B. RNAi and Cellular miRNAs in Infections by Mammalian Viruses. *Antivir. RNAi Concepts, Methods, Appl. Methods Mol. Biol.* **721,** 355–371 (2011).
257. Devi, G. R. siRNA-Based Approaches in Cancer Therapy. *Cancer Gene Ther.* **13,** 819–829 (2006).
258. Yim, E.-K. & Park, J.-S. The Role of HPV E6 and E7 Oncoproteins in HPV-Associated Cervical Carcinogenesis. *Cancer Res. Treat.* **37,** 319–324 (2005).
259. Jung, H. S. *et al.* The synergistic therapeutic effect of cisplatin with Human papillomavirus E6/E7 short interfering RNA on cervical cancer cell lines in vitro and in vivo. *Int. J. Cancer* **130,** 1925–1936 (2012).
260. Salazar-León, J. *et al.* Silencing of HPV16 E6 and E7 Oncogenic Activities by Small Interference RNA Induces Autophagy and Apoptosis in Human Cervical Cancer Cells. *J. Nucleic Acids Investig.* **2,** 59–69 (2011).
261. Butz, K. *et al.* siRNA Targeting of the Viral E6 Oncogene Efficiently Kills Human Papillomavirus-Positive Cancer Cells. *Oncogene* **22,** 5938–5945 (2003).
262. Zhou, J. *et al.* Transcriptional Gene Silencing of HPV16 E6/E7 Induces Growth Inhibition via Apoptosis in vitro and in vivo. *Gynecol. Oncol.* **124,** 296–302 (2012).
263. Jiang, M. & Milner, J. Selective Silencing of Viral Gene Expression in HPV-Positive Human Cervical Carcinoma Cells Treated with siRNA, a Primer of RNA Interference. *Oncogene* **21,** 6041–6048 (2002).
264. Chang, J. T.-C. *et al.* Highly Potent and Specific siRNAs Against E6 or E7 Genes of HPV16- or HPV18-Infected Cervical Cancers. *Cancer Gene Ther.* **17,** 827–836 (2010).
265. Lin, Q., Chen, J., Zhang, Z. & Zheng, G. Lipid-Based Nanoparticles in the Systemic Delivery of iRNA. *Nanomedicine* **9,** 105–120 (2014).
266. Hughes, D. E., Rebello, G. & Al-Nafussi, A. Integrin Expression in Squamous Neoplasia of the Cervix. *J. Pathol.* **173,** 97–104 (1994).
267. Rabinovitz, I., Nagle, R. B. & Cress, A. E. Integrin α6 Expression in Human Prostate Carcinoma Cells is Associated with a Migratory and Invasive Phenotype in vitro and in vivo. *Clin. Exp. Metastasis* **13,** 481–491 (1995).
268. Friedrichs, K. *et al.* High Expression Level of α6 Integrin in Human Breast Carcinoma Is Correlated with Reduced Survival. *Cancer Res.* **55,** 901–906 (1995).
269. Hozumi, K. *et al.* Cell Adhesive Peptide Screening of the Mouse Laminin α1 Chain G Domain. *Arch. Biochem. Biophys.* **503,** 213–222 (2010).
270. Boussif, O. *et al.* A Versatile Vector for Gene and Oligonucleotide Transfer into Cells in Culture and in vivo: Polyethylenimine. *Proc. Natl. Acad. Sci.* **92,** 7297–7301 (1995).
271. Liang, W. & Lam, J. K. W. Endosomal Escape Pathways for Non-Viral Nucleic Acid Delivery Systems. *Mol. Regul. Endocytosis* 429–456 (2012). doi:10.5772/46006
272. Levine, R. M., Pearce, T. R., Adil, M. M., Kokkoli, E. & Pierce, T. R. Preparation and Characterization of Liposome-Encapsulated Plasmid DNA for Gene Delivery. *Langmuir* (2013).
273. Adil, M. M., Levine, R. M. & Kokkoli, E. Increasing Cancer-Specific Gene Expression by Targeting Overexpressed α5β1 Integrin and Upregulated Transcriptional Activity of NF-κB. *Mol. Pharm.* **11,** 849–858 (2014).

274. Adil, M. M., Erdman, Z. S. & Kokkoli, E. Transfection Mechanisms of Polyplexes, Lipoplexes, and Stealth Liposomes in α5β1 Integrin Bearing DLD-1 Colorectal Cancer Cells. *Langmuir* **30,** 3802–3810 (2014).
275. Ma, P. L., Lavertu, M., Winnik, F. M. & Buschmann, M. D. New Insights into Chitosan-DNA Interactions using Isothermal Titration Microcalorimetry. *Biomacromolecules* **10,** 1490–1499 (2009).
276. Utsuno, K. & Uludağ, H. Thermodynamics of Polyethylenimine-DNA Binding and DNA Condensation. *Biophys. J.* **99,** 201–207 (2010).
277. Ferreira, E. & Cronjé, M. J. Selection of Suitable Reference Genes for Quantitative Real-Time PCR in Apoptosis-Induced MCF-7 Breast Cancer Cells. *Mol. Biotechnol.* **50,** 121–128 (2012).
278. Wang, X., Ramström, O. & Yan, M. Quantitative Analysis of Multivalent Ligand Presentation on Gold Glyconanoparticles and the Impact on Lectin Binding. *Anal. Chem.* **82,** 9082–9089 (2010).
279. Hong, S. *et al.* The Binding Avidity of a Nanoparticle-Based Multivalent Targeted Drug Delivery Platform. *Chem. Biol.* **14,** 107–115 (2007).
280. Margadant, C., Monsuur, H. N., Norman, J. C. & Sonnenberg, A. Mechanisms of Integrin Activation and Trafficking. *Curr. Opin. Cell Biol.* **23,** 607–614 (2011).
281. Choosakoonkriang, S., Lobo, B. A., Koe, G. S., Koe, J. G. & Middaugh, C. R. Biophysical Characterization of PEI/DNA Complexes. *J. Pharm. Sci.* **92,** 1710–1722 (2003).
282. Ikonen, M., Murtomäki, L. & Kontturi, K. Controlled Complexation of Plasmid DNA with Cationic Polymers: Effect of Surfactant on the Complexation and Stability of the Complexes. *Colloids Surfaces B Biointerfaces* **66,** 77–83 (2008).
283. Ketola, T.-M. *et al.* Independent versus Cooperative Binding in Polyethylenimine-DNA. *J. Phys. Chem. B* (2013).
284. Breunig, M. *et al.* Mechanistic Investigation of Poly(ethylene imine)-Based siRNA Delivery: Disulfide Bonds Boost Intracellular Release of the Cargo. *J. Control. Release* **130,** 57–63 (2008).
285. Mao, S. *et al.* Influence of Polyethylene Glycol Chain Length on the Physicochemical and Biological Properties of Poly(ethylene imine)-graft-Poly(ethylene glycol) Block Copolymer/siRNA Polyplexes. *Bioconjug. Chem.* **17,** 1209–1218 (2006).
286. Zheng, M. *et al.* Targeting the Blind Spot of Polycationic Nanocarrier-Based siRNA Delivery. *ACS Nano* **6,** (2012).
287. Ziebarth, J. D. & Wang, Y. Understanding the protonation behavior of linear polyethylenimine in solutions through Monte Carlo simulations. *Biomacromolecules* **11,** 1–29 (2011).
288. Wu, S. Y. & McMillan, N. A. J. Lipidic Systems for in vivo siRNA Delivery. *AAPS J.* **11,** 639–652 (2009).
289. Guo, Y. *et al.* How is mRNA expression predictive for protein expression? A correlation study on human circulating monocytes. *Acta Biochim. Biophys.* **40,** 426–36 (2008).
290. Chen, G. *et al.* Discordant protein and mRNA expression in lung adenocarcinomas. *Mol. Cell. Proteomics* **1,** 304–13 (2002).
291. Qi, Z. *et al.* Effect of simultaneous silencing of HPV-18 E6 and E7 on inducing apoptosis in HeLa cells. *Biochem. Cell Biol.* **88,** 697–704 (2010).
292. Burnett, J. C., Rossi, J. J. & Tiemann, K. Current Progress of siRNA/shRNA Therapeutics in Clinical Trials. *Biotechnol. J.* **6,** 1130–1146 (2011).
293. Xu, C. & Wang, J. Delivery Systems for siRNA Drug Development in Cancer Therapy. *Asian J. Pharm. Sci.* **10,** 1–12 (2014).
294. Li, S.-D., Chen, Y.-C., Hackett, M. J. & Huang, L. Tumor-Targeted Delivery of siRNA by Self-Assembled Nanoparticles. *Mol. Ther.* **16,** 163–169 (2008).
295. Hatakeyama, H. *et al.* Systemic Delivery of siRNA to Tumors using a Lipid Nanoparticle

Containing a Tumor-Specific Cleavable PEG-Lipid. *Biomaterials* **32,** 4306–4316 (2011).
296. Whitehead, K. a *et al.* Degradable lipid nanoparticles with predictable in vivo siRNA delivery activity. *Nat. Commun.* **5,** 4277 (2014).
297. Judge, A. D. *et al.* Confirming the RNAi-Mediated Mechanism of Action of siRNA-Based Cancer Therapeutics in Mice. *J. Clin. Invest.* **119,** 661–673 (2009).
298. Bartlett, D. W., Su, H., Hildebrandt, I. J., Weber, W. A. & Davis, M. E. Impact of Tumor-Specific Targeting on the Biodistribution and Efficacy of siRNA Nanoparticles Measured by Multimodality in vivo Imaging. *Proc. Natl. Acad. Sci.* **104,** 15549–15554 (2007).
299. Adil, M. M., Levine, R. M. & Kokkoli, E. Increasing Cancer-Specific Gene Expression by Targeting Overexpressed α5β1 Integrin and Upregulated Transcriptional Activity of NF-κB. *Mol. Pharm.* **11,** 849–858 (2014).
300. Merkel, O. M. *et al.* Nonviral siRNA Delivery to the Lung: Investigation of PEG-PEI Polyplexes and Their in vivo Performance. *Mol. Pharm.* **6,** 1246–1260 (2009).
301. Van Rompaey, E., Engelborghs, Y., Sanders, N., De Smedt, S. C. & Demeester, J. Interactions Between Oligonucleotides and Cationic Polymers Investigated by Fluorescence Correlation Spectroscopy. *Pharm. Res.* **18,** 928–936 (2001).
302. Sunshine, J. C., Peng, D. Y. & Green, J. J. Uptake and Transfection with Polymeric Nanoparticles are Dependent on Polymer End-Group Structure, but Largely Independent of Nanoparticle Physical and Chemical Properties. *Mol. Pharm.* **9,** 3375–3383 (2012).
303. Ghosh, P. S., Kim, C.-K., Han, G., Forbes, N. S. & Rotello, V. M. Efficient Gene Delivery Vectors by Tuning the Surface Charge Density of Amino Acid-Functionalized Gold Nanoparticles. *ACS Nano* **2,** 2213–2218 (2008).
304. Tseng, W.-C., Fang, T.-Y., Su, L.-Y. & Tang, C.-H. Dependence of Transgene Expression and the Relative Buffering Capacity of Dextran-Grafted Polyethylenimine. *Mol. Pharm.* **2,** 224–232 (2005).
305. Sioud, M. Induction of Inflammatory Cytokines and Interferon Responses by Double-Stranded and Single-Stranded siRNAs is Sequence-Dependent and Requires Endosomal Localization. *J. Mol. Biol.* **348,** 1079–1090 (2005).
306. Li, S. D. & Huang, L. Surface-Modified LPD Nanoparticles for Tumor Targeting. *Ann. N. Y. Acad. Sci.* **1082,** 1–8 (2006).
307. Yang, X. H. *et al.* CD151 Restricts the a6 Integrin Diffusion Mode. *J. Cell Sci.* **125,** 1478–1487 (2011).
308. Caswell, P. T. & Norman, J. C. Integrin Trafficking and the Control of Cell Migration. *Traffic* **7,** 14–21 (2006).
309. Sterk, L. M. T. *et al.* The Tetraspan Molecule CD151, a Novel Constituent of Hemidesmosomes, Associates with the Integrin alpha6beta4 and May Regulate the Spatial Organization of Hemidesmosomes Lotus. *J. Cell Biol.* **149,** 969–982 (2000).
310. Liu, L. *et al.* Tetraspanin CD151 Promotes Cell Migration by Regulating Integrin Trafficking. *J. Biol. Chem.* **282,** 31631–31642 (2007).
311. Dy, G. K. & Adjei, A. A. Understanding, Recognizing, and Managing Toxicities of Targeted Anticancer Therapies. *CA. Cancer J. Clin.* **63,** 249–279 (2013).
312. Saul, J. M., Annapragada, A. V & Bellamkonda, R. V. A Dual-Ligand Approach for Enhancing Targeting Selectivity of Therapeutic Nanocarriers. *J. Control. Release* **114,** 277–287 (2006).
313. Barnett, B. G., Tillman, B. W., Curiel, D. T. & Douglas, J. T. Dual Targeting of Adenoviral Vectors at the Levels of Transduction and Transcription Enhances the Specificity of Gene Expression in Cancer Cells. *Mol. Ther.* **6,** 377–385 (2002).
314. Barker, S. D. *et al.* Combined Transcriptional and Transductional Targeting Improves the Specificity and Efficacy of Adenoviral Gene Delivery to Ovarian Carcinoma. *Gene Ther.* **10,** 1198–1204 (2003).
315. Banerjee, D. & Sengupta, S. Nanoparticles in cancer chemotherapy. *Prog. Mol. Biol. Transl.*

Sci. **104,** 489–507 (2011).
316. Gerber, D. E. Targeted therapies: A new generation of cancer treatments. *Am. Fam. Physician* **77,** 311–319 (2008).
317. Davis, M. E., Chen, Z. G. & Shin, D. M. Nanoparticle therapeutics: an emerging treatment modality for cancer. *Nat. Rev. Drug Discov.* **7,** 771–782 (2008).
318. Sanna, V., Pala, N. & Sechi, M. Targeted therapy using nanotechnology: Focus on cancer. *Int. J. Nanomedicine* **9,** 467–483 (2014).
319. Izar, B., Rotow, J., Gainor, J., Clark, J. & Chabner, B. Pharmacokinetics, clinical indications, and resistance mechanisms in molecular targeted therapies in cancer. *Pharmacol. Rev.* **65,** 1351–1395 (2013).
320. Prabhu, R. H., Patravale, V. B., & Joshi, M. D. Polymeric nanoparticles for targeted treatment in oncology : current insights. *Int. J. Nanomedicine* **10,** 1001–1018 (2015).
321. Hughes, S. E. Differential expression of the fibroblast growth factor receptor (FGFR) multigene family in normal human adult tissues. *J. Histochem. Cytochem.* **45,** 1005–19 (1997).
322. Koretz, K., Schlag, P. & Möller, P. Expression of epidermal growth factor receptor in normal colorectal mucosa, adenoma, and carcinoma. *Virchows Arch. A. Pathol. Anat. Histopathol.* **416,** 343–9 (1990).
323. Parsons-Wingerter, P. *et al.* Uniform overexpression and rapid accessibility of alpha5beta1 integrin on blood vessels in tumors. *Am. J. Pathol.* **167,** 193–211 (2005).
324. Raschi, E. & De Ponti, F. Cardiovascular toxicity of anticancer-targeted therapy: emerging issues in the era of cardio-oncology. *Intern. Emerg. Med.* **7,** 113–31 (2012).
325. Matsumura, Y. & Maeda, H. A new concept for macromolecular therapeutics in cancer chemotherapy: mechanism of tumoritropic accumulation of proteins and the antitumor agent smancs. *Cancer Res.* **46,** 6387–92 (1986).
326. Lasic, D. D. & Needham, D. The 'Stealth' Liposome: A Prototypical Biomaterial. *Chem. Rev.* **95,** 2601–2628 (1995).
327. Yuan, F. *et al.* Mirovascular Permeability and Interstitial Penetration of Sterically Stabilized (Stealth) Liposomes in a Human Tumor Xenograft. *Cancer Res.* **54,** 3352–3356 (1994).
328. Mukhopadhyay, R., Theriault, R. L. & Price, J. E. Increased levels of alpha6 integrins are associated with the metastatic phenotype of human breast cancer cells. *Clin. Exp. Metastasis* **17,** 325–32 (1999).
329. Berry, M. G., Gui, G. P. H., Wells, C. a & Carpenter, R. Integrin expression and survival in human breast cancer. *Eur. J. Surg. Oncol.* **30,** 484–9 (2004).
330. Jia, Y. *et al.* Integrin fibronectin receptors in matrix metalloproteinase-1-dependent invasion by breast cancer and mammary epithelial cells. *Cancer Res.* **64,** 8674–81 (2004).
331. Chao, C. *et al.* A Function for the Integrin a6b4 in the Invasive Properties of Colorectal Carcinoma Cells. *Cancer Res.* **56,** 4811–4819 (1996).
332. Ellis, L. M. A targeted approach for antiangiogenic therapy of metastatic human colon cancer. *Am. Surg.* **69,** 3–10 (2003).
333. Gong, J. *et al.* Role of a5b1 integrin in determining malignant properties of colon carcinoma cells. *Cell Growth Differ.* **8,** 83–90 (1997).
334. Dedhar, S., Saulnier, R., Nagle, R. & Overall, C. M. Specific alterations in the expression of alpha 3 beta 1 and alpha 6 beta 4 integrins in highly invasive and metastatic variants of human prostate carcinoma cells selected by in vitro invasion through reconstituted basement membrane. *Clin. Exp. Metastasis* **11,** 391–400 (1993).
335. Rokhlin, O. W. & Cohen, M. B. Expression of cellular adhesion molecules on human prostate tumor cell lines. *Prostate* **26,** 205–12 (1995).
336. Livant, D. L. *et al.* Anti-invasive, antitumorigenic, and antimetastatic activities of the PHSCN sequence in prostate carcinoma. *Cancer Res.* **60,** 309–320 (2000).
337. Chen, J., De, S., Brainard, J. & Byzova, T. V. Metastatic properties of prostate cancer cells

are controlled by VEGF. *Cell Commun. Adhes.* **11,** 1–11
338. Cruz-Monserrate, Z. & O'Connor, K. Integrin α6β4 promotes migration, invasion through Tiam1 upregulation, and subsequent Rac activation. *Neoplasia* **10,** 408–417 (2008).
339. Mercurio, a M. & Rabinovitz, I. Towards a mechanistic understanding of tumor invasion--lessons from the alpha6beta 4 integrin. *Semin. Cancer Biol.* **11,** 129–41 (2001).
340. Uhlén, M. *et al.* Tissue-based map of the human proteome. *Science* **347,** 1260419–1260419 (2015).
341. Mercurio, A. M. *et al.* The metastatic odyssey: the integrin connection. *Surg. Oncol. Clin. N. Am.* **10,** 313–28, viii–ix (2001).
342. Laginha, K., Mumbengegwi, D. & Allen, T. Liposomes targeted via two different antibodies: assay, B-cell binding and cytotoxicity. *Biochim. Biophys. Acta* **1711,** 25–32 (2005).
343. Omolola Eniola, a & Hammer, D. a. In vitro characterization of leukocyte mimetic for targeting therapeutics to the endothelium using two receptors. *Biomaterials* **26,** 7136–44 (2005).
344. Kakimoto, S., Moriyama, T., Tanabe, T., Shinkai, S. & Nagasaki, T. Dual-ligand effect of transferrin and transforming growth factor alpha on polyethyleneimine-mediated gene delivery. *J. Control. Release* **120,** 242–9 (2007).
345. Singh, S. R. *et al.* Intravenous transferrin, RGD peptide and dual-targeted nanoparticles enhance anti-VEGF intraceptor gene delivery to laser-induced CNV. *Gene Ther.* **16,** 645–659 (2009).
346. Kluza, E. *et al.* Synergistic targeting of alphavbeta3 integrin and galectin-1 with heteromultivalent paramagnetic liposomes for combined MR imaging and treatment of angiogenesis. *Nano Lett.* **10,** 52–8 (2010).
347. Kluza, E. *et al.* Dual-targeting of α(v)β(3) and galectin-1 improves the specificity of paramagnetic/fluorescent liposomes to tumor endothelium in vivo. *J. Control. Release* **158,** 207–214 (2011).
348. Gunawan, R. & Auguste, D. Immunoliposomes that target endothelium in vitro are dependent on lipid raft formation. *Mol. Pharm.* **7,** 1569–1575 (2010).
349. Gunawan, R. & Auguste, D. The role of antibody synergy and membrane fluidity in the vascular targeting of immunoliposomes. *Biomaterials* **31,** 900–907 (2010).
350. Gunawan, R. C., Almeda, D. & Auguste, D. T. Complementary targeting of liposomes to IL-1α and TNF-α activated endothelial cells via the transient expression of VCAM1 and E-selectin. *Biomaterials* **32,** 9848–53 (2011).
351. Xu, L. *et al.* Heterobivalent ligands target cell-surface receptor combinations in vivo. *Proc. Natl. Acad. Sci. U. S. A.* **109,** 21295–300 (2012).
352. Rangger, C. *et al.* Tumor targeting and imaging with dual-peptide conjugated multifunctional liposomal nanoparticles. *Int. J. Nanomedicine* **8,** 4659–71 (2013).
353. Gao, H. *et al.* RGD and Interleukin-13 Peptide Functionalized Nanoparticles for Enhanced Glioblastoma Cells and Neovasculature Dual Targeting Delivery and Elevated Tumor Penetration. *Mol. Pharm.* **11,** 1042–1052 (2014).
354. Dixit, S. *et al.* Dual receptor-targeted theranostic nanoparticles for localized delivery and activation of PDT drug in glioblastomas. *Mol. Pharm.* **12,** 3250–3260 (2015).
355. Lauffenburger, D. A. & Linderman, J. *Receptors : Models for Binding, Trafficking, and Signaling*. (Oxford University Press, USA, 1993).
356. Ghaghada, K. B., Saul, J., Natarajan, J. V, Bellamkonda, R. V & Annapragada, A. V. Folate targeting of drug carriers: a mathematical model. *J. Control. Release* **104,** 113–28 (2005).
357. Handl, H. L. *et al.* Hitting multiple targets with multimeric ligands. *Expert Opin. Ther. Targets* **8,** 565–86 (2004).
358. Tassa, C. *et al.* Binding affinity and kinetic analysis of targeted small molecule-modified nanoparticles. *Bioconjug. Chem.* **21,** 14–9 (2010).

359. Müller, K. M., Arndt, K. M. & Plückthun, A. Model and simulation of multivalent binding to fixed ligands. *Anal. Biochem.* **261,** 149–58 (1998).
360. Haun, J. B. & Hammer, D. A. Quantifying nanoparticle adhesion mediated by specific molecular interactions. *Langmuir* **24,** 8821–8832 (2008).
361. English, T. J. & Hammer, D. A. Brownian adhesive dynamics (BRAD) for simulating the receptor-mediated binding of viruses. *Biophys. J.* **86,** 3359–3372 (2004).
362. Caplan, M. R. & Rosca, E. V. Targeting drugs to combinations of receptors: a modeling analysis of potential specificity. *Ann. Biomed. Eng.* **33,** 1113–24 (2005).
363. Nermut, M., Green, N. & Eason, P. Electron microscopy and structural model of human fibronectin receptor. *EMBO J.* **7,** 4093–4099 (1988).
364. Xiong, J.-P., Stehle, T., Goodman, S. L. & Arnaout, M. A. New insights into the structural basis of integrin activation. *Blood* **102,** 1155–9 (2003).
365. Hulme, E. C. & Trevethick, M. a. Ligand binding assays at equilibrium: validation and interpretation. *Br. J. Pharmacol.* **161,** 1219–37 (2010).
366. Fiske, C. & Subbarow, Y. The colorimetric determination of phosphorus. *J. Biol. Chem.* **66,** 375–400 (1925).
367. Johnson, I. & Spence, M. T. Z. *Molecular Probes Handbook*. (2010).
368. Li, N., Hill, K. S. & Elferink, L. A. Analysis of receptor tyrosine kinase internalization using flow cytometry. *Methods Mol. Biol.* (2008). doi:10.1016/j.bbi.2008.05.010
369. Weert, A. W. M. Van, Geuze, H. J., Groothuis, B. & Stoorvogel, W. Primaquine interferes with membrane recycling from endosomes to the plasma membrane through a direct interaction with endosomes which does not involve neutralisation of endosomal pH nor osmotic swelling of endosomes. **399,** 394–399 (2000).
370. Silverstein, S. C., Steinman, R. M. & Cohn, Z. A. Endocytosis. *Annu. Rev. Biochem.* **46,** 669–722 (1977).
371. Weddell, J. C. & Imoukhuede, P. I. Quantitative characterization of cellular membrane-receptor heterogeneity through statistical and computational modeling. *PLoS One* **9,** (2014).
372. Kimmig, R., Pfeiffer, D., Landsmann, H. & Hepp, H. Quantitative determination of the epidermal growth factor receptor in cervical cancer and normal cervical epithelium by 2-color flow cytometry: Evidence for down-regulation in cervical cancer. *Int. J. Cancer* **74,** 365–373 (1997).
373. Shankaran, H., Zhang, Y., Tan, Y. & Resat, H. Model-Based Analysis of HER Activation in Cells Co-Expressing EGFR, HER2 and HER3. *PLoS Comput. Biol.* **9,** (2013).
374. Hackel, B. J., Neil, J. R., White, F. M. & Wittrup, K. D. Epidermal growth factor receptor downregulation by small heterodimeric binding proteins. *Protein Eng. Des. Sel.* **25,** 47–57 (2012).
375. Pangburn, T. O., Bates, F. S. & Kokkoli, E. Polymersomes functionalized via ‘“ click ”’ chemistry with the fibronectin mimetic peptides PR _ b and GRGDSP for targeted delivery to cells with different levels of α5β1 expression. *Soft Matter* **8,** 4449–4461 (2012).
376. Schaffner, F., Ray, A. M. & Dontenwill, M. Integrin a5b1, the fibronectin receptor, as a pertinent therapeutic target in solid tumors. *Cancers (Basel).* **5,** 27–47 (2013).
377. Skubitz, A. P. N., Bast, R. C., Wayner, E. A., Letourneau, P. C. & Wilke, M. S. Expression of a64 integrins in serous ovarian carcinoma correlates with expression of the basement membrane protein laminin. *Am. J. Pathol.* **148,** 1445–1461 (1996).
378. Figini, M. *et al.* Reversion of transformed phenotype in ovarian cancer cells by intracellular expression of anti folate receptor antibodies. *Gene Ther.* **10,** 1018–1025 (2003).
379. Folgiero, V. *et al.* Induction of ErbB-3 expression by alpha6beta4 integrin contributes to tamoxifen resistance in ERbeta1-negative breast carcinomas. *PLoS One* **3,** e1592 (2008).
380. Chavez, K., Garimella, S. & Lipkowitz, S. Triple negative breast cancer cell lines: one tool in the search for better treatment of triple negative breast cancer. *Breast Dis.* **32,** 35–48 (2010).

381. Mardilovich, A. & Kokkoli, E. Patterned biomimetic membranes: effect of concentration and pH. *Langmuir* **21,** 7468–75 (2005).
382. Cluzel, C. *et al.* The mechanisms and dynamics of αvβ3 integrin clustering in living cells. *J. Cell Biol.* **171,** 383–392 (2005).
383. Roca-Cusachs, P., Gauthier, N. C., Del Rio, A. & Sheetz, M. P. Clustering of alpha(5)beta(1) integrins determines adhesion strength whereas alpha(v)beta(3) and talin enable mechanotransduction. *Proc. Natl. Acad. Sci.* **106,** 16245–16250 (2009).
384. Van Kooyk, Y. & Figdor, C. G. Avidity regulation of integrins: The driving force in leukocyte adhesion. *Curr. Opin. Cell Biol.* **12,** 542–547 (2000).
385. Erdmann, T. & Schwarz, U. S. Impact of receptor-ligand distance on adhesion cluster stability. *Eur. Phys. J. E* **22,** 123–137 (2007).
386. Jamali, Y., Jamali, T. & Mofrad, M. R. K. An agent based model of integrin clustering: Exploring the role of ligand clustering, integrin homo-oligomerization, integrin-ligand affinity, membrane crowdedness and ligand mobility. *J. Comput. Phys.* **244,** 264–278 (2013).
387. Lortat-Jacob, H., Chouin, E., Cusack, S. & van Raaij, M. J. Kinetic analysis of adenovirus fiber binding to its receptor reveals an avidity mechanism for trimeric receptor-ligand interactions. *J. Biol. Chem.* **276,** 9009–15 (2001).
388. Onodera, Y., Nam, J. M. & Sabe, H. Intracellular trafficking of integrins in cancer cells. *Pharmacol. Ther.* **140,** 1–9 (2013).
389. Wiseman, P. W. *et al.* Spatial mapping of integrin interactions and dynamics during cell migration by image correlation microscopy. *J. Cell Sci.* **117,** 5521–5534 (2004).
390. Gaborski, T. R., Clark, A., Waugh, R. E. & McGrath, J. L. Membrane mobility of beta2 integrins and rolling associated adhesion molecules in resting neutrophils. *Biophys. J.* **95,** 4934–4947 (2008).
391. Yokoyama, Y. & Ramakrishnan, S. Binding of endostatin to human ovarian cancer cells inhibits cell attachment. *Int. J. Cancer* **121,** 2402–9 (2007).
392. Godbey, W. T., Wu, K. K., Hirasaki, G. J. & Mikos, A. G. Improved packing of poly(ethylenimine)/DNA complexes increases transfection efficiency. *Gene Ther.* **6,** 1380–1388 (1999).
393. Jeong, J. H., Song, S. H., Lim, D. W., Lee, H. & Park, T. G. DNA transfection using linear poly(ethylenimine) prepared by controlled acid hydrolysis of poly(2-ethyl-2-oxazoline). *J. Control. Release* **73,** 391–9 (2001).

Appendix A: Binding Equations and Matlab Code Used to Create the Heteromultivalent Model

$$L + R \underset{k_r}{\overset{k_f}{\leftrightarrow}} C$$

$$R = R_0 - C$$

$$\frac{dL}{dt} = k_r C - k_f L R$$

L – unbound nanoparticle

q – valency of ligand A

r – valency of ligand B

R_a – unbound Receptor A

R_b – unbound Receptor B

R_{a0} – Initial Receptor A

R_{b0} – Initial Receptor B

C_{na} – complex between ligand A and receptor A of valency n

C_{mb} – complex between ligand B and receptor B of valency m

k_{fa} – forward reaction rate for binding of unbound nanoparticle to a cell via ligand A-receptor A interactions

k_{fb} – forward reaction rate for binding of unbound nanoparticle to a cell via ligand B-receptor B interactions

k_{xa} – forward reaction rate for binding of ligand A from an already bound nanoparticle

k_{xb} – forward reaction rate for binding of ligand B from an already bound nanoparticle

k_{ra} – rate of dissociation of ligand A

k_{rb} – rate of dissociation of ligand B

q=8, r=0

$$R_a = R_{a0} - (C_{1a}) - 2(C_{2a}) - 3(C_{3a}) - 4(C_{4a}) - 5(C_{5a}) - 6(C_{6a}) - 7(C_{7a}) - 8(C_{8a})$$

$$\frac{dL}{dt} = k_{ra}C_{1am} - 8k_{fa}LR_{am} + k_{ra}C_{1an} - 8k_{fa}LR_{an} + k_{ra}C_{1ap} - 8k_{fa}L$$

$$\frac{dC_{1a}}{dt} = 2k_{-xa}C_{2a} + qk_{fa}LR_a - C_{1a}[(q-1)k_{xa}R_a + k_{ra}]$$

$$\frac{dC_{2a}}{dt} = 3k_{-xa}C_{3a} + (q-1)k_{xa}C_{1a}R_a - C_{2a}[(q-2)k_{xa}R_a + 2k_{-xa}]$$

$$\frac{dC_{3a}}{dt} = 4k_{-xa}C_{4a} + (q-2)k_{xa}C_{2a}R_a - C_{3a}[(q-3)k_{xa}R_a + 3k_{-xa}]$$

$$\frac{dC_{4a}}{dt} = 5k_{-xa}C_{5a} + (q-3)k_{xa}C_{3a}R_a - C_{4a}[(q-4)k_{xa}R_a + 4k_{-xa}]$$

$$\frac{dC_{5a}}{dt} = 6k_{-xa}C_{6a} + (q-4)k_{xa}C_{4a}R_a - C_{5a}[(q-5)k_{xa}R_a + 5k_{-xa}]$$

$$\frac{dC_{6a}}{dt} = 7k_{-xa}C_{7a} + (q-5)k_{xa}C_{5a}R_a - C_{6a}[(q-6)k_{xa}R_a + 6k_{-xa}]$$

$$\frac{dC_{7a}}{dt} = 8k_{-xa}C_{8a} + (q-6)k_{xa}C_{6a}R_a - C_{7a}[(q-7)k_{xa}R_a + 7k_{-xa}]$$

$$\frac{dC_{8a}}{dt} = (q-7)k_{xa}C_{7a}R_a - C_{8a}[8k_{-xa}]$$

q=6, r=2

$$R_a = R_{a0} - (C_{1a} + C_{1a1b} + C_{1a2b}) - 2(C_{2a} + C_{2a1b} + C_{2a2b}) - 3(C_{3a} + C_{3a1b} + C_{3a2b}) - 4(C_{4a} + C_{4a1b} + C_{4a2b}) + 5(C_{5a} + C_{5a1b} + C_{5a2b}) + 6(C_{6a} + C_{6a1b} + C_{6a2b})$$

$$R_b = R_{b0} - (C_{1b} + C_{1a1b} + C_{2a1b} + C_{3a1b} + C_{4a1b} + C_{5a1b} + C_{6a1b}) - 2(C_{2b} + C_{1a2b} + C_{2a2b} + C_{3a2b} + C_{4a2b} + C_{5a2b} + C_{6a2b})$$

$$\frac{dL}{dt} = k_{ra}C_{1am} + k_{rb}C_{1bm} - L\left(qk_{fa}R_{am} + rk_{fb}R_{bm}\right) + k_{ra}C_{1an} + k_{rb}C_{1bn} - L\left(qk_{fa}R_{an} + rk_{fb}R_{bn}\right) + k_{ra}C_{1ap} + k_{rb}C_{1bp} - L(qk_{fa}R_{ap} + rk_{fb}R_{bp})$$

$$\frac{dC_{1a}}{dt} = 2k_{-xa}C_{2a} + k_{-xb}C_{1a1b} + qk_{fa}LR_a - C_{1a}((q-1)k_{xa}R_a + rk_{xb}R_b + k_{ra})$$

$$\frac{dC_{2a}}{dt} = 3k_{-xa}C_{3a} + k_{-xb}C_{2a1b} + (q-1)k_{xa}C_{1a}R_a - C_{2a}((q-2)k_{xa}R_a + rk_{xb}R_b + 2k_{-xa})$$

$$\frac{dC_{3a}}{dt} = 4k_{-xa}C_{4a} + k_{-xb}C_{3a1b} + (q-2)k_{xa}C_{2a}R_a - C_{3a}((q-3)k_{xa}R_a + rk_{xb}R_b + 3k_{-xa})$$

$$\frac{dC_{4a}}{dt} = 5k_{-xa}C_{5a} + k_{-xb}C_{4a1b} + (q-3)k_{xa}C_{3a}R_a - C_{4a}((q-4)k_{xa}R_a + rk_{xb}R_b + 4k_{-xa})$$

$$\frac{dC_{5a}}{dt} = 6k_{-xa}C_{6a} + k_{-xb}C_{5a1b} + (q-4)k_{xa}C_{4a}R_a - C_{5a}((q-5)k_{xa}R_a + rk_{xb}R_b + 5k_{-xa})$$

$$\frac{dC_{6a}}{dt} = k_{-xb}C_{6a1b} + (q-5)k_{xa}C_{5a}R_a - C_{6a}(rk_{xb}R_b + 6k_{-xa})$$

$$\frac{dC_{1b}}{dt} = k_{-xa}C_{1a1b} + 2k_{-xb}C_{2b} + rk_{fb}LR_b - C_{1b}(qk_{xa}R_a + (r-1)k_{xb}R_b + k_{rb})$$

$$\frac{dC_{1a1b}}{dt} = 2k_{-xa}C_{2a1b} + 2k_{-xb}C_{1a2b} + qk_{xa}C_{1b}R_a + rk_{xb}C_{1a}R_b - C_{1a1b}((q-1)k_{xa}R_a + (r-1)k_{xb}R_b + k_{-xa} + k_{-xb})$$

$$\frac{dC_{2a1b}}{dt} = 3k_{-xa}C_{3a1b} + 2k_{-xb}C_{2a2b} + (q-1)k_{xa}C_{1a1b}R_a + rk_{xb}C_{2a}R_b - C_{2a1b}((q-2)k_{xa}R_a + (r-1)k_{xb}R_b + 2k_{-xa} + k_{-xb})$$

$$\frac{dC_{3a1b}}{dt} = 4k_{-xa}C_{4a1b} + 2k_{-xb}C_{3a2b} + (q-2)k_{xa}C_{2a1b}R_a + rk_{xb}C_{3a}R_b - C_{3a1b}((q-3)k_{xa}R_a + (r-1)k_{xb}R_b + 3k_{-xa} + k_{-xb})$$

$$\frac{dC_{4a1b}}{dt} = 5k_{-xa}C_{5a1b} + 2k_{-xb}C_{4a2b} + (q-3)k_{xa}C_{3a1b}R_a + rk_{xb}C_{4a}R_b - C_{4a1b}((q-4)k_{xa}R_a + (r-1)k_{xb}R_b + 4k_{-xa} + k_{-xb})$$

$$\frac{dC_{5a1b}}{dt} = 6k_{-xa}C_{6a1b} + 2k_{-xb}C_{5a2b} + (q-4)k_{xa}C_{4a1b}R_a + rk_{xb}C_{5a}R_b - C_{5a1b}((q-5)k_{xa}R_a + (r-1)k_{xb}R_b + 5k_{-xa} + k_{-xb})$$

$$\frac{dC_{6a1b}}{dt} = 2k_{-xb}C_{6a2b} + (q-5)k_{xa}C_{5a1b}R_a + rk_{xb}C_{6a}R_b - C_{6a1b}((r-1)k_{xb}R_b + 6k_{-xa} + k_{-xb})$$

$$\frac{dC_{2b}}{dt} = k_{-xa}C_{1a2b} + (r-1)k_{xb}C_{1b}R_b - C_{2b}(qk_{xa}R_a + 2k_{-xb})$$

$$\frac{dC_{1a2b}}{dt} = 2k_{-xa}C_{2a2b} + qk_{xa}C_{2b}R_a + (r-1)k_{xb}C_{1a1b}R_b - C_{1a2b}((q-1)k_{xa}R_a + k_{-xa} + 2k_{-xb})$$

$$\frac{dC_{2a2b}}{dt} = 3k_{-xa}C_{3a2b} + (q-1)k_{xa}C_{1a2b}R_a + (r-1)k_{xb}C_{2a1b}R_b - C_{2a2b}((q-2)k_{xa}R_a + 2k_{-xa} + 2k_{-xb})$$

$$\frac{dC_{3a2b}}{dt} = 4k_{-xa}C_{4a2b} + (q-2)k_{xa}C_{2a2b}R_a + (r-1)k_{xb}C_{3a1b}R_b - C_{3a2b}((q-3)k_{xa}R_a + 3k_{-xa} + 2k_{-xb})$$

$$\frac{dC_{4a2b}}{dt} = 5k_{-xa}C_{5a2b} + (q-3)k_{xa}C_{3a2b}R_a + (r-1)k_{xb}C_{4a1b}R_b - C_{4a2b}((q-4)k_{xa}R_a + 4k_{-xa} + 2k_{-xb})$$

$$\frac{dC_{5a2b}}{dt} = 6k_{-xa}C_{6a2b} + (q-4)k_{xa}C_{4a2b}R_a + (r-1)k_{xb}C_{5a1b}R_b - C_{5a2b}((q-5)k_{xa}R_a + 5k_{-xa} + 2k_{-xb})$$

$$\frac{dC_{6a2b}}{dt} = (q-5)k_{xa}C_{5a2b}R_a + (r-1)k_{xb}C_{6a1b}R_b - C_{6a2b}(6k_{-xa} + 2k_{-xb})$$

q=4, r=4;

$$R_a = R_{a0} - (C_{1a} + C_{1a1b} + C_{1a2b} + C_{1a3b} + C_{1a4b}) - 2(C_{2a} + C_{2a1b} + C_{2a2b} + C_{2a3b} + C_{2a4b}) - 3(C_{3a} + C_{3a1b} + C_{3a2b} + C_{3a3b} + C_{3a4b}) - 4(C_{4a} + C_{4a1b} + C_{4a2b} + C_{4a3b} + C_{4a4b})$$

$$R_b = R_{b0} - (C_{1b} + C_{1a1b} + C_{2a1b} + C_{3a1b} + C_{4a1b}) - 2(C_{2b} + C_{1a2b} + C_{2a2b} + C_{3a2b} + C_{4a2b}) - 3(C_{3b} + C_{1a3b} + 2_{1a3b} + C_{3a3b} + C_{4a3b}) - 4(C_{4b} + C_{1a4b} + C_{2a4b} + C_{3a4b} + C_{4a4b})$$

$$\frac{dL}{dt} = (k_{ra}C_{1am} + k_{rb}C_{1bm}) - L(qk_{fa}R_{am} + rk_{fb}R_{bm}) + (k_{ra}C_{1an} + k_{rb}C_{1bn}) - L(qk_{fa}R_{an} + rk_{fb}R_{bn}) + (k_{ra}C_{1ap} + k_{rb}C_{1bp}) - L(qk_{fa}R_{ap} + rk_{fb}R_{bp})$$

$$\frac{dC_{1a}}{dt} = 2k_{-xa}C_{2a} + k_{-xb}C_{1a1b} + qk_{fa}LR_a - C_{1a}((q-1)k_{xa}R_a + rk_{xb}R_b + k_{ra})$$

$$\frac{dC_{2a}}{dt} = 3k_{-xa}C_{3a} + k_{-xb}C_{2a1b} + (q-1)k_{xa}C_{1a}R_a - C_{2a}((q-2)k_{xa}R_a + rk_{xb}R_b + 2k_{-xa})$$

$$\frac{dC_{3a}}{dt} = 4k_{-xa}C_{4a} + k_{-xb}C_{3a1b} + (q-2)k_{xa}C_{2a}R_a - C_{3a}((q-3)k_{xa}R_a + rk_{xb}R_b + 3k_{-xa})$$

$$\frac{dC_{4a}}{dt} = k_{-xb}C_{4a1b} + (q-3)k_{xa}C_{3a}R_a - C_{4a}(rk_{xb}R_b + 4k_{-xa})$$

$$\frac{dC_{1b}}{dt} = k_{-xa}C_{1a1b} + 2k_{-xb}C_{2b} + rk_{fb}LR_b - C_{1b}(qk_{xa}R_a + (r-1)k_{xb}R_b + k_{rb})$$

$$\frac{dC_{1a1b}}{dt} = 2k_{-xa}C_{2a1b} + 2k_{-xb}C_{1a2b} + qk_{xa}C_{1b}R_a + rk_{xb}C_{1a}R_b - C_{1a1b}((q-1)k_{xa}R_a + (r-1)k_{xb}R_b + k_{-xa} + k_{-xb})$$

$$\frac{dC_{2a1b}}{dt} = 3k_{-xa}C_{3a1b} + 2k_{-xb}C_{2a2b} + (q-1)k_{xa}C_{1a1b}R_a + rk_{xb}C_{2a}R_b - C_{2a1b}((q-2)k_{xa}R_a + (r-1)k_{xb}R_b + 2k_{-xa} + k_{-xb})$$

$$\frac{dC_{3a1b}}{dt} = 4k_{-xa}C_{4a1b} + 2k_{-xb}C_{3a2b} + (q-2)k_{xa}C_{2a1b}R_a + rk_{xb}C_{3a}R_b - C_{3a1b}((q-3)k_{xa}R_a + (r-1)k_{xb}R_b + 3k_{-xa} + k_{-xb})$$

$$\frac{dC_{4a1b}}{dt} = 2k_{-xb}C_{4a2b} + (q-3)k_{xa}C_{3a1b}R_a + rk_{xb}C_{4a}R_b - C_{4a1b}((r-1)k_{xb}R_b + 4k_{-xa} + k_{-xb})$$

$$\frac{dC_{2b}}{dt} = k_{-xa}C_{1a2b} + 3k_{-xb}C_{3b} + (r-1)k_{xb}C_{1b}R_b - C_{2b}(qk_{xa}R_a + (r-2)k_{xb}R_b + 2k_{-xb})$$

$$\frac{dC_{1a2b}}{dt} = 2k_{-xa}C_{2a2b} + 3k_{-xb}C_{1a3b} + qk_{xa}C_{2b}R_a + (r-1)k_{xb}C_{1a1b}R_b - C_{1a2b}((q-1)k_{xa}R_a + (r-2)k_{xb}R_b + k_{-xa} + 2k_{-xb})$$

$$\frac{dC_{2a2b}}{dt} = 3k_{-xa}C_{3a2b} + 3k_{-xb}C_{2a3b} + (q-1)k_{xa}C_{1a2b}R_a + (r-1)k_{xb}C_{2a1b}R_b - C_{2a2b}((q-2)k_{xa}R_a + (r-2)k_{xb}R_b + 2k_{-xa} + 2k_{-xb})$$

$$\frac{dC_{3a2b}}{dt} = 4k_{-xa}C_{4a2b} + 3k_{-xb}C_{3a3b} + (q-2)k_{xa}C_{2a2b}R_a + (r-1)k_{xb}C_{3a1b}R_b - C_{3a2b}((q-3)k_{xa}R_a + (r-2)k_{xb}R_b + 3k_{-xa} + 2k_{-xb})$$

$$\frac{dC_{4a2b}}{dt} = 3k_{-xb}C_{4a3b} + (q-3)k_{xa}C_{3a2b}R_a + (r-1)k_{xb}C_{4a1b}R_b - C_{4a2b}((r-2)k_{xb}R_b + 4k_{-xa} + 2k_{-xb})$$

$$\frac{dC_{3b}}{dt} = k_{-xa}C_{1a3b} + 4k_{-xb}C_{4b} + (r-2)k_{xb}C_{2b}R_b - C_{3b}(qk_{xa}R_a + (r-3)k_{xb}R_b + 3k_{-xb})$$

$$\frac{dC_{1a3b}}{dt} = 2k_{-xa}C_{2a3b} + 4k_{-xb}C_{1a4b} + qk_{xa}C_{3b}R_a + (r-2)k_{xb}C_{1a2b}R_b - C_{1a3b}((q-1)k_{xa}R_a + (r-3)k_{xb}R_b + k_{-xa} + 3k_{-xb})$$

$$\frac{dC_{2a3b}}{dt} = 3k_{-xa}C_{3a3b} + 4k_{-xb}C_{2a4b} + (q-1)k_{xa}C_{1a3b}R_a + (r-2)k_{xb}C_{2a2b}R_b - C_{2a3b}((q-2)k_{xa}R_a + (r-3)k_{xb}R_b + 2k_{-xa} + 3k_{-xb})$$

$$\frac{dC_{3a3b}}{dt} = 4k_{-xa}C_{4a3b} + 4k_{-xb}C_{3a4b} + (q-2)k_{xa}C_{2a3b}R_a + (r-2)k_{xb}C_{3a2b}R_b - C_{3a3b}((q-3)k_{xa}R_a + (r-3)k_{xb}R_b + 3k_{-xa} + 3k_{-xb})$$

$$\frac{dC_{4a3b}}{dt} = 4k_{-xa}C_{4a4b} + (q-3)k_{xa}C_{3a3b}R_a + (r-2)k_{xb}C_{4a2b}R_b - C_{4a3b}((r-3)k_{xb}R_b + 4k_{-xa} + 3k_{-xb})$$

$$\frac{dC_{4b}}{dt} = k_{-xa}C_{1a4b} + (r-3)k_{xb}C_{3b}R_b - C_{4b}(qk_{xa}R_a + 4k_{-xb})$$

$$\frac{dC_{1a4b}}{dt} = 2k_{-xa}C_{2a4b} + qk_{xa}C_{4b}R_a + (r-3)k_{xb}C_{1a3b}R_b - C_{1a4b}((q-1)k_{xa}R_a + k_{-xa} + 4k_{-xb})$$

$$\frac{dC_{2a4b}}{dt} = 3k_{-xa}C_{3a4b} + (q-1)k_{xa}C_{1a4b}R_a + (r-3)k_{xb}C_{2a3b}R_b - C_{2a4b}((q-2)k_{xa}R_a + 2k_{-xa} + 4k_{-xb})$$

$$\frac{dC_{3a4b}}{dt} = 4k_{-xa}C_{4a4b} + (q-2)k_{xa}C_{2a4b}R_a + (r-3)k_{xb}C_{3a3b}R_b - C_{3a4b}((q-3)k_{xa}R_a + 3k_{-xa} + 4k_{-xb})$$

$$\frac{dC_{4a4b}}{dt} = (q-3)k_{xa}C_{3a4b}R_a + (r-3)k_{xb}C_{4a3b}R_b - C_{4a4b}(4k_{-xa} + 4k_{-xb})$$

Parrallel equations were written and used for q and r combinations of 0,1; 0,2; 0;3, 0;4, 0;5, 0;6, 0,7; 0,8; 1,0; 1,1; 1,2; 2,3; 1,4; 1,5; 1,6; 1,7; 2,0; 2,1; 2,2; 2,3; 2,4; 2,5; 2,6; 3,0; 3,1; 3,2; 3,3; 3,4; 3,5; 4,0; 4,1; 4,2; 4,3; 4,4; 5,0; 5,1; 5,2; 5,3; 6,0; 6,1; 6,2; 7,0; 7,1; 8,0.

Matlab code for heteromultivalent kinetic model used in Chapter 4

```
%% dual targeting. graph Mtotal, Ntotal, Ptotal. Calculate Specificity

clear
clc
format shortg
c=clock
tic

p.N = 6.022e23;          %avagadro's number
p.V = 4e-9;              %Vol (L/cell) - 200 uL/50,000 cells
kfa = 3e2;               %on rate ligand-receptor pair a [1/(M*s)]
kda = 3.3e-6;            %dissociation rate [M]
kfb = kfa;               %on rate ligand-receptor pair a [1/(M*s)]
kdb = 3.3e-6;            %dissociation rate [M]
hwell = 6.22;            %height of media in the well (mm)
hbind = 2e-6;            %binding height (mm)
h = hwell/hbind;         %ratio of binding volume

p.kfa = kfa/(p.N*p.V);   %on rate ligand-receptor pair a [cell/(#*s)]
p.kra  = kda*kfa;        %off rate ligand-receptor pair a [1/s]
p.kxa = p.kfa*h;         %affinity on rate ligand-receptor pair a [cell/(#*s)]
p.k_xa = p.kra;          %affinity off rate ligand-receptor pair a [1/s]
p.kfb  = kfb/(p.N*p.V);  %on rate ligand-receptor pair a [cell/(#*s)]
p.krb = kdb*kfb;         %off rate ligand-receptor pair b [1/s]
p.kxb  = p.kfb*h;        %5e-6;%affinity on rate ligand-receptor pair b [cell/(#*s)]
p.k_xb = p.krb;          %affinity off rate ligand-receptor pair b [1/s]

p.tf=240000*3600;%diffEQ time (s)
p.Lg= 2.5e-14;

Mtotal = [NaN, NaN, NaN, NaN, NaN, NaN, NaN, NaN, NaN;NaN, NaN, NaN, NaN, NaN, NaN, NaN, NaN, NaN;NaN, NaN, NaN, NaN, NaN,
NaN, NaN, NaN, NaN;NaN, NaN, NaN, NaN, NaN, NaN, NaN, NaN, NaN;NaN, NaN, NaN, NaN, NaN, NaN, NaN, NaN, NaN;NaN, NaN, NaN, NaN,
NaN, NaN, NaN, NaN, NaN;NaN, NaN, NaN, NaN, NaN, NaN, NaN, NaN, NaN;NaN, NaN, NaN, NaN, NaN, NaN, NaN, NaN, NaN;NaN, NaN, NaN,
NaN, NaN, NaN, NaN, NaN, NaN];
```

```
    Ntotal = [NaN, NaN, NaN, NaN, NaN, NaN, NaN, NaN, NaN;NaN, NaN, NaN, NaN, NaN, NaN, NaN, NaN, NaN;NaN, NaN, NaN, NaN, NaN,
NaN, NaN, NaN, NaN;NaN, NaN, NaN, NaN, NaN, NaN, NaN, NaN, NaN;NaN, NaN, NaN, NaN, NaN, NaN, NaN, NaN, NaN;NaN, NaN, NaN, NaN,
NaN, NaN, NaN, NaN, NaN;NaN, NaN, NaN, NaN, NaN, NaN, NaN, NaN, NaN;NaN, NaN, NaN, NaN, NaN, NaN, NaN, NaN, NaN;NaN, NaN, NaN,
NaN, NaN, NaN, NaN, NaN, NaN];
    Ptotal = [NaN, NaN, NaN, NaN, NaN, NaN, NaN, NaN, NaN;NaN, NaN, NaN, NaN, NaN, NaN, NaN, NaN, NaN;NaN, NaN, NaN, NaN, NaN,
NaN, NaN, NaN, NaN;NaN, NaN, NaN, NaN, NaN, NaN, NaN, NaN, NaN;NaN, NaN, NaN, NaN, NaN, NaN, NaN, NaN, NaN;NaN, NaN, NaN, NaN,
NaN, NaN, NaN, NaN, NaN;NaN, NaN, NaN, NaN, NaN, NaN, NaN, NaN, NaN;NaN, NaN, NaN, NaN, NaN, NaN, NaN, NaN, NaN;NaN, NaN, NaN,
NaN, NaN, NaN, NaN, NaN, NaN];

    q=0;
    r=0;
    p.Ram0 = 200000;
    p.Rbm0 = p.Ram0;
    p.Ran0 = p.Ram0;
    p.Rbn0 = p.Rbm0/8;
    p.Rap0 = p.Ram0/8;
    p.Rbp0 = p.Rbm0;
    for countq=0:1:8
       for countr=0:1:8-countq
       q=countq;
       r=countr;
    %% initial conditions for bound complexes (all=0)
    p.C1am = 0;%all units #/cell
    p.C2am = 0;
    p.C3am = 0;
    p.C4am = 0;
    p.C5am = 0;
    p.C6am = 0;
    p.C7am = 0;
    p.C8am = 0;
    p.C1bm = 0;
    p.C1a1bm = 0;
    p.C2a1bm = 0;
    p.C3a1bm = 0;
    p.C4a1bm = 0;
    p.C5a1bm = 0;
```

```
p.C6a1bm = 0;
p.C7a1bm = 0;
p.C2bm = 0;
p.C1a2bm = 0;
p.C2a2bm = 0;
p.C3a2bm = 0;
p.C4a2bm = 0;
p.C5a2bm = 0;
p.C6a2bm = 0;
p.C3bm = 0;
p.C1a3bm = 0;
p.C2a3bm = 0;
p.C3a3bm = 0;
p.C4a3bm = 0;
p.C5a3bm = 0;
p.C4bm = 0;
p.C1a4bm = 0;
p.C2a4bm = 0;
p.C3a4bm = 0;
p.C4a4bm = 0;

p.C1an = 0;
p.C2an = 0;
p.C3an = 0;
p.C4an = 0;
p.C5an = 0;
p.C6an = 0;
p.C7an = 0;
p.C8an = 0;
p.C1bn = 0;
p.C1a1bn = 0;
p.C2a1bn = 0;
p.C3a1bn = 0;
p.C4a1bn = 0;
p.C5a1bn = 0;
p.C6a1bn = 0;
```

```
p.C7a1bn = 0;
p.C2bn = 0;
p.C1a2bn = 0;
p.C2a2bn = 0;
p.C3a2bn = 0;
p.C4a2bn = 0;
p.C5a2bn = 0;
p.C6a2bn = 0;
p.C3bn = 0;
p.C1a3bn = 0;
p.C2a3bn = 0;
p.C3a3bn = 0;
p.C4a3bn = 0;
p.C5a3bn = 0;
p.C4bn = 0;
p.C1a4bn = 0;
p.C2a4bn = 0;
p.C3a4bn = 0;
p.C4a4bn = 0;

p.C1ap = 0;
p.C2ap = 0;
p.C3ap = 0;
p.C4ap = 0;
p.C5ap = 0;
p.C6ap = 0;
p.C7ap = 0;
p.C8ap = 0;
p.C1bp = 0;
p.C1a1bp = 0;
p.C2a1bp = 0;
p.C3a1bp = 0;
p.C4a1bp = 0;
p.C5a1bp = 0;
p.C6a1bp = 0;
p.C7a1bp = 0;
```

```
p.C2bp = 0;
p.C1a2bp = 0;
p.C2a2bp = 0;
p.C3a2bp = 0;
p.C4a2bp = 0;
p.C5a2bp = 0;
p.C6a2bp = 0;
p.C3bp = 0;
p.C1a3bp = 0;
p.C2a3bp = 0;
p.C3a3bp = 0;
p.C4a3bp = 0;
p.C5a3bp = 0;
p.C4bp = 0;
p.C1a4bp = 0;
p.C2a4bp = 0;
p.C3a4bp = 0;
p.C4a4bp = 0;
%% ODE and total complexes summation
modelname=sprintf('%s%d%s%d', 'modelq', q,'r',r);
modelname2=str2func(modelname);
totalname=sprintf('%s%d%s%d', 'totalq', q,'r',r);
totalname2=str2func(totalname);
%setting initial conditions
y0=[p.Lg p.C1am p.C2am p.C3am p.C4am p.C5am p.C6am p.C7am p.C8am p.C1bm p.C1a1bm p.C2a1bm p.C3a1bm p.C4a1bm p.C5a1bm
p.C6a1bm p.C2bm p.C1a2bm p.C2a2bm p.C3a2bm p.C4a2bm p.C5a2bm p.C6a2bm p.C3bm p.C1a3bm p.C2a3bm p.C3a3bm p.C4a3bm p.C4bm
p.C1a4bm p.C2a4bm p.C3a4bm p.C4a4bm p.C1an p.C2an p.C3an p.C4an p.C5an p.C6an p.C7an p.C8an p.C1bn p.C1a1bn p.C2a1bn p.C3a1bn
p.C4a1bn p.C5a1bn p.C6a1bn p.C2bn p.C1a2bn p.C2a2bn p.C3a2bn p.C4a2bn p.C5a2bn p.C6a2bn p.C3bn p.C1a3bn p.C2a3bn p.C3a3bn
p.C4a3bn p.C4bn p.C1a4bn p.C2a4bn p.C3a4bn p.C4a4bn p.C1ap p.C2ap p.C3ap p.C4ap p.C5ap p.C6ap p.C7ap p.C8ap p.C1bp p.C1a1bp
p.C2a1bp p.C3a1bp p.C4a1bp p.C5a1bp p.C6a1bp p.C2bp p.C1a2bp p.C2a2bp p.C3a2bp p.C4a2bp p.C5a2bp p.C6a2bp p.C3bp p.C1a3bp
p.C2a3bp p.C3a3bp p.C4a3bp p.C4bp p.C1a4bp p.C2a4bp p.C3a4bp p.C4a4bp];
%passing constants, initial conditions to ODE solver and diffEQs
 options = odeset('AbsTol', 1e-7, 'RelTol', 1e-5);
    [t,y] = ode15s(modelname2, [0 p.tf], y0, options, p);
    [M,N,P,Mu,Nu,Pu] = totalname2(y);
    [u,~]=size(y);
```

```
    Mtotal(countq+1,countr+1)=Mu;
    Ntotal(countq+1,countr+1)=Nu;
    Ptotal(countq+1,countr+1)=Pu;
    Q(countq+1)=q;
    R(countr+1)=r;
   end
toc
end

    SpecN=Mtotal./Ntotal;
    SpecP=Mtotal./Ptotal;
    Spec = min(SpecN, SpecP);
%     [maxSpecN,ind] = max(SpecN(:));
% [h,k] = ind2sub(size(SpecN),ind);
% maxQN = Q(h)
% maxRN = R(k)
% [maxSpecP,ind] = max(SpecP(:));
% [H,K] = ind2sub(size(SpecP),ind);
% maxQP = Q(H)
% maxRP = R(K)
%     [maxSpecN,ind] = max(Spec(:));
% [h,k] = ind2sub(size(SpecN),ind);
% maxQ = Q(h)
% maxR = R(k)
% %verify that equilibrium has been reached
% figure(1)
% plot(t,y)
%plot Binding vs. Receptor Density and Q
figure('units','inches','position',[0 0 6 6],'Color',[1,1,1]);
subplot(2,2,1)
pcolor(Q,R,Mtotal)
%colorbar
xlabel('Ligand B (Valency)')
ylabel('Ligand A (Valency)')
axis([0 8 0 8])
%title('++/++ Cell Line')
```

```
caxis([0 55])
colormap parula
set(gca,'FontSize',10)
set(findall(gcf,'type','text'),'FontSize',10,'FontName','Arial')

subplot(2,2,2)
pcolor(Q,R,Ntotal)
xlabel('Ligand B (Valency)')
ylabel('Ligand A (Valency)')
axis([0 8 0 8])
%colorbar
%title('++/+ Cell Line')
caxis([0 55])
colormap parula
set(gca,'FontSize',10)
set(findall(gcf,'type','text'),'FontSize',10,'FontName','Arial')

subplot(2,2,3)
pcolor(Q,R,Ptotal)
axis([0 8 0 8])
%colorbar
xlabel('Ligand B (Valency)')
ylabel('Ligand A (Valency)')
%title('+/++ Cell Line')
caxis([0 55])
colormap parula
set(gca,'FontSize',10)
set(findall(gcf,'type','text'),'FontSize',10,'FontName','Arial')

subplot(2,2,4)
pcolor(Q,R,Spec)
axis([0 8 0 8])
%colorbar
xlabel('Ligand B (Valency)')
ylabel('Ligand A (Valency)')
%title('Specificity')
```

```
caxis([0 55])
colormap parula
set(gca,'FontSize',10)
set(findall(gcf,'type','text'),'FontSize',10,'FontName','Arial')

toc
```

Appendix B: Heteromultivalent Kinetic Model Sensitivity Analysis

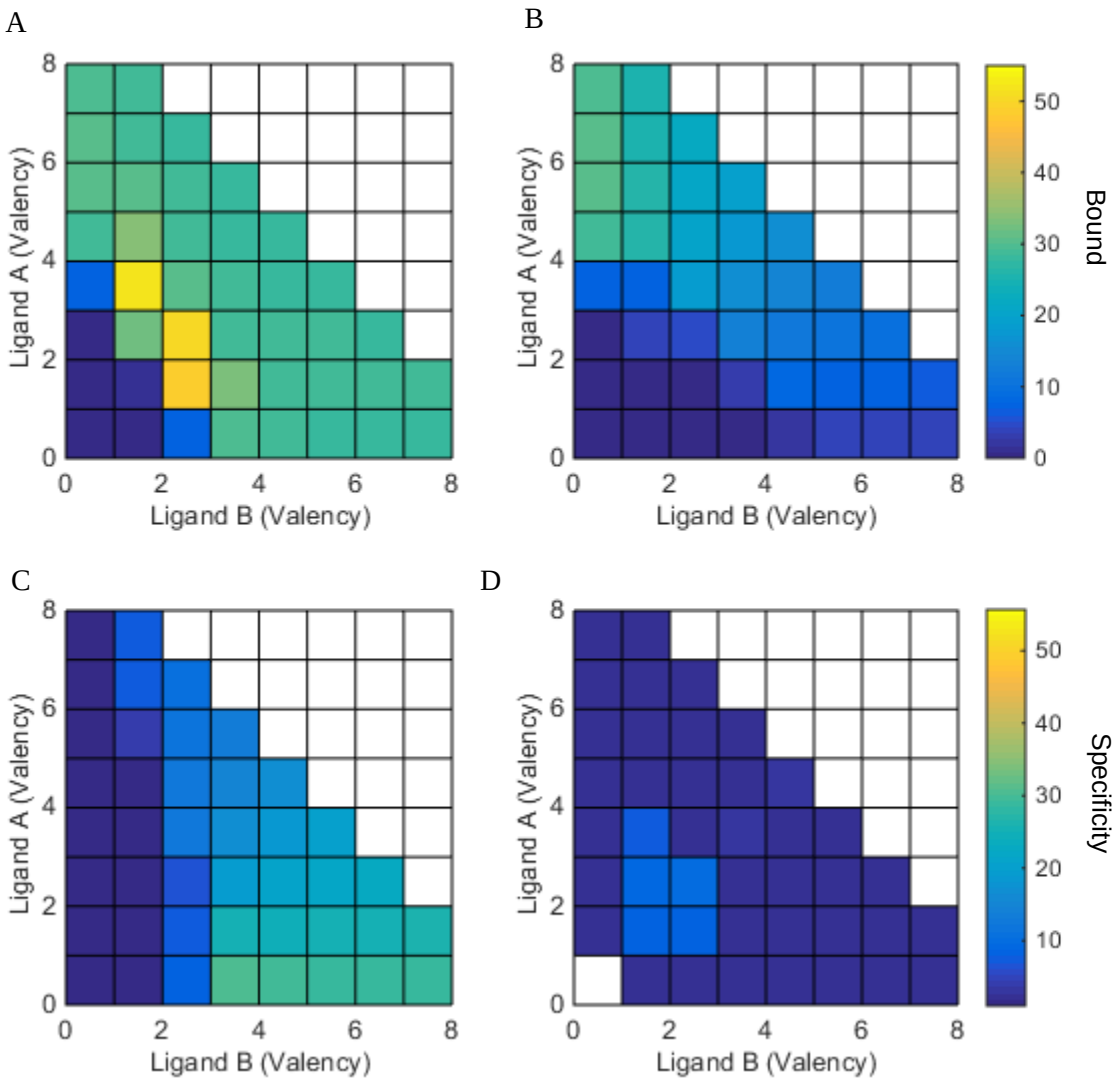

Figure B1. Theoretical Binding of Heteromultivalent Nanoparticles to 3 Representative Cell Types
The heteromultivalent kinetic binding model was used to calculate nanoparticles bound to cells with high dual expression of receptors (R_A=200,000, R_B=200,000) (A), higher expression of receptor A (R_A=200,000, R_B=25,000) (B) of higher expression of receptor B (R_A=25,000, R_B=200,000) (C). Valency of ligand A and B were varied 0-4 and binding to each cell was measured, as well as specificity (D) of (A) compared to (B) and (C). L = $2.5*10^{-14}$ nanoparticles, K_{da}= $3.3*10^{-6}$ M, K_{db}=$0.367*10^{-6}$ M , k_{fa}=k_{fb}=300 $M^{-1}s^{-1}$, k_{ra}=k_{rb}=K_{da}*k_{fa}, k_{-xa}= k_{-xb} =k_{ra}, k_{xa}= k_{xb} =$9.3*10^{8}$ $M^{-1}s^{-1}$.

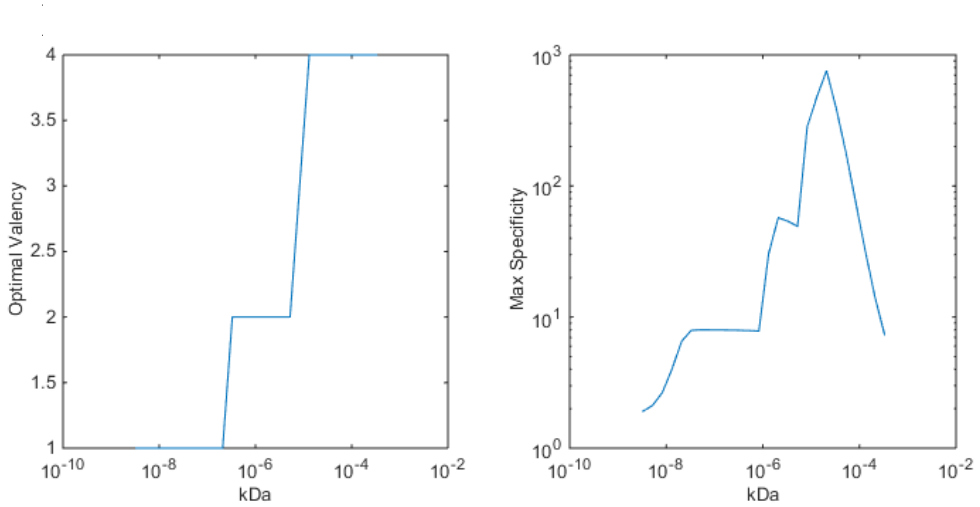

Figure B2. Maximum specificity and dual valency that achieves maximum specificity were calculated with varying K_d. All other variables are the same as in Figure B1.

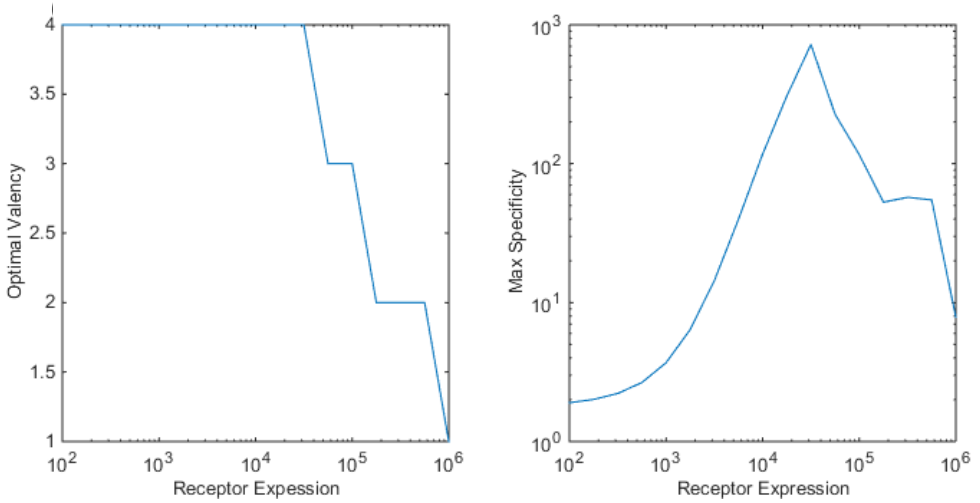

Figure B3. Maximum specificity and dual valency that achieves maximum specificity were calculated at various receptor expression levels. All other variables are the same as in Figure B1.